

**APPLIED PHYSICS REVIEWS****Ion and electron irradiation-induced effects in nanostructured materials**A. V. Krasheninnikov<sup>1,2,a)</sup> and K. Nordlund<sup>1,b)</sup><sup>1</sup>*Department of Physics, University of Helsinki, P.O. Box 43, Helsinki FI-00014, Finland*<sup>2</sup>*Department of Applied Physics, P.O. Box 1100, FI-00076 Aalto University, Finland*

(Received 22 July 2009; accepted 18 January 2010; published online 6 April 2010)

A common misconception is that the irradiation of solids with energetic electrons and ions has exclusively detrimental effects on the properties of target materials. In addition to the well-known cases of doping of bulk semiconductors and ion beam nitriding of steels, recent experiments show that irradiation can also have beneficial effects on nanostructured systems. Electron or ion beams may serve as tools to synthesize nanoclusters and nanowires, change their morphology in a controllable manner, and tailor their mechanical, electronic, and even magnetic properties. Harnessing irradiation as a tool for modifying material properties at the nanoscale requires having the full microscopic picture of defect production and annealing in nanotargets. In this article, we review recent progress in the understanding of effects of irradiation on various zero-dimensional and one-dimensional nanoscale systems, such as semiconductor and metal nanoclusters and nanowires, nanotubes, and fullerenes. We also consider the two-dimensional nanosystem graphene due to its similarity with carbon nanotubes. We dwell on both theoretical and experimental results and discuss at length not only the physics behind irradiation effects in nanostructures but also the technical applicability of irradiation for the engineering of nanosystems. © 2010 American Institute of Physics. [doi:10.1063/1.3318261]

**TABLE OF CONTENTS**

I. INTRODUCTION. . . . .	2	H. Kinetic Monte Carlo approach. . . . .	11
A. Scope of the review. . . . .	3	I. Summary of simulation methods and their limitations. . . . .	11
B. Organization of the paper. . . . .	3	V. IRRADIATION EFFECTS IN CARBON NANOSYSTEMS. . . . .	12
II. PRODUCTION OF DEFECTS IN SOLIDS UNDER ION AND ELECTRON IRRADIATION. . . . .	4	A. Defect production in carbon nanosystems under irradiation. . . . .	12
A. Production of defects in bulk targets. . . . .	4	1. Production of defects in SWNTs under ion irradiation. . . . .	12
B. Creation of defects in nanoscale materials under irradiation. . . . .	5	2. Production of defects in multiwalled and bundled-up nanotubes. . . . .	14
III. EXPERIMENTAL TECHNIQUES USED TO IDENTIFY DEFECTS IN NANOSTRUCTURED MATERIALS. . . . .	6	3. Ion irradiation of fullerenes and fullerene-nanotube systems. . . . .	14
IV. COMPUTATIONAL ATOMISTIC METHODS USED FOR MODELING IRRADIATION EFFECTS IN SOLIDS. . . . .	7	4. Simulations of electron irradiation of carbon nanosystems. . . . .	15
A. Binary collision approximation-based methods. . . . .	8	5. Carbon atom displacement energy. . . . .	15
B. Molecular dynamics with empirical potentials. . . . .	8	B. Irradiation-induced defects in carbon nanosystems and their properties. . . . .	16
C. Simulation setup. . . . .	8	1. Vacancies in graphene and carbon nanotubes. . . . .	17
D. Density functional theory-based methods. . . . .	9	2. Carbon adatoms as interstitials in single-walled carbon nanotubes. . . . .	19
E. Tight-binding methods. . . . .	9	3. Carbon adatoms on graphene. . . . .	19
F. Time-dependent DFT simulations. . . . .	10	4. Stone-Wales defects. . . . .	19
G. Phenomenological descriptions of electronic excitation. . . . .	10	5. Irradiation-induced defects in MWNTs and nanotube bundles. . . . .	20
		6. Annealing of irradiation-induced defects. . . . .	20
		7. Relationship between point defects in nanotubes, those in multilayer graphene, and those in graphite. . . . .	22

<sup>a)</sup>Electronic mail: akrashen@acclab.helsinki.fi.<sup>b)</sup>Electronic mail: knordlun@acclab.helsinki.fi.

C. Electron irradiation of carbon nanostructures. . . . .	22	C. Phase changes in nanoparticles. . . . .	53
1. Electron irradiation of graphene. . . . .	23	D. Irradiation of quantum dots. . . . .	55
2. Electron irradiation of freestanding single-walled carbon nanotubes. . . . .	23	1. InAs quantum dots. . . . .	55
3. Irradiation-induced links between single-walled carbon nanotubes in bundles. . . . .	24	2. Other quantum dots. . . . .	55
4. Electron irradiation of multiwalled carbon nanotubes. . . . .	24	IX. IRRADIATION EFFECTS IN EMBEDDED NANOCCLUSERS (NCS). . . . .	56
5. Welding and coalescence of carbon nanotubes under electron beam. . . . .	25	A. Effects of radiation on embedded NCs. . . . .	56
6. Engineering carbon nanostructures with a focused electron beam. . . . .	26	1. Si and Ge NCs in silica. . . . .	56
D. Ion irradiation of carbon nanomaterials. . . . .	28	2. Metal NCs. . . . .	57
1. Ion irradiation of graphene. . . . .	28	3. Inverse Ostwald ripening. . . . .	58
2. Experiments on heavy ion irradiation of carbon nanotubes. . . . .	29	B. Elongation of nanoclusters by swift heavy ions. . . . .	58
a. High-dose irradiation. . . . .	29	X. CONCLUSIONS AND OUTLOOK. . . . .	60
b. Low-dose irradiation. . . . .	32	APPENDIX: WIKIPEDIA ARTICLES RELATED TO THE TOPIC. . . . .	61
3. Light ions: Proton irradiation of carbon nanotubes. . . . .	33		
4. Welding of nanotubes by ion beams. . . . .	34		
5. Ion-irradiation-induced links between nanotubes and substrates. . . . .	34		
6. Irradiation-mediated doping of carbon nanotubes with foreign atoms. . . . .	34		
7. Carbon nanotubes as masks against ion irradiation. . . . .	35		
8. Channeling of ions in nanotubes. . . . .	35		
E. Irradiated carbon nanotubes and onions as high-pressure cells. . . . .	36		
F. Influence of defects on the properties of nanocarbon systems. . . . .	38		
1. Mechanical properties. . . . .	38		
2. Electronic properties. . . . .	39		
3. Magnetic properties. . . . .	40		
VI. IRRADIATION EFFECTS IN BORON NITRIDE (BN) NANOSYSTEMS. . . . .	40		
A. Electron irradiation. . . . .	40		
B. Ion irradiation. . . . .	41		
C. Theory of point defects in BN nanotubes. . . . .	42		
D. Boron and nitrogen atom displacement energies. . . . .	43		
E. Engineering boron nitride nanosystems with the electron beam. . . . .	44		
VII. EFFECTS OF IRRADIATION ON NANOWIRES (NWS). . . . .	45		
A. Silicon-based NWS. . . . .	45		
B. Implantation of compound semiconductor NWS. . . . .	46		
C. Electron beam modification. . . . .	47		
D. Ion beam synthesis of NWS. . . . .	49		
E. Ion tracks and NWS. . . . .	50		
F. Simulation of radiation effects in NWS. . . . .	50		
VIII. IRRADIATION EFFECTS IN FREESTANDING NANOCCLUSERS. . . . .	51		
A. Sputtering of nanoparticles. . . . .	51		
B. Sputtering of nanoparticles by swift heavy ions. . . . .	52		

## I. INTRODUCTION

Irradiation of solids with energetic particles, such as electrons or ions, normally gives rise to formation of atomic defects in the target and spoils the material properties. Historically, the necessity to understand the irradiation-induced degradation of metal and graphitic components of fission and, later on, fusion reactors was the initial driving force for studying effects of irradiation on solids.<sup>1-3</sup>

However, in spite of the damage, irradiation may overall have a beneficial effect on the target. A good example is the industrially very important ion implantation onto semiconductors.<sup>4</sup> This application motivated further studies of defect production under irradiation because each implanted atom creates many lattice defects in the sample.<sup>5</sup> Another important example of a positive effect of irradiation coming from biophysics is the radiation-assisted treatment of cancer.

It has been demonstrated that irradiation, especially when combined with heat treatment, can also have beneficial effects on nanostructured materials. Experiments carried out for the technologically important carbon nanomaterials, such as nanotubes and graphene, showed that their atomic structure and morphology can be changed in a controllable manner by irradiation.<sup>6-16</sup> Besides, it was demonstrated that nanotubes can be interconnected or merged<sup>9,12,17,18</sup> and that irradiation can give rise to many interesting phenomena, such as extreme pressure inside nanotubes<sup>19</sup> or fullerene-like “onions,”<sup>6,20</sup> so that these systems can be used as nanolaboratories for studying pressure-induced transformations at the nanoscale. Furthermore, recent experiments indicate that ion,<sup>21-38</sup> electron,<sup>6,39-52</sup> and high energy photon<sup>53-56</sup> irradiation can be used to tailor the mechanical,<sup>8,10</sup> electronic,<sup>11,21-23</sup> and even magnetic<sup>57,58</sup> properties of nanostructured carbon materials.

Examples of irradiation-assisted manipulation of noncarbon nanoscale materials are the patterning or ordering of the magnetic properties of ultrathin ferromagnetic films,<sup>59,60</sup> fabrication of nanodots<sup>61</sup> and silicon carbide clusters,<sup>62</sup> the self-organization of ensembles of embedded nanoclusters due to the inverse Ostwald ripening effect,<sup>63</sup> the transformation of spherical nanocolloids into ellipsoids with the aim to build a

photonic crystal,<sup>64</sup> doping of Si nanowires (NWs),<sup>65</sup> or the creation of metallic nanoparticles in dielectric matrices,<sup>64</sup> just to mention a few.

Irradiation of nanostructures may give rise to quite unexpected and even counterintuitive results. For example, ordering of fullerene and carbon nanotube thin films under high energy ion irradiation (200 MeV Au and 60 MeV Ni ions) has been reported,<sup>66</sup> probably due to effects of ion-beam heating and a vanishingly small probability for defect production in a very thin target. Thus, harnessing irradiation as a tool for improving the properties of nanomaterials requires full microscopic understanding of such phenomena as defect production in nanoscale systems under irradiation, damage accumulation and annealing, as well as the knowledge of how the defects affect the material properties. Although various experimental techniques can be used to characterize defects, the vast majority of experiments are carried out *ex situ*. An exception is the transmission electron microscopy (TEM), which makes it possible to not only create defects, but also visualize them *in situ*. However, even TEM cannot give any information on the defect creation process, as it occurs on the picosecond time scale. At the same time, atomistic computer simulations have provided lots of insight into irradiation damage creation in bulk metals and semiconductors, as well as in nanostructures, as such simulations allow one not only to calculate the characteristic of the materials with defects, but also to model the defect production in real time. Recently, substantial progress in understanding the irradiation effects and properties of defects in various nanomaterials was achieved. This was possible in part due to the advent of high-performance computers, which stimulated the development of computational tools for realistic simulations of nanostructured systems.

### A. Scope of the review

In this review, we give a summary of the most recent experimental results on irradiation effects in various zero-dimensional (0D) and one-dimensional (1D) nanoscale systems, such as semiconductor and metal clusters and NWs, nanotubes, and fullerenes. We also consider the two-dimensional (2D) nanosystem graphene due to its similarity with carbon nanotubes. We restrict our consideration to selected papers reporting results of irradiation with ions or electrons and do not review effects of neutron or photon irradiation and also consider irradiation of bulk materials *with* nanoclusters to fall outside the scope of the current review, although this certainly also is a very interesting topic (see, e.g., Refs. 67–71).

Due to the success of atomistic simulations in getting insights into irradiation-induced phenomena in nanomaterials, we also give an overview of recent computational work and the simulation methods used. We discuss at length not only the physics behind irradiation of nanostructures but also the technical applicability of irradiation for nanoengineering of nanosystems. We stress that although several review articles on the subject focused on carbon nanosystems,<sup>72–74</sup> ion implantation onto nanomaterials,<sup>75</sup> atomistic simulations of irradiation effects,<sup>76,77</sup> and focused electron/ion beams<sup>78</sup>

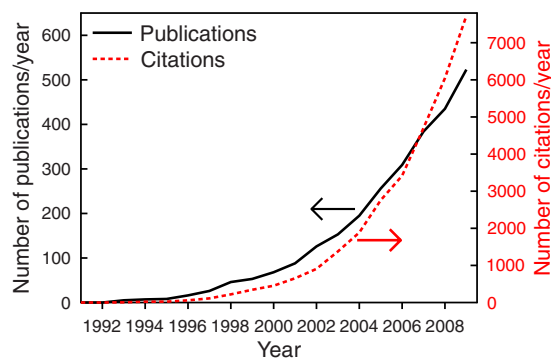


FIG. 1. (Color online) Results of a Web of Science (Ref. 81) search carried out on January 6, 2010, using the advanced search keyword “TS=(irradiation or implantation or collision cascade or radiation effects) AND TS=(nanocluster or NC or nanoparticle or NW or nanotube).” Web of Science covers the titles, keywords, and abstracts of all major refereed publication series in the natural sciences since 1949. The search gave no hits before 1993. The strong and continued growth of the field and its impact (number of citations) is obvious from the graph.

have recently been published, the field has been developing quite fast following the discoveries of new important nanomaterials, such as graphene,<sup>79,80</sup> which motivates reanalyzing and reviewing the literature.

To quantify the growth of the field, we carried out a Web of Science<sup>81</sup> search on irradiation effects and 0D or 1D nanostructures, see Fig. 1. The results show that both the number of publications and their impact, as measured in the number of citations, are in a strong and continued growth.

### B. Organization of the paper

The paper is organized as follows. In Sec. II, we briefly review the well-established basic aspects of interaction of energetic particles—electrons and ions with kinetic energies clearly above thermal ones—with bulk and nanoscale targets. A short overview of the experimental tools, which can be used to detect and characterize native and irradiation-induced defects in nanostructures, is given in Sec. III. Computational techniques used for simulations of defect production in bulk and nanomaterials under irradiation are discussed in Sec. IV. We stress that simulations of irradiation effects in solids require modifications of the conventional molecular dynamics (MD) and electronic structure calculations algorithms, so that we pay particular attention to the technical issues important for modeling electron and ion bombardment. In Sec. V, we dwell on irradiation effects in carbon nanomaterials. We discuss at length production of defects in carbon nanosystems under ion and electron irradiation, analyze the structure and properties of the most prolific irradiation-induced defects, and give an overview of the most interesting examples of engineering the structure and properties of carbon nanomaterials with electron and ion beams. Irradiation effects in BN nanosystems, which are closely related to carbon nanomaterials, are reviewed in Sec. VI. The bombardment of semiconductor and metal NWs with energetic ions and electrons is discussed in Sec. VII, and irradiation effects in free-standing and embedded clusters are discussed in Secs. VIII and IX.

## II. PRODUCTION OF DEFECTS IN SOLIDS UNDER ION AND ELECTRON IRRADIATION

### A. Production of defects in bulk targets

When an energetic particle—ion or electron—penetrates a solid, it collides with the nuclei and the electrons of the target, so that the projectile energy is transferred to the target atoms. Although the low-energy (eV or keV) incoming ions are quickly neutralized by capturing electrons from the target,<sup>82</sup> in what follows, the incoming ion or atom is always referred to as “ion” to differentiate between the projectile and recoil atoms. If the target recoil atom acquires kinetic energy enough to leave its position in the atomic network, various atomic-scale defects may appear in the target. Many of the point defects, e.g., vacancy-interstitial pairs, disappear immediately after the impact (on the picosecond time scale), but some defects may remain in the system or form more complicated defect structures.

The slowing down of an energetic ion moving in a solid target can be separated into two different mechanisms.<sup>83,84</sup> electronic and nuclear stopping. The nuclear stopping originates from ballistic collisions between the ion and the nuclei of atoms in the target, so that the ion kinetic energy is partly transmitted to a target atom as a whole, resulting in its translational motion. The energy loss is determined by screened Coulomb interactions and momentum transfer. A common feature for all ions is that the nuclear stopping is dominant only for relatively slow ( $E_{kin} \lesssim 100$  keV/amu) ions. The nuclear collisions at higher energies usually occur as a sequence of independent binary collisions of atoms, between which the ion moves in an almost straight path, and its energy loss is predominantly by electronic stopping. For the concept of independent collisions to be meaningful, the distances between successive collisions need to be at least about two interatomic spacings, i.e.,  $\geq 5$  Å. In this initial stage of a cascade, the system is not thermodynamic at all since the atomic motion occurs much faster than the thermodynamic relaxation time scale of atoms (which is of the order of 100 fs or more). Once the ion has lost enough energy, or if several recoils happen to occur close to each other, numerous collisions may occur in close vicinity of each other. In this case, the binary collision concept does not work any more, but the cascade becomes a complex many-body phenomenon, which leads to the complete breakup of the lattice. Due to the high kinetic energy of the recoils, the region of overlapping collisions can in some sense be considered to be “hot”<sup>85–88</sup> and is hence called a “heat spike” or “thermal spike.” In bulk materials, this hot region cools down rapidly due to heat conduction to the surrounding lattice. Heat spikes can become important for heavy projectiles in dense materials.

The electronic stopping is governed by inelastic collisions between the moving ion and the electrons in the target, which can be either bound or free. Many different physical processes contribute to the electronic stopping: ionization of the target atoms, excitation of electrons into the conduction band, collective electronic excitations such as plasmons, etc.<sup>89–102</sup>

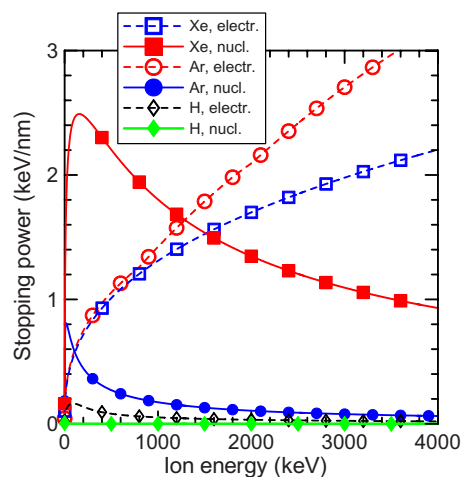


FIG. 2. (Color online) Electronic and nuclear stopping power as a function of ion energy for H, Ar, and Xe ions moving in a C target, as calculated within the Ziegler–Biersack–Littmark (Ref. 83) formalism. At low ion energies, the nuclear stopping prevails, except for very light ions such as H and He.

Electronic stopping dominates at high ion energies (see Fig. 2). The crossover between the nuclear and electron stopping depends on the ion mass (in case of a carbon target 100 keV for Ar ions and 1 MeV for Xe). For hydrogen ions (protons), electronic stopping always dominates.

Due to the different mechanisms of conversion of electronic excitations into heat, the electronic structure of the target strongly affects the outcome of the ion impact. In metals, the electronic excitations are delocalized due to the presence of conduction electrons. This makes the excitations less likely to lead to atom motion, so that radiation damage comes mostly from knock-on atom displacements.

In insulators (e.g., diamond<sup>103</sup> or silica<sup>64</sup>), above a certain electronic energy deposition threshold,<sup>104</sup> excitations may result in a strong heating of the lattice and damage by a cylindrical form of heat spikes.<sup>105</sup> To reach this deposition regime requires high energy (tens of MeV or more) heavy ion irradiation, whence the regime is called “swift heavy ion irradiation.” Swift heavy ions can give rise to so-called “tracks”—amorphous regions that appear along the trajectory of the high energy ion. The same effect has been observed in fullerenes.<sup>106</sup> Normally the tracks are well aligned with respect to the beam directions and themselves can be viewed as nanostructures inside bulk materials. The track cores can be etched away and filled with some other material, which enables production of long straight NWs. The tracks may also have an internal structure, being underdense in the center and overdense in the surroundings, at least in silica.<sup>107</sup>

As for electron irradiation, energetic electrons interact with the nuclei and the electron system in the target.<sup>72</sup> Because of momentum conservation, only a small fraction of the impinging electron energy can be transferred to a nucleus, so that a rather high electron energy (“threshold energy”) is needed to displace an atom. The energy transfer occurs via electron-nucleus scattering. For example, an electron energy of 100 keV is needed to transfer approximately 20 eV to a carbon atom. This is close to the threshold for

displacing the atom from the lattice site in a graphitic structure. Electron-electron scattering, on the other hand, is already possible at low electron energies and may cause ionization or bond breaking. This kind of energy transfer does not normally lead to atom displacements but may damage the target due to beam-stimulated local chemical reactions.<sup>108–111</sup> The cross sections of both nuclear and electron scattering decreases with increasing electron energy.

Both electron and ion beams can be focused onto an area of several nanometers (and even down to 0.6 Å in some TEMs), which makes it possible to create defects in predetermined areas of the sample. We stress that even at the maximum currents available (for highly focused electron beams, currents in a TEM can be about  $10^5$  A cm<sup>-2</sup> so that 100 displacement per carbon atom can be achieved), the typical time between the impacts of the particles onto the same area is normally much longer than the typical time during which the extra energy is dissipated into the environment, so that one can neglect temporal correlations between collision cascades, and consider the initial damage from impacts of energetic particles “one by one.”

The effects of an ion or electron impact on a material may extend beyond the region of initial collisions due to several physical effects. The defects (both point and extended ones) produced during the irradiation can, unless they recombine during the cascade development with each other, migrate in principle arbitrarily far in the sample. A cascade may also “raise” impurities from essentially immobile positions into mobile ones.

The electronic stopping power can excite electrons to relatively high (keV) energies,<sup>112</sup> and such electrons (known often as  $\delta$  electrons) can travel far in the lattice. This can at least in principle produce damage far from the nuclear collision region and is certainly a significant factor behind transporting electron excitation energy away from the central region of a swift heavy ion track.<sup>113,114</sup> It is also well known that nuclear collision cascades, especially in the heat spike regime, also induce a sound/shock wave in the materials.<sup>115,116</sup> Such a shock wave can in principle cause emission of material far away from the impact site, although in practice this is likely to occur if the material is in an unstable state to begin with.<sup>115</sup> More likely is the situation of the pressure wave or long-term stress relaxation causing plastic deformation of the material outside, also far from the region of atomic collisions.<sup>117</sup>

Any kind of irradiation can also generate phonons. These have relatively low energies and are thus unlikely to cause any materials modification. However, it has been proposed that anharmonic longitudinal vibrations, so called “discrete breathers,” can dramatically enhance N atom migration in steels.<sup>118</sup>

Electronic excitations associated with irradiation can naturally also cause photon emission when the electrons decay to lower-energy states. In materials with a band gap, the photons can travel far from the impact site. It is very unlikely that such photons could cause significant damage to the material as they are emitted in random directions and the radiation intensity decays rapidly with distance. However, the

light emission, known as ionoluminescence, may be useful as a source of information during ion beam analysis of materials.<sup>119</sup>

Near surfaces, all of the processes described in this section can lead to sputtering. Linear cascades produce sputtering if a recoil is backscattered through the surface. Heat spikes can lead to massive sputtering yields by a combination of evaporation and flow of liquid material from the heat spike.<sup>68,120</sup> Low-energy can also sputter material at energies below the physical sputtering threshold via bond-weakening and breaking mechanisms.<sup>121</sup> Well-described examples of this are the so called Küppers cycle, in which ion bombardment weakens chemical bonds so that molecules can then desorb thermally<sup>122</sup> and swift chemical sputtering, in which hydrogen isotopes with energies of the order of 10 eV can break bonds athermally by entering between two atoms.<sup>123–125</sup> Swift heavy ions can also cause massive sputtering via the heat spikes induced in them.<sup>126</sup> Electron irradiation can naturally lead to sputtering if the kinetic energy transfer from the electron to sample atoms is above the threshold energy for sputtering. Also much lower energy electrons can lead to sputtering of insulators via promotion of electrons in chemical bonds to antibonding states.<sup>127</sup>

The typical time scale for defect production and sputtering is as follows. An energetic electron transfers energy to a nucleus essentially instantly (for  $10^{-21}$  s, Ref. 72), and similarly most of the transfer of electronic energy from swift heavy ions to sample atoms via electron-phonon coupling (EPC) occurs on time scales less than 10 fs.<sup>128</sup> The ballistic phase of a collision cascade after an impact of an electron or ion takes of the order of 100 fs, after which a heat spike may form in dense materials. The “extra” energy brought in by the energetic particle is, for all kinds of irradiations, dissipated to the surroundings (either by heat conduction or near surfaces also by sputtering) on nanosecond time scales, after which defects are formed. These defects would be fully stable at 0 K, but may, at finite temperatures, start migrating and thus recombining or forming larger defect complexes or adatoms on surfaces.<sup>129</sup>

The relatively short time scale of defect creation makes dynamic atomistic simulation of defect production feasible. The thermal annealing of defects occurs on a macroscopic time scale, so that special techniques such as accelerated<sup>130</sup> and parallel replica<sup>131</sup> MD or kinetic Monte Carlo (KMC) approaches<sup>132</sup> should be used.

## B. Creation of defects in nanoscale materials under irradiation

Production of defects in irradiated nanosystems is different from that in bulk materials. This is due to a small system size in one or more dimensions, which affects the dissipation of energy brought in by the energetic particle. An illustration of the difference in energy distribution between a three-dimensional (3D) and 1D system is presented in Fig. 3 by snapshots of atom kinetic energy profiles (“temperature”<sup>134</sup>) taken several femtoseconds after the ion impacts. The reduced dimensionality may give rise to a higher local kinetic energy after the impact so that the local temperature may exceed the melting temperature of the material. This is par-

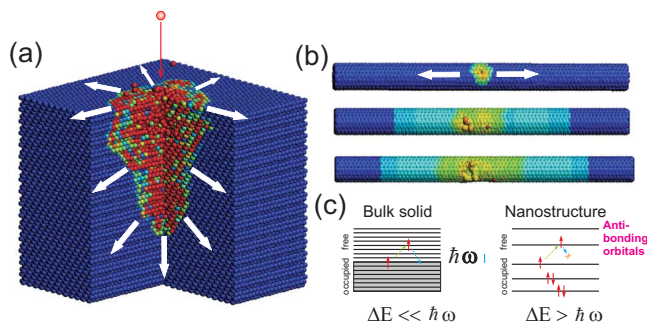


FIG. 3. (Color online) Conversion of the projectile initial kinetic energy into thermal energy in bulk and nanosystems. (a) Impact of an energetic ion onto a bulk metal target. The ion kinetic energy is transferred ballistically to the target atom, which results in temperature raise. The excess energy is dissipated in essentially a 3D system. The atoms are colored according to their kinetic energy from blue (zero energy) to high (red) energies. A quarter of the target was cut out for a better visualization. (b) Impact of an ion onto a carbon nanotube, a quasi-1D system. The excess energy is dissipated in only two directions, which may affect the temperature profile and give rise to additional defects. (c) The sketch of the electronic structure of bulk and nanoscale objects, illustrating the so-called “phonon bottleneck” problem (Ref. 133). The excitation relaxation time is enhanced when the spacing between the size-quantized energy levels  $\Delta E$  is larger than the vibrational energy  $\hbar\omega$ . This mechanism is discussed for illustration purposes only. There are many other nonradiative relaxation channels in nanosystems which affect the excitation lifetimes.

ticularly important for zero-dimensional objects. For example, only  $E_i=30$  eV transferred to an atom in an isolated fullerene  $C_{60}$  will raise temperature to  $T^* \sim 1/3E_i/k_B/60 \sim 2000$  K, where  $k_B$  is the Boltzmann constant, and an additional factor of 0.5 was introduced due to the equipartition theorem.

Three other important points should be taken into account, which are as follows: (1) a big surface area of nanosystems results in a high sputtering yield, including sideward and forward sputtering;<sup>135</sup> (2) high surface-to-volume ratio may also give rise to enhanced annealing; and (3) at high energies of impinging particles normally only a small part of the projectile energy is deposited onto the nanosystem, contrary to the case of irradiation of bulk systems when all the energy is eventually dispersed in the sample. This is related to a drop in the cross section for defect production at high energies of the particle.<sup>74</sup> Correspondingly, the total amount of damage to a nanoscale object decreases with the particle energy, contrary to the situation in bulk solids.

For ion irradiation, the application of the conventional theory of ion stopping to nanosystems is somewhat questionable, as the theory is based on averaging over many collisions of the projectile with the target atoms, which is obviously incorrect for nano-objects. Besides this, the conventional separation of the ion energy loss into two components ignores the possible correlation between hard nuclear collisions and inelastic losses due to electronic excitations, which may be particularly important for nano-objects. The conventional approach to ion-nanosystem interactions has been demonstrated to be inadequate in certain cases for fullerenes<sup>136</sup> and very thin targets,<sup>83</sup> or at least it should be used cautiously, e.g., for LiF clusters<sup>137</sup> or graphene.<sup>138</sup>

The finite size of the system also affects the electronic structure and thus the mechanisms of conversion of electronic excitations to atom kinetic energy.<sup>136</sup> As the electronic spectrum of the system may be discrete with a separation between the levels exceeding the typical phonon energies (the so-called “phonon bottleneck” problem,<sup>133</sup>) the lifetime of excitations may be longer than in bulk solids, and when the excitations are localized and antibonding orbitals are populated, this can result in the appearance of defects. We stress, however, that there are other channels (electron-electron interactions affected by the reduction of dynamic screening, Auger recombination, etc.) of nonradiative electron relaxation in nanoscale objects, which may, on the contrary, decrease the excitation decay time.<sup>139</sup> The detailed discussion of these channels is beyond the scope of this review.

### III. EXPERIMENTAL TECHNIQUES USED TO IDENTIFY DEFECTS IN NANOSTRUCTURED MATERIALS

In this section, we briefly outline the experimental techniques used to analyze irradiation-induced and native defects in nanostructures. The defects in nanomaterials can be detected by various experimental techniques. Although most materials analysis techniques have been developed originally for studying bulk materials or micrometer-thin films, we discuss here the methods that are also well suited for nanostructures.

Defects can be directly observed by scanning tunneling microscopy (STM)<sup>32,140,141</sup> and TEM.<sup>7,39,72</sup> Even individual point defects can be imaged with the both methods, for examples see Sec. V B. Atomic force microscopy (AFM) does not normally allow one to see point defects in carbon materials, but may provide useful information on the amount of disorder.<sup>142</sup>

In STM and other scanning probe microscopy methods, a thin needle is moved above the sample with subangstrom lateral resolution via the use of piezoelectric crystals. For STM in particular, the shape of the surfaces is measured from the electron tunneling current. The interpretation of STM images, however, is not straightforward, as it does not measure the atomic positions directly, but the source of the current comes from the outermost occupied electronic levels. Thus the local electronic structure should be taken into account in the analysis.<sup>143</sup>

In TEM, a high energy electron beam is passed through the sample to be imaged, and an image can be formed as in a conventional light microscope thanks to the use of the quantum mechanical wave nature of electrons.<sup>144</sup> Traditional TEMs could already image extended defects such as dislocations in nanosystems consisting of heavy elements.<sup>145</sup> Now the new generation of aberration-corrected field emission TEM (which can also work in the scanning mode) with spatial resolution better than 1 Å (Ref. 146) have made it possible to get images of not only individual point defects in light elements such as carbon, but also to study defect evolution in real time. The limiting factor here is the mechanical stability (drift) of the sample and time resolution limited by the noise-to-useful signal ratio, which in practice does not allow us to record more than about 40 frames/s. Scanning electron microscopy (SEM) makes it possible to detect

irradiation-induced changes in the morphology of nanotubes (e.g., welding due to irradiation<sup>23</sup>), but this technique does not provide enough resolution to detect point defects.

Elemental composition and nanosize precipitates in metals and some compounds can be examined using field ion microscopy and its more modern variants known as the 3D atom probe or tomographic atom probe.<sup>147–149</sup> In this method, a sharp needle is fabricated out of the material to be studied, and it is placed under a high electric field in ultra-high vacuum. The field gradient at the needle tip is high enough (of the order of 10 GV/m) to lead to field evaporation of ions from the sample. These are accelerated over the electric field and detected at a position-sensitive detector with single-atom sensitivity. Time-of-flight (TOF) data are collected for each ion. The position at the detector can be used to calculate backward the atom position inside the sample, and the TOF data gives the atom type.

One of most widely used techniques for defect identification in covalently bonded carbon,<sup>24,27–29,150,151</sup> BN,<sup>152</sup> or Si (Refs. 65, 153, and 154) nanostructures is Raman scattering. This is a noncontact and nondestructive tool. In sp<sup>2</sup>-bonded carbon, the ratio of the intensity of the so-called “D-band” at around 1300 cm<sup>-1</sup> to the intensity of the “G-band” at 1590 cm<sup>-1</sup> can be used as a parameter for estimating the amount of disorder.<sup>155</sup> The ratio increases (as compared to the pristine sample) when defects are present and satellite structures appear.<sup>27</sup> The dependence of the ratio on the irradiation dose is, however, nonmonotonic and the first increase of the ratio at small irradiation doses can be followed by a saturation<sup>156,157</sup> or even a drop<sup>158</sup> at high doses when the structure becomes completely amorphous. The positions of the peaks (Raman shift) can also change with the irradiation dose.<sup>151,157</sup> As the pristine materials may have native defects (for example, the D/G ratio is normally quite big in nonirradiated MWNTs<sup>156,157</sup>) getting quantitative information on defect concentration from Raman spectra is a challenging task. Moreover, if one wants to compare irradiation-induced damage in the samples irradiated with ions having different energies, a nonuniform distribution of the damage and the thickness of the skin layer probed by the Raman technique must be taken into account.

The signatures of defects in carbon nanomaterials can be detected with x-ray photoelectron spectroscopy (XPS)<sup>29–31,159,160</sup> by monitoring changes in the C 1s peak shape, which is very sensitive to the type of carbon bonding, and with the electron spin resonance (ESR) method.<sup>161,162</sup> The polarization dependence (linear dichroism) of the C 1s x-ray absorption spectrum of individual carbon nanotubes measured using scanning transmission x-ray microscopy<sup>163</sup> can be used to assess the anisotropy of the atomic network of the system and thus the concentration of defects.

Synchrotron radiation x-ray methods, such as extended x-ray absorption fine structure (EXAFS) and x-ray absorption near edge structure (XANES), can be used to characterize the bond lengths, local atomic neighborhood, and densities in nanoclusters and tracks.<sup>107,164–166</sup> In these approaches, the x-ray absorption in a sample is measured near an absorption edge. For an isolated atom in a gas, the absorption intensity distribution would have a relatively simple shape, but

inside a condensed material, the scattered electron wave interacts with the atoms near the absorbing atom. This results in a fine structure of the absorption spectrum, which depends on the local atomic neighborhood. Analysis of the fine structure can be used to extract information on, e.g., the bond lengths, pair correlation function, and coordination numbers of atoms. Moreover, since the absorption edges are specific to the element, the analysis can be carried out separately for different elements, a feature which is very useful in compounds. The main drawback of these methods is that they can be practically carried out only at synchrotrons and requires elements heavy enough to have energy levels suitable for x-ray analysis.

Electronic transport measurements for individual nanostructures, and first of all, carbon nanotubes<sup>11,26</sup> and macroscopic nanotube samples<sup>48,167</sup> can provide useful, although indirect, information on irradiation-induced defects. A special technique based on selective electrochemical deposition and on probing the local electronic resistance of nanotubes was recently developed for identifying defects in carbon nanotubes.<sup>168</sup>

At the same time, some of the standard techniques used for identification of defects in semiconductors<sup>169</sup> cannot be applied to nanostructures because of their nanometer scale and unusual structure. For example, positron annihilation can hardly be used for defect identification in carbon nanotubes due to the abundance of open space in these materials, so that positron-electron annihilation will more likely occur there rather than at irradiation-induced vacancies. Similarly, Rutherford backscattering/channeling is normally not sensitive enough to detect defects in quantum dots on surfaces.<sup>170</sup> On the other hand, both methods could be suitable for analysis of large concentrations of nanoclusters embedded in the bulk.

#### IV. COMPUTATIONAL ATOMISTIC METHODS USED FOR MODELING IRRADIATION EFFECTS IN SOLIDS

In this section, we overview the methods that are widely used to simulate irradiation effects in nanostructured and bulk solids. We focus on atomistic models. The target is considered as an agglomerate of atoms that interact with each other [except for the binary collision approximation (BCA)] and the projectile. Most of the methods can also be applied to simulations of the behavior of irradiation-induced and native defects. At the same time, many simulation models widely used for studying dynamical processes in solids (e.g., diffusion) cannot be directly applied to irradiation simulations, and require modifications. For example, most empirical potentials (EPs) used in MD are inappropriate at the small interatomic separations, which can be reached in energetic atomic collisions. Potentials with an exponential term in the repulsive part, such as the Morse and Tersoff-like potentials<sup>171,172</sup> are too soft as they do not have the Coulombic  $1/r$  term to describe internuclear repulsion. On the other hand, Lennard-Jones-type potentials<sup>173</sup> are too hard, as they have a  $1/r^{12}$  repulsion. The reason for these shortcomings is that in normal thermodynamic systems the atoms never come very close to each other, so that most potential developers

did not fit parameters to reproduce repulsive interaction of close atoms. To circumvent this problem, the potentials are normally augmented<sup>174–176</sup> with a pair potential, which describes interaction of atoms at small separations reasonably.

### A. Binary collision approximation-based methods

The standard program to evaluate the amount of damage produced by irradiation in a solid target is TRIM/SRIM.<sup>177</sup> The code is based on the BCA approach and uses statistical algorithms to calculate how the moving ion loses its energy in the target. It is not able to distinguish when a cascade goes over from the linear cascade to the heat spike regime, but keeps treating the collisions as independent binary collisions regardless of the collision density. Nevertheless, the code often gives reasonable deposited energy and range distributions for various materials, including nanotubes and nanoclusters.<sup>178,179</sup> However, TRIM can hardly be used for quantitative estimates of the radiation damage and defect distribution in strongly anisotropic nanosystems, as it treats the irradiated sample as an amorphous structure with a homogeneous mass density, which is obviously not relevant to highly anisotropic covalent systems such as, e.g., nanotubes. Besides this, only binary collisions between the ion and the sample atoms are taken into consideration, while many-atom effects are important, especially in the heat spike regime.

### B. Molecular dynamics with empirical potentials

MD simulations involve numerical solution of the Newton equations of motion to determine the time evolution of a system of interacting particles.<sup>180,181</sup> These methods have provided a lot of insight into the damage production in nanostructures under impacts of energetic ions and electrons and facilitated the interpretation of the experimental results. The interaction between the target atoms and the ion can be described at different levels of theory (within the framework of different force models): EP, tight-binding (TB), and density functional theory (DFT) force models are normally used.

MD simulations of radiation effects are usually most valuable in providing insights into qualitative mechanisms, which cannot be studied directly by experiments. The simplest variety of MD, direct solution of the equations of motion, is ideally suited to study ion-induced radiation effects since this scheme correctly accounts for the nonequilibrium ballistic motion of high energy ions as well as the subsequent thermalization of the ion.<sup>182</sup> Efficient and realistic simulation of radiation effects often requires the basic MD methods<sup>181</sup> to be amended with a few solutions specific to radiation effects. These may account for electronic stopping as a frictional force,<sup>183</sup> realistic high energy repulsive interactions<sup>83</sup> (see above) and making the time step adaptive to the maximum kinetic energy and force in the system in the ballistic phase of the cascade,<sup>183</sup> while reducing it to a normal constant equilibrium time step after the cascade.

To dissipate the heat emanating from the cascade away from the simulation cell, temperature scaling (velocity damping) at the boundaries is often carried out, Fig. 4, although sometimes this step is left out and the temperature is simply allowed to spread out in the simulation cell. If the cell is

large enough that the associated temperature rise is not significant, this can be considered acceptable. Multiple time step schemes<sup>187</sup> may be useful for speeding up the initial stages of the simulation when atoms have highly disparate velocities.

The empirical (or analytical) potentials involve a set of analytical equations with the parameter fitted to empirical and/or DFT data. Many EPs have been developed for carbon systems, the most popular being the Brenner potential<sup>188</sup> and its extensions.<sup>189,190</sup> For metals, the Finnis–Sinclair and embedded-atom method potentials and their functional equivalents are widely used,<sup>191–194</sup> while for covalently bonded materials Tersoff-like bond order potentials<sup>172,188,195</sup> have proven to be quite successful. For compounds of different types of materials, far fewer potentials are available, but since the Tersoff and Finnis–Sinclair-like potentials are fundamentally similar,<sup>188,196</sup> a Tersoff-like formalism has proven to be useful in development of potentials for carbides, oxides, and nitrides.<sup>196–200</sup>

Although these potentials have been fitted to reproduce a large number of reference systems, the drawback of the empirical approach is its low transferability (the ability to describe systems different from those used for fitting the parameters, for example, correctly describe defect behavior). Nevertheless, the methods have been demonstrated to give valuable results. In the following discussion, many examples of applications of the above methods to simulations of irradiation effects in nanostructures will be given.

### C. Simulation setup

The typical simulation setups used in atomistic modeling of irradiation effects in solids are sketched in Fig. 4. These setups is common for MD simulations with both classical and quantum mechanical force models. The simulation cell is normally chosen to be as big as possible (unless a nanoparticle, e.g., fullerene C<sub>60</sub> or metal nanocluster, is simulated). The atomic structure is fully optimized (if the simulation temperature is zero) or atom velocities are scaled accordingly by using special techniques (e.g., Nose–Hoover<sup>201</sup> or Berendsen<sup>202</sup> temperature control) to correspond to a certain temperature.

In ion impact simulations, the ion is placed beyond the interaction range and then it is directed toward the surface or nanosystem with the velocity corresponding to its initial energy, Figs. 4(a), 4(e), and 4(f). During the development of the collisional cascade after the ion impact, the atoms in the middle of the cell are allowed to move without any constraints, while the velocities of atoms at the borders of the cell are scaled to allow for energy dissipation and thus eliminate spurious pressure waves reflected from the border cells. To avoid displacement of the cell as a whole due to momentum transfer, the total momentum of a bulk simulation cell may be scaled to zero, or some atoms may be kept fixed. After the collision cascade and heat spikes have cooled down, so that the formation of additional defects is unlikely, the velocities of all the atoms are scaled toward the initial

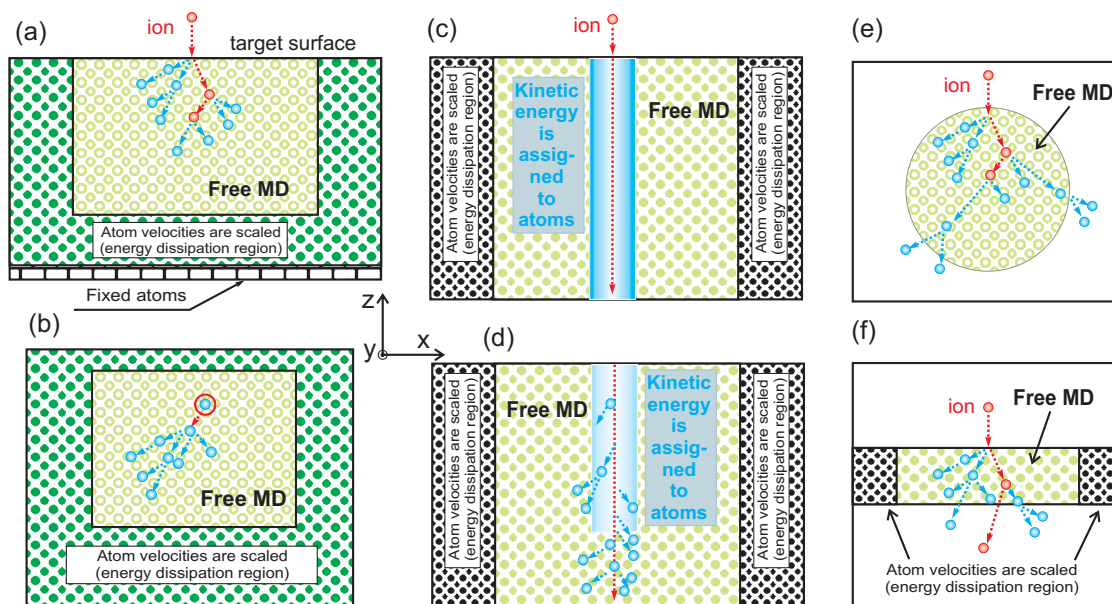


FIG. 4. (Color online) Typical simulation setups used in atomistic simulations of irradiation effects in solids and nanosystems. The areas are hatched differently depending on how the velocities of atoms in the areas are treated. (a) Ion implantation simulations, (b) Electron, neutron, or high energy ion irradiation simulations. Since  $\geq 100$  keV electrons, neutrons, and MeV ions penetrate deep into solids, it is usually most appropriate to only simulate the recoils they produce. The recoil energies can for electrons be obtained from the McKinley–Feshbach model (Ref. 184), for neutrons from empirical tabulations (Ref. 185), and for ions from BCA codes such as SRIM (Refs. 83 and 186) or MD range (Ref. 183) calculations. (c) Swift heavy ion, when electronic stopping prevails. The conversion of the deposited energy from electronic into atomic degrees of freedom resulting into local melting of the target is modeled by assigning kinetic energy to atoms in the track area, and the ion is slowed down by the same amount of energy. The ion moves essentially in a straight path, and hence it is natural to simulate a segment of its movement employing periodic boundaries in the  $z$  direction. The swift heavy ion itself is not part of the simulation, only the heating it causes. (d) The same as in (c), but in addition to electronic stopping, ballistic collisions of the ion with the target atoms are taken into account. The swift heavy ion can either be simulated explicitly and removed from the system after it passes the bottom periodic boundary, or the recoil energies are obtained from recoil spectra. (e) Simulation of an isolated nanoparticle in gas phase or only weakly bound to a substrate. (f) Simulation of a nanotube or NW. The  $y$  direction (out of the paper) is in all cases except (f) treated the same as the  $x$  (horizontal) direction. In case (f), velocity scaling is used only in the  $x$  direction. A nanoparticle strongly bound to a substrate can be simulated with setup (a) placing the particle in the middle of the surface. In many cases, the layer of fixed atoms is not needed, but it is sufficient to have an energy dissipation region.

temperature. This is done as slowly as possible to take into account annihilation of defects, normally close vacancy-interstitial pairs.

As for simulations of electron or neutron irradiation in carbon systems, some energy (due to impact of an energetic electron or neutron) is instantaneously assigned to an atom, Fig. 4(b), then the procedure is essentially the same as for ion irradiation simulations. For swift heavy ions, the electronic energy loss is translated into heating of the atoms around the track core,<sup>107,203,204</sup> Figs. 4(c) and 4(d). However, the details of how and at what rate the atoms should be heated are still unclear. We would also like to note that in covalently bonded materials, the bond breaking induced by the electron beam can also be included into simulations.<sup>111</sup>

#### D. Density functional theory-based methods

The DFT approach (for a detailed overview of the formalism and its computational realization, see Ref. 205) is based on two theorems by Hohenberg, Kohn, and Sham, which state that (i) the ground state energy of a nondegenerate electronic state is a unique functional (density functional) of its density and (ii) the energy can be obtained by variation of the universal density functional with respect to the charge density. This implies that calculation of the wave function of the many-electron system is not required in order to find the

total energy, we must know only the charge density. However, the exact density functional is not known and some approximate functionals are used instead.

DFT-based and other quantum mechanical methods (e.g., Hartree–Fock methods) have a high accuracy but are computationally very expensive (simulations are normally limited to systems composed of a few hundred atoms and picosecond time scales), which makes the use of such methods in practice impossible for tackling most of irradiation-related problems, e.g., formation of defects under irradiation or direct dynamical simulations of defect diffusion. However, such simulations should be feasible in the near future due to more and more powerful computers, as recent works<sup>206,207</sup> indicate. As DFT methods describe well the atomic structure of defects, the methods have successfully been used for simulations of the behavior of various defected systems.

#### E. Tight-binding methods

As all *ab initio* methods are computationally very demanding, a number of computationally cheaper methods have been developed, such as TB techniques. In the TB method, the energy is calculated by solving the Schrödinger equation for electrons in the field of atom cores, although the exact many-body Hamiltonian operator is replaced with a parametrized Hamiltonian matrix. The basis set usually is

atomiclike so that it has the same symmetry properties as the atomic orbitals.

The TB methodology has been successfully applied to simulations of irradiation effects in covalently bonded systems such as silicon, graphite, or hexagonal boron-nitride. A nonorthogonal self-consistent charge TB method<sup>208,209</sup> in which the parameters of the Hamiltonian were derived from DFT calculations (a second-order expansion of the Kohn–Sham total energy in DFT with respect to charge density fluctuations) has been widely used for simulations of impacts of energetic electrons onto C,<sup>46,210,211</sup> BN,<sup>212</sup> and SiC (Ref. 213) nanosystems.

Thus, no empirical parameter is present in the method and despite the approximations made, this method retains the quantum-mechanical nature of bonding in materials, ensuring that the angular nature of the bonding is correctly described in far-from-equilibrium structures. Due to parameter fitting to the density functional results, this method, unlike other TB schemes (where the parameters are chosen to describe equilibrium structures) describes the interaction of atoms even at relatively small interatomic separations, i.e., upon energetic collisions. This approach has been found to work well in modeling various systems<sup>214</sup> and the results are in agreement with those obtained by the first-principles methods.<sup>215,216</sup> Another widely used parametrization for carbon by Xu *et al.*<sup>217</sup> has been successfully applied to simulations of irradiation effects in carbon nanomaterials.<sup>12,18,218</sup>

## F. Time-dependent DFT simulations

The conventional MD simulations (even based on DFT) are carried out within the Born–Oppenheimer approximation. It is assumed that the electronic structure is always in the ground state (the situation is somewhat different in the Car–Parrinello approach, but a detailed discussion of this is beyond the scope of this review).

Obviously, this is not true when the ion velocity is much higher than the Fermi velocity  $v_F$  in the target material, and/or the original charge state of the ion is high, which may give rise to a Coulomb explosion in the system.<sup>219</sup> In graphitic structures,  $v_F = 8 \times 10^5$  m/s, which, assuming hydrogen as a projectile, corresponds to ion energy of around 3 keV. Although the role of nonadiabaticity is, to some extent, smeared out due to good conducting properties of nanotubes, several attempts have been made to assess the role of electronic excitations in ion collisions with carbon nanostructures.<sup>136,138,220</sup> Some other nanosystems have been studied as well.<sup>137</sup>

In particular, a combination of time dependent DFT and classical MD for ions,<sup>221</sup> can be used to obtain an unbiased microscopic insight into the interaction of energetic particles with target atoms, since time-dependent (TD) DFT-MD treats electron and ion dynamics on the same footing in real time. The advantage of the approach is that it explicitly takes into account the electronic structure of the target and thus discriminates among different carbon allotropes, including diamond and graphite. In addition to irradiation simulations,

the method has proven useful to describe photo-chemical processes<sup>222</sup> and understand the damping mechanism of electronic excitations<sup>223</sup> in carbon nanotubes.

## G. Phenomenological descriptions of electronic excitation

As mentioned in Sec. IV B, electronic stopping can be handled by adding it as a frictional force slowing down the motion of atoms. The magnitude of the force can be obtained from analytical or empirically tabulated electronic stopping powers.<sup>83,92,180,224</sup> Numerous comparisons of experimental depth distributions of implanted ions with BCA and MD range calculations have shown that this approach is sufficient to describe at least the penetration depths of energetic ions.<sup>225–229</sup>

Implementing electronic effects as a purely frictional force does not, however, in any way account for the possibility that electrons transfer heat back to the ionic system. There are several important physical processes where such a transfer happens. Laser and light irradiation of solids first heats up the electronic system,<sup>230,231</sup> as does swift heavy ion irradiation.<sup>104,114</sup> Also slow highly charged ions<sup>82,219</sup> lead to a strong local electronic excitation of a material near the surface.

In ion-induced collision cascades in metals, the energy that is first transferred to atoms in nuclear collisions will transfer partly to electrons, resulting in faster cooling of the cascade since electronic processes dominate the heat conductivity. This effect is known as EPC.

In principle, all such effects could be handled by TDDFT-MD approaches, but these remain too slow for practical use in most effects related to ion irradiation, which typically involve thousands or millions of atoms. Hence it is natural that several phenomenological models have been developed to enable practical treatment of electronic excitations in BCA and MD simulations.

Nonequilibrium irradiation by any particle, with any of the processes mentioned above, can lead to excitations of electrons. These electrons can gain fairly high energies (approximately keV) and travel far in the lattice, being then called “secondary electrons” or “delta electrons.”<sup>112</sup> In insulators and semiconductors, valence band electrons can be promoted to the conduction band, and in metals free electrons can also be simply promoted to higher-lying states in the conduction band.

The initial kinetic energy distribution of the excited electrons need not be a thermal (Maxwell–Boltzmann) distribution. However, it is a fair assumption that the electrons are rapidly (femtosecond time scales) thermalized, and after this their behavior can be described as a diffusion (heat conduction) process of hot electrons. The thermalized hot electronic subsystem (with a temperature  $T_e(\vec{r})$ ) is coupled to the ionic subsystem [with a temperature  $T_i(\vec{r})$ ] with some EPC mechanism.

Several models based on this general physical picture have been developed to treat the electronic excitations. To describe swift heavy ion energy deposition, Toulemonde and co-workers<sup>114,128,232</sup> have developed the “two-temperature”

model, which solves the heat conduction equation for the coupled system of electrons and ions, with an EPC constant  $g$  related to the electron mean-free path  $\lambda$ . With some reasonable assumptions of what ionic temperature is related to damage production, this approach has been quite successful in predicting track radii in insulators.<sup>114,128</sup> On the other hand, Coulomb explosion models have also been used to describe the track formation, but most recent studies indicate that the two models are at least partly consistent with each other.<sup>105,233</sup>

For MD simulations of track formation, the simplest approach is to use an instantaneous heating of the atoms in the beginning of the simulation.<sup>107,234–236</sup> This simple approach can be motivated by the observation from the two-temperature models that most of the transfer of energy from electrons occurs on femtosecond time scales, i.e., much slower than the time needed for significant ionic displacements. In spite of its simplicity, the approach has given good agreement on track radii in comparisons with experiments.<sup>107</sup> Recently models have also been developed where the solution of the electronic heat conduction is embedded into the MD simulations.<sup>204,237</sup> This allows for a much more realistic description of how the electronic subsystem transfers energy to the ionic one since the solution of the heat conduction equation gives both the spatial and temporal distribution of energy. On the other hand, the uncertainty of how the coupling of the electronic and ionic subsystems should exactly be handled remains. Two-temperature models have also been implemented into MD simulations of laser ablation<sup>231,238</sup> as well as shock simulations.<sup>239</sup>

In BCA or MD simulations of EPC in collision cascades, the EPC can be described as a frictional force or Langevin term affecting the atom motion.<sup>240–243</sup> Recently also two-temperature models have been implemented to examine EPC in cascades.<sup>244</sup> However, the problem is not symmetric with laser ablation and swift heavy ions since in cascades the ionic system is heated first and the electronic one later. Moreover, the ionic system is already distorted by nuclear collisions when it starts transferring energy to electrons, and hence EPC models derived for perfect lattices may not be appropriate. Very recently, the first TDDFT simulations of low-energy cascades have been performed,<sup>245</sup> and these may give crucial insight into how EPC and low-energy electronic stopping should be implemented in cascades.

The two-temperature approach for cascades has been extended by Duvenbeck *et al.*<sup>246</sup> to also include explicit description of collisional excitation and transport of hot electrons. This approach has been applied to examine the role of electronic excitations on surface cascades, and in particular the energy distribution of hot electrons.<sup>247</sup>

## H. Kinetic Monte Carlo approach

Juxtaposition of MD data with experiments is often complicated by the limited time scale (typically of the order of nanoseconds) of MD simulations. Hence most diffusion processes and long-term relaxation of molecular structures are not included in the MD, which may completely hinder comparison of MD results with experiments. KMC methods can

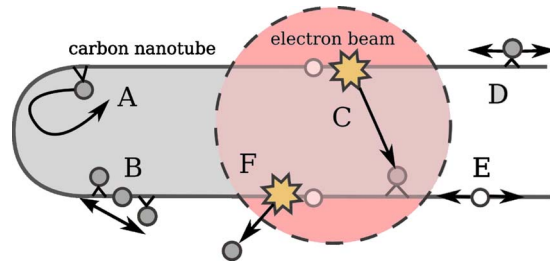


FIG. 5. (Color online) Schematic representation on the most important processes included in a KMC model (Ref. 132) developed for simulations of the response of carbon nanotubes to electron irradiation. The model includes the following “elementary” events. (a) A diffusing endohedral adatom is reflected back from a cap. (b) Endohedral-exohedral transformation of an adatom through the exchange mechanism. (c) Electron impact creating a defect pair (white sphere—a vacancy, gray sphere—an adatom) by displacing a carbon atom. [(d) and (e)] Adatom and vacancy migration, respectively. (f) Creation of a vacancy by sputtering the displaced atom.

sometimes solve this problem.<sup>132,248–250</sup> The method takes as input the rates of relevant processes in a system, which typically are the defect migration rates and incoming ion flux, and simulates the time evolution of the objects. The algorithm selects the processes proportionally to their rate, so no effort is wasted in time steps with no events occurring. In atomic KMC (AKMC) simulations, all atom coordinates are included but only one or a few defects (typically vacancies) at a time are moving.<sup>251</sup> In other modifications of the method, only the mobile defects are followed, and the lattice atoms are not explicitly described at all (such methods are known as object, reaction, event,<sup>252</sup> or first-passage<sup>253</sup> KMC). Since only the objects of interest are simulated, this allows for simulation of macroscopic time (up to several hours) and length scales.

An AKMC approach that is used for simulations of the response of a nanosystem to ion or electron bombardment should allow for sputtering and other irradiation-induced effects. Such a method was developed in Ref. 132. It enabled one to simulate the behavior of irradiated nanotubes on macroscopic time scales, Fig. 5. Within the model, the paths and energy barriers for the diffusion of irradiation-induced defects are obtained from DFT-based calculations.<sup>215,216</sup>

## I. Summary of simulation methods and their limitations

The range of applicability (both space and time wise) of the different simulation methods can be summarized as follows. The binary collision approaches, when they involve also primary and secondary recoil atoms, are well suited for obtaining the spatial extent of the ballistic collisions, but cannot tell anything about the thermodynamic aspects of a cascade or detailed nature of defects. MD simulations can, in addition to the ballistic phase of the cascade, describe the formation of heat spikes, their thermalization, formation of a sound/shock wave, and how it spreads beyond the region of ballistic collisions. MD simulations can also predict the nature of defects produced. However, there are major uncertainties in how reliable classical potentials are with respect to defect types and properties. Quantum mechanical methods (DFT and TB) can provide a much more reliable picture of

defect properties, but are quite limited in the number of atoms and time scale they can handle. There is an additional complication related to small atom-atom separations during the development of a cascade. If pseudopotential or similar methods such as the projected augmented wave<sup>254</sup> technique are used, the separation between the atoms can be smaller than the core radii, which limits the maximum energy of the impinging ion. Different KMC approaches are well suited to describe atom migration on both space and time scales exceeding those in MD by orders of magnitude, but great effort is often needed to parametrize the KMC reliably.

Electronic and optical excitations can in principle be fully described by TDDFT, but this approach is extremely time consuming, and treatment of all possible excitations, transport, and recombination processes in the collisional phase of a cascade in a dense material will remain beyond reach far into the future. Phenomenological models can be used to treat electronic and possibly also optical excitations on a case-by-case basis.

## V. IRRADIATION EFFECTS IN CARBON NANOSYSTEMS

The big interest in irradiation effects in carbon nanomaterials, such as fullerenes,<sup>255</sup> single- and multiwalled nanotubes<sup>256</sup> (SWNTs and MWNTs), graphene,<sup>79</sup> and nanodiamonds,<sup>57</sup> stems from the high technological importance of these systems due to their unique mechanical and electronic properties which can further be tailored by irradiation. The rich physics and intriguing behavior of nanostructured carbon under irradiation comes from the unique ability of carbon atomic networks to reorganize their structures like no other material can do. New bonds around defects restructure the lattice by creating a modified but coherent network, which can retain many of its original properties. In addition to  $sp^2$ -hybridized structures including graphene and nanotubes, carbon also exists in  $sp^3$  (diamond) and  $sp^1$  (linear carbene chains) forms,<sup>257,258</sup> as well as in hybrid structures.<sup>259</sup> The difference in cohesive energies corresponding to different phases of carbon systems is very small. By using energetic particle beams one can drive the system away from equilibrium due to beam heating effects, defect creation and annealing and different responses of different phases due to irradiation. Then, under certain conditions, one can quench it into a metastable atomic configuration. For example, irradiation can give rise to transformations of graphite to diamond at the nanoscale,<sup>6</sup> cause BN fullerene growth,<sup>260,261</sup> or stimulate the formation of carbon nanotubes by injecting sputtered carbon atoms into metal particles.<sup>262,263</sup>

As in bulk solids, irradiation effects in nanoscale materials cannot be fully understood without the precise knowledge of how defects are formed. The damage production in  $sp^2$ -bonded carbon nanomaterials is somewhat different from that observed in most other solids. For example, due to the open structure of the nanotubes (isolated or bundled up), even recoils that have received energy only slightly above the threshold energy can be displaced quite far, which is in contrast to many other types of materials (e.g., in densely packed metals a stable interstitial-vacancy pair is normally

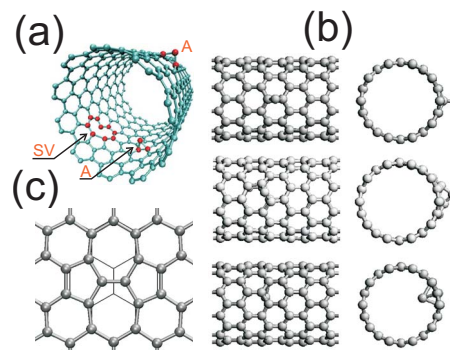


FIG. 6. (Color online) Molecular models of carbon nanotubes with point defects. (a) Short fragment of a SWNT with a SV and double-coordinated carbon atoms (a) adsorbed onto the outer and inner surfaces of the tube. (b) Carbon adatoms in different configurations on a zigzag nanotube. (c) SW topological defect associated with the rotation of a C–C bond. Thin lines correspond to the atomic network of the pristine tube.

formed by a replacement collision sequence<sup>264</sup>). Likewise, every displacement of a carbon atom from a suspended graphene sheet should give rise to formation of a defect (unless the displaced atom remains attached to the graphene sheet). There are many other peculiarities in defect production, as detailed below.

Because nanotubes, graphene, and graphite are excellent heat and charge conductors, the irradiation-induced changes in these  $sp^2$ -bonded carbon systems are governed by knock-on atom displacements<sup>72</sup> under electron or ion beams. This appears to be true for both metallic and narrow-band semiconducting carbon systems, e.g., nanotubes, as the gap in the latter is quite small, around 1 eV.<sup>256</sup>

### A. Defect production in carbon nanosystems under irradiation

As mentioned in Sec. I, the experimental techniques used to detect and characterize irradiation-induced defects in materials cannot give any information on the defect creation process, as it occurs on the picosecond time scale, but atomistic computer simulations have provided lots of insight into irradiation damage creation. In this section, we dwell on defect production in various carbon nanomaterials as revealed by calculations and corroborated by many experiments.

#### 1. Production of defects in SWNTs under ion irradiation

Computer simulations<sup>30,174,176,265–274</sup> of electron and ion irradiation of nanotubes proved to be a very useful tool for understanding the defect production mechanisms, relative abundance of particular types of defects, and defect atomic structures. The simulations showed that if the energy of the impinging particle (electron or ion) is high enough, the collision of the particle with a carbon atom in a SWNT will result in displacement of the atom, i.e., formation of a vacancy [single vacancy (SV) or multivacancies, see Figs. 6 and 16] and a number of primary recoil atoms which leave the tube. Energetic recoils can displace other atoms from the SWNT. The displaced C atoms frequently adsorb onto the tube walls, Figs. 6(a) and 6(b). These adsorbed atoms (adatoms) play the role of interstitials<sup>174,175</sup> in nanotube samples.

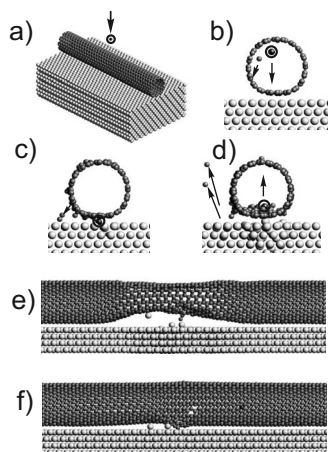


FIG. 7. Illustration of the production of defects in carbon nanotubes deposited on Pt substrates. The initial movement direction of the impinging Ar ion (circled) is designated by the arrow. The light spheres represent Pt atoms and the darker ones C atoms. The first snapshot (a) shows the original atom configuration in the nanotube-Pt substrate system. The Ar ion creates vacancies in the uppermost part of the nanotube wall as well as primary C recoils (b). Some other C atoms are sputtered from the nanotube. The Ar ion hits the substrate and gives rise to the development of a collision cascade (c). The Ar ion is reflected back from the surface creating some extra damage in the nanotube (d). A pressure wave has developed in the nanotube (e). The final configuration after cooling down the system to the zero temperature (f). From Ref. 175.

Notice that due to the quasi-1D morphology, all displaced atoms can be sputtered from the SWNT, so that no interstitial can exist in the system (placing an atom in the center of a hexagon would be geometrically easy, but is chemically extremely unfavorable). Due to voids in the SWNT, the interstitial-vacancy (Frenkel pair) separation can be large, preventing instant recombination even at modest energies of incident particles.

An illustration of the production of defects in single-walled carbon nanotubes deposited on a Pt substrate is presented in Fig. 7. The initial motion direction of the impinging Ar ion (circled) is designated by the arrow. The light spheres represent Pt atoms and the darker ones C atoms. The first snapshot (a) shows the original atom configuration in the nanotube-Pt substrate system. The Ar ion creates vacancies in the uppermost part of the nanotube wall as well as primary C recoils, Fig. 7(b). Some other C atoms are sputtered from the nanotube. The Ar ion hits the substrate and gives rise to the development of a collision cascade, Fig. 7(c). The Ar ion is reflected back from the surface creating some extra damage in the nanotube, Fig. 7(d). A pressure wave has developed in the nanotube Fig. 7(e). The final configuration after cooling down the system to the zero temperature is shown in Fig. 7(f).

As for ion irradiation of isolated nanotubes, impacts of 50–3000 eV Ar ions onto SWNTs were modeled in Refs. 174 and 175 by the EP MD method. The SWNTs were assumed to be suspended by their ends (such nanotubes can be experimentally manufactured<sup>275</sup>). It was found that SVs were the most prolific defects in nanotubes that appeared after ion impacts. Carbon adatoms on both external and internal sides of the nanotube walls were also common. Besides this, other complex defects such as SW defects and amorphous regions were observed.

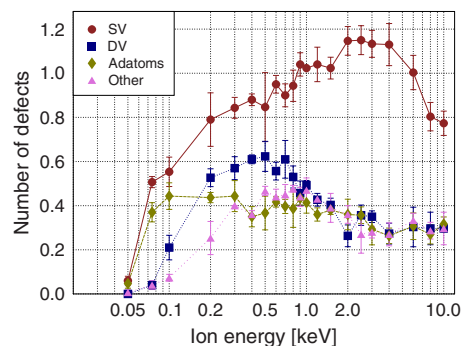


FIG. 8. (Color online) Average numbers of SVs, DVs, adatoms, and other defects per Ar ion impact as functions of ion energy in a (8,8) SWNT. The symbols are simulation results, lines are guides to the eye, from Ref. 276.

The average number of defects in a freestanding (suspended) (8,8) SWNT per ion impact is presented in Fig. 8. The total number of defects increases with ion energy and reaches its maximum at an ion energy of about 0.7 keV. The reason for such behavior is that at low energies the damage production grows with ion energy since there is simply more energy available for it. At higher energies the number of SVs increases slightly (up to  $\sim 2$  keV) while the number of divacancies (DVs) drops. The number of other defects is maximal at 1.0 keV and slowly decreases at higher energies. Such a behavior originates from a drop in the cross section for defect production at high ion energies.<sup>175,178,276</sup> The number of multivacancies is less than 10% for all ion energies. Multivacancies normally appear when the ion tangentially hits the sides of the tubes. The abundance of SVs and multivacancies does not correlate with their relative stability<sup>277–280</sup> at room and lower temperatures, but at temperatures above 300 °C multivacancy abundance may be affected by their energetics due to defect coalescence. At high ion energies, a further drop in the number of defects is expected. This is fundamentally different from the production of defects under ion irradiation in bulk materials, where the total number of defects always grows with ion energy, but the peak in the defect density is moved farther away from the surface.

The number of defects produced by the ion is larger in supported nanotubes (lying on a substrate) due to backscattered ions and atoms sputtered from the substrate, Fig. 9. Here the total damage is characterized by the number of C atoms with a coordination other than three (recall that all carbon atoms in the intact nanotube are three coordinated). It is also evident that high-temperature annealing decreases the number of defects 20%–50% due to recombination of Frenkel pairs. The residual damage after annealing was found to be practically independent of the substrate type.<sup>175</sup>

Qualitatively similar results were obtained for other types of ions<sup>178,265</sup> with energies up to 1 keV. It is interesting to notice that in this interval of energies Xe and Kr ions create approximately the same amount of damage (despite the difference in ion masses). This behavior can be understood in terms of the cross section for the defect production in a SWNT. The cross sections for different ions were estimated<sup>178,265</sup> by calculating the maximum impact parameter for which the ion transfers at least 25 eV to a C atom in a binary collision (25 eV is slightly above the experimental

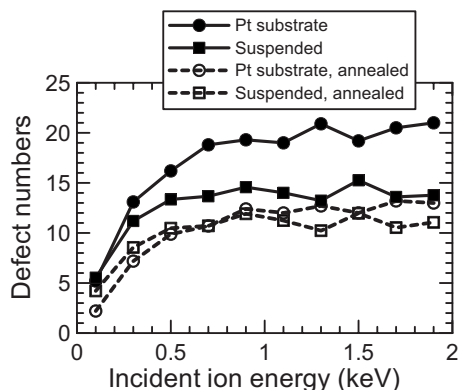


FIG. 9. Average coordination defect numbers for irradiated SWNTs as functions of incident Ar ion energy. Full circles/squares stand for the number of C atoms with a coordination other than three for suspended/supported nanotubes. Open circles/squares are the corresponding coordination defect numbers after 100 ps annealing at 1500 K.

value of the threshold energy for displacing an atom in the nanotube, see Sec. V A 5, but this is the threshold energy for displacing a C atom in the EP Brenner model used in the MD simulations) The cross sections  $S$  ( $S = \pi p^2$  where  $p$  is the impact parameter) for various ions are presented in Fig. 10. It is evident that the averaged cross sections for Kr and Xe ions are roughly the same. This is why the damage created by these ions is approximately equal in the energy range considered.

## 2. Production of defects in multiwalled and bundled-up nanotubes

In addition to the simple point defects discussed above, MD simulations<sup>178,271,272,281,282</sup> showed that a number of more complex defects can be formed in MWNTs and bundles of SWNTs. Important examples of these defects are intershell covalent bonds (formed, e.g., by two dangling bonds at the vacancies in the adjacent shells) in MWNTs, see Fig. 11(a). Likewise, defect-mediated covalent bonds between adjacent SWNTs in the bundle can appear, Fig. 11(b).

In Ref. 282, the formation of cross-links between neighboring carbon nanotubes within a bundle under self-irradiation (irradiation with C ions) was studied by classical

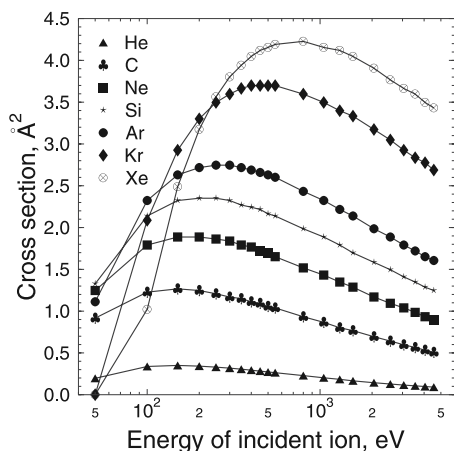


FIG. 10. Cross section for the defect production in nanotubes as a function of incident ion energy for various ions.

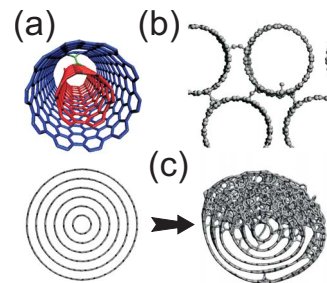


FIG. 11. (Color online) Irradiation induced links between nanotubes. (a) A covalent bond between two nearby vacancies in the adjacent shells of a MWNT. (b) Covalent bonds between SWNTs in a nanotube bundle. (c) The atomic network of a MWNT before and after 300 eV Ar ion irradiation with a dose of  $2 \times 10^{16} \text{ cm}^{-2}$  as simulated with EP MD.

MD. It was shown that it is possible to polymerize carbon nanotubes through irradiation. Cross-links were found to be created mainly in the direction perpendicular to the surface, and for higher energies, defects are created deeper in the rope. Qualitatively similar results were reported for Ar ion<sup>283</sup> and  $\text{CH}_3$  (Ref. 272) radical irradiation. High irradiating doses eventually amorphize the tubes, Fig. 11(c).

## 3. Ion irradiation of fullerenes and fullerene-nanotube systems

The interest in ion irradiation of fullerenes was stimulated by reports on formation of diamond nanocrystals (NCs) inside carbon onions (multishell fullerenes) under Ne ion irradiation.<sup>284</sup>

Besides this, ordering of fullerene thin films under high-energy ion irradiation (200 MeV Au and 60 MeV Ni ions) has been reported,<sup>66</sup> probably due to effects of ion-beam heating and a vanishingly small probability for defect production in a very thin target. Besides this, fullerene films irradiated with 250 keV Ar and 92 MeV Si ions showed magnetic response,<sup>285</sup> as evidenced by magnetic measurements using a superconducting quantum interference device and magnetic force microscopy. A ferromagnetic behavior increasing with ion fluence was observed. The magnetization was attributed to the formation of an amorphous carbon network and to the incorporation of oxygen in the irradiated films. Low-dose irradiation also gave rise to another interesting phenomenon: conducting NWs parallel to each other, embedded in fullerene matrix were synthesized by high energy heavy ion bombardment of thin fullerene films.<sup>106</sup> The typical diameter of the conducting tracks was about 40–100 nm. The creation of conducting wires could be explained by transformation of fullerene to conducting forms of carbon in the ion track, surrounded by the polymerized zone.

Theoretically, the interaction of Ar ions with  $\text{C}_{60}$ @ $\text{C}_{240}$ @ $\text{C}_{540}$  carbon onions were studied by EP MD.<sup>286</sup> It was shown that the pentagons in the graphitic network and their nearest environment are the least stable regions in the carbon onion under irradiation. The energy threshold for the formation of a vacancy in a pentagon of the onion fullerene shell was examined in two temperature regimes (300 and 1000 K), and it was found that the threshold for defect formation decreases with temperature. The simulation results provided direct confirmation of the possibility of formation

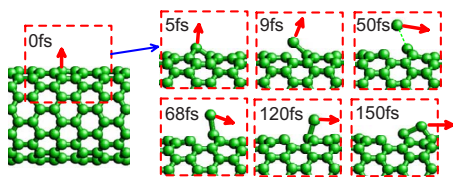


FIG. 12. (Color online) The setup used in simulations of electron irradiation of carbon nanotubes (side view) and several snapshots showing the atom positions after electron impact onto a zigzag nanotube. The initial energy of the recoil atom is just above the threshold for defect production.

of a diamond structure upon ion irradiation of carbon onions. Additional information on the mechanism of diamond nucleation in the fullerene cores was obtained from DFT-based TB simulations<sup>287</sup> of irradiation of a prototype icosahedral two-shell fullerene  $C_{60}@C_{240}$ . It was possible to identify regions in which almost all carbon atoms become  $sp^3$ -bonded. Additionally, a counteracting tendency for the carbon atoms to form shell-like substructures was observed. Thus it was shown that, to shift the balance between these two processes toward diamond nucleation, strongly nonequilibrium conditions are required.

MD simulations<sup>273</sup> were also used to study ion irradiation-induced transformations in other hybrid systems, such as carbon nanopeapods (fullerenes encapsulated inside carbon nanotubes). The results confirmed the effectiveness of ion bombardment in inducing chemical modifications of nanopeapods. The simulations showed that the coalescence of  $C_{60}$  molecules starts with the damage of fullerenes and intermolecular bridging. The cross-linking of  $C_{60}$  molecules to the tube wall was also predicted. This cross-linking results in changes in the electronic band structure as compared to the unmodified nanopeapod, which was investigated using DFT methods. Further information on the type of irradiation-induced bonds and their effects on the local electronic structure was obtained from hybrid Hartree–Fock/DFT calculations.<sup>288</sup>

#### 4. Simulations of electron irradiation of carbon nanosystems

As discussed in Sec. II, the electron-atom collision time is extremely short ( $10^{-21}$  s, Ref. 72), so that the impacts of energetic electrons onto carbon nanosystems can be modeled<sup>43,46,210,212,271,289</sup> by assigning some kinetic energy to a carbon atom in the atomic network and then by using the MD method to simulate the subsequent atom motion to understand if the impact gave rise to the formation of a defect. The orientation of the initial velocity vector can be chosen either randomly if the main goal is to simulate the response of the system to a prolonged irradiation or in the direction,<sup>43</sup> which will more likely result in the formation of a defect, if the defect formation energy is the quantity of interest. The typical simulation setup with the initial velocity vector being perpendicular to the tube surface and several snapshots showing the atom positions after electron impact onto a zigzag nanotube are presented in Fig. 12. The initial energy of the recoil atom was chosen just above the threshold for defect production.

Such a setup has been successfully used to calculate the displacement energies of atoms from graphene and carbon nanotubes,<sup>46,210,212</sup> as well as from SiC nanotubes,<sup>213</sup> see Sec. V A 5. However, for simulations of high dose irradiation, the MD simulations for atoms should be combined with an algorithm that could make it possible to generate a realistic distribution of initial velocities of recoil atoms.

Such an attempt was recently made<sup>290</sup> by augmenting MD with a Monte Carlo method using the elastic-scattering cross section, which described the interaction between a high energy incident electron and the recoil carbon atom. The model was applied to carbon nanotubes and provided reasonable agreement with the experiments. The advantage of the model is that it made it possible to correlate the response of nanotubes to irradiation with incident electron energy, tube diameter, and tube temperature. The drawback of the approach is an unrealistically high current density (ten orders of magnitude higher than in experiments) required in simulations due to computational limitations on the time interval between consecutive impacts of electrons into the system (otherwise the simulation time would have been prohibitively long). Besides, the EP MD with the Brenner model was used, which is inferior to TB model due to a lower accuracy and inadequate description of bond breaking due to artificial cutoff functions.<sup>291</sup>

#### 5. Carbon atom displacement energy

The displacement threshold energy  $T_d$  is an important characteristic describing the radiation hardness of a material.  $T_d$  can be defined as the minimum kinetic energy that must be delivered to an atom due to the impact of an energetic particle, in order for the atom to leave its position in the atomic network and either take a metastable (interstitial) position in the lattice or leave the system.  $T_d$  is different for different carbon allotropes,<sup>72,292</sup> as it is related to not only the bond energy but also the local chemical bonding and the availability of open space in the structure.  $T_d$  is smaller in  $sp^2$ -bonded carbon (15–20 eV) than in diamondlike structures (30–48 eV).

Moreover,  $T_d$  may depend on the system geometry, for example, on the diameter of a nanotube, that is, on the curvature of the atomic network, or on nanotube chirality. Early experimental and theoretical studies<sup>42,43</sup> revealed a strongly anisotropic threshold for atomic displacement, but did not report any dependence on the chirality. It was shown that in an isolated SWNT with a diameter over 1 nm, a lower energy (roughly half the value) is required to displace a carbon atom into the direction perpendicular to the tube surface ( $T_d \sim 15$ –17 eV), than into the tangential direction (30–50 eV). This value (perpendicular direction) was very close to the corresponding value for graphite (15–20 eV).<sup>72</sup>

Later calculations<sup>46,210</sup> showed that for small nanotubes with diameters less than 1 nm,  $T_d$  indeed depends on the tube diameter and chirality. Figure 13 shows  $T_d$  as a function of tube diameter for armchair nanotubes. The energy was calculated by a DFTB-based TB model dynamically (diamonds) and statically (triangles). In the dynamical approach, some kinetic energy was assigned to a carbon atom in the nanotube network, then the MD method was used to simulate the be-

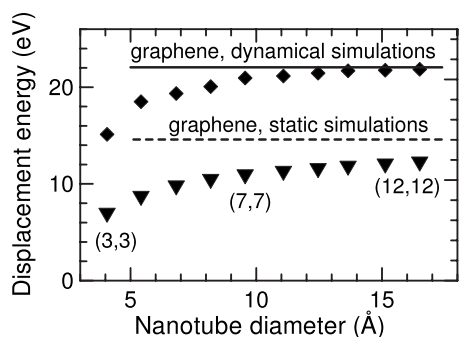


FIG. 13. Threshold energy  $T_d$  needed to displace carbon atoms from arm-chair SWNTs and graphene, calculated dynamically (diamonds) and statically (triangles) as a function of tube diameter. The lines are the corresponding results for graphene.

havior of the system.  $T_d$  was determined as the minimum kinetic energy of the atom to escape from the system. In the static simulation setup,  $T_d$  was calculated as

$$T_d = E(N+1) + E(N-1) - 2E(N), \quad (1)$$

where  $E(N+1)$  is the total energy of the system with a carbon adatom,  $E(N-1)$  is the energy of the system with a vacancy, and  $E(N)$  stands for the energy of the perfect system composed of  $N$  atoms. Physically, this expression gives the energy of a spatially separated vacancy-interstitial pair, which is obviously related to the formation energies of SVs and adsorption energy of carbon adatoms.

The static approach gives the lower bound on  $T_d$ , while the dynamical approach likely overestimates the value.<sup>210</sup> Independent of the absolute value of  $T_d$  (the true value should be somewhere in between the two bounds), both simulation setups showed that  $T_d$  is less for nanotubes with smaller diameters, which can be related to the curvature-induced strain in the nanotube atomic network. Later TEM experiments<sup>293</sup> on the response of SWNTs with different diameters to electron irradiation confirmed that nanotubes with diameters 1.3 nm and larger are more stable than those with diameters about 1 nm, and that stability increases with diameter.

Knowing  $T_d$ , one can estimate the minimum, or threshold, electron energy  $eV_{el}$  and TEM voltage  $V_{el}$  for damage production in nanotubes under electron irradiation. Based on the simple classical binary collision formula, an estimate can be done as

$$eV_{el} \approx 0.25 \frac{m_C}{m_e} T_d, \quad (2)$$

where  $m_e$  is the mass of the electron and  $m_C$  is the mass of a carbon atom. More accurate calculations can be made using the McKinley–Feshbach formalism.<sup>184</sup> For  $T_d=15$  eV, Eq. (2) gives  $eV_{el}=82$  eV, which is close to the experimentally reported value of 86 keV for MWNTs (Ref. 42) and 80 keV for SWNTs.<sup>293</sup>

Using the same head-on BCA, and the value of  $T_d$ , one can also estimate the threshold energy  $E_{th}$  of the impinging ion (the minimum kinetic energy of the ion to displace a carbon atom),

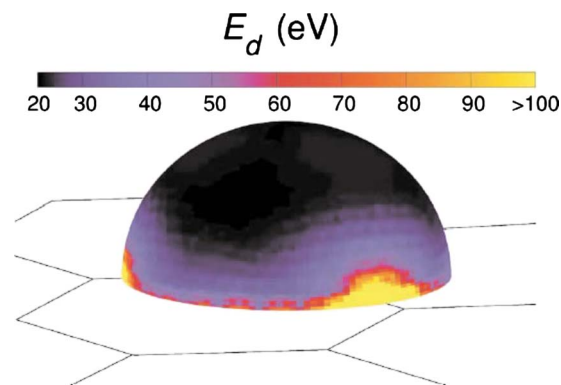


FIG. 14. (Color online) 3D representation of the map of the emission threshold function  $T_d(\delta, \gamma)$  for a carbon atom in a graphitic layer as a function of the spherical coordinates and  $\delta$  and  $\gamma$ . The color scale indicates the emission energy values from 20 to more than 100 eV. The sphere indicates the emission direction for the ejected carbon atom. The sphere is centered on the initial position of the targeted C atom. Reprinted from Ref. 212.

$$T_d = \frac{4m_C m_I}{(m_C + m_I)^2} E_{th}, \quad (3)$$

where  $m_I$  is the mass of the ion and  $m_C$  is the mass of a carbon atom. This would be a lower bound on the energy, as a part of the energy is always transferred to the atoms neighboring the recoil atom.

The computational approach used to calculate the minimum value of  $T_d$  in monatomic carbon systems<sup>46,210</sup> and systems doped with nitrogen atoms<sup>211</sup> was further extended<sup>212</sup> to account for the anisotropy of the atomic network in nanostructured carbon systems and thus for the dependence of  $T_d$  on the direction of the initial velocity of the recoil atom. In a first step, the anisotropy of the atomic emission energy threshold was obtained within extended MD simulations based on the DFT-based TB method. Atom emission from both flat graphene and curved systems was studied, see Figs. 14 and 15. In a second step, the total Mott cross section was numerically derived for different emission sites as a function of the incident electron energy. Two regimes were described. At low irradiation energies (below 300 keV), the atoms are preferentially ejected from the upper and lower parts of the tube, while at high energies (above 300 keV), the atoms are preferentially ejected from the side walls. Typical values from a fraction of a barn (at a side wall for 150 keV electron) up to around 20 barn (for 1 MeV electrons) were obtained for the total cross section of knock-on processes. These values were somewhat smaller than those previously reported using isotropic models and the values obtained from the experiments. Although electronic excitations (which are beyond this Born–Oppenheimer computational approach) may lower the threshold value of  $T_d$  and thus increase the cross section, more work is required to fully understand the origin of the discrepancy.

## B. Irradiation-induced defects in carbon nanosystems and their properties

Similar to defects in bulk materials, the defects in nanotubes can conventionally be divided into point (atomic scale) defects such as interstitial-vacancy pairs and defects of

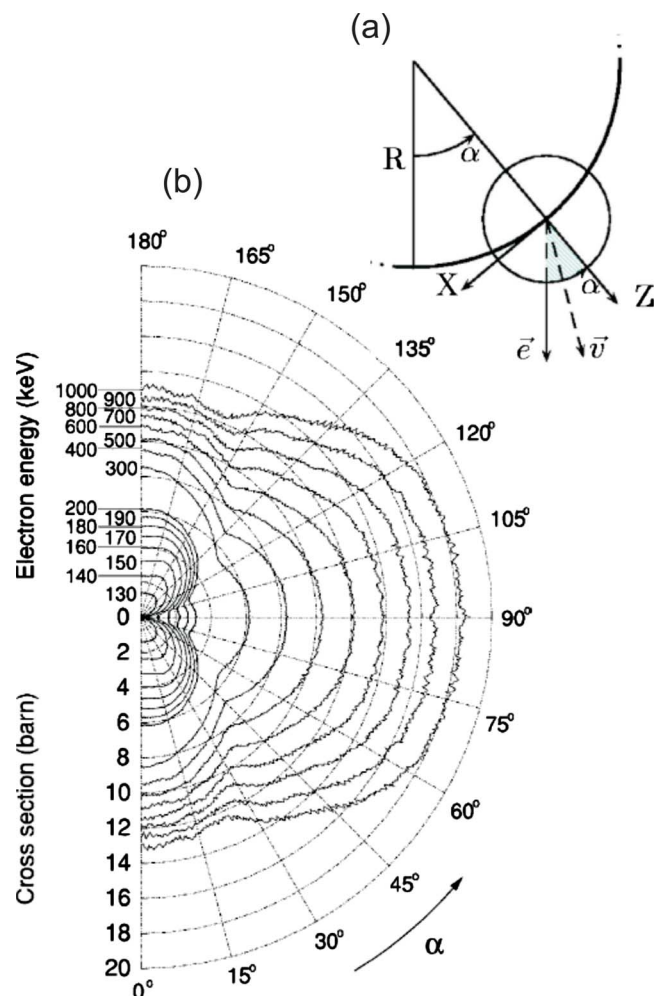


FIG. 15. (Color online) (a) Schematic representation of the irradiation geometry for a carbon nanotube, radius  $R$ , projected onto the  $XZ$  plane. The nanotube has its axis along  $Y$  perpendicular to the incident electron beam. (b) Total knock-on cross section for carbon atoms in a single-walled carbon nanotube as a function of their position around the tube circumference. Angles  $\alpha=0^\circ$  and  $\alpha=90^\circ$  refer, respectively, to carbon atoms in the tube base and in the tube side. The electron beam is entering vertically from the top of the figure. Total cross section for the full tube ( $0^\circ < \alpha < 90^\circ$ ) can be obtained by symmetrization of the plot. The curves are plotted for incident electron energies between 130 keV and 1 MeV representative of the voltages used in TEM. Reprinted from Ref. 212.

higher dimensions, for example, a local change in the chirality can be interpreted as a dislocation.<sup>7</sup> Dislocations should be particularly abundant in mechanically strained nanotubes.<sup>294</sup> Dislocation lines have also been observed in graphene.<sup>295</sup> As mentioned above, the most prolific point defects, which appear under both electron and ion irradiation in carbon nanosystems, are SVs and multivacancies, adatoms, and interstitials. In this section, we briefly discuss the atomic structure and properties of the defects.

### 1. Vacancies in graphene and carbon nanotubes

Unlike metals,<sup>296</sup> where the structure of a vacancy is essentially a missing atom in the lattice, carbon nanotubes exhibit a strong reconstruction of the atomic network near the vacancy, which, as discussed below, results in many interesting effects, e.g., pressure buildup inside irradiated nanotubes.<sup>19,297</sup>

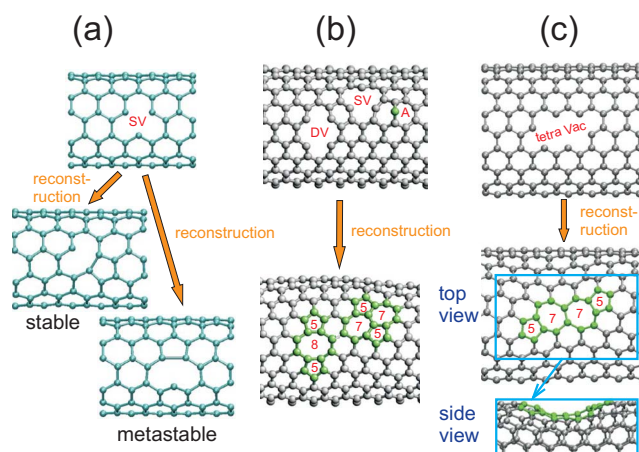


FIG. 16. (Color online) Reconstructions of the atomic network near vacancies in single-walled carbon nanotubes. Only front walls of the nanotubes are shown. (a) Reconstruction of a SV in a (6,6) armchair carbon nanotube. The top panel shows the original nonreconstructed configuration which is unstable with respect to the Jahn–Teller distortion. Depending on the orientation of the new weak “pentagon bond,” the reconstructed configurations can be metastable (when the bond is parallel to the tube axis) or stable (when the bond is almost perpendicular to the tube axis). The latter configuration has lower energy. (b) Reconstructions of the atomic network of a (10,10) carbon nanotube with several point defects. A DV transforms to an agglomeration of five- and eight-membered rings. A SV and an adatom may form a metastable SW (5757) defect. (c) Reconstruction of a tetravacancy. Note that the effective size of the “hole” decreases at the expense of local diameter reduction, so that carbon nanotubes can be referred to as self-healing materials.

DFT and DFT-based TB calculations<sup>216,298–302</sup> showed that SVs in nanotubes reconstruct by saturating two dangling bonds and forming a pentagon, see Fig. 16. In graphite, SVs reconstruct as well due to the Jahn–Teller distortion.<sup>303–305</sup> However, in nanotubes, the reconstruction is much stronger due to the curvature and inherent nanosize of the system. It is easier for the tube to contract locally to “heal” the hole and thus saturate energetically unfavorable dangling bonds. The curvature gives rise to a shorter bond in the pentagon (as compared to the bond in graphite) and a considerable drop in the vacancy formation energy  $E_{sv}$ , Fig. 17 ( $E_{sv} \sim 7.5$  eV in

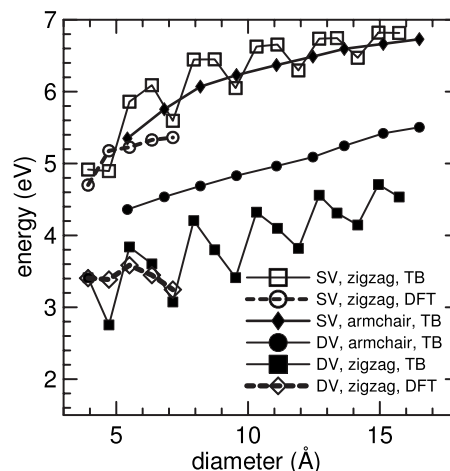


FIG. 17. Formation energies of SVs and DVs in armchair and zigzag nanotubes as functions of nanotube diameter as calculated by the TB and DFT methods (Ref. 216).

graphite<sup>305,306</sup>). Here  $E_{sv}$  is calculated as usual through the formula

$$E_{sv} = E(N-1) + E(N)/N - E(N), \quad (4)$$

where  $E(N)$  is the total energy of the system composed of  $N$  carbon atoms.  $E_{sv}$  is positive and physically defines the energy required to remove an atom from the system and place it into a vacant position at the surface far away from the original position of the atom.

As curvature breaks the trigonal symmetry of the graphene sheet, the configuration when the new bond in the pentagon is parallel (or nearly parallel) to the tube axis is higher in energy as compared to the case when the bond is perpendicular to the axis, Fig. 16(a). Similar phenomena occur in nanotubes with other chiralities, and  $E_{sv}$  is affected by the orientation of the new bond.

DVs in nanotubes also reconstruct, see Fig. 16(b). One can expect the DV formation energy  $E_{dv}$  in nanotubes to be smaller than the formation energy of *two* SVs, as there are no dangling bonds in the system. The DV formation energy  $E_{dv}=8.7$  eV in graphite<sup>305</sup> is indeed lower than twice  $E_{sv}=7.7$  eV.  $E_{dv}$  was calculated<sup>216</sup> for armchair and zigzag nanotubes as a function of nanotube diameters (see Fig. 17). Similar to  $E_{sv}$  for SVs,  $E_{dv}$  decreases when the diameter becomes smaller, which can be understood in terms of the easier reconstructions of the nanotube atomic network. The diameter locally decreases, so no dangling bond or strongly strained bonds (typical for the case of graphite) are present. However, most surprising is that for nanotubes  $E_{dv}$  is smaller than the formation energy of *one* SV. Such behavior is inherently related to the nano size and the unique atomic structure of SWNTs and is fundamentally different from that of most monoatomic solids,<sup>307</sup> including graphite.<sup>305</sup> Extrapolating the data presented in Fig. 17, one can assume that this is the case for nanotubes with diameters under 30 Å or even larger. It is important that, unlike DVs, SVs always have a dangling bond, so that a perfect reconstruction around a SV is not possible.

Saturation of dangling bonds and the local contraction of the nanotube also take place for multivacancies.<sup>277</sup> Thus carbon nanotubes can be referred to as self-healing materials under irradiation. An additional piece of evidence for self-healing of irradiation-induced defects in nanotubes was recently obtained in experiments on controlled telescopic motion of MWNTs in a TEM.<sup>308</sup> Defects with dangling bonds intentionally introduced in the MWNTs by electron irradiation led to temporary mechanical dissipation, but self-healing rapidly optimized the atomic structure and restored smooth motion.

Further reconstructions of nanotube atomic network can occur by rotations of carbon-carbon bonds near vacancies. For example, a DV, which can be referred to as a 585 defect (two pentagons and one octagon), see Fig. 18, can be transformed to a 555 777 defect, which is energetically more favorable in nanotubes with large (about 5 nm) diameters,<sup>309</sup> graphene,<sup>310</sup> and graphene ribbons.<sup>311</sup>

The advent of high-resolution TEMs equipped with aberration correctors made it possible to achieve a resolution of better than 1 Å and directly see individual point defects in

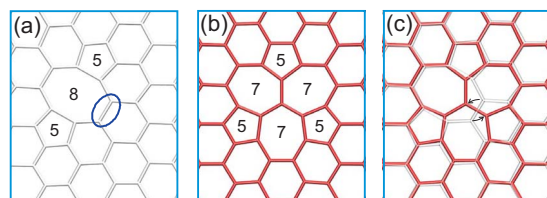


FIG. 18. (Color online) Formation of a 555 777 defect from a DV by bond rotation. (a) The atomic structure of a DV, which can be referred to as a 585 defect (two pentagons and one octagon). The bond to be rotated is circled. (b) 555 777 defect which is energetically more favorable in nanotubes with large diameters and graphene. (c) Both structures are presented in the same image.

carbon systems, especially in graphene membranes.<sup>295,312</sup>

Figure 19 shows defects found in TEM image sequences, and among them, Figs. 19(e)–19(g), a reconstructed vacancy: (e) original image and (f) showing atomic configuration; a pentagon is indicated in green. The unperturbed lattice was imaged after 4 s (g), possibly due to recombination of the vacancy with a carbon adatom. Note that electron beam energy was 80 keV, close to the threshold value to displace a carbon atom from a graphene sheet, Sec. V A 5, so that the observed defects were likely created by the electron beam.

Isolated SVs and DVs and defect constellations have also been observed in graphene by a TEM operating at 100 kV.<sup>295</sup> It was assumed that these defects had been produced by electron bombardment. Figure 20 shows the TEM images and the atomic structure of the defects. The atomic network appears to be slightly distorted, possibly due to mechanical stress induced by nearby defects.

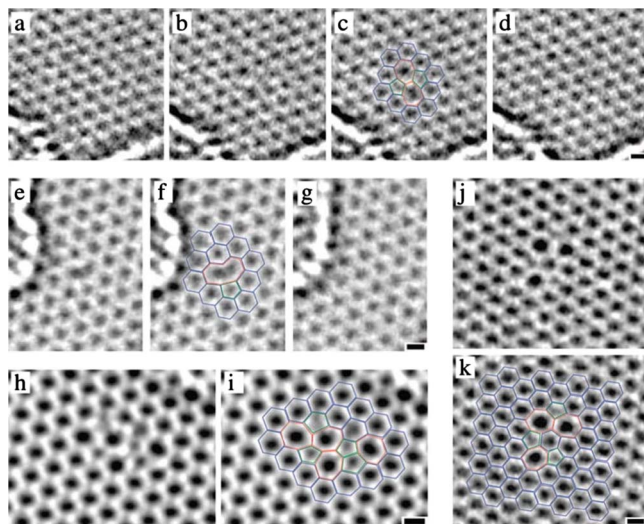


FIG. 19. (Color online) Defects found in HRTEM image sequences. [(a)–(d)] SW defect: (a) unperturbed lattice before appearance of the defect, (b) SW defect (c) same image with atomic configuration superimposed, (d) relaxation to unperturbed lattice (after approximately 4 s). [(e)–(g)] Reconstructed vacancy: (e) original image and (f) showing atomic configuration; a pentagon is indicated in green. (g) Unperturbed lattice, 4 s later. [(h) and (i)] Defect image and configuration consisting of four pentagons (green) and four heptagons (red). Note the two adjacent pentagons. [(j) and (k)] Defect image and configuration consisting of three pentagons (green) and three heptagons (red). This defect returned to the unperturbed lattice configuration after 8 s. In spite of the odd number of five to seven pairs, this is not a dislocation core (it is compensated by the rotated hexagon near the center of the structure). All scale bars are 2 Å. From Ref. 312.

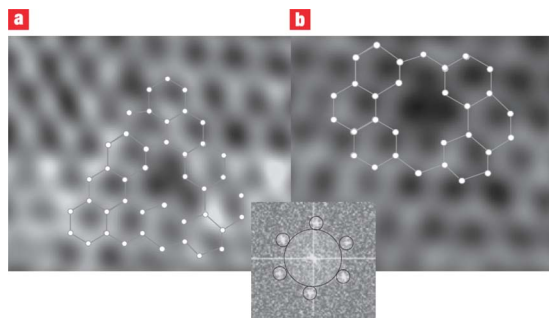


FIG. 20. (Color online) High resolution TEM images of defects in graphene lattice. (a) SV and (b) DV. The images were obtained with a filter applied to the FFT of the raw images as indicated by the inset. From Ref. 295.

## 2. Carbon adatoms as interstitials in single-walled carbon nanotubes

The adsorption of carbon adatoms onto nanotubes<sup>215</sup> was recently studied by DFT-based methods. It was found that the adatom on the outer surface of the SWNT occupies the bridge position above the C–C bond. Similar to vacancies, due to the SWNT curvature the adatom adsorption onto sites above C–C bonds being parallel and perpendicular to the nanotube axis results in different adsorption energies and local atom arrangements, see Fig. 6(b). Adatoms inside the SWNT are displaced from the bridge position due to curvature-enhanced interactions with the neighbor atoms.

In Fig. 21, the adatom adsorption energies are shown as functions of nanotube diameters for armchair SWNTs. For adatoms on the outer surface, the absolute value of  $E_a$  decreases with an increase in the SWNT diameter. This seems to be a general tendency: similar behavior of Al, H,<sup>313</sup> and N (Ref. 314) adatoms on SWNTs has been reported. The adsorption energy is always lower for configurations when the adatom is above the C–C bond oriented perpendicular to the SWNT axis than for the “parallel” configuration. This can be understood from simple carbon bonding considerations. In the “perpendicular” case, it is easier for the adatom to pull the two adjacent nanotube atoms apart (notice that the bond

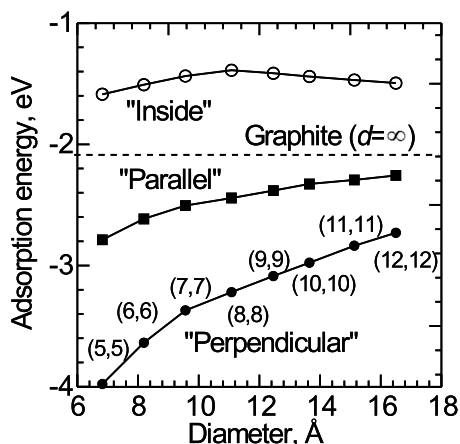


FIG. 21. Adsorption energies of carbon adatoms on armchair SWNTs as functions of tube diameter as calculated with a TB method. The numbers stand for the tube chirality indices.

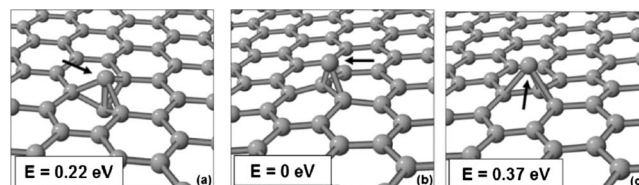


FIG. 22. Single adatoms on graphene and their relative energies: (a) dumbbell configuration, (b) bridge position with an adatom above the midpoint of a graphene C–C bond, and (c) an adatom displaced (off-top) from a top position. The positions of adatoms are indicated with arrows, from Ref. 320.

is actually broken, thus avoiding the energetically unfavorable four-coordinated atom configurations). Similar results were obtained for zigzag nanotubes.<sup>215,315</sup>

## 3. Carbon adatoms on graphene

Carbon adatoms<sup>316</sup> on graphene, which have been also referred to as self-interstitials, have received particular attention due to their possible contribution to intrinsic magnetism in all-carbon systems<sup>316,317</sup> and in the context of engineering the atomic network of  $sp^2$ -bonded nanostructures.<sup>318–320</sup>

The adatoms occupy the position on top of the middle of a C–C bond in graphene, Fig. 22(b). Besides this, two other metastable configurations with slightly higher energies are possible,<sup>320,321</sup> as shown in Fig. 22(a) and 22(c). The adatoms can easily migrate over the graphene surface with a migration barrier of about 0.4 eV.<sup>215,315</sup> This means that adatoms on flat graphene flakes are highly mobile at room and elevated temperatures and can hardly be detected with TEM or STM. At the same time, as curvature decreases adatom diffusivity, Sec. V B 6, the interpretation of TEM observations<sup>7</sup> in terms of adatoms can be consistent with theoretical results, if the graphene surface is slightly curved. The dumbbell configuration is important in the context of migration of carbon interstitials in graphite and onions in the direction perpendicular to carbon layers, as discussed in Sec. V B 6.

When two adatoms form a dimer, they can be incorporated into the network of  $sp^2$ -hybridized carbon atoms at the expense of local curvature of the network,<sup>318</sup> Figures 23(a) and 23(b). Such defects which look like two pentagons and two heptagons were named as “inverse Stone–Wales (ISW) defects.” Their formation energy is about 6 eV, even higher than that of Stone–Wales (SW) defects so the concentration of such defects in as-grown carbon nanostructures should be very small. However, such defects can appear under irradiation if two atoms displaced from their positions and adsorbed on a graphenic structure form a dimer. Such defects are immobile under ambient conditions, and their agglomeration may locally change the curvature of graphene flakes and even give rise to blisters,<sup>318</sup> Figs. 23(c)–23(f).

## 4. Stone–Wales defects

Along with vacancy- and interstitial-type defects (atoms are missing or extra atoms are present), defects of another type may exist in  $sp^2$ -hybridized carbon materials: the pentagon/heptagon SW defects<sup>322</sup> associated with a rotation of a bond in the nanotube atomic network, Fig. 6(c). Note

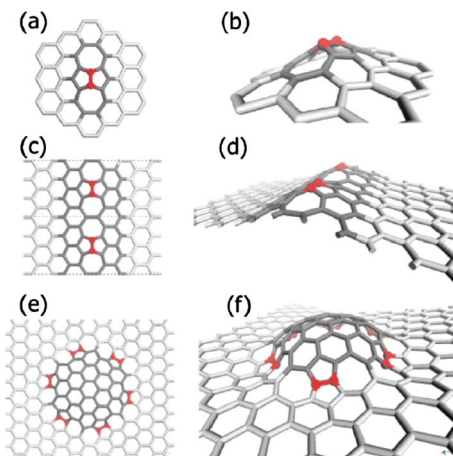


FIG. 23. (Color online) SW defects and their agglomerations. [(a) and (b)] Single inverse SW defect. [(c)–(f)] Multiple defects, which can be aligned to form ridged contours which can be straight, curved, or even closed, from Ref. 318.

that the number of atoms is the same as in the pristine network, and that all atoms are three coordinated, so we have an example of topological disorder. Note also that in a SW defect the two heptagons have a common C–C bond, while the pentagons have a common bond in an ISW defect. An experimental TEM image<sup>312</sup> of a SW defect is shown in Fig. 19(b) and 19(c).

SW defects can appear in carbon nanotubes and other  $sp^2$ -bonded covalent nanostructures, e.g., SiC nanotubes,<sup>323</sup> after impacts of energetic ions<sup>175</sup> and electrons.<sup>46,210</sup> SW defects can be produced directly by the impact of an energetic particle or by partial recombination of an adatom and a vacancy, as shown in Fig. 16(b), which may explain experimental observations,<sup>324</sup> of SW defect migration under the electron beam.

SW defects are also thought to be responsible for the release of excessive strain under axial mechanical load of nanotubes.<sup>325–327</sup> The formation energy of SW defects proved to be dependent on the tube diameter and chirality,<sup>328–330</sup> analogously to other point defects. Overall, MD simulations showed that the concentration of SW defects after impact of energetic ions<sup>174,175,178,265</sup> and electrons<sup>210</sup> is much smaller than those for adatoms and interstitials.

With regard to the atomic structure of SW defects in graphene, very recent DFT and quantum Monte Carlo simulations<sup>331</sup> showed that the structure of the defects may be more complex than reported in the original paper.<sup>322</sup> It was demonstrated that rather than being a simple in-plane transformation of two carbon atoms, out-of-plane wavelike defect structures that extend over several nanometers may exist with the formation energy being lower by 0.2 eV than that for the flat structure. Thus irradiation-induced SW defects may enhance the tendency of graphitic layers to roll up into nanotubes and fullerenes and may also play a role in the intrinsic rumpling of graphene.

### 5. Irradiation-induced defects in MWNTs and nanotube bundles

As discussed in Sec. V A, in addition to simple point defects, a number of more complex defects can be formed in

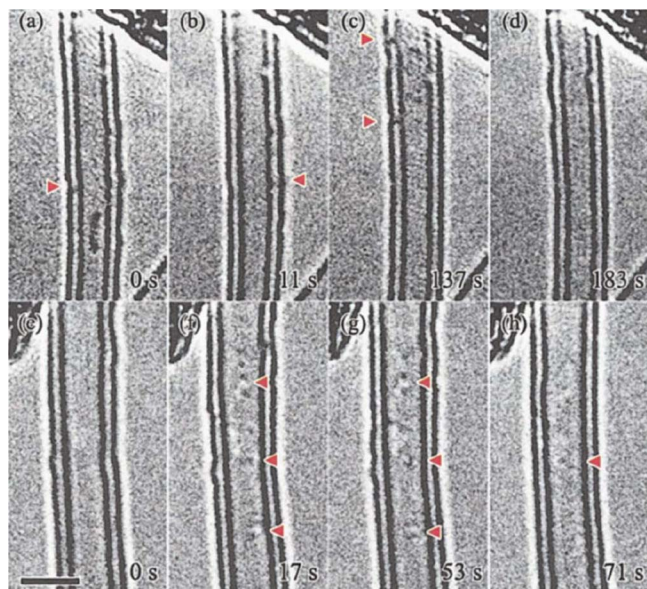


FIG. 24. (Color online) Sequential TEM images of the interlayer defects which appear and disappear in DWNTs recorded at 573 K. In the [(a)–(d)] side wall, several bridges connecting two graphene layers frequently appear in dark contrast (marked by red arrows) and disappear just after the observation. Also in the [(e)–(h)] top wall, pairs of dark and bright contrast often appear and then vanish (marked by red arrows). From Ref. 39.

MWNTs and bundles of SWNTs. Important examples of these defects are intershell covalent bonds (formed, e.g., by two dangling bonds at the vacancies in the adjacent shells) in MWNTs, see Fig. 11(a). Likewise, defect-mediated covalent bonds between adjacent SWNTs in the bundle can appear, Fig. 11(b). The bonds can be due to vacancies or the so-called Wigner defects,<sup>332</sup> a metastable atom configuration formed by a vacancy and a nearby interstitial. Such structures were experimentally found in TEM images of irradiated double-walled nanotubes (DWNTs),<sup>39</sup> Fig. 24. The behavior of these complex irradiation-induced defects is governed in part by annealing and diffusion of original defects—vacancies and interstitials. As shown below, these defects have a profound effect on the mechanical properties of the nanotubes.

The presence of nearby walls changes the behavior of vacancies. The focused electron beam in a TEM was recently used to create individual vacancies in predefined positions of single- and double-walled carbon nanotubes.<sup>333</sup> Individual vacancies in SWNTs were reported to be unstable and cause an immediate reconstruction of the lattice between 20 and 700 °C likely due to vacancy migration and coalescence. Note that in the geometry of the experiment, vacancies could have been generated in both upper and lower parts of the nanotube directly above each other. In double-walled tubes, vacancies were stable and observable up to at least 235 °C, whereas above 480 °C a relaxation of the lattice occurred, which may be associated with intershell links between the vacancies in the neighbor shells and thus lower mobility of the vacancies.

### 6. Annealing of irradiation-induced defects

Experiments on electron<sup>72</sup> and ion<sup>334</sup> irradiation of both SWNTs and MWNTs indicate that much of irradiation-

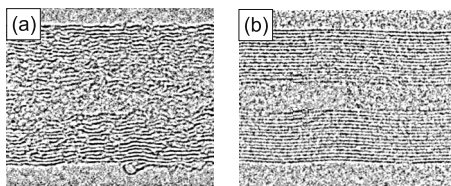


FIG. 25. MWNT after electron irradiation at room temperature (a) and at 700 °C (b). Courtesy of F. Banhart.

induced damage in nanotubes can be annealed *in situ* at temperatures higher than 300 °C, Fig. 25. Thus radiation damage in nanotubes can be avoided at relatively high temperatures. Note that in most common fcc metals, close Frenkel pairs annihilate well below room temperature (“stage I” annealing).<sup>129</sup>

Two mechanisms govern the defect annealing.<sup>175</sup> The first mechanism is vacancy healing through dangling bond saturation and by forming nonhexagonal rings, as described in Sec. V B 1.

The second mechanism of annealing is the migration of carbon interstitials and vacancies, followed by Frenkel pair recombination. The interstitial can migrate over the surface of SWNTs (isolated or bundled up). Early calculations<sup>335,336</sup> indicated that the adatom migration energy  $E_m^{(a)}$  is very low, but more rigorous recent results<sup>215,316</sup> give higher values (0.5–1 eV, the actual value depends on the tube diameter and chirality), which is in a good agreement with experimental values of  $E_m^{(a)} \sim 0.8$  eV.<sup>337</sup> Recent direct observations of the migration of individual point defects in nanotubes<sup>39</sup> and nanoscale graphite species<sup>7</sup> are also in line with the theoretical results. Interstitials (adatoms) inside SWNT and hollow cores of MWNTs are highly mobile, with the migration energy of 0.1–0.4 eV (depending on the diameter and chirality of the tube), as simulations<sup>46</sup> indicate.

The high mobility of carbon interstitials inside SWNTs has been experimentally confirmed,<sup>46</sup> and the migration barrier was measured<sup>338</sup> to be about 0.25 eV. To do this, the irradiation dose necessary to cut nanotubes repeatedly with a focused electron beam was measured as a function of the

separation between the cuts and at different temperatures. As the cutting speed is related to the migration of displaced carbon atoms trapped inside the tube and to their recombination with vacancies, as sketched in Fig. 26, information about the mobility of the trapped atoms was obtained within a simple 1D diffusion picture. By fitting the theoretical data to the experimental curves, the migration barrier was estimated. The remarkably high mobility of interstitial atoms inside carbon nanotubes shows that nanotubes have potential applications as pipelines for the transport of carbon and other atoms.

Migration of interstitials in the open spaces between the adjacent shells in MWNTs seems to be similar to that in graphite. Although there are some relevant theoretical<sup>306,321</sup> and experimental<sup>339</sup> data for graphite, further studies are required to confirm that the migration energy of interstitials in MWNTs is the same as in graphite.

Much less is known about the migration of carbon interstitials in graphite, MWNTs, and onions in the direction perpendicular to carbon layers. The exchange mechanism of diffusion with an activation barrier of about 1.7 eV, which includes the dumbbell [Fig. 22(a)] as an intermediate configuration has been proposed.<sup>321</sup> Earlier simulations<sup>340</sup> gave a value of 2.3 eV. However, experiments<sup>341</sup> on relaxation of strain in carbon onions carried out in a TEM indicate that the migration barrier may be much higher, about 5 eV, in agreement with early data on the diffusivity of interstitials along the c axis in graphite.<sup>339</sup>

Recent simulations<sup>216</sup> showed that the vacancy migration energy  $E_m^{(v)}$  is above 1 eV, larger than  $E_m^{(a)}$ . Nevertheless, SVs should be mobile already at 200 °C. The mechanism of vacancy migration is quite complicated, and it includes two steps: bond switching and “actual” migration of the vacancy (motion of the atom), as illustrated in Fig. 27. Besides annihilating with interstitials, SVs will form DVs that are practically immobile at temperatures under 1000 °C or disappear at the open ends of the tubes.

As for SW defects, the annealing should result in the restoration of the perfect atomic network, especially if an

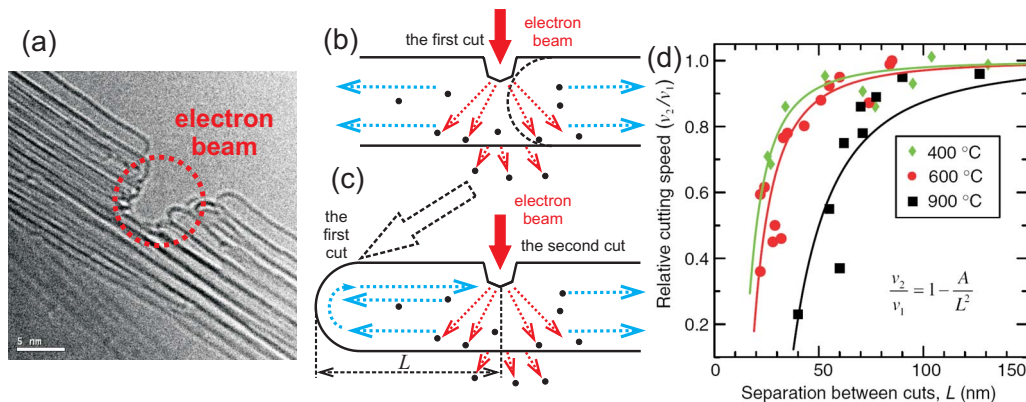


FIG. 26. (Color online) Nanotubes cut by the electron beam. (a) TEM picture of a nanotube bundle partially cut by the beam. It is evident that tubes develop caps at the cuts. (b) Schematic representation of a nanotube within the bundle when the first cut is being made. The interstitials created by the beam migrate away from the cut in both directions and disappear. (c) During the development of the second cut, the interstitials have a higher probability of arriving at the cut due to “reflection” from the cap and annihilating with vacancies thus slowing down the cutting speed. (d) Relative cutting speed  $v_2/v_1$  at various temperatures as a function of separation between the cuts  $L$ . Symbols stand for the experimental data, solid lines are fits obtained within a simple picture of 1D diffusion. From Ref. 338.

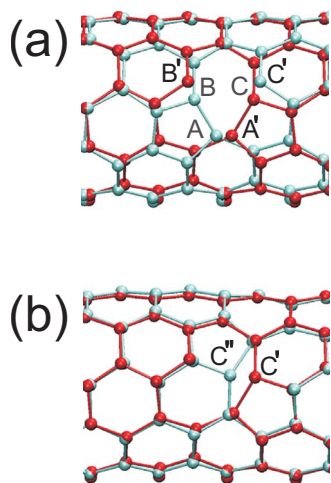


FIG. 27. (Color online) Atomic networks of (5,5) nanotubes with SVs in a ball-and-stick representation illustrating migrations and bond switching for a SV. Atoms in the back part of the tube are not shown for the sake of clarity. Each panel depicts the initial and the final configurations (shown in different colors) for every migration event. Atoms in the final configurations are labeled by letters with primes. (a) Switching of the dangling bond on atom B to atom C. Atom A moves along the tube axis. (b) Migration of atom C.

extra carbon adatom (which works as the catalyst for the transformation thus substantially reducing the defect annihilation barrier) is nearby.<sup>342</sup>

It is important that efficient annealing occurs only when the temperature is high during the irradiation. Irradiation at lower temperatures and subsequent annealing does not fully remove the radiation damage, probably due to low mobility of big defect clusters formed during low-temperature irradiation. Big vacancy agglomerations can move, however, under Joule heating of nanotubes, possibly due to electromigration effects.<sup>343</sup>

The role of defect annealing during continuous electron irradiation over macroscopic times was studied by a KMC method.<sup>132</sup> It was found that the irradiation temperature has a significant effect on defect concentration (i.e., vacancy concentration defined as a ratio of missing atoms to the total number of atoms in the irradiated area) in the irradiated carbon nanotube. At low temperatures (near 300 K), mobilities of both vacancies and carbon adatoms are low enough for the defect creation rate to introduce new defects faster than the old ones can escape from the irradiated area. This leads to defect agglomeration and thus to formation of amorphouslike structures. As the temperature increases (about 300–900 K), adatoms are mobile enough to either annihilate with the vacancies or to escape from the irradiated area. Vacancies, however, still typically coalesce to multivacancies. At even higher temperatures, both the vacancies and adatoms are mobile enough to escape from the irradiated area before coalescing, thus leaving the lattice undamaged. A defect concentration as a function of temperature is presented in Fig. 28.

### 7. Relationship between point defects in nanotubes, those in multilayer graphene, and those in graphite

The atomic structure of carbon nanotubes is closely related to that of graphite, and multilayer graphene is essen-

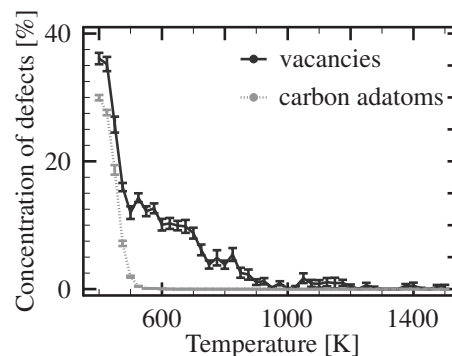


FIG. 28. Defect concentration in a (10,10) carbon nanotube after 60 s of electron irradiation as a function of the temperature as simulated with a KMC method. Courtesy of J. Kotakoski.

tially a thin graphite film. Thus, one can expect the behavior of point defects in carbon nanostructures and graphite to have much in common.

As graphite is an important moderator material in fission reactors, point defects in graphite have been studied both experimentally<sup>339,344–346</sup> and theoretically.<sup>303–306,346–348</sup> Based on the results of early experiments on defect migration in graphite, it was argued that the carbon interstitial does not form bonds with the atoms in the lattice, and it can easily migrate in the hollow regions between the graphene layers with an activation barrier of 0.1 eV.<sup>339</sup> Contrary to the above, recent theoretical calculations demonstrated that interstitials<sup>306</sup> and adatoms<sup>143,316,335</sup> form covalent bonds with atoms in graphene planes and diffuse with a migration barrier of around 1.5 eV (Refs. 306 and 321) and 0.4 eV,<sup>316</sup> respectively.

For vacancies, the interpretation of indirect experiments carried out mostly in the 1960s assigned SVs a migration barrier of around 3 eV.<sup>339</sup> Again, the results of calculations differ, predicting a barrier of around 1.6 eV,<sup>305,347</sup> much less than the experimental value.

The discrepancies in the migration energies come, on the one hand, from the uncertainties in the interpretation of the results of indirect experiments (for example, it is not clear which particular type of defects can be associated with the annealing peaks recorded during annealing experiments). On the other hand, the conventional DFT theory with the local density approximation or generalized gradient approximation functionals for exchange and correlations does not properly take into account van der Waals (vdW)-type interactions between graphite layers (see the discussion in Ref. 349 and references therein), which may be important for defect migration in layered materials.

As graphene and SWNTs have a simpler structure than graphite, simulations and direct experimental probing of individual point defects in these systems by TEM should provide lots of valuable information on the behavior of point defects in graphite and resolve long-standing contradictions between the theory and experiments.

### C. Electron irradiation of carbon nanostructures

Effects of electron irradiation on the structure and properties of carbon nanostructures have been studied mostly in

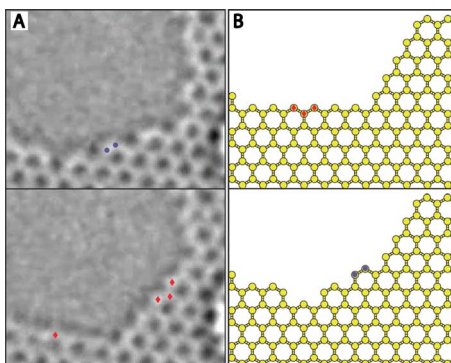


FIG. 29. (Color online) Edge reconfiguration. (a) Conversion of an armchair edge (top) to a zigzag edge (bottom). The two atoms marked as blue dots in the upper frame are gone in the lower frame, where four new carbon atoms are indicated as red diamonds. The seven-hexagon armchair edge is transformed into a nine-hexagon zigzag edge with a  $60^\circ$  turn. The transformation occurs due to migration of atoms along the edge. (b) Similar behavior is observed in the KMC simulation of hole growth, where three zigzag atoms (red diamonds, top) disappear and two armchair atoms (blue dots, bottom) appear. From Ref. 13.

the TEM, as the TEM cannot only create the damage in nanotubes by energetic (up to 1.25 MeV) electrons in a controllable manner but also monitor the irradiation-induced changes *in situ*. Moreover, as in modern aberration-corrected TEMs with field emission guns the electron beam can be focused onto areas of dimensions less than  $1 \text{ \AA}$ , the nanostructures can selectively be modified on the atomic scale by displacing or removing atoms from predefined regions. In addition to the TEM, carbon nanotubes have been irradiated by energetic electrons in a Van de Graaff electron accelerator operating at 2.5 MeV,<sup>161</sup> and graphene samples have been exposed to 1 MeV electron beam.<sup>350</sup>

### 1. Electron irradiation of graphene

Although graphene is the parent material for all  $sp^2$ -bonded carbon nanostructures and graphite, individual graphene sheets were extracted only recently,<sup>79</sup> so that relatively few papers on the response of graphene to electron irradiation have appeared so far. Nevertheless, as graphene has a very simple and well-defined structure, it is instructive to start with an overview of the response of  $sp^2$ -bonded carbon nanomaterials to electron irradiation with graphene.

Studies of freestanding graphene sheets in the TEM (Ref. 351) not only revealed the structure of pristine sheets, but also made it possible to create and directly observe defects,<sup>7,295,312</sup> such as single and DVs, as well as SW defects, see Figs. 19 and 20. Prolonged irradiation resulted in the appearance of big holes in graphene flakes<sup>13</sup> and even in the formation of carbon atomic chains across the holes.<sup>257,258</sup> The response of graphene to electron irradiation proved to be consistent with the theoretical models based on the extrapolation of the data on nanotube behavior under irradiation. It was also demonstrated that the morphology and the shape of graphene edges can be controlled by the electron beam, Fig. 29, due to a combination of electron-beam mediated displacement of atoms at the edge and their subsequent diffusion.

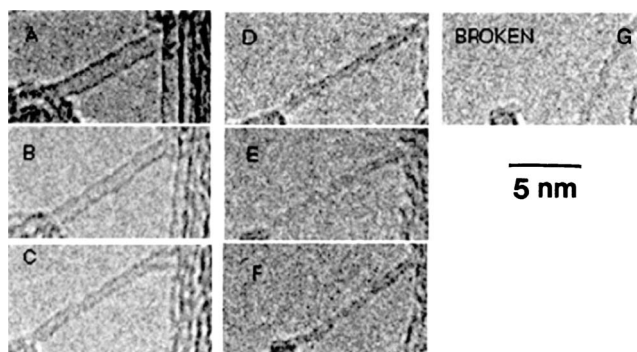


FIG. 30. Controlled electron irradiation of a SWNT segment bridged across a hole in a carbon grid. The diameter of the original nanotube (a) is approximately 1.4 nm. The tube has shrunk drastically in diameter during the irradiation. The image in (f) shows the smallest diameter ( $\sim 0.4 \text{ nm}$ ) that was visible before the tube broke (g). From Ref. 41.

In the TEM experiments described above, the beam energy (80–120 keV) was close to the displacement threshold, Sec. V A 5. Much higher energies of 1 MeV were used to create defects in multilayer graphene grown on 6H-SiC(0001) substrate<sup>350</sup> and functionalize the surface, as confirmed by XANES. Modifications of graphene properties due to low-energy (5–20 keV) electron irradiation were also reported.<sup>352</sup> The increase in the number of defects was detected by Raman spectroscopy. As the electron energy was much lower than the threshold value of about 86 keV required for ballistic defect production, Sec. V A 5, the defects likely appeared due to chemical etching of graphene surface by reactive OH and other radicals formed under the beam.

### 2. Electron irradiation of freestanding single-walled carbon nanotubes

Early experiments<sup>40</sup> showed that SWNTs exposed to focused electron irradiation were locally deformed and developed necklike features due to removal of carbon atoms by knock-on displacements. Uniform irradiation of SWNTs (Ref. 41) resulted in surface reconstructions and drastic dimensional changes, as a corollary of which the apparent diameter of the nanotubes decreased from 1.4 to 0.4 nm, and finally the tube broke, see Fig. 30. The reason for these transformations is saturation of dangling bonds at vacancies on the walls of the SWNTs created by energetic electrons, see Sec. V B 6.

Experimental and theoretical studies also demonstrated that the electron beam creates defects nonuniformly. When the electron energy is not very high (slightly above the threshold energy), carbon atoms are most rapidly removed from surfaces lying normal to the beam direction.<sup>42–44</sup> For higher energies, large-angle scattering dominates because of a higher cross section. The anisotropy in damage production was shown<sup>44</sup> to afford the ability to selectively modify the nanotube structure even with a uniform irradiation, for example, tangential irradiation of edge-on flattened nanotubes produced micron-long carbon ribbons.<sup>44</sup>

Very recently, the diameter-dependent stability of SWNTs (see Sec. V A 5) under electron irradiation was studied<sup>293</sup> in a TEM operating at 80 kV. It was found that SWNTs with small diameters of 1 nm are damaged by the

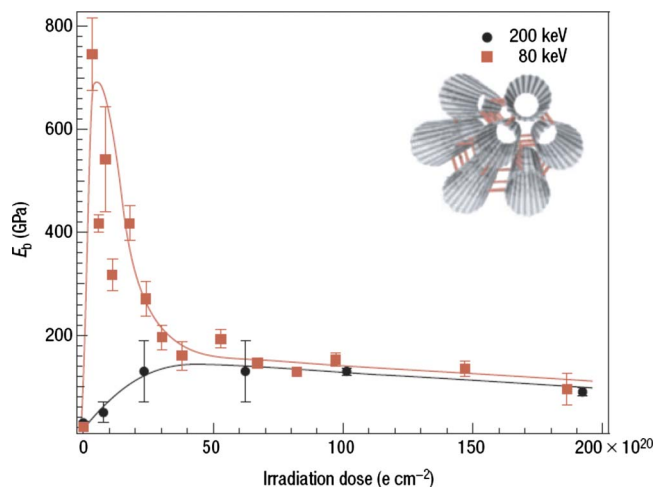


FIG. 31. (Color online) Behavior of the bending modulus of different carbon nanotube ropes as a function of electron irradiation dose for two incident electron energies. For 200 keV, the bending modulus increases on short exposures due to cross-linking and degrades at higher exposures because of structural damage. The rope irradiated with 80 keV electrons shows a much stronger and sharper increase of the bending modulus. Lines are given to guide the eye. The inset shows a sketch of cross-linked nanotubes in the rope. From Ref. 10.

electron beam and that defects produced in the side walls can lead to their destruction. SWNTs with diameters of 1.3 nm and larger were found to be more stable against degradation, and stability increased with diameter.

### 3. Irradiation-induced links between single-walled carbon nanotubes in bundles

High dose electron irradiation of SWNT bundles in the TEM gave rise to gradual amorphization of the nanotubes with the irradiation dose.<sup>10</sup> At moderate doses, however, irradiation resulted in a dramatic increase (one to two orders of magnitude) in the bundle bending modulus  $E_b$ , as measured by the AFM, Fig. 31. As the bending modulus is related to the shear modulus (proportional to the force required to move a tube in the bundle with respect to other tubes), this was interpreted in terms of irradiation-mediated covalent bonds. Early EP MD simulations<sup>283</sup> predicted formation of such bonds under ion irradiation, see Fig. 11(b), so one could expect that similar bonds could appear due to interactions of the nanotubes with energetic electrons. The structure of the bonds was theoretically studied at length by *ab initio* methods.<sup>332</sup>

Experiments<sup>10</sup> showed that at irradiation doses over  $50 \times 10^{20} \text{ e/cm}^2$ , the bending modulus started decreasing, which was understood in terms of the damage accumulation in SWNTs, and thus, a drop in the Young's (axial) modulus of individual tubes.<sup>353,354</sup> It is interesting that the increase in the bending modulus was observed at not only high (200 keV) electron energies (above the threshold) but also at energies under the threshold (80 keV). This observation may be explained by the presence of SWNTs with small diameters in the bundle, and thus lower threshold energies required to displace C atoms and form links, see Sec. V A 5, or by cross-links originating from irradiation-mediated chemical reactions between nanotubes and carboxyl groups.<sup>10</sup>

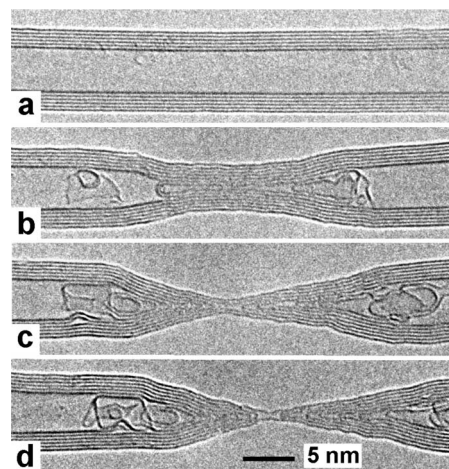


FIG. 32. Morphological evolution of a multiwalled carbon nanotube under electron irradiation. An electron beam with a diameter of 15 nm and a beam current density of approximately  $450 \text{ A/cm}^2$  was focused onto the central part of the tube. Irradiation time: (a)  $t=0$  (starting point); (b)  $t=150 \text{ s}$ ; (c)  $t=300 \text{ s}$ ; (d)  $t=800 \text{ s}$ . Specimen temperature:  $600 \text{ }^\circ\text{C}$ . From Ref. 46.

Another piece of evidence for irradiation-induced links between SWNTs in the fibers was obtained by measuring *in situ* the electrical properties of nanotubes irradiated in the TEM.<sup>48</sup> The resistivity of the irradiated SWNT-bundles assembled to form a macroscopic fiber was measured as a function of irradiation dose. A minimum was found, which, similar to mechanical measurements,<sup>10</sup> can be interpreted as an interplay between two effects of irradiation. Formation of covalent bonds enhancing intertube conductance and amorphization of the sample at high doses, which decreases the conductivity of each tube.

### 4. Electron irradiation of multiwalled carbon nanotubes

Similar to SWNTs, electron irradiation of MWNTs at room temperature resulted in the formation of vacancies on their walls and eventual amorphization upon high-dose irradiation,<sup>49,72</sup> see Fig. 25(a). In general, MWNTs seem to be more stable under electron irradiation than SWNTs,<sup>72</sup> supposedly because the atoms sputtered from inner shells remain in the MWNT and Frenkel pairs created inside the MWNT can easily recombine. The irradiation-induced damage manifested itself in the deterioration of mechanical properties of MWNTs exposed to prolonged 2 MeV electron irradiation.<sup>49</sup> It also affected the electronic properties of the tubes near the Fermi level, as assessed by ESR.<sup>49,50</sup>

High-dose irradiation of MWNTs at high temperatures ( $600 \text{ }^\circ\text{C}$ ) resulted in very interesting effects. Figure 32 shows the structural evolution of a MWNT under the electron beam. Intense irradiation (several hundred  $\text{A/cm}^2$ ) led to almost spontaneous shrinkage of all shells and collapse of the tube. Surprisingly, all shells remained temporarily intact (no breakage or disintegration) although material was lost (the surface area was decreasing). However, when the collapse proceeded, the innermost shell finally disintegrated. During the collapse, an aggregation of material in the shape of irregular graphitic cages occurs in the hollow core just outside the irradiated area, Fig. 32(b)–32(d). The initially

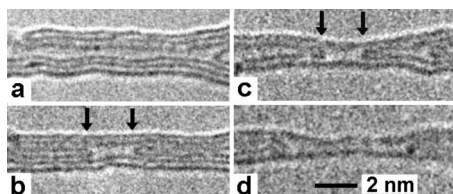


FIG. 33. Central part of a collapsing tube showing the successive loss of shells in detail. Electron beam diameter: 18–28 nm [increased deliberately from (a) to (d)]; corresponding beam current densities: 155–65 A/cm<sup>2</sup>; irradiation times: (a)  $t=0$  (starting point); (b)  $t=540$  s; (c)  $t=1400$  s; (d)  $t=2000$  s; specimen temperature: 600 °C. The three-shell tube in (a) was generated by transforming a bundle of SWNTs into a MWNT under electron irradiation. The caps closing the ends of the shells are arrowed. From Ref. 46.

cylindrical structure collapsed into a morphology of a double cone. As soon as the collapse was complete (the innermost tube had a diameter of a typical SWNT), an unexpected morphological evolution was observed, Figs. 32 and 33. Whereas the outer shells shrank but remained undamaged, the inner shells were successively broken until a SWNT in the center was left. It is always the innermost layer which breaks in such a way that the two halves form cones with closed caps. This is a counterintuitive result, as in a naive picture, one can expect the outermost shell should break first since atoms displaced from inner shells remain in the nanotube and can recombine with the vacancies thus increasing the stability, in contrast to a displacement event for an atom in the outermost shell, which corresponds to sputtering. The cone from the innermost tube moved outwards (in axial direction), and the cones from the other shells moved up. Eventually, the last remaining shell broke so that two separate multishell cones were left (not shown in the figures). Such a behavior was explained<sup>46,210</sup> in terms of a lower stability of the inner shells under irradiation due to a higher curvature of the atomic network (see Sec. V A 5) and fast diffusion of carbon interstitials through the inner hollow in the axial direction.

Concurrently with the experiments<sup>46,210</sup> on electron irradiation of MWNTs with many shells, qualitatively similar results<sup>39</sup> were obtained for DWNTs at different temperatures, see Fig. 34. Efficient annealing of the radiation damage due to interstitial migration along the inner hollow indicated that carbon nanotubes can be used as pipes for effective transport of interstitial carbon and foreign atoms.

### 5. Welding and coalescence of carbon nanotubes under electron beam

Observations of the saturation of irradiation-induced dangling bonds in carbon nanotubes, combined with the inherent ability of carbon atoms to form structures with different coordination of the atoms, opened new ways for electron-beam-assisted engineering of carbon nanotubes at high temperatures.

The coalescence of two parallel SWNTs under electron irradiation was demonstrated<sup>12</sup> at 600–800 °C. These transformations were found to proceed due to vacancies via a zipperlike mechanism, imposing a continuous reorganization of atoms in individual tube lattices along adjacent tubes. The

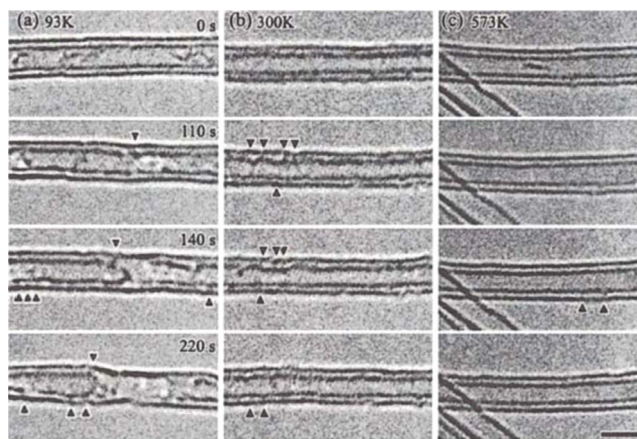


FIG. 34. (Color online) Sequential TEM images for the formation rates of the interlayer defects at different temperatures with the same time scale (0–220 s). (a) At 93 K, the defects due to electron irradiation are quite prolific, and the nanotube inside quickly damages due to the complex defects. (b) At 300 K, the nanotubes are more resistive but the defects can also be found frequently. (c) At 573 K, the defect formation can hardly be seen and the DWNTs are completely resistive due to the electron beam irradiation. The arrows indicate possible interlayer defects. Scale bar 2 nm. From Ref. 39.

electron-beam-induced coalescence of nanotubes may, in principle, be employed for improving on the control over the nanotube diameter distribution.

Irradiation of crossed SWNTs in the TEM was shown<sup>18</sup> to give rise to nanotube welding. Various stable “X,” “Y,” and “T” junctions were created, see Fig. 35. Two crossed *pristine* tubes would not normally join, even at high temperatures, as the structure of the junction containing nonhexagonal rings and strongly distorted bonds is less stable than the two perfect tubes. However, irradiation-induced vacancies and energy gain by dangling bond saturation apparently made it possible to weld the tubes together. This result suggests that it may be possible to fabricate nanotube networks

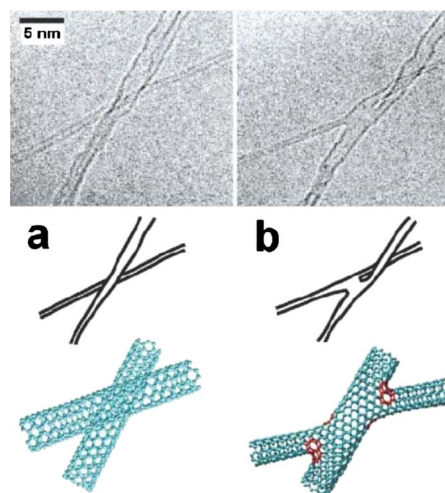


FIG. 35. (Color online) (a) A SWNT with a diameter of approximately 2.0 nm (running from bottom-left diagonally toward top right) crossing with an individual SWNT of approximately 0.9 nm diameter. (b) 60 s of electron irradiation promotes a molecular connection between the thin and the wide tubes, forming a X junction. Schematics show that this junction is twisted out of the plane. Molecular models of each image are provided. From Ref. 18.

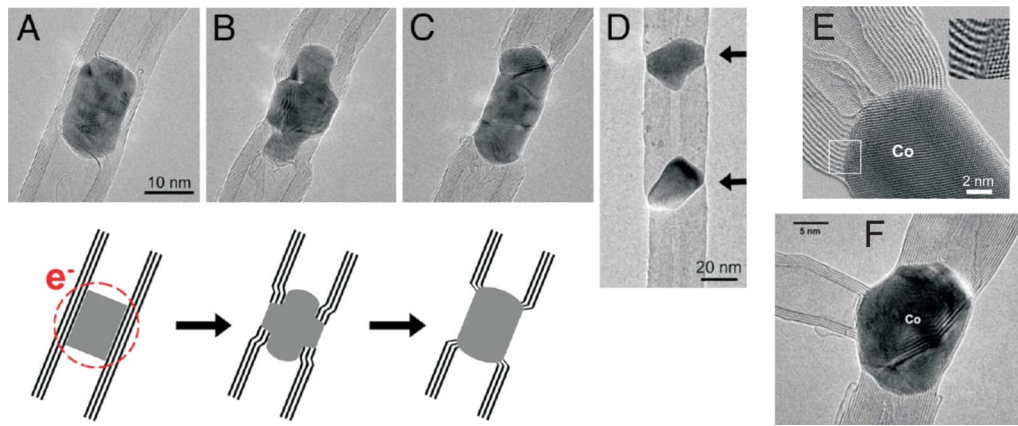


FIG. 36. (Color online) Formation of a MWNT-Co-MWNT junction from a Co-filled MWNT subjected to electron irradiation (200 keV) at 700 °C. (a) The Co-filled MWNT at the beginning of the experiment. (b) The focused electron beam damages the tube, and the Co NW is expelled to the surface, experiencing shape changes after 6 min of irradiation. (c) Finally, the Co particle acts as a link between the two MWNT segments. The sketch at the bottom shows the mechanism of the process. The circle indicates the zone subjected to electron irradiation. (d) Periodic FeCo—MWNT heterojunction, formed by repeated irradiation at different positions of a FeCo-filled nanotube. Arrows indicate metal particles. (e) Bright-field TEM image (Cs corrected) of a MWNT-Co interface. The Co particle has a fcc structure (the image shows an alignment close to the [110] zone axis projection of the Co fcc lattice). Strain is introduced at the interface as can be seen by the local bending of the graphitic layers at the interface. The inset shows a detail of the interface (white square) after noise filtering, where the bending of the nanotube layers to match the metal lattice is visible, from Ref. 358. (f) Junction between three MWNTs and a Co particle as made by electron irradiation of a metal-carbon nanotube composite. Courtesy of F. Banhart.

by growing crossed nanotubes or moving them mechanically, followed by controlled electron irradiation at high temperatures. The use of a highly localized electron beam with diameter of several nanometers, and high temperature annealing of the samples after irradiation, should minimize the damage outside the junction area, which is particularly important for applications of SWNT-based circuits in nanoelectronics. Simulations<sup>289</sup> showed that the welded nanotube structures should be mechanically stable in spite of many defects near the contact area.

Electron irradiation can also be used to fuse together the fullerenes inside carbon nanotubes (peapods).<sup>355,356</sup> The resulting structures consisted of corrugated tubules nested inside the original SWNT. These carbon nanostructures exhibited pentagonal, hexagonal, heptagonal, and octagonal rings and resembled the theoretically proposed Haeckelite structures.<sup>357</sup>

Besides carbon nanotubes, irradiation-mediated fusion of fullerenes was implemented inside boron-nitrogen nanotubes.<sup>17</sup> As a result, a carbon nanotube was obtained inside the BN nanotube. Because BN nanotubes are insulating, the use of the electron beam for producing such structures (a metal wire inside an insulating cylinder) opens new ways for making complex nano systems with predetermined electrical properties.

Another very interesting approach for contacting nanotubes with the use of electron beam was recently put forward. The controlled formation of heterojunctions between carbon nanotubes and different metal NCs (Fe, Co, Ni, and FeCo) was demonstrated.<sup>358</sup> The heterojunctions were formed from metal-filled MWNTs via intense electron beam irradiation in a TEM at elevated temperatures in the range of 450–700 °C. Under irradiation, the segregation of metal and carbon atoms occurred, leading to the formation of heterojunctions between metal and graphite, Fig. 36. Metallic conductivity of the metal-nanotube junctions was found by using

*in situ* transport measurements in an electron microscope. Mechanical tests of the contacts showed that these structures are mechanically strong, while TEM studies indicated that the bonding at the metal-carbon interface is covalent. DFT calculations confirmed the covalent nature of bonding and pointed out that the electronic states at and around the Fermi level are delocalized across the entire system. These properties are essential for the application of such heterojunctions as contacts in electronic devices and vital for the fabrication of robust nanotube-metal composite materials. An example of a three-terminal junction that has been made by electron irradiation of two crossing MWNTs with a metal particle on top of the junction is shown in Fig. 36(f). More data on irradiation-mediated contacts between carbon and metal nanosystems can be found in a recent review article.<sup>359</sup>

## 6. Engineering carbon nanostructures with a focused electron beam

The structure and the shape of nanotubes can be further tailored by electron irradiation with a focused electron beam (just a couple of nanometers in diameter) and at high temperatures. MWNTs irradiated with an electron beam of the size roughly equal to the tube wall thickness were shown<sup>47</sup> to bend due to the removal of carbon atoms from one side of the tube (Fig. 37). The bending angle could be controlled precisely by the irradiation dose. The changes in the shape apparently originated from the saturation of dangling bonds at the cut.

It was also demonstrated that a focused electron beam can be used to fabricate nanoholes and nanoconstrictions in MWNTs<sup>360</sup> and graphene sheets.<sup>13,257,258,361</sup> Such nanoholes may be applicable to DNA sequencing or work as graphene.<sup>362</sup> Such narrow ribbons in graphene have recently received a lot of attention due to their interesting electronic properties. Finite width opens up a gap in graphene ribbons<sup>363,364</sup> making feasible the development of graphene-

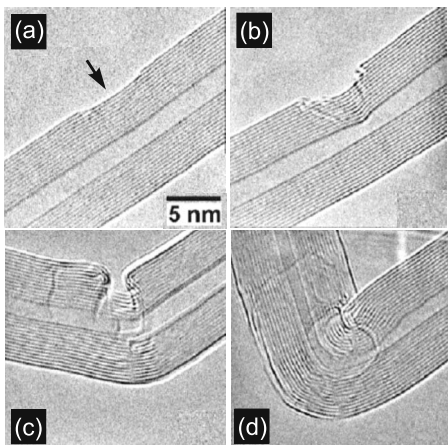


FIG. 37. Multiwalled carbon nanotube under spatially localized electron irradiation. The sequence shows the bending of the nanotube when the beam spot size equals the wall thickness (5 nm). Irradiation time: (a) 3 min, (b) 5 min, (c) 11 min, and (d) 15 min. Beam current density  $10^3$  A/cm<sup>2</sup>. Courtesy of F. Banhart.

based electronics. Moreover, as defects at the edges present a big problem in electronic transport through the ribbons,<sup>80</sup> electron beam treatment may decrease the number of defects at the edge of a ribbon. As the displacement energy of undercoordinated atoms is lower than that for three-coordinated atoms,<sup>210</sup> by adjusting the beam energy and focusing the beam on the edge it should be possible to produce a smooth edge of either zigzag or armchair type. Indeed, recent experiments<sup>16</sup> indicate that electron beam irradiation at an accelerating voltage of 80 kV preferentially sputters unsaturated carbon atoms surrounding vacancies and big holes. Migration of displaced carbon atoms along the edge<sup>13</sup> should also contribute to the development of an edge with the desired characteristics.

The irradiation of a SWNT bundle with an electron beam of 20 nm in diameter resulted<sup>47</sup> in the collapse of the bundle in the irradiated area, followed by graphitization and transformation of SWNTs into a MWNT, see Fig. 38. In such a

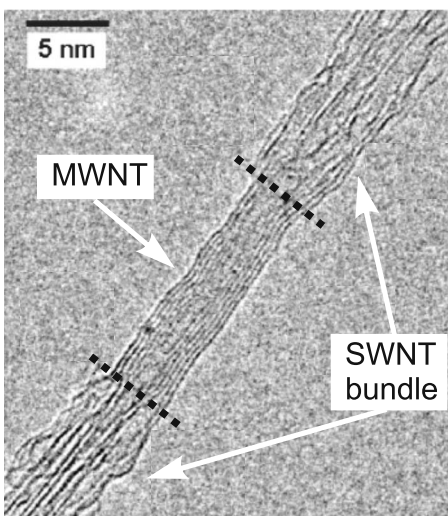


FIG. 38. Coherent transition from a bundle of single-wall tubes to a multiwall tube. The irradiation of the bundle of single-wall tubes for 28 min with moderate beam intensity (50 A/cm<sup>2</sup>) leads to the transformation into a multiwall tube in the irradiated area. Courtesy of F. Banhart.

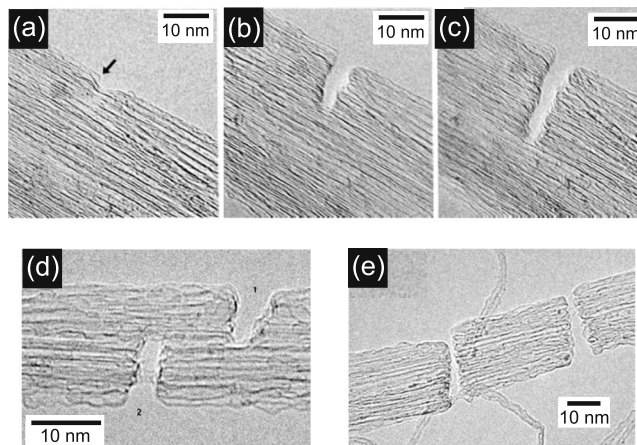


FIG. 39. Image series [(a)–(c)] shows the cutting of a gap in a bundle of SWNTs by moving a focused electron beam across the bundle. Cutting the second gap in that same bundle (d). Complete sectioning of the bundle (e). Courtesy of F. Banhart.

way, a coherent junction between SWNTs in the bundle and a MWNT can be created.

Experiments<sup>45,338</sup> also showed that bundles of SWNTs could be cut by the electron beam, see Fig. 39, either partly or completely. The cutting speed was obviously determined by the beam intensity, and surprisingly, by the existence of close cuts. For example, the cutting speed decreased when the cut reached the tubes that had been cut from the other side of the tube, as in Fig. 39(d). As the ends of the tubes at the cuts are normally closed, this observation could be interpreted as an evidence for efficient migration of interstitials inside SWNTs. If the tube was closed by a cap, the interstitials could not escape from the irradiated area and thus the defect annihilation rate was higher. This effect made it possible to even measure the migration barrier of interstitials,<sup>338</sup> see also Sec. V B 6. Note that the nanotubes were cut due to ballistic collisions of energetic electrons with nanotube atoms, but not by electron-beam-stimulated chemical reactions in the presence of gaseous species such as water molecules, as in Ref. 365.

Other aspects of electron-beam engineering were addressed in Refs. 51, 52, and 366. In particular, it was shown<sup>51</sup> that electron beam can be used to puncture carbon nanotubes with nitrogen molecules inside and to produce amorphous CN<sub>x</sub> islands. As for electron irradiation of nitrogen-doped nanotubes, very recent simulations<sup>211</sup> indicate that the dopant nitrogen atoms can be displaced more easily than the host carbon atoms. Thus spatially localized electron irradiation of N-doped nanotubes can be used for local atomic and band structure engineering by selectively removing N atoms from the predetermined areas. Likewise, this approach can also be used for the local atomic and band structure engineering of nanotubes with nitrogen-molecule-functionalized groups,<sup>367</sup> and for B–C–N nanotubes.<sup>368,369</sup>

Finally, as the electron beams can now be focused onto the areas with diameters of less than 1 Å, displacement of individual carbon atoms<sup>333</sup> followed by “plugging” of the vacancies with noncarbon atoms may give rise to novel nanostructures with very interesting electronic and magnetic properties.<sup>370</sup> Indeed, recent simulations<sup>371,372</sup> indicate that

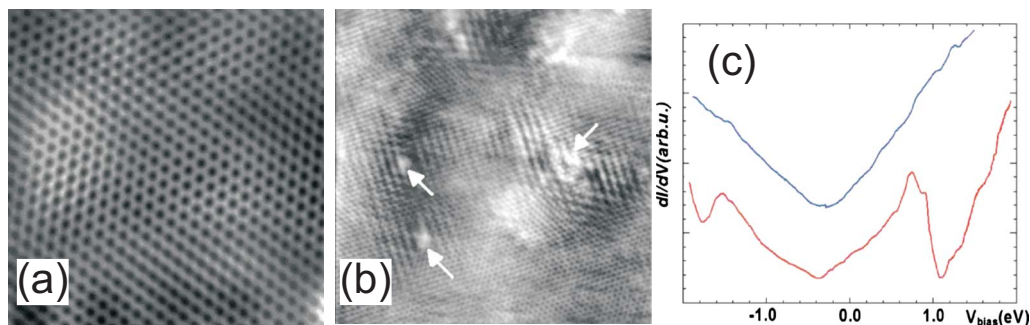


FIG. 40. (Color online) Ion irradiation of graphene. (a) Atomic resolution STM image ( $6 \times 6 \text{ nm}^2$ ) of pristine graphene on  $\text{SiO}_2$  substrate, displaying the honeycomb carbon lattice characteristic for single graphene layers. (b) Atomic resolution STM image ( $20 \times 20 \text{ nm}^2$ ) of irradiated graphene, revealing electron-density oscillations near defect sites (small hillocklike protrusions indicated by arrows). (c) Scanning tunneling spectra of graphene taken on the defect-free region (the upper curve) and at a defect site of the irradiated graphene (the lower curve). From Ref. 141.

bonding of transition metal atoms to defects in graphenic structures is strong, while metal adatoms on graphene surface are mobile at room and elevated temperature, so that it should be possible to produce such structures by depositing metal atoms on the irradiated surface of graphene or nanotubes and by raising then the temperature in such a way that the adatoms become mobile, and the defects will pin the adatoms.

#### D. Ion irradiation of carbon nanomaterials

Depending on ion mass, the ions used in materials science for irradiation and implantation are traditionally split into two categories: light and heavy ions. Normally H, He, and sometimes Li ions are referred to as “light,” while ions of other chemical elements are treated as “heavy.” Another important parameter is the irradiation dose. One can define “low dose” as the dose corresponding to the situation when the defected regions created by different ions do not overlap. Conversely, “high dose” irradiation means that many ions hit the same microscopic area of interest.

##### 1. Ion irradiation of graphene

From the viewpoint of fundamental aspects of ion-solid interaction, graphene is an extremely interesting target. Indeed, contrary to bulk solids, every displacement of atoms from a suspended monoatomic graphene under ion irradiation should give rise to the formation of a defect, as the displaced atoms will be sputtered away, so that recombination of vacancy-interstitial pairs is not possible. Due to a well controlled structure, graphene can be an ideal system for studying effects of ion irradiation on solid targets in various regimes corresponding to the nuclear and electronic stopping, Sec. II. The techniques which can detect individual defects such as STM (Ref. 141) or TEM,<sup>295,312</sup> can be combined with transport measurements, micro-Raman<sup>150</sup> and other spectroscopic techniques to get the signal from specific regions of the sample.

The first ion irradiation experiments have been carried out, however, on graphene samples deposited on substrates. The main motivation of these experiments was to study the effect of atomic scale defects and disorder on the low-energy electronic structure of graphene and the electronic transport.

Mechanically exfoliated graphene layers deposited on  $\text{SiO}_2$  substrates were irradiated with 30 keV Ar ions.<sup>141</sup> The irradiated samples were investigated by STM and STS techniques. The defect sites were identified, Fig. 40, and new states close to Fermi energy spatially localized at irradiation-induced defect were revealed, as predicted earlier.<sup>373</sup> It was found that defect sites, besides acting as scattering centers for electrons through local modification of the on-site potential, also induce disorder in the hopping amplitudes. The most important consequence of the induced disorder is the substantial reduction in the Fermi velocity, revealed by bias-dependent imaging of electron-density oscillations near defect sites. The types of the defects were not identified, however. It should also be pointed out that the hillocks in STM images may have originated not only from the defects in graphene (probably some substitutional defects, as the sample was subjected to ambient conditions) but also from the defects in the substrates such as charged impurities. Most defects in graphene were probably created not by the ion beam directly but by the atoms sputtered from the substrate, as the density of the defects in Fig. 40 appears to be higher than one could expect from the irradiation dose used ( $5 \times 10^{11} \text{ ions/cm}^2$ ).

Effects of irradiation with 500 eV Ne and He ions on graphene on  $\text{SiO}_2$  substrate were studied as well.<sup>150</sup> The presence of defects was confirmed by Raman spectroscopy, as evident from Fig. 41. It was also found that the defect

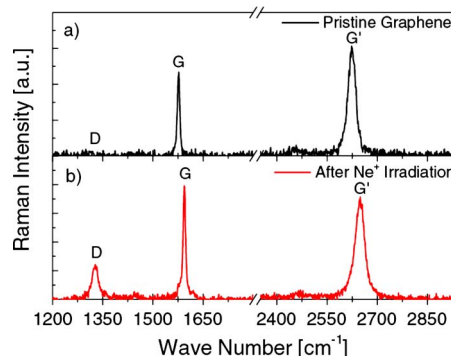


FIG. 41. (Color online) Raman spectra (wavelength 633 nm) for (a) pristine graphene and (b) graphene irradiated by 500 eV Ne ions at a dose of  $5 \times 10^{12} \text{ ions/cm}^2$ . Note increase of the intensity of the D band associated with defects. From Ref. 150.

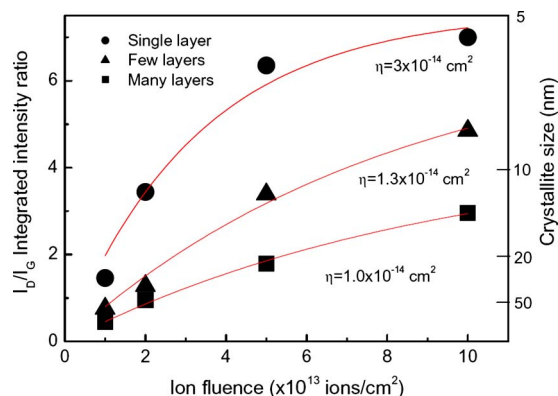


FIG. 42. (Color online) Ratio of the D peak and G peak intensities ( $I_D/I_G$ ) as a function of the ion fluence  $\nu$  for a single layer, a double layer, and a multilayer of graphene. From Ref. 142.

scattering gives a conductivity proportional to charge carrier density, with mobility decreasing as the inverse of the ion dose. Defected graphene showed a diverging resistivity at low temperature, indicating insulating behavior. The results were explained by ion-induced formation of lattice defects that result in midgap states. Although the results provided a plethora of information on the effects of disorder on electronic transport, the microscopic structure of irradiation-induced defects remains unknown.

As for high energy irradiation, when electronic stopping dominates over nuclear stopping, single layers, bilayers, and multilayers of graphene deposited on  $\text{SiO}_2$  substrate were irradiated with 500 keV carbon ions.<sup>142</sup> The combined use of Raman spectroscopy and AFM techniques allowed one to assess the effects of nearby graphene layers and substrate on defect production. It was found that the ratio between the D and G peak intensities in the Raman spectra of single layers is higher than for bilayers and multilayers (Fig. 42) indicating a higher amount of disorder and the importance of the environment (that is the substrate) on defect production rate. It was also found using AFM that for irradiation at fluences higher than  $5 \times 10^{13} \text{ cm}^{-2}$ , the morphology of single layers becomes fully conformed to that of the  $\text{SiO}_2$  substrate, i.e., graphene ripples are completely suppressed, while ripples are still present on bilayers and multilayers.

Graphene flakes on  $\text{SiO}_2/\text{Si}$  substrate were also irradiated with 0.4–0.7 MeV protons.<sup>374</sup> The irradiated samples were studied by Raman spectroscopy and AFM. No increase in D band intensity was reported. This is not surprising, as protons with MeV energies should not produce much damage in graphene. AFM probing of the irradiated sample revealed bubblelike features, which appeared on the sample surface after irradiation. These features were explained in terms of agglomerations of gas molecules under the graphene layer. As irradiation doses were quite small, of the order of  $10^9 \text{ ions/cm}^2$ , the gas molecules were not hydrogen but probably oxygen, water, and other molecules released from the  $\text{SiO}_2$  substrate under the beam. It was concluded that one atom thick sheets can serve as robust membranes capable of holding mesoscopic volumes of gas.

Overall, despite the first interesting experimental results on ion irradiation of graphene, the response of graphene to

ion irradiation has not yet been thoroughly studied, and future experiments and simulations should reveal the defects that appear under ion irradiation in this unique, only one atom thick, target.

## 2. Experiments on heavy ion irradiation of carbon nanotubes

*a. High-dose irradiation* Early experiments on heavy ion irradiation of MWNTs with diameters of about 10 nm with 3 keV Ar ions, followed by XPS and TEM probing,<sup>159</sup> demonstrated that the bombardment resulted in the appearance of carbon dangling bonds, which can be understood in terms of single- and multiatom vacancies. A gradual amorphization of the carbon network was reported, and for maximum irradiation doses used (i.e., more than  $10^{19} \text{ ions/cm}^2$ ) MWNTs with originally hollow cores were transformed into nanorods composed of amorphous carbon. The amorphization of MWNTs by 3 keV Ar ions was achieved<sup>33</sup> with a much lower irradiation dose of  $4 \times 10^{16} \text{ ions/cm}^2$ . Irradiation of MWNTs with 2 MeV Ag ions was reported<sup>158</sup> to give rise to complete destruction of nanotubes at an irradiation dose of  $1 \times 10^{16} \text{ ions/cm}^2$ . Note that ions with different masses and energies produce a different number of defects in the target, so that the comparison of the irradiation doses which give rise to the complete amorphization of the sample is not straightforward. The displacement per atom should be estimated taking into account the actual finite thickness of the target.

Multiwalled carbon nanotubes were also irradiated by 40 keV C, N, Si, and Ar ion beams with different doses, with an aim to produce networks of amorphous NWs.<sup>156</sup> It was found that for lighter ions, the threshold dose for the formation of NWs is higher than it is for the heavier ions, which is relevant to the fact that the heavier ions produced more collision cascades than lighter ions. The formation of NWs proceeds through the three following stages: local amorphization of nanotubes, formation of simple junctions, and formation of NW networks. The effects of irradiation induced defects on Raman spectra were studied as well, Fig. 43. Note that, in contrast to Raman spectra of SWNTs, Fig. 50, and graphene, Fig. 41, the number of defects in pristine MWNTs is relatively high, so that the ratio of intensities of the D and G bands does not change much and cannot provide quantitative information on defect concentration.

Although the first experiments reported essentially destructive effects of irradiation on nanotubes, later works provided evidence that heavy ion irradiation can be used in a creative way. Irradiation of arc-evaporated MWNTs with 30 and 50 keV Ga ions resulted in very interesting structural transformations in the nanotubes.<sup>22</sup> For 50 keV ions with doses of  $\sim 10^{13} \text{ ions/cm}^2$ , the outer shells of the MWNTs remained intact, while the inner layers reorganized into highly ordered pillboxlike nanocompartments with diameters of about 5 nm and of varying lengths between 2 and 20 nm, see Fig. 44. Increasing the dose to  $10^{14} \text{ ions/cm}^2$  resulted in the gradual disordering of the graphitic shells and destroyed the nanocapsules, while at doses of about  $10^{15} \text{ ions/cm}^2$  the

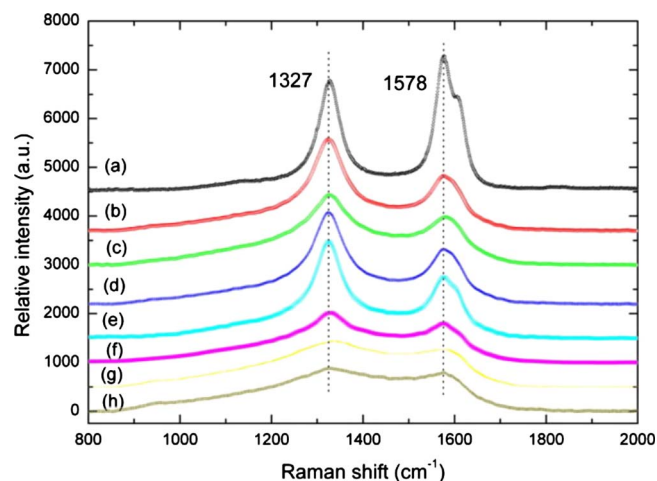


FIG. 43. (Color online) Typical Raman spectra of the as-grown MWNTs and MWNTs irradiated with Ar ion beam with different doses: (a) as-grown, (b)  $5 \times 10^{14}$  ions/cm<sup>2</sup>, (c)  $1 \times 10^{15}$  ions/cm<sup>2</sup>, (d)  $5 \times 10^{15}$  ions/cm<sup>2</sup>, (e)  $1 \times 10^{16}$  ions/cm<sup>2</sup>, (f)  $5 \times 10^{16}$  ions/cm<sup>2</sup>, (g)  $1 \times 10^{17}$  ions/cm<sup>2</sup>, and (h)  $5 \times 10^{17}$  ions/cm<sup>2</sup>. Compare to Raman spectra of irradiated SWNTs, Fig. 50 and graphene, Fig. 41. From Ref. 156.

graphitic shells collapsed into the hollow, resulting in the formation a homogeneous amorphous rod. Irradiating nanotubes with 30 keV ions gave similar results, but at higher doses.

The formation of similar bamboolike structures in MWNTs irradiated with 4 MeV Cl<sup>2+</sup> ions with a dose of  $3 \times 10^{16}$  ions/cm<sup>2</sup> was reported<sup>34</sup> as well. In addition to the changes in the shape of the tubes, irradiation resulted in their swelling, as a result of which the average diameter of the tubes increased from 70 to 180 nm, possibly due to intercalation of Cl atoms and due to defect-mediated changes in the atomic structure. Both Ga and Cl ion high dose irradiation fully amorphized the samples, as evident from the TEM images, as well as from growing resistance of the tubes and increase in the area ratio of D-peak to G-peak in the Raman spectra.<sup>34</sup>

Self-irradiation with 100 eV C<sup>+</sup> ions was used for making nanotube-amorphous diamond nanocomposites<sup>35</sup> in which conducting mats of SWNTs were protected against wear by 50 nm amorphous diamond films. Experiments also indicate that magnetized-plasma ion irradiation can be used

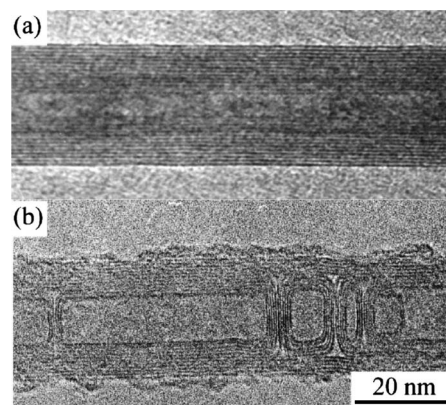


FIG. 44. TEM micrograph of a pristine MWNT and a MWNT irradiated with a  $5 \times 10^{15}$  ions/cm<sup>2</sup> dose of 30 keV Ga ions. From Ref. 22.

for encapsulating fullerenes<sup>376</sup> and intercalating cesium inside SWNTs (Ref. 377) via irradiation-induced defects in the tube walls.

10 and 30 keV focused beams of Ga ions were shown<sup>23</sup> to be able to thin, slice, and alter the structure and composition of MWNTs at precise locations along the nanotube axis. This strategy of harnessing ion-beam-induced defect generation and doping could be attractive for modulating chemical and electrical properties along the nanotube length, and fabricating nanotube heterostructures, and networks for device applications.

An interesting irradiation-assisted way for manufacturing nanotube networks consisting of perfectly straight and suspended structures was demonstrated.<sup>27</sup> SWNTs grown suspended between pillars of Si/SiO<sub>2</sub> structures were irradiated with 30 keV Ga<sup>+</sup> ions. The typical ion dose was around  $1.5 \times 10^{14}$  ions/cm<sup>2</sup>. The nanotubes were straightened by ion beam scans. In addition, the ion irradiation selectively removed nanotubes lying on the substrate, leaving the suspended nanotubes in place. Although ion irradiation induces structural modifications to nanotubes and introduces defects into the nanotube lattice, the form, and dimensions of the nanotubes remained close to those of the original structures.

Irradiation-induced enhancement in the field emission properties of nanotubes has been reported.<sup>28</sup> Argon irradiation treatment straightened as-grown curly nanotubes, see Fig. 45, similarly to Ga ion irradiation.<sup>27</sup> As a result, the

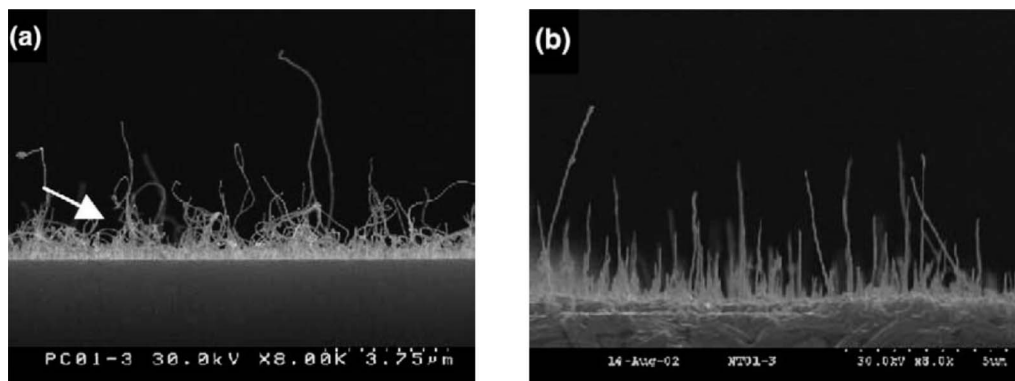


FIG. 45. SEM images of nanotubes (a) before and (b) after Ar ion irradiation. Nanotubes were straightened by the ion beam. From Ref. 28.

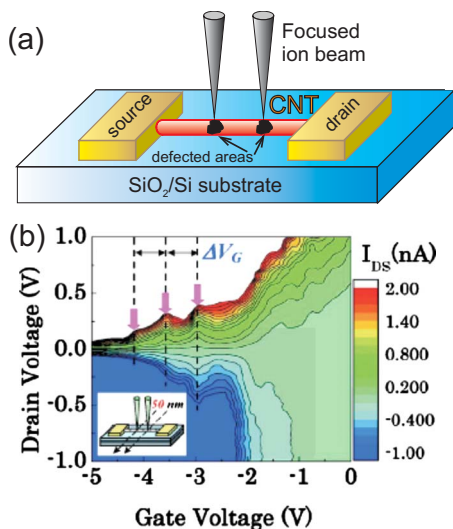


FIG. 46. (Color online) Using ion irradiation for making nanotube-based electronic devices. (a) Schematic illustration of the fabrication of a quantum dot in a carbon nanotube by using FIBs. (b) Contour plots of source-drain currents for the system shown in (a) at room temperature as functions of source-drain voltage after ion bombardment. The arrows indicate the irradiation-induced features corresponding to the Coulomb blockade regime. Reprinted from Ref. 379.

local electric field was enhanced due to the increased aspect ratio and reduced mutual shield effect. Additional contributions may have come from irradiation-induced defects, which made nanotube effective surfaces more active, thus emitting more electrons. The electron field emission from nanotubes has also been enhanced by Si ion beam irradiation.<sup>378</sup> The irradiation-induced defects and the adsorbed molecules on the nanotubes were responsible for the enhancement of electron field emission. Thus ion irradiation appears to be a tool to improve the electron field emission properties of carbon nanotubes.

As for the beneficial effects of ion irradiation on nanotube electronic properties, spatially localized Ar ion irradiation (with doses up to  $\sim 10^{16}$  ions/cm<sup>2</sup>) of individual MWNTs deposited on SiO<sub>2</sub> substrates was used<sup>25,379</sup> to create a defective region which worked as a potential tunnel barrier for electrons in the MWNT, Fig. 46. A fast increase in the tube resistance with the irradiation dose was reported. It was demonstrated that a double-barrier structure fabricated by such method can work as a quantum dot. However, the types of defect and their spatial distribution were not identified, although knowing this is important for understanding the Coulomb oscillations observed in the system and how the current flows through the damaged MWNT shells. Spatially localized ion irradiation was also used for the fabrication of a single-electron inverter in MWNTs.<sup>26</sup>

Because irradiation-induced defects normally increase the reactivity of nanotubes (e.g., due to dangling bonds at the surface defects), focused-ion-beam irradiation, followed by mild chemical treatment, was used to functionalize nanotubes at preselected locations,<sup>24</sup> Fig. 47. The bombardment with Ga ions having energies of 10–30 keV and with irradiation doses of  $\sim 10^{15}$ – $10^{17}$  ions/cm<sup>2</sup> resulted in the desired effect. Controlled chemical modification was also achieved with 2 keV argon ions,<sup>29</sup> but at much smaller doses of about

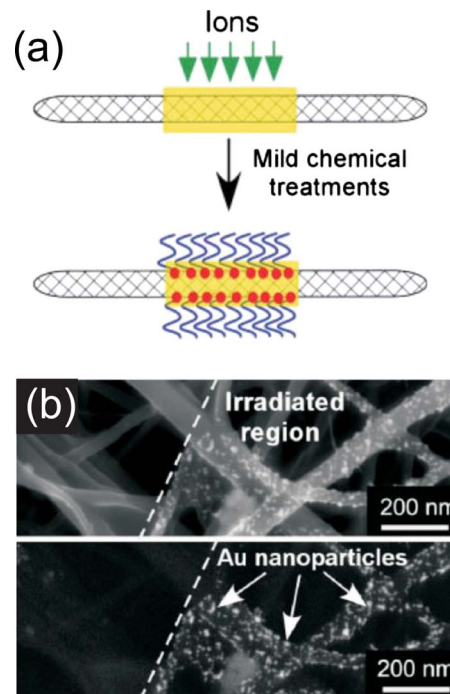


FIG. 47. (Color online) Ion-beam-assisted site-selective functionalization of carbon nanotubes. (a) Schematic illustration of the experimental setup. (b) Immobilization of Au nanoparticles on ion irradiated regions of carbon nanotubes. Reprinted from Ref. 24.

$\sim 10^{13}$  ions/cm<sup>2</sup>. The lower doses may, however, give a comparable number of surface defects, as the production of defects at the nanotube surface should drop with increasing ion energy, see Sec. V A. Ion-beam-assisted functionalization can also be used<sup>380</sup> for the modification of graphene properties.

Effects of ion irradiation were also studied by Raman spectroscopy in DWNTs.<sup>151</sup> As this method allows one to differentiate signals from the outer and inner shells of a DWNT, the differences in the response of the shells to irradiation could be probed. Highly pure DWNTs were irradiated with 170 keV Si and 100 keV C ions. The bombardment was performed at room temperature with ion doses ranging between  $1^{13}$  and  $1 \times 10^{15}$  ions/cm<sup>2</sup>. As expected, heavier Si ions created more disorder than C for the same irradiation dose. As in other works discussed above, the “D-band” intensity increased, while the “G-band” intensity decreased with the dose, indicating increased lattice disorder. With increasing ion dose, the radial breathing modes (RBMs) of the outer tubes disappeared before the respective RBM bands from the inner tubes, suggesting that the outer nanotubes are more affected than the inner nanotubes by the ion irradiation. After Si ion bombardment to a dose of  $1 \times 10^{15}$  ions/cm<sup>2</sup>, the Raman spectrum resembled that of highly disordered graphite, indicating that the lattice structures of the inner and outer nanotubes were almost completely destroyed. However, laser annealing partially restored the crystalline structure of the nanotubes, as evidenced by the re-emergence of the G and RBM bands and the significant attenuation of the D band in the Raman spectrum.

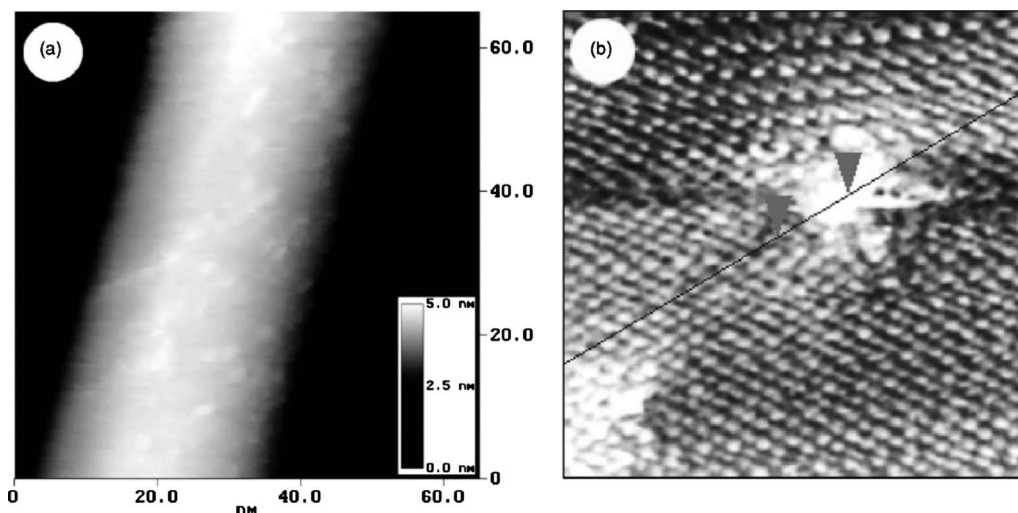


FIG. 48. MWNTs with defects (hillocklike protrusions) created by Ar ion irradiation (a). Atomic resolution STM image of a nanotube defect (b). From Ref. 32.

*b. Low-dose irradiation* Effects of single ion impacts on the atomic structure and properties of nanotubes can be studied by low-dose ion irradiation combined with other techniques that can detect signatures of irradiation-induced defects.

MWNTs dispersed on a graphite substrate were irradiated<sup>32</sup> with 30 keV ions with a dose of around  $10^{11}$  ions/cm<sup>2</sup>. STM measurements carried out under ambient conditions revealed hillocklike protrusions on the nanotube walls (Fig. 48), which were associated with individual vacancies, in agreement with the theoretical predictions.<sup>174,381,382</sup> Annealing in nitrogen atmosphere of the irradiated samples at 450 °C demonstrated that defects in nanotubes tend to heal already at moderate temperatures, which was in line with the TEM results.<sup>72</sup>

Low dose irradiation of individual SWNTs with 120 eV Ar ions (this energy is just above the threshold to produce defects in SWNT, see Sec. V A) and electronic transport measurements on the irradiated nanotube made it possible to assess the effect of individual defects on nanotube conductance.<sup>11</sup> At such low energies, irradiation with Ar ions should result in the formation of single and DVs, which give rise to a dramatic drop in the conductance of the nanotube due to the 1D nature of the system and thus a very small number of conduction channels. Theoretical transport calculations showed that mostly DVs contribute to the resistance increase and that just 0.03% of DVs produced an increase of three orders of magnitude in the resistance of a 400 nm long SWNT.

The impact of low-dose ( $\sim 10^{12}$  ions/cm<sup>2</sup>) ion irradiation on bundles of SWNTs was experimentally studied as well.<sup>21</sup> The bundles were irradiated with an 500 eV Ar<sup>+</sup> ion beam followed by transport measurements. The results suggest that irradiation gives rise to current redistribution between the damaged and undamaged tubes in the same rope, which can be interpreted as evidence for the formation of irradiation-mediated links between individual SWNTs in the bundle. The links appear to be of the same origin as the intertube links in electron-irradiated nanotube bundles.<sup>10,48</sup>

The formation of covalent bonds between bundled-up nanotubes under impacts of low energy (below 50 eV) CF<sub>3</sub><sup>+</sup> ions was also reported.<sup>30</sup> The cross-links, however, should appear only near the bundle surface at such low ion energies.

Low dose ion irradiation has also been used to alter the characteristics of nanotube bucky paper (NBP) (see also Sec. V F 1). A remarkable correlation between frequency shifts in G<sup>+</sup>, D, and D\* Raman modes and changes in the conductivity and Young's modulus of freestanding SWNT networks was found<sup>167</sup> (Fig. 49). Under 30 keV Ar ion irradiation with

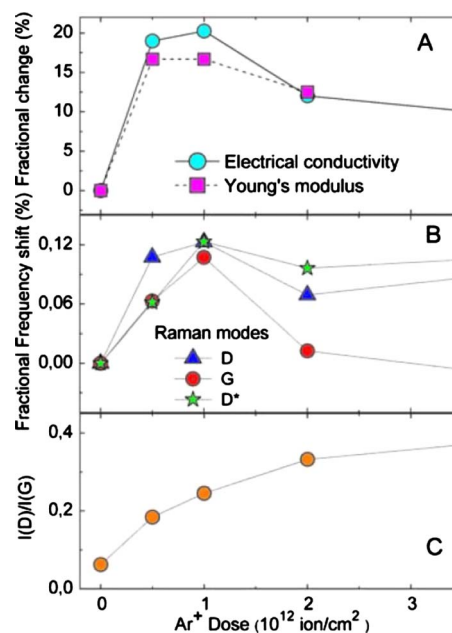


FIG. 49. (Color online) (a) Fractional increase of electrical conductivity and Young's modulus of a piece of an SWNT paper sample relative to their values before irradiation with low doses of Ar ions. (b) Fractional shifts in the frequencies of Raman D (1310 cm<sup>-1</sup>), G<sup>+</sup> (1585 cm<sup>-1</sup>), and D\* (2600 cm<sup>-1</sup>) modes of a piece of the same sample, as a function of Ar irradiation dose. The lines in (a) and (b) join the data points (the lines on the right extrapolate to data points at a dose of  $5.5 \times 10^{12}$  ions/cm<sup>2</sup>). (c) Increase in the intensity ratio I(d)/I(g) for the D and G modes on irradiation. From Ref. 167.

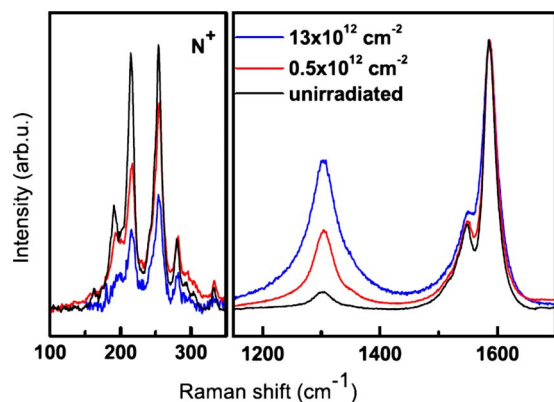


FIG. 50. (Color online) Raman spectra of an unirradiated SWNTs sample and of samples irradiated by 30 keV N ions with different irradiation doses. Resonant breathing modes (left panel) and the D ( $1300\text{ cm}^{-1}$ ) and the G ( $1590\text{ cm}^{-1}$ ) bands (right panel). From Ref. 375.

doses up to  $5.5 \times 10^{12}$  ions/cm<sup>2</sup>, all these properties show similar peaks as a function of irradiation dose. Small irradiation doses gave rise to an increase in conductivity and mechanical properties of the sample, which could be interpreted as evidence for irradiation-induced interconnection of nanotubes or functionalization of SWNTs at irradiation-induced defects by various chemical species due to the contacts with air accompanied by chemical doping. Experiments<sup>383</sup> also indicated that thermal annealing of tunneling barriers between individual nanotubes by heat released during collisions of energetic ions with the target atoms may be a possible reason for the improvement in conducting properties, although irradiation-mediated adsorption/desorption of various molecules and cross-linking could also contribute to the observed changes in conductivity. Although the role of ion beam heating on the SWNT mats and their Raman spectra, Fig. 50, has been studied<sup>375</sup> later on, the reason for the observed increase in mechanical properties and conductivity remains unclear, as both functionalization and cross-linking may contribute to the observed phenomena.

### 3. Light ions: Proton irradiation of carbon nanotubes

Several experiments<sup>36–38,384</sup> on irradiation of SWNTs with high energy (a couple of MeV range) protons were recently carried out. Both purified SWNTs<sup>36,37</sup> and those assembled as a NBP<sup>385–387</sup> representing a highly interconnected network of SWNT bundles<sup>384</sup> were irradiated. Effects of proton irradiation on nanotubes embedded into a polymer matrix were studied as well.<sup>38</sup> In addition to fundamental aspects of energetic proton interactions with highly anisotropic carbon-based nanomaterials, the interest in the response of nanotubes to proton irradiation was stimulated by the possible use of nanotubes in space applications, in particular, as components of solar cells.<sup>384</sup>

SWNTs deposited onto TEM grids for subsequent analysis were irradiated<sup>36</sup> in air at room temperature with 3 MeV protons with doses ranging from  $6\ \mu\text{C}$  to  $0.72\ \text{mC}$ , or correspondingly, from  $1.2 \times 10^{13}$  to  $3 \times 10^{16}$  protons/cm<sup>2</sup> (the beam diameter was reported to be 4 mm). Evident morphological changes such as curving of SWNTs and formation of short pieces were observed at doses of about 0.1 mC. Further

irradiation resulted in nearly full amorphization of the nanotubes (a significant fraction of the tubes were still present as pieces of different lengths). Based on the results of the experiments, it was concluded that for the typical near-Earth space condition during “quiet sun” periods (typical proton energies of around 1 GeV, much lower fluxes) SWNTs will undergo no detectable alterations for practically unlimited time.

A  $0.5\ \mu\text{m}$  thick SWNT film and a similar one placed below a  $16.75\ \mu\text{m}$  Xe film were irradiated at 15 K with 1 MeV protons.<sup>37</sup> The maximum irradiation doses were  $9.6 \times 10^{14}$  and  $5.5 \times 10^{14}$  protons/cm<sup>2</sup>, respectively. The analysis of the irradiated samples done by Fourier transform infrared and Raman spectroscopy evidenced formation of CH bonds and defects in nanotubes, accompanied by some changes in nanotube diameters.

Effects of proton irradiation on optical properties of SWNTs matrixed in poly(3-octylthiophene) were investigated<sup>38</sup> by an optical absorption technique. Two interband transitions were observed, at 0.71 and 1.28 eV in a sample that was subject to 2 MeV proton irradiation to fluences ranging between  $5.0 \times 10^{10}$  and  $5.6 \times 10^{15}$  protons/cm<sup>2</sup>. The results indicate that proton irradiation to fluences as high as  $5.6 \times 10^{15}$  has little effect on the interband transitions in carbon nanotubes. However, small radiation-related degradation has been observed as judged by the broadening of the interband transition spectra and by the reduction of the RBM intensity observed by Raman scattering.

The radiation tolerance of NBP was also analyzed in the context of the application of nanotubes in space photovoltaic applications in combination with quantum dots.<sup>384</sup> Irradiation with 2 MeV protons caused the room temperature resistivity of the NBP samples to increase nearly linearly up to a fluence of  $7 \times 10^{16}$  protons/cm<sup>2</sup>. Based on the comparison of the irradiation-induced changes in NBP resistivity (the defects in the samples were not characterized at the microscopic level), it was concluded that the sensitivity of the nanotube paper falls between that of individual nanotubes and graphite. This was a somewhat unexpected result, for systems such as NBP which are composed of radiation-soft components [recall that nanotubes are radiation-soft themselves; irradiation dose of  $3 \times 10^{16}$  protons/cm<sup>2</sup> resulted in complete amorphization and fracture of SWNTs (Ref. 36)]. It was also concluded that the solar cells based on quantum dots and NBP paper should be five orders of magnitude more resistant to radiation damage than the conventional bulk solar cells.

As seen from the experimental results, irradiation doses  $\leq 10^{17}$  protons/cm<sup>2</sup> should completely amorphize the samples. However, the estimates of the radiation damage in SWNT created by protons with such energies and doses using the TRIM code<sup>177</sup> give dpa (displacement per atom) values of around  $10^{-4}$  (Ref. 388). This value means that on average, one atom out of 10 000 was displaced during irradiation. Obviously, this is not enough for sample amorphization, and the nuclear stopping can be excluded. The electronic stopping for 1 MeV protons is some two to three orders of magnitude larger than the nuclear one, but the

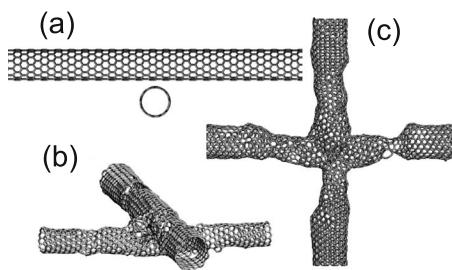


FIG. 51. Two crossed carbon nanotubes before irradiation (a). Atomic networks of (10,10)&(12,0) and (10,10)&(10,10) nanotubes [panels (b) and (c), respectively] welded together by energetic Ar ions, as simulated (Ref. 389) with the EP MD method.

nanotubes are excellent heat and charge conductors, so that the deposited energy should be quickly redistributed over the sample. Note that for the typical metals such as copper irradiated with light ions, the TRIM code gives dpa values<sup>182</sup> which are at least in qualitative agreement with the experiments. Although chemically reactive species (such as water and oxygen radicals which appear due to irradiation) may be present in the system and play some role, similar to irradiation of nanotubes with low-energy electrons<sup>365</sup> or ultraviolet light,<sup>54</sup> the precise mechanism of the damage creation by high energy protons is unknown at the moment.

#### 4. Welding of nanotubes by ion beams

As discussed in Sec. V C 5, a focused electron beam can be used<sup>18</sup> for welding nanotubes together at high temperatures. As MD simulations<sup>389</sup> pointed out, ion irradiation combined with high-temperature annealing should also result in welding of crossed nanotubes, both suspended and deposited on substrates, see Fig. 51. For the latter, the optimum Ar ion energies were predicted to be about 0.5 keV, whereas the optimum irradiation doses should be about  $10^{15}$  ions/cm<sup>2</sup>. Higher doses will result in heavy damage of the carbon network.<sup>389</sup>

The theoretical predictions were corroborated later on by experiments. Irradiation of overlapping nanotubes with 10 keV Ga ions with doses up to  $10^{16}$  ions/cm<sup>2</sup> resulted in the welding of nanotubes,<sup>23</sup> see Fig. 52. Similar results were obtained with 50 keV carbon ions,<sup>390</sup> although the irradiation

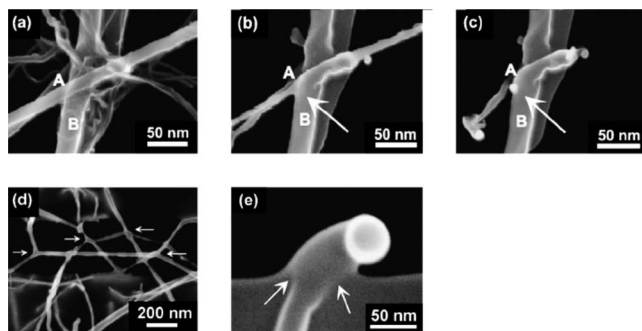


FIG. 52. SEM micrographs of overlapping nanotubes marked A and B, (a) prior to irradiation, and after exposure to (b)  $10^{16}$  and (c)  $2 \times 10^{16}$  ions/cm<sup>2</sup> of 10 keV Ga ions. (d) An example of a nanotube network formed by several welds indicated by arrows. (e) SEM micrograph showing a nanotube welded to the edge of the SiN membrane (see the arrows) by exposure to  $10^{17}$  ions/cm<sup>2</sup> of 30 keV Ga ions. From Ref. 23.

dose of  $10^{15}$  ions/cm<sup>2</sup> used converted the tubes into amorphous rods. As the experiments,<sup>23,390</sup> were carried out at room temperature, irradiation of nanotubes at higher temperatures and/or subsequent annealing should minimize the amount of damage in the nanotubes.

The welding of the MWNTs has been realized at elevated temperature by 40 keV Si ion beam irradiation.<sup>391</sup> It was found that both the irradiation dose and temperature greatly affect the welding of the MWNTs. At the irradiation dose of  $5 \times 10^{16}$  Si ions/cm<sup>2</sup>, the formed MWNT junctions had well-ordered structure at the temperature range of 600–850 K. This work gives another confirmation that ion irradiation technology combined with heating can be used for interconnecting nanotubes in future nanodevices.

#### 5. Ion-irradiation-induced links between nanotubes and substrates

As simulations predict,<sup>175,270</sup> ion irradiation of supported nanotubes should result in the pinning of the nanotubes to metallic and graphite<sup>175</sup> substrates, as well as to Si (Ref. 270) surfaces. This should happen through the formation of chemical bonds between the nanotube and substrate atoms near irradiation-induced defects (by saturating dangling bonds), thus increasing the nanotube-substrate adhesion.

MWNTs were experimentally welded to SiN substrates.<sup>23</sup> The experiments<sup>392</sup> also showed that electrical contact resistance of MWNTs deposited on gold contact fingers can be decreased by orders of magnitude when the contact areas are selectively exposed to the electron beam in a SEM. The local focused electron beam irradiation was also reported<sup>393</sup> to make good thermal contacts between the nanotubes and platinum nanofilm sensors. Thus one may hope that ion irradiation will improve not only mechanical but also electronic/thermal properties at the interfaces between the tubes and the environment.

#### 6. Irradiation-mediated doping of carbon nanotubes with foreign atoms

Chemical doping of nanostructured carbon systems such as carbon nanotubes, fullerenes, and peapods is a possible route toward controllable modification of their structural, mechanical, and, first of all, electronic properties. Doping may be implemented by intercalating foreign atoms into the open space in the carbon network<sup>394–396</sup> or by substituting the host atoms with impurities.<sup>218,397–405</sup>

As for substitutional doping, much attention has recently been given to the doping of nanotubes with boron and nitrogen atoms. This is a natural choice of the dopant, as B and N atoms are the neighbors of C in the Periodic Table and thus have roughly the same atomic radius as C, while they possess one electron less or more than C, respectively. Several methods based on arc-discharge techniques<sup>399,406</sup> and substitutional reactions<sup>401</sup> have been developed for doping. Unfortunately, instead of occupying the substitutional sp<sup>2</sup> position in the graphitic network, a substantial part of the dopant is chemisorbed<sup>407</sup> on the nanotube surface or binds to irregular carbon structures in sp<sup>3</sup> sites.<sup>399</sup> Problems with incorporating

B atoms into the carbon lattice of nanotubes have also been reported.<sup>406</sup> All of these issues further limit the applicability of these techniques.

Low-energy ion-irradiation was suggested<sup>267,408</sup> as an alternative way to introduce B/N impurities into nanotubes. The simulations<sup>267,408</sup> showed that up to 40% of the impinging ions can occupy directly the  $sp^2$  positions in the nanotube atomic network. Ion beams have been successfully used to implant  $N^+$  ions into graphite<sup>409</sup> and fullerene solids,<sup>410</sup> so the technique was also expected to work with nanotubes.

Indeed, doping of nanotubes with N atoms through irradiation was implemented experimentally.<sup>31,411–413</sup> SWNTs were bombarded with low energy [70 eV (Ref. 411) and 500 eV (Ref. 31)]  $N_2^+$  ions. XPS experiments showed that the N 1s core level spectra for N-doped nanotubes could be interpreted in terms of two peaks related to  $sp^2$  and  $sp^3$  hybridization of N atoms in the C network. AFM nanoindentation of the irradiated tubes also provided evidence for the appearance of  $sp^3$ -hybridized bonds, as manifested by an increase in hardness. Overall, the experimental results were in line with the theoretical predictions.<sup>267,408</sup> Overall, the results indicated that irradiation-mediated doping of nanotubes is a promising way to control the nanotube electronic and even mechanical properties due to impurity-stimulated cross-linking of nanotubes.

In addition to substitutional doping, MD simulations<sup>268</sup> also demonstrated that intercalation of K atoms into the open space of nanotubes can be achieved by means of irradiation. The formation of clusters from the implanted potassium atoms was studied as well. It was found that for MWNTs with one to three shells, the highest ratio of K atoms in clusters per total number of K ions should be obtained at irradiation energy of about 100 eV. Such low energies should also minimize the damage created in nanotubes by energetic ions.

### 7. Carbon nanotubes as masks against ion irradiation

Another quite interesting application of irradiation of nanotubes on metallic substrates has been reported. Experiments demonstrated that ion bombardment and nanotubes may be employed for fabricating metal NWs using MWNTs as masks.<sup>414</sup> By irradiating with 300 eV  $Ar^+$  ions, a Au/Ti wire about 10 nm in width has been formed underneath a MWNT lying on a thin Au/Ti layer deposited earlier on a  $SiO_2$  substrate.<sup>414</sup> The key idea is illustrated in Fig. 53.

After forming the NW due to metal layer sputtering everywhere except for the area beneath the nanotube, the MWNT could be removed by an atomic force microscope (AFM) or dissolved. Because nanotubes are micrometer-long and nanometer-wide objects and since they can be positioned very accurately using the AFM by pushing them mechanically,<sup>415</sup> the described technique may potentially be employed for developing a large and complicated network of metal NWs.

A computational study<sup>281</sup> was done to estimate the theoretical limit for the minimum width of a metal NW which could be produced using this method. MD simulations of Ar ion irradiation of MWNTs showed that the bombardment results in the sputtering of carbon atoms from the MWNT,

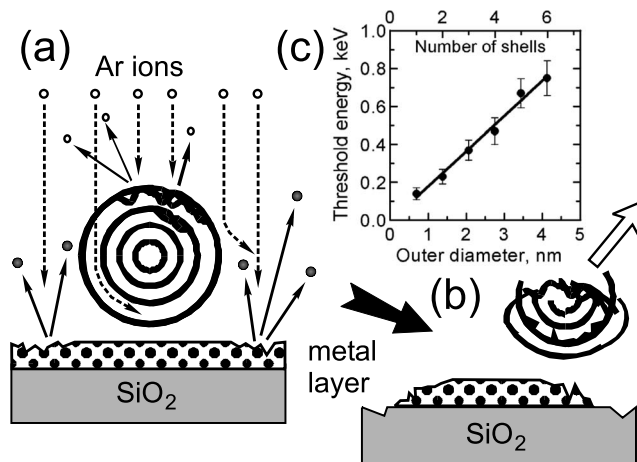


FIG. 53. Schematic illustration of the setup for using MWNTs as masks against ion bombardment. (a) Before irradiation, a nanotube has been deposited on a thin metal layer on a  $SiO_2$  substrate. Ion irradiation results in sputtering of metal atoms and nanotube amorphization. (b) After irradiation the nanotube can be removed by AFM. (c) Threshold energy of incident ions (the maximum energy at which no energetic recoil hit the area below the nanotube) as a function of tube outer diameter (number of shells).

formation of vacancies on the MWNT walls, and insertion of interstitial atoms between the shells. High irradiation doses lead to the complete amorphization of the MWNT, but the amount of  $sp^3$  bonds is very small, which is in agreement with experimental results.<sup>159</sup> By estimating the sputtering yield from a MWNT (notice that the yield is lower for carbon than for typical metals) and taking into account the thickness of the metal layer, a universal equation was derived which for a given NW material allows one to estimate the theoretical limit on the minimum width of the wire as a function of the original thickness of the metal layer. It was shown that this technique potentially provides a better resolution than the present-day electron beam lithography, although a low AFM operation speed prevents mass production of metal wires using nanotubes as masks against ion bombardment.

This setup may also be used for spatially selective ion implantation into the parts of the sample which have not been covered with nanotubes. Thus, the threshold energy of incident ions (the maximum energy at which no energetic recoil hit the area below the nanotube) is an important characteristic. The threshold energy as a function of the MWNT outer diameter (number of shells) was evaluated<sup>281</sup> for various MWNTs. The threshold energy was found to grow linearly with the number of shells, see Fig. 53(c). An analytical approximation was derived which makes it possible to estimate the minimum diameter of a MWNT needed to prevent the substrate below the MWNT from sputtering and ion implantation for a given energy of the incident ion.

### 8. Channeling of ions in nanotubes

The tubular shape of carbon nanotubes, as well as their hollow cores, high aspect ratio, and a low concentration of defects suggest another possible application for nanotubes: conduits for energetic ions.

This potential application of nanotubes is related to a phenomenon which is important for present-day semicon-

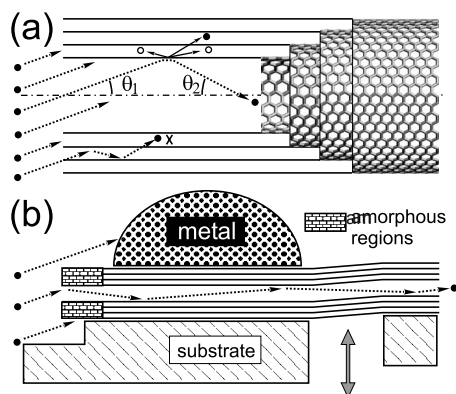


FIG. 54. (a) Schematic representation of a beam of Ar ions colliding with a multiwalled carbon nanotube with an open end. Depending on ion energy, impact point, and angle  $\theta_1$ , the ion hitting the inner shell of the tube can either remain in the core region or go through the shell. (b) The basic idea for a nanotube-based aperture. From Ref. 417.

ductor technology:<sup>84,416</sup> channeling of energetic ions through solids. When an energetic ion moves nearly parallel to a major axis or plane in a single crystal, it can be steered down the open channel between the aligned rows of atoms, thereby avoiding violent collisions with the host atoms and giving rise to deeper implantation and less lattice disorder.

The channeling of heavy ions with keV energies through MWNTs was theoretically studied<sup>417–419</sup> by MD simulations and within the framework of the classic electromagnetic theory.<sup>420</sup> It was shown that under certain conditions of the tube alignment with respect to the ion beam and of ion energies, the ions can efficiently channel through the empty cores of the nanotubes. Suggestions were made for making a nanotube-based conduit for energetic ions, which should work as an aperture and allow one to manipulate ion beams at the nanoscale, see Fig. 54. Note also that nanotubes have been suggested as possible conduits for atoms and molecules with thermal energies.<sup>421–423</sup> Extensions to higher energies of the particles might also result in developing other promising applications in biology and materials science. The main experimental challenge would be the stability of the tubes under irradiation, as defect formation will result in the accumulation of the displaced atoms in the nanotube core, which will quickly block the tube for the ions. Also, wall scattering has high probability for stopping low energy ions.

The channeling of carbon ions in nanotube bundles has been studied as well<sup>424</sup> by classical MD. The carbon ions were fired into the rope on the outside of the nanotubes in a direction almost parallel to the longitudinal axis. It was found that channeling takes place when the incidence angle is smaller than a critical angle and that the dependence of the critical angle on the energy follows an inverse square root function. The calculations also showed that the dependence of the critical angle on the energy is very similar for intra- and intertube channeling. The dependence of the critical angle  $\Psi_c$  on ion energy and mass was also addressed,<sup>425</sup> and the square root rules  $\Psi_c \sim E^{-1/2}$  and  $\Psi_c \sim M^{-1/2}$  were confirmed.

The motion of high energy light ions (protons) through freestanding SWNTs<sup>426–429</sup> and nanotubes embedded in various dielectric media<sup>430</sup> has received even bigger attention

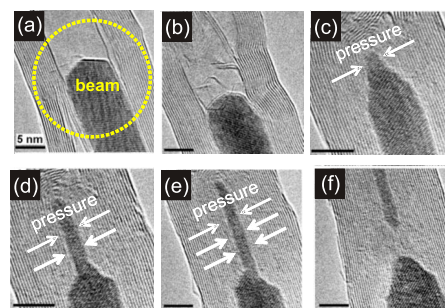


FIG. 55. (Color online) Typical evolution of a MWNT partly filled with a  $\text{Fe}_3\text{C}$  NW under electron irradiation with an electron beam (about 60 nm in diameter, more than the area schematically shown in the figure) and 200–400  $\text{A}/\text{cm}^2$  in intensity) during a total period of 50 min at a specimen temperature of 600 °C. (a) Tube before irradiation. [(b)–(e)] Irradiation leads to a collapse of the tube and deformation of the  $\text{Fe}_3\text{C}$  crystal. (f) Tube collapse cuts off the thinned  $\text{Fe}_3\text{C}$  crystal. Scale bars 5 nm. See Ref. 19 for details.

than that of heavy ions. The driving force for these studies was the possibility to use SWNT bundles for steering beams of high energy (GeV) protons, which would otherwise require cumbersome and expensive magnetic systems. However, despite an extensive theoretical analysis and first experimental results<sup>431</sup> it is not clear at all if nanotubes can in practice be used for this purpose, as the sample may quickly be destroyed by the beam, as experiments on proton irradiation of SWNTs indicate.

### E. Irradiated carbon nanotubes and onions as high-pressure cells

Another very interesting irradiation-induced phenomenon in carbon nanotubes and onions was recently reported.<sup>19,20</sup> When the shells of carbon onions or nanotubes contract due to irradiation-induced knock out of carbon atoms, followed by reconstructions of the atomic network (see Fig. 32), they should inevitably exert pressure on the material encapsulated inside the shells.

Controlled electron irradiation of MWNTs was demonstrated to cause large pressure buildup within the nanotube cores that can plastically deform, extrude, and break solid materials that are encapsulated inside the core. It had been earlier shown that closed-shell carbon nanostructures, such as carbon onions, can act as self-contracting high-pressure cells under electron<sup>6</sup> and ion<sup>284</sup> irradiation, and that high pressure buildup in the onion cores can even induce graphite-diamond transformations (see Ref. 72 for a review). However, it was not obvious that high pressure can be achieved inside nanotubes, as the difference in the geometry (cylinder versus sphere) may have been critical for pressure buildup.

MWNTs encapsulating Fe,  $\text{Fe}_3\text{C}$ , or Co NWs were irradiated<sup>19</sup> in a TEM with a field emission gun and an acceleration voltage of 300 kV at a temperature of 600 °C. Figure 55 shows the evolution of a nanotube partly filled with a  $\text{Fe}_3\text{C}$  NW under irradiation. The initial configuration is presented in Fig. 55(a) Irradiation of the section at the end of the wire leads to a nonuniform collapse of the tube. The hollow noncollapsed part of the tube fills up with graphitic filaments [Fig. 55(b)]. Carbon material migrates from the open side of the channel and aggregates at the end of the

Fe<sub>3</sub>C wire by closing the inner hollow with graphene sheets. Therefore, the number of shells increases locally. The tube now collapses in the region of the carbide crystal by deforming the crystal. The diameter of the Fe<sub>3</sub>C wire decreases from 9 to 2 nm while the solid carbide is squeezed through the hollow core downward along the tube axis, as in an extrusion process. The final collapse of the tube pinches and cuts off the thinned wire [Fig. 55(b)]. The compressive effect is also manifested in a decrease in lattice spacing between graphitic shells and in the encapsulated crystal.

Qualitatively similar results were obtained for Co crystals. Note that the collapse of the tubes and the extrusion of encapsulated material occurred only under electron irradiation, not under heating. Additional heating of the specimen by the electron beam was negligible because the rate of inelastic energy loss of the electrons is low and nanotubes are excellent heat conductors, so the transferred energy could dissipate into the environment.

Atomistic computer simulations by the DFTB method and continuum theory modeling shed light on the origin of the pressure. As discussed in Sec. V A 5, knock-on displacements of carbon atoms due to energetic electrons create vacancies and interstitials in the nanotubes. SVs are mobile enough<sup>216</sup> to form divacancies (see also Fig. 16), which are energetically favorable over SVs. DVs are essentially immobile even at 600 °C, as their migration energy is more than 5 eV. On the contrary, carbon interstitial atoms between the shells of MWNTs are highly mobile and can easily migrate away from the irradiated region, so it was assumed that no interstitials were left in the irradiated area, and that only DVs were present. Calculations of the atomic structure of free-standing (without encapsulates) nanotubes with various numbers of DVs showed contraction of the nanotube due to reconstructions of the atomic network, Fig. 56(b). For nanotubes encapsulating materials, this should exert pressure on the material inside. As the carbon-carbon covalent bond is very strong, one can expect a substantial pressure buildup, before the tube breaks.

Very recently carbon onions were used as extrusion cells.<sup>20</sup> Au, Pt, Mo, and W crystals of a few nanometers in size were encapsulated inside graphitic shells by coevaporation in an arc discharge<sup>432</sup> and irradiated with electrons (300 keV) in a temperature range of 300–1000 °C in the heating stage of a TEM. Under intense electron irradiation in a wide beam, the particles became spherical due to surface stress, which is exerted by the graphitic shells upon the removal of atoms and reconstruction. Then the electron beam was focused onto a spot of 2 nm in diameter and directed onto a point at the projected circumference of the graphitic shells. After 10–20 s, this caused a hole<sup>366</sup> (2–3 nm in diameter) through which the material under pressure could escape. Then the beam diameter was spread again over the whole particle. During the continuing collapse of the shells,<sup>19,432,433</sup> pressure was built up and the solid metal was gradually extruded through the hole, Fig. 57. Due to the slow contraction of graphitic shells, the deformation occurred on a scale of 0.1–1 nm/s. This made it possible to study the stability of NCs in detail under continuous load. The correlation with atomistic simulations showed that the observed slow plastic

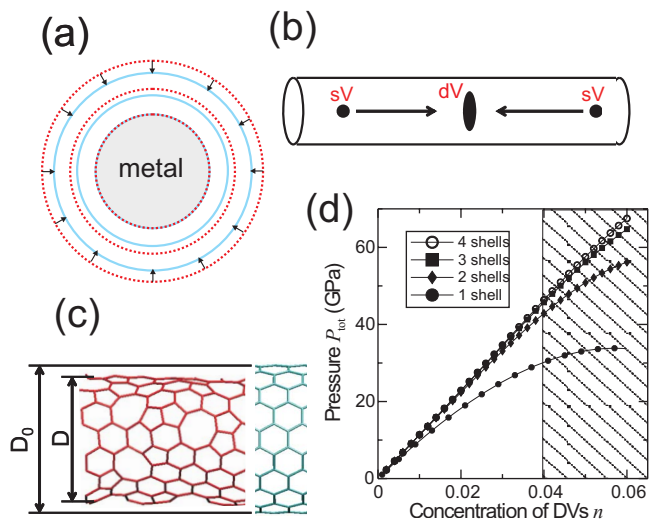


FIG. 56. (Color online) Pressure buildup inside carbon nanotubes. (a) Schematic cross section of a MWNT contracting (indicated by the small arrows) because of the removal of atoms from the shells (solid circles) under the electron beam. The dashed circles indicate the shells in the pristine tube. The inner core of the tube is filled with an incompressible material. (b) Formation of DVs from SVs due to SV migration and coalescence. (c) Atomic networks of a pristine (10, 10) (right) and irradiated nanotube (left). Note a decrease in the average tube diameter due to the reconstruction of the atomic network near vacancies. (d) Pressure inside a SWNT and MWNTs with different numbers of shells as a function of DV concentration. The hatched area corresponds to a high concentration of DVs, which may cause breakup of the tube walls and loss of pressure.

deformation is due to dislocation activity. The results also provided evidence that the vacancy concentration in a nanoscale system can be smaller than in the bulk material.

Simulations<sup>19,20</sup> showed that pressure inside irradiated nanotubes and onions can be as high as 40 GPa, only an order of magnitude below the pressure in the center of Earth (~360 GPa) or the highest pressure that has been achieved in diamond anvil cells (~400 GPa). However, phase transformations in many materials are within this range. Moreover, the advantage of the technique is that the evolution of the system can be monitored *in situ* with high spatial and temporal resolution, as the experiment is carried out inside the TEM. This technique can also be used for creating and studying new phases of materials which can exist only at the nanoscale and at high pressures.

Concurrently with electron irradiation of nanotubes with encapsulates, an experiment similar in spirit was carried out.<sup>297</sup> MWNTs with typical diameters of 20–30 nm and encapsulating nickel nanorods were irradiated with high energy (100 MeV) Au<sup>+7</sup> ions. TEM studies of the irradiated samples

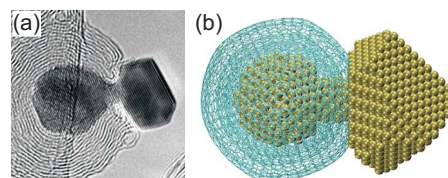


FIG. 57. (Color online) Extrusion of metals from carbon onion due to the irradiated-induced pressure buildup. (a) TEM image of a partly extruded gold crystal. (b) Schematic illustration of the process and simulation setup. From Ref. 20.

showed that irradiation resulted in a decrease in the interplanar spacing of nanotube walls and nickel (111) planes. The effect was relatively weak, as the irradiation dose was small (of the order of  $3 \times 10^{13} \text{ cm}^{-2}$ ), and because irradiation was done at room temperature, which was not enough for efficient annealing of defects in nanotube walls, and thus high pressure was not generated. Contrary to Ref. 19, irradiation-induced defects in the metal rods were reported. This is particularly interesting, as the energy loss rate in the metal (through electronic stopping) was not high enough to produce defects in Ni. More studies are necessary to understand the mechanism of damage production in the nanoscale composite nanotube-metal systems.

## F. Influence of defects on the properties of nanocarbon systems

### 1. Mechanical properties

The atomic structure of MWNTs, SWNTs in bundles, and other macroscopic forms of nanotubes such as NBP is governed by two kinds of atom-atom interaction: short-ranged covalent bonding between the C atoms within the graphene planes and long-ranged vdW-type interactions between atoms in different SWNTs or different shells in MWNTs. The covalent interaction is very strong; the carbon-carbon covalent bond in graphite and nanotubes is one of the strongest bonds known. At the same time, vdW interactions are three orders of magnitude weaker. Due to different types of interactions and highly anisotropic atomic structure, carbon nanotubes have anisotropic mechanical properties. The axial properties, such as Young's modulus  $Y$ , are excellent ( $Y \sim 1 \text{ TPa}$ , Ref. 434), while the properties associated with the vdW forces (e.g., the bending modulus of a nanotube bundle<sup>10</sup>) are much worse. The strength of macroscopic materials is also very low, as tubes can easily slide with respect to each other.

As shown in Sec. V B, either electron or ion irradiation results in the formation of defects in nanotubes. These defects, especially vacancies, have a deleterious effect—deterioration of axial mechanical properties of nanotubes, as computer simulations<sup>291,354,435–438</sup> indicate. Experiments<sup>10</sup> showed that during electron irradiation with doses over  $50 \times 10^{20} \text{ e/cm}^2$ , the bending modulus started decreasing, which was understood in terms of the damage accumulation in SWNTs, and thus, a noticeable drop in the Young's (axial) modulus of individual tubes.<sup>353,354</sup> Simulations demonstrated that small vacancies (from one to three missing atoms) relatively weakly affect  $Y$  (Ref. 354). Due to the quasi-1D structure of individual nanotubes, the effect of vacancies on the tensile strength and critical strain of nanotubes proved to be much stronger (20%–30%, Refs. 354 and 435). Interestingly enough, the theoretical fracture strength of nanotubes with point defects is still much higher than the experimental values for supposedly pristine tubes.<sup>439</sup> This discrepancy can be attributed<sup>435</sup> to the presence of large-scale defects, such as those that may arise from oxidative purification processes. Indeed, by omitting chemical treatments from the sample preparation process, and thus avoiding the formation of defects, the tensile strength of MWNTs was increased by a

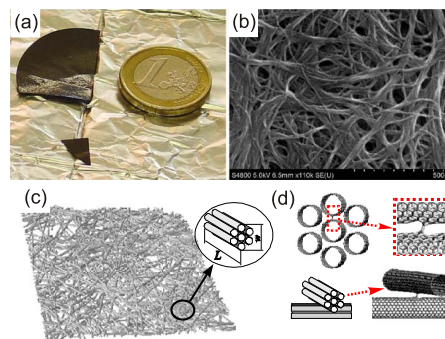


FIG. 58. (Color online) (a) Image of SWNT bucky paper on aluminum foil compared in size with a 1 Euro coin. (b) SEM image of the same sample. Courtesy of K. Arstila. (c) Nanotube mats used in simulations (Ref. 266) and schematic representation of an individual bundle. (d) Molecular models of nanotubes with irradiation-induced covalent bonds between two tubes in the same bundle and in different bundles.

factor of 3 (Ref. 8) as compared to previous experiments. The measured values of about 100 GPa were close to the theoretically predicted values of 90–120 GPa.<sup>354,435</sup>

At the same time, irradiation may give rise to irradiation-induced covalent bonds between tubes, Fig. 11. Thus, provided that the drop in the axial properties is not that big, the overall strength of the nanotube material may increase. Assuming that the axial mechanical properties remain roughly the same under moderate irradiation, formation of covalent bonds between nanotubes in a bundle would increase the Young's modulus of the bundle,<sup>353</sup> in agreement with the experimental results,<sup>10</sup> and its tensile strength (assuming that only the outermost nanotubes in the bundle are clamped and that inner shells in pristine samples do not carry mechanical load). Likewise, a small amount of defects can increase the interlayer shear strength of MWNTs by several orders of magnitude,<sup>440</sup> which would have a strong effect<sup>271,441</sup> on the failure of nanotubes by the sword-in-sheath mechanism. In agreement with theoretical predictions, recent experiments<sup>308</sup> on the telescopic motion of MWNTs demonstrated that irradiation-induced SVs at the telescopic interface lead to an increase in friction, but annealing of defects restores smooth motion of the sliding shells. Moreover, electron irradiation of MWNTs at 200 keV led to improvements in the maximum sustainable loads by more than an order of magnitude.<sup>8</sup> This effect is attributed to cross-linking between the shells, so that the mechanical load was shared between the shells. In a standard tensile strength measurement, the load is carried out only by the outermost shell, and when it breaks, the tube is fragmented by the sword-in-sheath mechanism.

Irradiation can also increase the tensile strength of macroscopic nanotube products, such as NBP,<sup>266</sup> Fig. 58. Due to a low density (or correspondingly, high porosity  $\sim 80\%$ , Ref. 386) and weak interactions between the bundles, the experimentally measured tensile modulus, strength and strain to failure of the NBP mats proved to be several orders of magnitude smaller<sup>385,387</sup> than those for individual nanotubes. Simulations demonstrated that the stiffness and tensile strength of NBP and nanotube fibers<sup>442–444</sup> can be substantially (several orders of magnitude) increased by irradiation. Physically, an increase in stiffness is mainly due to

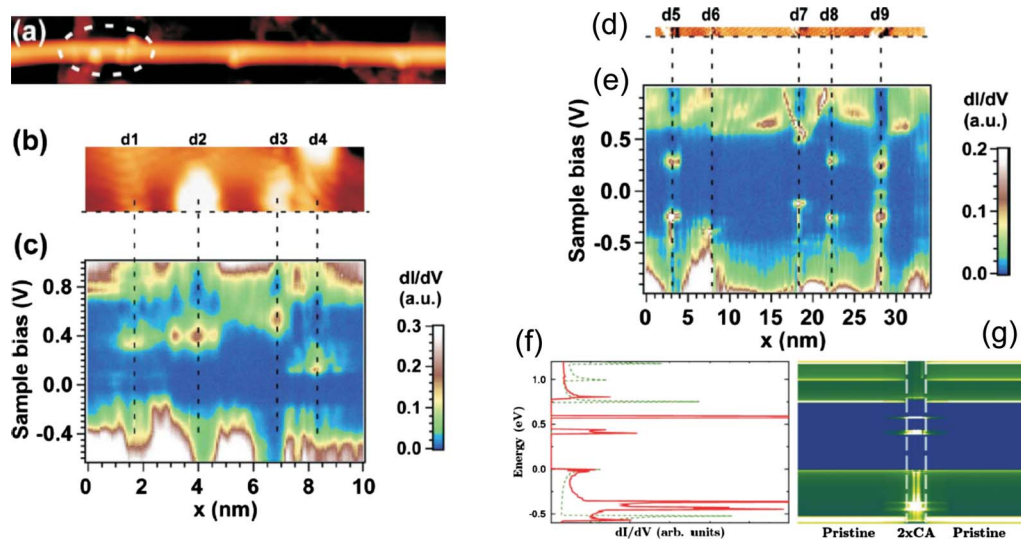


FIG. 59. (Color online) STM/STS images of semiconducting SWNT exposed to 200 eV Ar ions. (a) STM topography image. (b) Detailed image of the tube section with defect sites d1–d4 inside the dashed ellipse drawn in panel (a). (c)  $dI/dV$  scan, which can be associated with the local density of states, recorded along the horizontal dashed line. Irradiation gave rise to defects which are manifested by single peaks in the band gap. (d) STM/STS images of a segment of another semiconducting SWNT with five defect sites d5–d9. (e)  $dI/dV$  scan recorded along the horizontal dashed line, see Ref. 452 for details. Examples of simulations: (f) Local density of states near two carbon adatoms on a (10,0) SWNT. (g) The corresponding calculated  $dI/dV$  scan.

irradiation-induced intertube covalent bonds at the bundle contact areas, Fig. 58. Several experiments indeed indicate that Young modulus of SWNT bucky paper can be increased due to irradiation,<sup>167,383</sup> as discussed in Sec. V D 2. Thus, irradiation may have overall beneficial effect on the mechanical properties of nanotubes.

## 2. Electronic properties

As demonstrated in numerous theoretical studies<sup>11,445–451</sup> the presence of even a small number of defects can have a strong effect on electron transport in nanotubes, due to their quasi-1D structure. Experiments<sup>11,21</sup> also indicate that irradiation-induced defects strongly affect the resistivity of the samples, which normally increases by several orders of magnitude, depending on the original sample perfection and the conductivity regime.

For macroscopic oriented SWNT ropes, the effect of irradiation proved to be more complicated.<sup>48</sup> A minimum in resistivity as a function of irradiation dose was found, which was interpreted to be a result of a twofold effect of the irradiation: the formation of covalent bonds between tubes in a bundle due to broken bonds in the tube walls and the amorphization of the sample at high dose.

Irradiation-induced defects affect the local electronic structure of the tubes near the Fermi level, as assessed by ESR.<sup>49,50</sup> As mentioned in Sec. V D 2, spatially localized Ar ion irradiation of individual MWNTs (Ref. 25) creates defective regions that represent potential tunnel barriers for electrons in the MWNT. A double-barrier structure fabricated by such method can work as a quantum dot. Spatially localized ion irradiation has also been used for the fabrication of a single-electron inverter in MWNTs.<sup>26</sup>

Spatially localized ion irradiation can also be used for local controllable modification of the electronic structure of carbon nanomaterials. With regard to semiconducting carbon nanotubes, individual irradiation-induced defects produced

by Ar plasmas were shown to give rise to single and multiple peaks in the band gap of the nanotubes, and a similar effect has been demonstrated when several defects are close to each other<sup>452</sup> (Fig. 59). Similar effects were observed after H-plasma treatment of SWNTs.<sup>453</sup> Defect-induced states in the gap of semiconducting nanotubes can have important implications in SWNT-based photonics and quantum optics in the light of recent observations of exciton localization in SWNTs due to the presence of disorder.<sup>454</sup>

Ion irradiation has also been used to change the characteristics of NBP. An increase in sample conductivity was reported<sup>167</sup> under 30 keV Ar ion irradiation with doses of about  $1 \times 10^{12}$  ions/cm<sup>2</sup>. This could be interpreted as evidence for irradiation-induced interconnection of nanotubes or functionalization of SWNTs at irradiation-induced defects by various chemical species due to the contact with air accompanied by chemical doping. Further experiments<sup>383</sup> indicated that thermal annealing of tunneling barriers between individual nanotubes by heat released during collisions of energetic ions with the target atoms may be a possible reason for the improvement in conducting properties. By contrast, high energy irradiation of the samples with 23 MeV C<sup>4+</sup> ions did not give rise to any enhancement in conductivity.<sup>455</sup> An increase in electrical conductivity of carbon nanotube sheets irradiated with Ar and H ions at a temperature of 800 K has also been reported.<sup>456</sup> The conductivity improvement was associated with the formation of covalent cross-links between nanotubes induced by the ion beam irradiation at the elevated temperature. Although the reason for the observed increase in conductivity remains unclear (as both functionalization and cross-linking may contribute to the observed phenomena), overall, defects, and thus irradiation, can also be used in a beneficial way to tailor the nanotube electronic properties and improve the functionality of the nanotube-based devices.

### 3. Magnetic properties

Observations of ferromagnetism in various metal-free carbon systems, such as polymerized fullerenes and graphite,<sup>285,457–460</sup> have stimulated much experimental and theoretical research work on the magnetic properties of all-carbon systems, for an overview, see Ref. 461 and references therein. The driving force behind these studies was not only to create technologically important, light, nonmetallic magnets with a Curie point well above room temperature, but also to understand a fundamental problem: the origin of magnetism in a system which traditionally has been thought to show diamagnetic behavior only.

The observed magnetism may originate from defects<sup>462,463</sup> in the graphitic network such as undercoordinated atoms, e.g., vacancies,<sup>303,464–468</sup> interstitials,<sup>469</sup> carbon adatoms,<sup>316</sup> and atoms on the edges of graphitic nanofragments with dangling bonds either passivated with hydrogen atoms<sup>470–472</sup> or free.<sup>471,473</sup> Structural defects, in general, give rise to localized electronic states, a local magnetic moment, flat bands associated with defects and thus to an increase in the density of states at the Fermi level, and eventually to the development of magnetic ordering. Magnetism may also originate from impurity atoms which are nonmagnetic by themselves, but due to unusual chemical environment, e.g., due to bonding to defects in the graphitic network, give rise to local magnetic moments, or from a combination of both. It should be pointed out that magnetic impurities, e.g., Fe atoms, cannot be the origin of the observed magnetism, as the measured concentration of magnetic impurities is much too low.<sup>461</sup> Moreover, it was recently demonstrated<sup>474</sup> that irradiation with hydrogen or iron ions with energies in the MeV range produced different effects on graphite. Only proton irradiation gives rise to magnetism, while implanted Fe ions result in paramagnetic behavior.

Irradiation of graphite with protons<sup>58,474</sup> resulted in a significant ferromagnetic response, which was explained in terms of vacancy-hydrogen interstitial atom complexes.<sup>303</sup> High energy (100 keV) nitrogen ion irradiation of nanosized diamond (which is graphitized at high irradiation dose), followed by magnetic measurements on the doped samples, showed ferromagnetic order at room temperature.<sup>57</sup> The magnetic moment observed was in a good agreement with the results of DFT simulations,<sup>269,475</sup> which reported net magnetic moments at several N-interstitial defect configurations. In addition to hydrogen and nitrogen, reports<sup>476</sup> on the appearance of magnetic signal after irradiation of graphite with carbon ions have recently appeared.

## VI. IRRADIATION EFFECTS IN BORON NITRIDE (BN) NANOSYSTEMS

Boron nitride nanostructures, such as BN nanotubes,<sup>477,478</sup> fullerenes,<sup>260,261</sup> and individual sheets<sup>479,480</sup> have the same atomic structure as their carbon counterparts, but alternating B and N atoms substitute for C atoms in graphenelike planes with almost no change in atomic spacing. The interest in BN nanotubes and related structures has been large due to the fact that the BN tube is always an insulator with a band gap of about 5.5 eV, independent of

tube chirality and morphology,<sup>481</sup> in contrast to C nanotubes which can be metallic or semiconducting. Besides, layered BN structures have outstanding mechanical properties comparable to those of carbon nanotubes, but are more thermally and chemically stable.<sup>481</sup>

In spite of their technological importance and the necessity to know the behavior of these materials in an irradiation-hostile environment, the effects of electron and especially ion irradiation on BN nanostructures have been scantily studied. At the same time, very little information relevant to defect production in BN nanostructures under irradiation can be deduced from the experiments on irradiation of bulk hexagonal and cubic BN systems<sup>482–484</sup> or thin BN films.<sup>485</sup> Nevertheless, although the data on the response of these nanomaterials to different kinds of irradiation are quite fragmented, in this section, we try to analyze the available experimental and theoretical results and make conclusions on the general behavior of BN nanosystems under impacts of energetic particles.

### A. Electron irradiation

Numerous experiments carried out in a TEM working at a voltage of 300 kV showed that BN MWNTs are more resistant to electron irradiation than their carbon counterparts. An electron irradiation dose that completely amorphized a carbon MWNT created almost no visible damage to BN nanotubes.<sup>486</sup> This is an unexpected result, as the structure of BN and C nanotubes is the same (except for a higher polygonization degree in BN nanotubes), and atomic masses of B and N are close to that of C. Moreover, as discussed in Sec. VI C, simulations of displacement energies of B and N atoms from BN nanotubes and sheets gave lower values than in the corresponding C systems.<sup>212</sup> At the same time, the stability of BN SWNTs appears to be roughly the same as, or lower than, that of their carbon counterparts.

Moreover, low-dose irradiation was reported<sup>487</sup> to even give rise to the annealing of defects formed during the growth of the nanotubes. If the walls of a pristine BN nanotube exhibited numerous undulating, dangling BN sheets and irregular spacing between adjacent BN layers, striking changes in their morphology occurred with increasing irradiation time. The tubular BN sheets became straight and aligned in the direction of the initial tube growth, while almost complete ordering of the nanotube shells occurred. The origin of this effect is not fully understood. Beam heating is normally quite low, except for the situation when the irradiated object is loosely connected to its environment or the beam is focused onto a very small area. Longer irradiation times of BN MWNTs resulted in gradual amorphization of BN shells,<sup>488</sup> as shown in Fig. 60, and then in the complete destruction of the nanotube morphology, leaving the material with the consecutive appearance of a near-amorphous BN rod and rectangular onionlike nanoparticle.

The effects of electron irradiation on BN nanotubes were recently studied<sup>489</sup> at length in a TEM operating at a voltage of 200 kV. It was demonstrated that electron irradiation of BN MWNTs can be used to cut the tubes by displacing B and N atoms. The response of BN nanotubes to electron irradiation

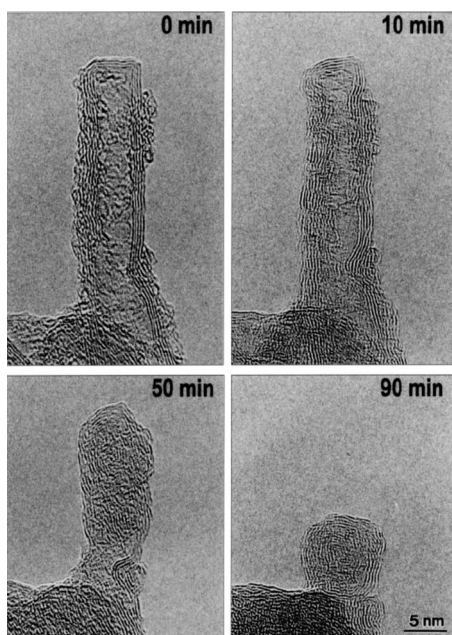


FIG. 60. Consecutive TEM images demonstrating structural changes of a BN MWNT into a nested, highly defective octahedral-like BN onion under electron irradiation with a approximately  $30 \text{ A cm}^{-2}$  current density at 300 kV. The irradiation time is shown on the figure panels. From Ref. 487.

tion at low (104 K) temperatures was studied as well.<sup>489</sup> Surprisingly, amorphization was not observed at low temperatures after considerable irradiation. Based on this result, the authors argued that the damage production and annealing mechanisms in BN nanotubes are different from those in carbon nanotubes where the sample temperature is a major factor in irradiation response. However, BN nanotubes have not yet been irradiated at high temperatures, and future experiments and simulations should shed light on the mechanisms of point defect production under irradiation at elevated temperatures, defect evolution, and annealing.

Very recently, the response of single BN sheets (structural analogs of graphene membranes) to electron irradiation was studied simultaneously by two groups.<sup>490,491</sup> The samples, composed of few BN layers, were prepared by peeling bulk hexagonal boron nitride as in Ref. 479 and deposited on TEM grids. Further thinning was performed in the TEM by sputtering BN layers one by one. Irradiation of a single sheet gave rise to formation of single and multivacancies, Fig. 61. Boron SVs were found to be preferably formed and the dominating zigzag-type edges were proved to be nitrogen terminated. Prolonged irradiation gave rise to formation of large holes with a triangular shape as N atoms with dangling bonds near B-vacancies could easily be displaced, which resulted in the growth of vacancy clusters. No evidence for SW defects or reconstructed vacancies was found, as such defects would have involved B–B and N–N bonds, which are less favorable than B–N bonds. DVs were not reported either. It is interesting to note that similar results were obtained in TEMs operating at different voltages (80 kV was used in Ref. 491 and 120 kV in Ref. 490). In the former case, the voltage was higher than the displacement threshold of boron while lower than that of nitrogen,<sup>212</sup> (see also Fig. 62) so that the selective knock out of B atoms can

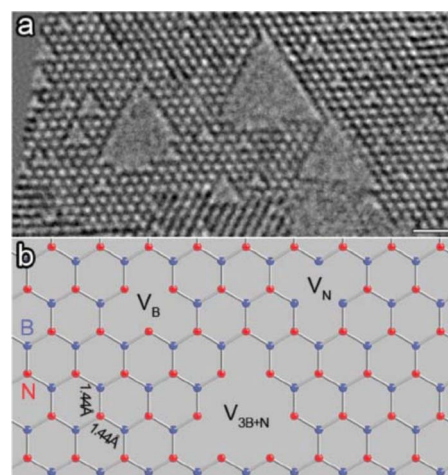


FIG. 61. (Color online) Atomic defects in h-BN monolayer. (a) A typical HRTEM single frame showing the lattice defects in h-BN such as SVs and larger vacancies, all of which are triangular in shape with the same orientation. (b) Models for the atomic defects in h-BN.  $V_B$  and  $V_N$  stand for boron and nitrogen SV, respectively. Note that the  $V_B$  and  $V_N$  should have an opposite orientation, while the  $V_B$  and  $V_{3B+N}$  (missing three boron and one nitrogen atoms) are in the same orientation and surrounded by two-coordinated nitrogen atoms. Scale bar is 1 nm. Reprinted from Ref. 490

naturally be understood. However, boron SVs also dominated even when a 120 kV acceleration voltage was employed, higher than the threshold for either boron or nitrogen. Besides, it is not fully clear why triangle-shape (not hexagon-shape) holes appeared. This means that the displacement thresholds should be calculated by a more sophisticated technique, and the mechanism of damage creation requires further studies.

## B. Ion irradiation

In contrast to electron irradiation, the influence of ion irradiation on BN nanomaterials has not been studied at all. The only experiment,<sup>492</sup> which was recently carried out, indicated that BN MWNTs subjected to 40 keV  $\text{Ar}^+$  ion beam are amorphized at irradiation doses of  $\sim 10^{15} \text{ cm}^{-2}$  (Fig. 63) and that the amount of damage can be considerably reduced if the sample is kept at elevated temperatures (600 °C.) The irradiation dose at which amorphization occurred corresponded to  $\sim 2.5 \text{ dpa}$ , which is close to the values typical for the amorphization of carbon nanotubes. Overall, the results provided evidence that multiwalled BN nanotubes have similar or even better stability under heavy ion irradiation than their carbon counterparts.

As for high energy irradiation corresponding to the regime of electronic stopping, no data have been reported, and future experiments should shed light on the behavior of BN nanostructures under swift ion bombardment. The comparison of the response of C and BN nanotubes to high energy irradiation should be particularly interesting, as the electronic structure of BN tubes (wide band gap semiconductor) may give rise to new effects as compared to carbon nanotubes (metals, narrow band gap semiconductors).

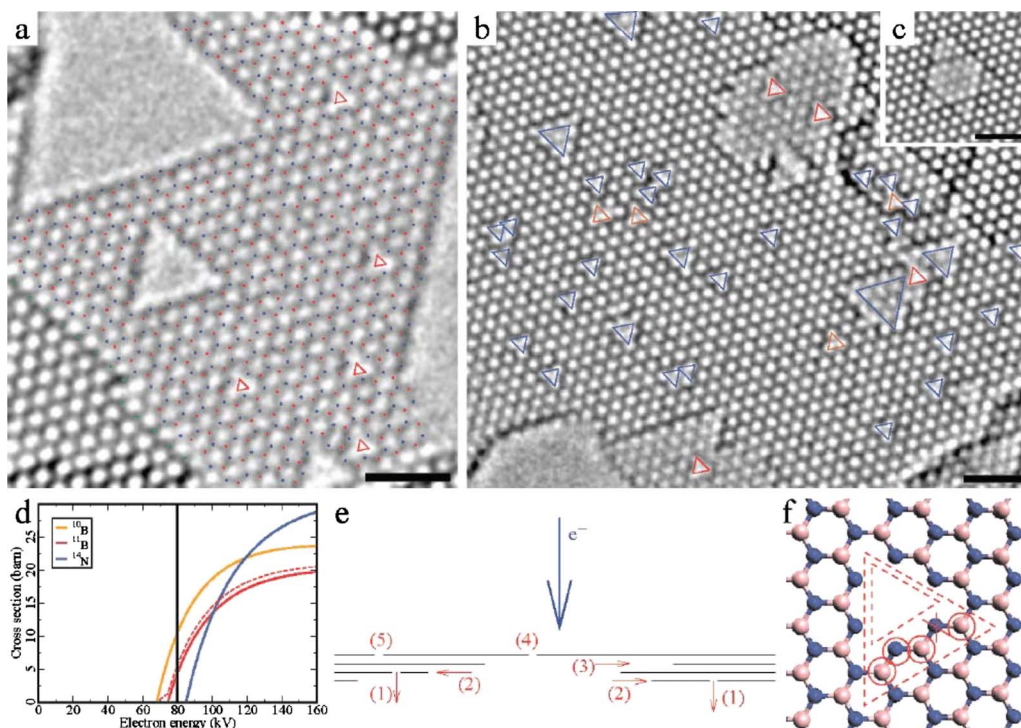


FIG. 62. (Color online) Radiation damage mechanism in h-BN membranes. (a) Single-layer h-BN membrane. All isolated vacancies (one missing atom; red triangles) exclusively appear on the same sublattice. The orientation of the triangle-shaped holes is maintained as the holes expand. The more stable element in the bulk (blue dots) is also the edge termination. Also the edge of the second layer (lower left corner, green dots) is terminated by the same element. (b) A mostly two-layer h-BN membrane in the same sample. Here, all SVs appear on the other sublattice (blue triangles), with few exceptions (brown). Red triangles are again vacancies in single-layer regions. (c) Triangles growing in opposite orientation in two adjacent layers of a three-layer h-BN membrane. (d) Total knock-on cross sections for B and N atoms vs. electron energy for h-BN membranes. Red dashed line is the average, weighted by relative abundances, for the two B isotopes. (e) Schematic of the damage mechanism. (1) Individual atoms are sputtered off on the exit surface layer. (2) Holes grow from these defects, predominantly within the layer. (3) Edges can even recede behind an adjacent layer, as seen in panel (c). (4) Vacancy in the last layer. (5) Exception case of an atom sputtered off on the beam entrance surface, identified as such because it remains in the last layer at a later time. (f) Growth of oriented holes from vacancies. We start with the smaller triangle-shaped hole (inner dashed line), which is terminated with the blue atoms, and rather stable in the beam. After random removal of an edge atom (crossed out in red), all two-coordinated red and single-coordinated blue atoms that are formed in the process (red circles) are quickly removed too. The result is again a blue-atom terminated triangle-shaped hole with the same orientation (outer dashed line). Scale bars (a)–(c) are 1 nm. Reprinted from Ref. 491.

### C. Theory of point defects in BN nanotubes

It was realized already at the early stages of BN nanotube investigations<sup>481</sup> that pristine BN nanotubes normally are more defective than their carbon counterparts. TEM studies revealed numerous cross-links between the shells of BN MWNTs, dislocations, and polygonizations of the tube cross sections possibly due to intershell covalent bonds, etc. Point defects such as vacancies likely exist in nonirradiated nanotubes as well, although there is no direct experimental evidence for their presence.

However, point defects should be created by energetic electron and ion beams. SW defects may also appear under

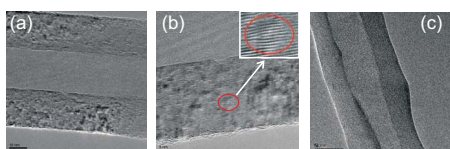


FIG. 63. (Color online) TEM images of BN MWNTs irradiated with 40 keV Ar ions. (a) Ion dose  $2 \times 10^{13} \text{ cm}^{-2}$ . Black areas correspond to the areas damaged by the ion beam. Irradiation gives rise to interrupted shells and dislocations, as shown in panel (b). Such defects are also common in pristine nanotubes, but their density in irradiated tubes is much higher. (c) High-dose irradiation ( $10^{15} \text{ cm}^{-2}$ ) resulted in the complete amorphization of nanotube walls, but the tubular structure was still preserved. From Ref. 492.

large tension, as simulations<sup>493</sup> indicate. Thus the properties of point defects in BN nanosystems have been studied in a considerable body of theoretical papers<sup>212,494–500</sup> within the framework of DFT.

The formation energies of B and N SVs ( $E_{sv}^B$  and  $E_{sv}^N$ ) have been calculated by several authors for BN nanotubes<sup>494,497,500,501</sup> and monolayers.<sup>495,497,498</sup> The formation energies (with neutral charge states) can be defined as

$$E_{sv}^X = E(K-1) + \mu_X - E(K), \quad (5)$$

where  $E(K)$  is the total energy of the system composed of  $K/2$  N and  $K/2$  B atoms,  $\mu_X$  is the chemical potentials (which generally depends on the environment conditions) for atom X, where  $X=N$  or B, cf. Eq. (4). It should be pointed out that for binary systems such as BN nanotubes the vacancy formation energy can be defined in different ways, since several reference states corresponding to different chemical potentials are possible.

For example, if the energy of an isolated  $N_2$  molecule is chosen as the reference, then  $\mu_N = E(N_2)/2$ , where  $m E(N_2)$  is the total energy of the  $N_2$  molecule. One can say that  $E_{sv}^N$  defined this way corresponds to a nitrogen-rich system.<sup>501</sup>

For N-rich systems, one can further assume that the BN nanotube is in equilibrium with the  $N_2$  gas. The chemical potential for the B atom,  $\mu_B$ , is then fixed by the growth condition

$$\mu_B + \mu_N = \mu_{BN}^{\text{tube}} \quad (6)$$

When the system is grown in a B-rich condition, the hexagonal structure of bulk B can be taken as the reference state.<sup>501</sup> Then the B chemical potential is defined by  $\mu_B = \mu_B^{\text{bulk}}$  and the N chemical potential is fixed by relation (6). Other authors chose the  $B_{12}$  cluster as the reference state,<sup>212,497</sup> which obviously gave different (although close) numbers for defect formation energies. Besides, the energy of an isolated N or B atom was taken as the corresponding chemical potential in Ref. 494, which does not allow one to estimate the thermodynamic concentration of defects, but only the relative abundance of B and N vacancies.

The formation energies of vacancies for N (N-rich systems) and B (B-rich systems) proved to be in the range of 7–9 eV. It was also found that, similar to the case of carbon nanotubes,<sup>216,298</sup> the energies are smaller for nanotubes with small diameters,<sup>494,497</sup> approaching the limit of a single BN sheet for large diameter nanotubes.<sup>497</sup>

It was also found that the formation of DVs (note that the BN DV can be considered as an intimate vacancy pair example of a Schottky defect pair, i.e., a pair of oppositely charged defect centers) from two SVs is energetically favorable.<sup>497</sup> Moreover, once a vacancy forms, the formation energy for a subsequent neighboring vacancy is close to zero; thus the probability of forming a second neighboring vacancy is higher than at any other site. This strong driving force suggests that vacancies in irradiated BN nanostructures will likely appear as boron-nitrogen pairs, in spite of the appearance of homonuclear bonds.<sup>497</sup> It should be pointed out, however, that very recent experiments<sup>490,491</sup> on electron irradiation of BN sheets did not provide any evidence for the existence of DVs.

Within the framework of a DFT-based TB model, both single and DVs were found<sup>497</sup> to give rise to new states in the gap. SVs introduce half-filled shallow acceptor states and they may be expected to act as electron acceptors. The electronic structure of the neutral DV was reported to be different from those of SVs with no half-filled shallow state available. It was argued that the optical properties and conductivity of BN nanostructures may be altered by the presence of DVs, and the new states should be readily detectable via optical spectroscopy.<sup>497</sup> Later first-principles simulations<sup>496,502–504</sup> confirmed the appearance of new states in the gap and specified the positions of the corresponding peaks in the electronic density of states. It is interesting to note that both B and N SVs were reported to induce spontaneous magnetization.<sup>502,503</sup> The same effect was theoretically found in BN nanoribbons,<sup>505</sup> which can be viewed as structural analogs of graphene nanoribbons.<sup>363</sup>

SW defects which may be formed due to the incomplete recombination of Frenkel pairs were also shown to exist in BN nanostructures.<sup>493,494,506</sup> The formation energy of these defects is a function of tube diameter and it is about 5 eV for nanotubes with diameters about 1 nm,<sup>493,494</sup> lower than the

energies for SVs. Note, however, that in contrast to the situation for graphene, SW defects have not been found in single BN sheets irradiated in a TEM.<sup>490,491</sup>

The migration of vacancies in hexagonal boron nitride layers has been studied as well.<sup>500</sup> This issue is of particular importance for understanding the response of BN nanostructures to prolonged irradiation, as migration of point defects should govern the annealing of irradiation-induced defects. DFT and TB simulations<sup>500</sup> gave the migration barriers for B and N vacancies about 3 and 6 eV, respectively. The DVs with a migration barrier of about 5 eV (for the B atom motion) can also become mobile at high temperatures.

The migration barriers for vacancies in BN nanostructures are higher than those in carbon systems, see Sec. V B 6, due to two types of atoms present. Large barriers point out that the higher stability of BN MWNTs under prolonged electron irradiation (as compared to carbon nanotubes) may likely be due to a higher mobility of interstitial atoms between the shells, which results in an efficient recombination of Frenkel pairs. However, at the moment there are no reliable data on the mobility of B and N interstitials in the h-BN bulk systems and BN nanotubes. Note also that this mechanism of defect annealing should not work for BN SWNTs, since a considerable number of atoms are sputtered in this case, so that few interstitials are available for recombination with vacancies.

In the context of triangular-shape vacancy-type defects produced by electron irradiation in BN sheets,<sup>490,491</sup> the energetics and electronic structure of multiatomic vacancies was recently studied<sup>507</sup> by DFT methods as well. It was found that the energetics of vacancies (up to four missing atoms) strongly depends not only on the environmental condition of boron and nitrogen chemical potentials but also on electron chemical potentials of these systems. The triangular vacancy comprised of one nitrogen and three boron atoms was reported to be a geometrically favorable structure under nitrogen- and electron-rich conditions. Such structures were indeed experimentally found in BN sheets after electron irradiation. However, as defects appeared under nonequilibrium conditions, and moreover, BN sheets may have been positively charged due to electron knock out, further studies are required to fully understand the formation of multivacancies in BN sheets under high-dose electron irradiation.

## D. Boron and nitrogen atom displacement energies

The response of a system to irradiation strongly depends on the threshold displacement energies  $T_d$  (also referred to as emission threshold energies) for the atoms the system is composed of, as discussed in Sec. V A 5 by the example of carbon nanosystems. The displacement energies of B and N atoms from BN sheets and nanotubes were computed through the TB method and by using the simulation setup described in Sec. V A 5 for various orientations of the initial velocity vectors of the atom with respect to the atomic network.<sup>212</sup> For a BN sheet, calculations gave the following values for the threshold values, corresponding to the atom emission direction perpendicular to the plane:  $T_d^N = 14$  eV and  $T_d^B = 15$  eV. A higher value of  $T_d^C = 23$  eV was obtained

for a graphene sheet, which indicates that BN sheets should be less stable under electron irradiation than graphene. Note, however, that the value for graphene appears to be overestimated, as the atom sputtering mechanism was considered as a pure knock-on process without any beam-induced electronic excitations. The excitations can reduce the bonding energy between the struck atom and the lattice by promoting the electrons to antibonding states and, in turn, reduce the kinetic energy necessary for atom emission.

A difference of about 1 eV between the most favorable emission energy for N and B atoms was reported. This corresponds to different formation energies for the vacancies: B and N vacancies in a BN sheet have formation energies of 11.22 and 8.91 eV, respectively.<sup>497</sup> However, the atomic mass dependence of the transmitted energy calculated within the McKinley–Feshbach model<sup>184</sup> results in a higher threshold electron beam energy for N atoms at which atom emission occurs. A beam energy of 74 keV corresponds to a maximum energy transfer of 15 eV for a B atom and the emission conditions are satisfied. However, for the same beam energy, the maximum energy transferred to a N atom is only 11.6 eV, lower than the minimum emission energy threshold. Emission conditions for nitrogen are only satisfied by increasing the incident electron energy to 84 keV. Thus, for beam energies between 74 and 84 keV, emission conditions are only satisfied for boron atoms, whereas above 84 keV, nitrogen atoms can also be sputtered. These theoretical results seem to be corroborated by recent experiments<sup>490,491</sup> carried out in an aberration-corrected TEM operating at 80 keV: vacancies were created on one sublattice only, and the displaced atoms were indeed B atoms. The rapid sputtering of B atoms followed by displacement of the neighboring N atoms under prolonged irradiation resulted in triangle-shaped holes with sharp edges. Note, however, that boron SVs also dominated even at a acceleration voltage of 120 kV,<sup>490</sup> indicating that the mechanism of damage creation requires further studies.

As for the effects of the atomic network curvature on the threshold displacement energy of B and N atoms and the total cross section in BN nanotubes, the behavior of the system appears to be the same as for carbon nanotubes. Lower formation energies of vacancies in nanotubes with small diameters<sup>494</sup> should result in smaller threshold energies than in BN sheets. The total knock-on cross sections for B and N atoms in a single-walled BN nanotube as functions of their position around the tube circumference are shown in Fig. 64. Similarly to the case of carbon nanotubes, at low beam energies it is much easier to displace a B or N atom from the area of a tube which is perpendicular to the beam direction than from the side part of the tube (parallel to the incident beam). At high beam energies, the cross section is maximal in sections parallel to the beam.

### E. Engineering boron nitride nanosystems with the electron beam

Similar to carbon nanostructures, it has been demonstrated that electron irradiation in a dedicated TEM can be used for engineering the atomic structure and thus properties of BN nanosystems.

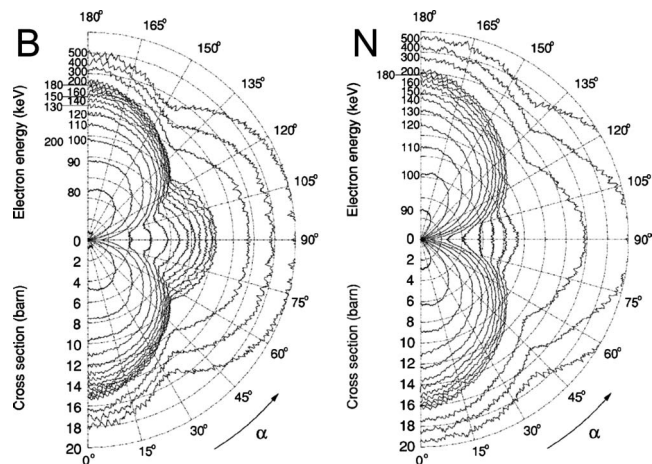


FIG. 64. Total knock-on cross sections for B and N atoms in a single-walled BN nanotube as functions of their position around the tube circumference. From Ref. 212.

Cutting and thinning of BN MWNTs by a focused electron beam was recently demonstrated<sup>489</sup> as for carbon nanotubes.<sup>45,338,365</sup> Electron beam cutting was observed when a focused electron beam with a diameter much smaller than the tube diameter was used. Cutting was accompanied by the formation of nanoarches, as seen in Fig. 65. It was also shown that irradiation of BN MWNTs can be used to form sharp crystalline conical tips. The formation of a conical tip under irradiation was reported when a shaped, disk-like, electron beam with a diameter comparable to the nanotube was used. The tip formation was driven by layer peeling and by the collapse of the inner walls of the nanotube, which was different from the formation of nanoarches observed during cutting. It was suggested that a combination of shaping and cutting can be used to fabricate atomically sharp tips for field emitters, nanoimaging, and manipulations.

The thinning of BN samples composed of few BN layers was demonstrated,<sup>490,491</sup> so that even a single BN sheet could be manufactured. This was done by sputtering BN layers one by one, as it is much easier to displace an atom from the last layer (with regard to the beam direction which was perpendicular to the layers) than from a layer in the middle of the sample.

It was also shown that electron irradiation can be used as a nanoelectron-lithography technique allowing the controlled reshaping of single walled BN nanotubes.<sup>499</sup> The required irradiation conditions were optimized on the basis of total knock-on cross sections calculated within density functional

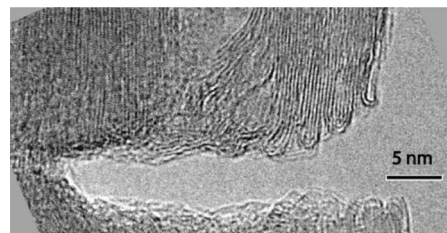


FIG. 65. Multiwalled BN nanotube partially cut. A small electron beam with a diameter of 3 nm was used to make the cut. Nanoarches can be seen along the cut surface in the BN nanotube.

based methods, as discussed in Sec. VI D. It was then possible to induce morphological modifications, such as a local change of the tube chirality, by sequentially removing several tens of atoms with a spatial resolution of about 1 nm.

Bearing self-organization aspects of irradiation of nano-systems in mind, it worth mentioning that the formation of small BN cage-like molecules under electron-irradiation experiments of BN samples was reported.<sup>508</sup> Depending on the starting material, either close-packed agglomerates of small fullerenes, or small nested fullerenes (onions) with up to six layers were found as irradiation derivatives. The diameters of the smallest and most observed cages were in the range from 0.4 to 0.7 nm, and were close to those of the  $B_{12}N_{12}$ ,  $B_{16}N_{16}$ , and  $B_{28}N_{28}$  octahedra which were predicted to be magic clusters for the BN system. Formation of BN fullerenes with a reduced number of layers (typically less than 3) and rectangle-like shapes due to electron irradiation was also demonstrated<sup>260</sup> at 20 and 490 °C.

## VII. EFFECTS OF IRRADIATION ON NANOWIRES (NWS)

The effects of particle irradiation on NWs—other than carbon or BN nanotubes—have been studied from many different points of view. Although nanotubes can of course be considered a type of NW, the crucial difference between C and BN nanotubes and most other NWs is that the former are hollow in the middle, whereas the latter are filled with atoms. In this section, we treat specifically NWs which are not hollow in the middle, but contain material at approximately the bulk density everywhere up to their side surfaces and ends.

NWs can be made in a wide variety of different ways,<sup>509</sup> such as growth,<sup>510</sup> the vapor-liquid-solid (VLS) approach,<sup>511</sup> etching away material to form nanopillars, using focused ion beams (FIBs) for selective growth,<sup>512</sup> elongation of nanoclusters,<sup>513</sup> or by sputtering material into grooves.<sup>514</sup> They can also be made of all classes of materials and may not be circular but also flattened in cross section (nanobelts or nanoribbons).<sup>509</sup> Hence, in contrast to the case of carbon nanotubes, it is hardly possible to give almost any common characteristics of how NWs behave under irradiation, with the obvious exception that surface effects can be expected to be significant.

For the further discussion, we briefly review the VLS approach<sup>511</sup> for NW synthesis, as this is a quite versatile and widely used method to grow NWs.<sup>509,515–517</sup> In the VLS method, liquid nanoclusters of one material A are first formed on a surface. These are subsequently exposed to a vapor of another material B. Provided the phase thermodynamics is suitable, the nanocluster will become saturated in B, after which a layer of B can form on the surface. From this surface layer, a NW of B can start growing, pushing the liquid A nanocluster upwards. Thus continued growth of a NW can be achieved, and if the balance between the involved surface and interface free energies is suitable, the wire can grow straight indefinitely.<sup>515</sup>

NWs do differ from nanotubes in the respect that surface reconstructions can be expected to be important in them, whereas nanotubes normally have the pristine hexagonal structure. A wide range of surfaces in vacuum are known to

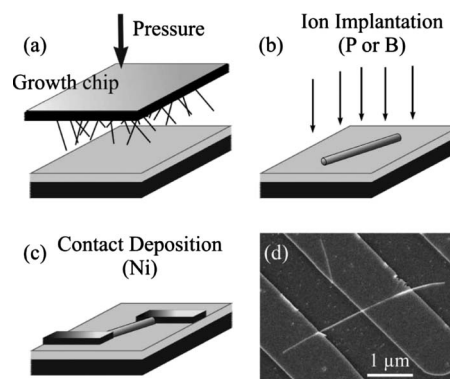


FIG. 66. Fabrication of Si NW FETs and their ion beam doping. From Ref. 65.

reconstruct, i.e., spontaneously rearrange the atom structure to lower the surface energy,<sup>518</sup> and thus it is natural to expect that NWs made out of the same material will also undergo reconstructions. The reconstruction can even determine the shape of the wire, for instance, the  $\{112\}$  surface of Si can reconstruct to a relatively low energy configuration<sup>519,520</sup> (see Fig. 78). Moreover, six different  $\langle 112 \rangle$  crystal directions can be perpendicular to a single  $\langle 111 \rangle$  direction. Hence Si NWs with the axis in a  $\langle 111 \rangle$  crystal direction be surrounded by six  $\{112\}$  planes and hence to be hexagonal in cross section.

In the following subsections, we review literature on some classes of NWs that have been either made or modified by ion, plasma, or electron irradiation. We do not review electron beam lithographic manufacturing of NWs on surfaces since this does not involve atom displacement processes (except maybe in the polymer mask). In general, we note that the topic of irradiation of NWs as compared to carbon nanotubes has to date been examined to a quite limited extent, considering how many different kinds of combinations of materials, radiation conditions and effects exist.

### A. Silicon-based NWs

The effects of energetic ions on the growth of Si NWs have been examined. Si NWs were manufactured with a plasma-ion assisted chemical vapor deposition approach, using Au nanoparticles as the VLS growth seed.<sup>522</sup> It was shown that the use of a plasma enhanced the growth. Formation of NWs on Si made possible by O implantation of the Si followed by annealing in an Ar gas was reported to lead to Si NWs with a small amount of oxygen.<sup>523</sup>

Pure silicon NWs have been doped to grow both *n*- and *p*-type field effect transistors (FETs) using P and B ion implantation,<sup>65</sup> Fig. 66. The NWs were grown by an Au-catalyzed VLS method and had 5–10 nm thick oxide shells surrounding a 10–20 nm diameter crystalline core. They were mechanically transferred to an oxidized Si wafer, and implanted with P and B with energies (7 and 2.5 keV, respectively) suitable to give a doping of the core of the NW. After the implantation, metal contacts were deposited on the wires and the electrical characteristics measured. Functionality as *n*- and *p*-type FETs was demonstrated. The NWs were disordered to a limited amount by the irradiation, but 800 °C

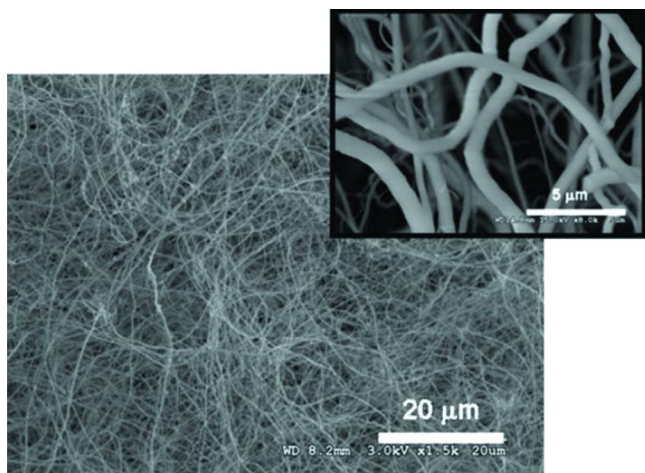


FIG. 67. (Color online) Silica NWs on Si. From Ref. 527.

was sufficient to achieve annealing.<sup>65</sup> FETs based on 70–150 nm Si NWs were fabricated with a similar Au-catalyzed VLS approach, and it was shown that 10 keV P ion implantation and subsequent annealing at 850–1000 °C temperatures could render them to work with clear *n*-type characteristics.<sup>524</sup>

Si NWs were also synthesized by thermal decomposition of SiO powder at 1320 °C in an Ar–H<sub>2</sub> ambient gas, and subsequently implanted with Ni or Co ions using a metal vapor vacuum arc (MEVVA) implanter at a voltage of 5 kV.<sup>525</sup> This resulted in a Ni–Si or Co–Si mixture in the top layers of the approximately 20 nm diameter wires. After annealing, the samples showed evidence of the formation of NiSi<sub>2</sub> surface layers and CoSi<sub>2</sub> nanoclusters.

Vertical doping, i.e., doping along the NW axis, was also demonstrated. By selecting combinations of suitable ion irradiation energies and species, the same kind of nanotube could be doped either to be *n*- or *p*-type on top and the opposite type in the lower parts. Electrical measurements showed that a single NW could act as a *p*-*n* junction with rectifying behavior.<sup>526</sup>

Silica (SiO<sub>x</sub>) NWs were made on Si substrates by sputter deposition of Pd on the surface, and subsequent annealing at 1100 °C for 4 h in an Ar atmosphere.<sup>527,528</sup> This treatment produced a dense network of randomly oriented silica NWs due to VLS growth from molten metal particles that formed from the sputter deposition,<sup>527</sup> see Fig. 67. The silica NW network was subsequently doped with 30 or 110 keV ErO molecular ions to introduce Er atoms into the NWs. Er is known to be optically active in bulk Si and silica, emitting efficiently around the 1.54 μm wavelength. The Er-implanted NWs showed an emission around the same wavelength, but with a photoluminescence (PL) intensity up to an order of magnitude stronger than that from bulk silica.<sup>527</sup> Furthermore, Au and Er coimplantation showed that Er could have a dual role of both catalyst and dopant.<sup>528</sup> In summary, ion implantation appears to be a very promising tool for modifying both the electrical and optical properties of silicon NWs.

## B. Implantation of compound semiconductor NWs

The compound semiconductors GaN and ZnO are interesting in that they have a relatively large band gap and can thus be used for emission of blue light. SiC is considered promising for high-power and high-temperature applications. NWs made of these materials are considered promising for 1D optoelectronic nanodevices and for applications requiring high radiation hardness such as space environments.

GaN NWs were grown on Si substrates by using an Au catalyst and a chemical vapor deposition (CVD) technique at 900 °C and ammonia as the reactant gas.<sup>529</sup> The NWs were subsequently implanted with 50 keV Ga. The implanted wires showed a blueshift in the PL emission compared to unimplanted wires, which was attributed to accumulation of N vacancies.<sup>529</sup>

The radiation hardness of GaN NW FETs made by electron beam lithography on Si wafers has also been studied. The NWs were grown by a direct reaction of gallium vapor with ammonia at about 900 °C.<sup>530</sup> The as-grown NWs had an interesting coaxial structure, with a 30–40 nm diameter wurtzite-structured core surrounded by a 20–60 nm zincblende outer shell. The authors showed that the GaN NW circuit resisted an irradiation fluence of  $3.3 \times 10^7$  125 MeV/amu Kr ions/cm<sup>2</sup>, a dose at which comparable conventional circuits failed. TEM investigations showed that the wires remained largely intact during the irradiations, with the exception of some strongly damaged regions at the surfaces.

ZnO NWs are also of interest with respect to radiation hardness because ZnO has already in the bulk phase considerably higher radiation hardness than even GaN, apparently due to major point defect recombination, even at low temperatures.<sup>531–535</sup> ZnO NW FETs were fabricated and irradiated with 35 MeV protons.<sup>536</sup> It was found that relatively low fluences in the range of  $(0.4–4) \times 10^{12}$  protons/cm<sup>2</sup> caused significant changes to the electrical characteristics of the FETs. This suggests that although damage levels in ZnO remain low, the electrical characteristics can be modified strongly (apparently an effect analogous to the case of carbon nanotubes where a single divacancy can affect the electrical characteristics of a long wire, see Sec. V D 2 b)

ZnO NWs were also subjected to Ti plasma immersion ion implantation (PIII) at pulse voltages of 5 and 10 kV, to a dose estimated to be  $5 \times 10^{14}$  ions/cm<sup>2</sup>, see Figs. 68 and 69.<sup>537</sup> Although some damage was visible in the NW, the crystal structure was clearly retained after the irradiation, as shown by the continuity of the lattice planes and the electron diffraction pattern in the figure. However, FETs manufactured from the NWs showed that the PIII decreased the resistivity of the wires by more than four orders of magnitude, showing that Ti irradiation can be efficiently used to tune the resistance of the wires. The irradiated “metallic” NWs with a resistivity around 10<sup>-2</sup> Ω cm were also reported to have a high current carrying capacity, with a maximal current density of  $2.75 \times 10^7$  A/cm<sup>2</sup>. In comparison, this is an order of magnitude higher than the current carrying capacity of noble metal lines,<sup>537</sup> but on the other hand carbon, nanotubes have been reported to have a current carrying capacity of up to

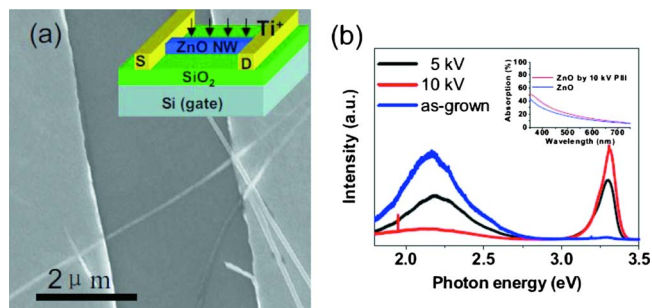


FIG. 68. (Color online) (a) SEM image of a ZnO NW FET, with a schematic inset showing the Ti plasma immersion ion implantation treatment. (b) PL spectra of the as-grown NW and after different Ti-PIII treatments. The inset shows the absorption of ZnO NWs before and after 10 kV Ti treatment. From Ref. 537.

$10^9$  A/cm<sup>2</sup>.<sup>538</sup> Also the optical characteristics of the NWs were changed by the irradiation, exhibiting a shift in the PL spectra from a peak at 2.2 eV to one at 3.3 eV, see Fig. 68(b).

ZnO light-emitting diodes were fabricated from 200 to 500 nm wide ZnO nanorods grown on tin-oxide coated sapphire surfaces by a vapor-phase transport method.<sup>539</sup> The nanorods were doped to *p*-type with 50 keV P ion implantation and subsequent annealing at 900 °C. An Au top electrode layer was fabricated by sputtering to obtain *p-n* homojunction diodes. The diodes were demonstrated to exhibit electroluminescence (EL) in the ultraviolet.<sup>539</sup>

The radiation tolerance of ZnO FETs was studied from a different point of view in a multilayer transistor setup where the NW was embedded below a SiO<sub>2</sub> passivation layer.<sup>540</sup> The NWs were irradiated with 10 MeV protons to fluences of  $10^{10}$  and  $5 \times 10^{11}$  protons/cm<sup>2</sup> [doses of 5.71 and 285 krad(Si)], corresponding to doses expected over 2 weeks and 2 years in low-earth orbit in space. SiO<sub>2</sub>-based transistor structures were found to be highly sensitive to the irradiations, with already the lower dose leading to strong changes in electrical characteristics. On the other hand, transistors where the gate dielectric was a self-assembled superlattice (SAS) organic material instead of SiO<sub>2</sub> were much less sensitive to the irradiation. The difference was attributed to the generation of significantly less bulk oxide traps and interface traps in the SAS under proton irradiation.<sup>540</sup>

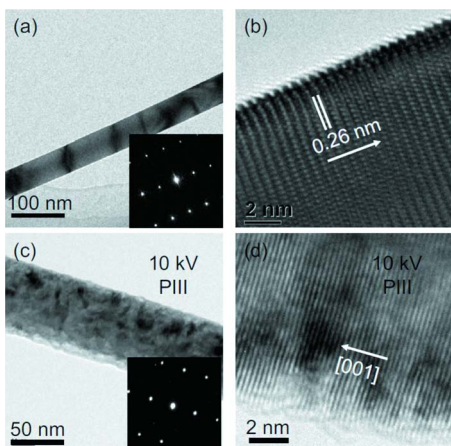


FIG. 69. (Color online) Atomic-resolution image of a ZnO NW before [(a) and (b)] and after [(c) and (d)] Ti plasma immersion ion implantation. From Ref. 537.

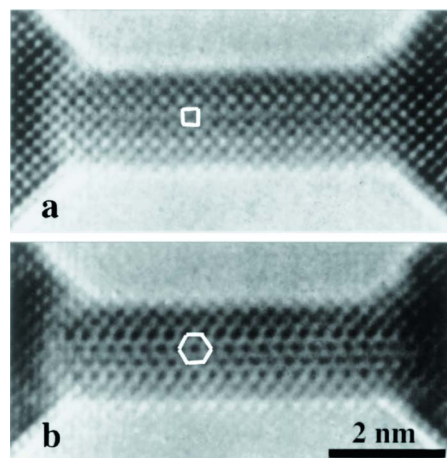


FIG. 70. (Color online) Atomic-resolution images of a gold NW formed by electron irradiation in an electron microscope. The white square and hexagon illustrate that one of the NWs has a square and the other one a hexagonal surface structure. From Ref. 544.

Er doping of ZnO NWs using 50 keV MEVVA ion implantation of Er to a dose of  $5 \times 10^{15}$  ions/cm<sup>2</sup> was examined with optical applications in mind.<sup>541</sup> After oxygen annealing at 800 °C, the implanted NWs were reported to retain a high crystalline quality and show room temperature luminescence at 1.54  $\mu$ m, suggesting the NWs could be used as functional units for optical communication applications.<sup>541</sup>

Hybrid silicon carbide-carbon NWs were prepared by irradiating carbon nanotubes with high fluence 40 keV Si irradiation employing a metal vapor vacuum arc ion source.<sup>542</sup> At doses of  $5 \times 10^{16}$  ions/cm<sup>2</sup>, the carbon nanotubes had transformed into an amorphous NW. XPS analysis showed the presence of Si-C covalent bonds, indicating formation of SiC. On the other hand, also Si-I bonds were observed, indicating oxidation due to a low vacuum level.<sup>542</sup> SiC NWs were also made in a very different way by first creating ion tracks with 450 MeV Xe ions in polycarbosilane films.<sup>543</sup> This causes cross-linking of the polymer and formation of a gel containing cylindrical nanostructures. By subsequently heating these NWs at 1000 °C in Ar gas, the precursor wires were transformed into SiC ceramic wires.

In summary, ion implantation can have a strong effect on both the electrical and optical properties of compound semiconductors. This can be used to adjust e.g., the resistivity of them in an, at least in principle, controllable manner.

### C. Electron beam modification

Similarly to the case of carbon nanotubes, electron beams (typically used *in situ* in an electron microscope) have also been used to manufacture and modify NWs. Gold NWs were for instance made by making holes into an initially 3 nm thick gold foil, forming NWs of 0.8–3 nm thickness between the holes,<sup>544</sup> similar to the case of cutting graphene to make nanoribbons (see Sec. V C 6). The NWs were proposed to have a structure of a hexagonal prism, with close-packed hexagonal layers on the outside, see Fig. 70.

NWs of different kinds were modified with electron beams.<sup>545</sup> Metal NWs were synthesized by electrochemical

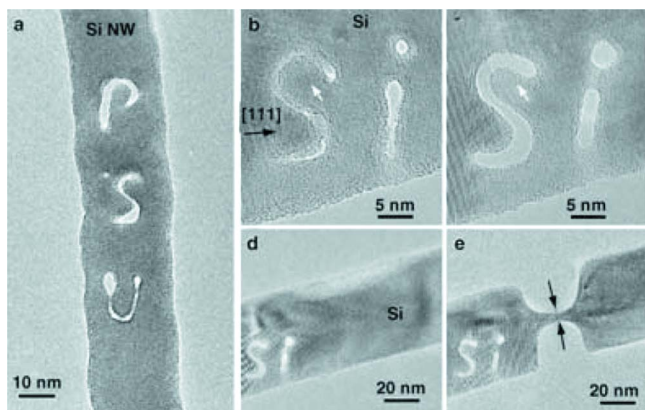


FIG. 71. (Color online) Writing of letters and cutting of Si NWs with a high-intensity electron beam in an electron microscope. From Ref. 545.

deposition, and Si NWs using Au particles as a catalyst. The authors irradiated Si, Au, Ag, Cu, and Sn NWs using a high-intensity electron beam and demonstrated the fabrication of holes, grooves, and even writing of hollow letters on Si NWs with a native oxide coating of about 2 nm and total thicknesses of tens of nanometers. The wires could also be cut in a localized region without modifying the surroundings (see Fig. 71). Also hole drilling and writing on metallic NWs was carried out. When metallic NWs were initially on top of each other, they could be welded together, similarly to welding of nanotubes (see Sec. V C 5). In hybrid systems, consisting of two different metal NWs next to each other, or a Si NW next to a metal one, the authors demonstrated the welding of the systems together to form a hybrid NW system. In the case of metals, intermetallics and alloys such as AuSn and AuSi were observed to be formed in the interface region.

Holes in MWNTs, Nb NWs and SiN membranes were made with a 200 keV electron beam in a TEM.<sup>360</sup> Multiple holes in a Nb NW were drilled, and it was found that grains of the material typically formed near the drilled holes.

Au/Si NW heterojunctions were examined under an electron microscope.<sup>432</sup> NW junctions were manufactured in a high-temperature vacuum furnace, forming Si NWs with Au rods inside. Electron irradiation of the Au near the end of the rod showed that the electron beam can induce flow of Au either into or away from the Si region, likely due to creation of mobile defects.

Ga<sub>2</sub>O<sub>3</sub> ribbon-shaped nanotubes with diameters of the order of 500 nm, which were partially or fully filled with an inner Sn NW, were fabricated using a high-temperature vacuum furnace with GaN and SnO precursors.<sup>546</sup> The inner Sn NWs were subsequently modified with an electron beam. The Sn NW, with a thickness of the order of 50 nm, was cut into two distinct parts, but also rejoining of the parts was demonstrated by utilizing beam-induced heating away from the original cut position.

Similar modification of compound semiconductor NWs was reported in Ref. 547, where holes into ZnO NWs were made and thinned to form nanobridges only a few atom layers thick. The hole formed in a crystalline NW was demonstrated to have a clearly hexagonal shape that followed the crystallographic planes of the NW.

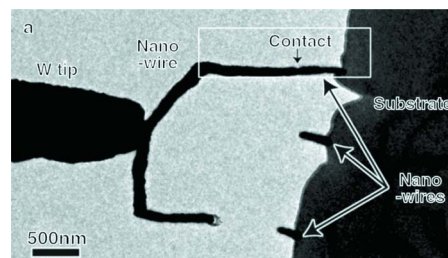


FIG. 72. (Color online) NW contact formed between a W tip and Mo substrate using electron-beam directed growth and careful sample positioning. From Ref. 549.

It was also shown that the conductivity of ZnO NW FETs was sensitive to 10 keV SEM electron irradiation, which was attributed to O absorption stimulated by the electron beam.<sup>548</sup> While interesting in itself, it was further shown that measurements of the electrical conductivity properties of ZnO NWs even in high vacuum without any irradiation was sensitive to molecule adsorption on the NW associated with electronic effects on the surface, analogous to the electron irradiation condition.<sup>548</sup>

A quite different approach to making NWs is using electron beam induced deposition to grow NWs with a width of about 100 nm between a Mo substrate and a W tip that was placed close to the substrate.<sup>549</sup> The NWs were formed out of iron carbonyl precursor gas employing a 30 kV SEM beam. After the formation of the NWs separately on the substrate and tip, the wires were positioned to come into contact with each other (see Fig. 72). The initial contact had a relatively high resistivity ( $>0.01 \Omega \text{ m}$ ) and high contact resistance (no current was detected for voltages below 1 V) due to the presence of an insulating interface layer. However, after the contact was irradiated with 300 kV electrons, the contact resistance decreased dramatically down to about  $5 \times 10^{-5} \Omega \text{ m}$ . This was attributed to a transformation of an insulating amorphous carbon interface layer into a conductive graphitelike structure.

In<sub>2</sub>O<sub>3</sub>/Sn core-shell NWs were manufactured using a physical vapor deposition approach, obtaining NWs with an In<sub>2</sub>O<sub>3</sub> core surrounded by Sb metal.<sup>550</sup> The Sb layer about 5 nm thick was reported to be initially amorphous, but to crystallize after electron beam irradiation. This was attributed to beam heating. About 100 nm diameter GeO<sub>2</sub> NWs were manufactured using self-catalytic VLS growth with a Ge powder as precursor and heating to 1050 °C in a carrier gas containing oxygen.<sup>517</sup> The wires were reported to amorphize in a matter of seconds when high-resolution (HR)TEM was attempted on the wires.

Single crystalline PbO<sub>2</sub> NWs were fabricated with an average diameter of about 40 nm using a nanoporous alumina membrane as a template and spin coating to introduce the oxide.<sup>551</sup> Under electron beam irradiation, the NWs were reported to undergo a partial structural transformation, from an initial phase of orthorhombic  $\alpha$ -PbO<sub>2</sub> into a state where orthorhombic  $\alpha$ -PbO<sub>2</sub> and orthorhombic  $\beta$ -PbO coexist. This was attributed to beam heating leading to loss of oxygen and thus a phase transition.<sup>551</sup>

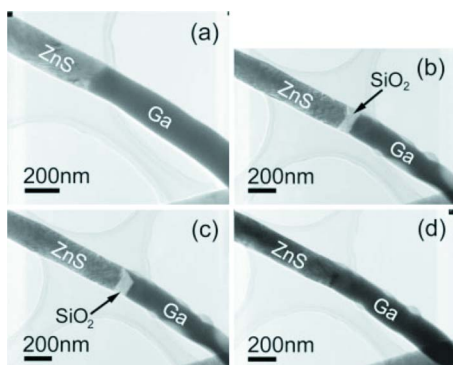


FIG. 73. (Color online) Hybrid Ga-ZnS NWs inside larger silica tubes. (a) Initial structure, (b) after cutting with an electron beam, (c) recovery stage when beam is kept away from the junction but close to the cut, and (d) fully recovered structure with no beam effect. From Ref. 552.

The fabrication of NWs is not even limited to a single material. Hybrid NWs consisting of Ga and ZnS segments, occasionally interspersed by SiO<sub>2</sub> were made and subsequently processed with electron beams, which were able to cut the NW by melting the Ga part.<sup>552</sup> On the other hand, after removal of the beam the junction was regenerated, see Fig. 73.

Also polymer nanostructures can be modified with electron beams. Conducting polymer poly (3,4-ethylenedioxythiophene) NWs were irradiated with 2 MeV electrons and found to undergo structural and conformational changes due to the irradiation.<sup>553</sup> The irradiation was also reported to induce a transition from a conducting to a semi-conducting state in the wires.<sup>553</sup> In summary, electron beams are a highly versatile tool for the modification of NWs, as they can be used to e.g., drill holes in NWs, crystallize or amorphize them, and make and break contacts between wires.

#### D. Ion beam synthesis of NWs

Also low-energy (keV) ion beams can be used for NW synthesis. As described in Sec. V D 7, carbon nanotubes can be used masks and sputtering can be used to remove material everywhere else except below the nanotube to form a wire. Another, more obvious approach is to use FIB processing to sputter away everything except the NWs. This approach has the advantage that the NWs can be placed accurately where desired, but on the other hand contamination of the material from the (typically Ga) ion beam can be a serious issue.<sup>554</sup> FIBs have been used to manufacture both NWs lying on substrates<sup>512,554-556</sup> and also standing NWs.<sup>557</sup> FIB processing has also been used to improve on the electrical contact between NWs and electrodes.<sup>558</sup> The NW formation on surfaces can be enhanced by annealing to form, e.g., metal silicides,<sup>512,554,556,559</sup> (see Fig. 74) approach can be combined with etching methods to enhance the processing speed and obtain high-aspect ratio standing NWs.<sup>560</sup>

Another approach for ion beam synthesis of NWs is to use sputtering to thin an initially broad wire. Fabrication of metal NWs as narrow as 10 nm has been demonstrated to be possible using this approach.<sup>561-563</sup> These NWs are narrow enough that quantum fluctuations of the superconducting

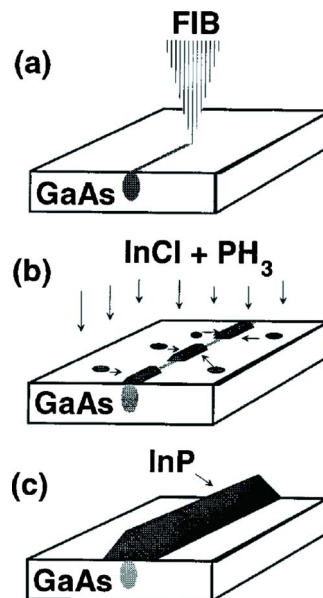


FIG. 74. (Color online) Principle for growth of NWs using FIB writing followed by annealing to induce nucleation along the written line. From Ref. 512.

transition can directly be observed in them.<sup>564</sup> Moreover, the nature of the irradiating ion was shown to be significant in the thinning process. Ga irradiation of Au wires lead to surface nanocondensation of Ga, hampering the process of downsizing, while irradiation with chemically inert Ar did not show this effect.<sup>563</sup>

Another less direct approach to form NWs lying on substrates was introduced by in Ref. 514. V-shaped grooves on Si were first formed with anisotropic etching. After this, Ge was implanted on the wafer. The Ge concentration became the highest at the bottom of the V groove due to sputtering and redeposition downwards from the side walls. After annealing, Ge atoms at the bottom formed a NW about 35 nm in diameter. This NW was, however, reported to be metastable. At long annealing times or high temperatures, it would break up into individual nanoclusters due to the Rayleigh (pearling) instability.<sup>514,565</sup> This effect could, however, also be beneficial in itself, as it could be used to produce an array of roughly equisized and equidistant nanoclusters.<sup>514</sup>

We note that the Rayleigh instability<sup>565</sup> applies to all NWs, and any NW can be expected to break down into isolated clusters if the annealing temperature is too high compared to the width and surface/interface energy of the wire material. Indeed, several reports of NW breakup do exist.<sup>554,556,566</sup>

An even more complex process was demonstrated in Ref. 510. Pd was first implanted into Si to form nanoclusters, then these nanoclusters were used as seeds for a VLS growth of NWs (see Fig. 75). The same approach has been used to grow Si NWs on Si using implantation of Au to form nanoclusters that act as the catalysts for VLS growth.<sup>567</sup> Also, Ga FIB processing of GaSb has been used to induce VLS growth of amorphous NWs containing embedded GaSb nanocrystallites.<sup>568</sup>

NiSi<sub>2</sub> NWs have been embedded inside Si using Ni implantation of Si and subsequent laser annealing.<sup>569</sup> The an-

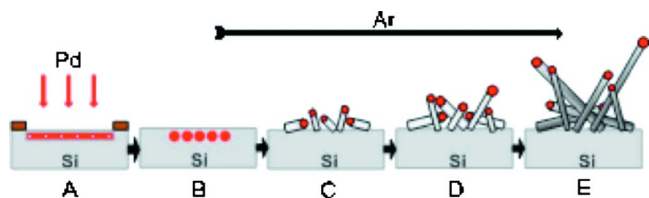


FIG. 75. (Color online) Principle for growth of NWs using implantation to form Pd nanoclusters in Si and subsequent VLS growth with these nanoclusters as the seeds. From Ref. 510.

nealing lead to epitaxial regrowth of Si. During the regrowth, Ni segregated to the grain boundaries, leading to the formation of nanorods. During annealing conditions when the Si regrowth lead to columnar grains, the nanorods become oriented perpendicular to the surface (see Fig. 76). A field emission current consistent with the Fowler–Nordheim equation for an enhancement factor of more than 600 (corresponding to thin long wires) was demonstrated from the samples.<sup>569</sup>

Very high-dose noble gas implantation can lead to bubble formation and eventual blistering and flaking/exfoliation of materials.<sup>570</sup> This normally harmful effect has been used to fabricate Cd NWs.<sup>571</sup> Cd<sub>2</sub>Nb<sub>2</sub>O<sub>7</sub> surfaces were irradiated with 3 MeV He up to doses of  $1.2 \times 10^{18}$  to induce exfoliation. Cd nanoparticles were formed at the ion-cut surface, and NWs with lengths up to tens of micrometers were observed to grow on the cut surface.<sup>571</sup> What is remarkable (compared to NW growth on metals or common semiconductors) is that the NW growth in this oxide material was reported to occur at room or lower temperatures.<sup>571</sup>

In summary, ion irradiation can be used to form NWs in many different ways. The irradiation can be used to synthesize nanoclusters that act as seeds for VLS growth of NWs, used to sputter NWs into grooves, or manufacture them directly using FIB processing.

### E. Ion tracks and NWs

Several groups have employed swift heavy ion tracks to grow NWs.<sup>572–579</sup> Heavy ions (typical examples are Xe, I, and Au) accelerated to energies of the order of 1 MeV/amu or higher, are well known to travel in straight paths deep into materials. If the energy lost to electronic excitations (electron stopping) exceeds some material-specific threshold, the ions can produce a nanometer-wide damage track in insulators and semiconductors.<sup>104,114</sup> The damaged track can in many materials be etched away, leaving behind a long straight nanopore which can (at least in principle) be filled with another material to form an embedded NW. If further the matrix can be thereafter etched away, the approach can also be used to make freestanding NWs.

Examples of NWs grown with this approach include CuSCN wires,<sup>572</sup> Ni,<sup>574,576,580</sup> Co,<sup>578</sup> Cu,<sup>577</sup> and Au.<sup>579</sup> Although usually the NWs obtained in this manner are cylindrical, e.g., He irradiation of mica has been shown to produce diamond-shaped etch traps and thus prism-shaped NWs.<sup>580</sup> Sometimes the morphology is even more complex, for instance, agglomeration of the wires after they have grown long enough, can lead to a beautiful starlike pattern (see Fig. 77).

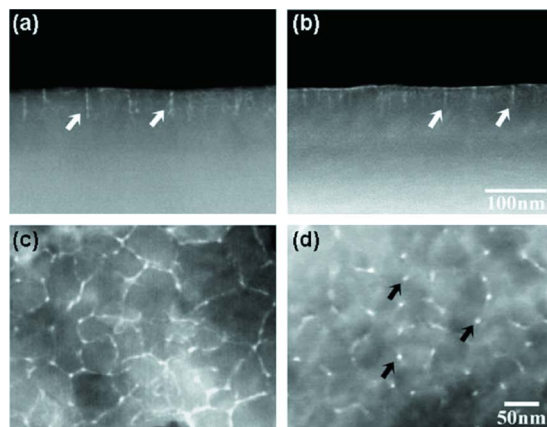


FIG. 76. (Color online) Nickel silicide NWs embedded into Si formed by Ni implantation and subsequent laser annealing. The NWs were formed at the grain boundaries of recrystallized Si grains. From Ref. 569.

A slightly different approach to making NWs is to use the track phase transformation to form a more stable structure than the original matrix. Polymers can be cross-linked by the irradiation, hardening them.<sup>581</sup> This allows selective etching of the remaining material to form NWs,<sup>573,582</sup> which has, for instance, been used to grow cross-linked polysilane wires.<sup>573</sup>

The NWs grown with this approach have also been demonstrated to have potential practical applications. Vertical NW transistors in flexible polymer foils have been fabricated, and it has been reported that the resulting devices are comparatively insensitive to mechanical motion of the foil.<sup>572</sup> This was attributed to be due to the plastic environment absorbing most of the mechanical stress. Also interconnected NW clusters for 3D flexible circuits and magnetic sensing applications have been created,<sup>574</sup> as well as nano-sized capacitors made by placing both conducting and insulating material inside a track.<sup>575</sup> Electron field emission was demonstrated from patch arrays of Au NWs in Ref. 579, and emission at currents that were about a factor of 5 higher than expected from a simple calculation based on the aspect ratio and Fowler–Nordheim equation has been shown in Ref. 577. Ni wires have also been functionalized with porphyrin to become fluorescent.<sup>580</sup>

In summary, swift heavy ion tracks can be etched to form hollow cylinders into which NWs can be grown. Alternatively, in certain materials, the track itself can be more stable than its surroundings, and thus form a NW.

### F. Simulation of radiation effects in NWs

While the effects of ion and electron irradiation on carbon nanotubes have been studied extensively with MD simulations, very few studies have considered the effects of irradiation on NWs. Defect formation energies in Cu NWs have been studied with classical MD simulations.<sup>583</sup> It was reported that the formation energy of vacancies is the lowest in the middle of the NW. On the other hand, the formation energy of adatoms was reported to decrease with decreasing NW diameter. The authors also considered the recombination mechanisms of vacancies and adatoms in detail.<sup>583</sup> Si NWs with a hexagonal cross section have also been classically

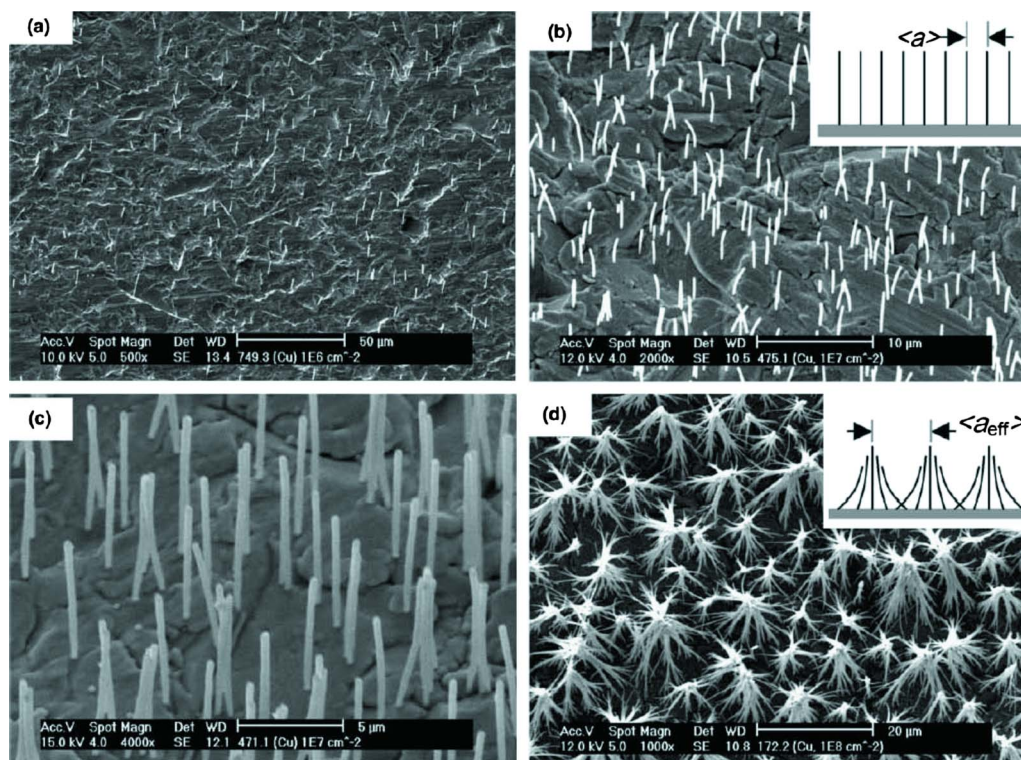


FIG. 77. (Color online) SEM images of straight and agglomerated Cu NWs on Au/Cu backing layers formed by growth of NWs into swift heavy ion tracks. From Ref. 577.

simulated, comparing two different potentials, the Tersoff<sup>584</sup> and Stillinger–Weber<sup>585</sup> ones.<sup>586</sup> In certain crystallographic directions, the two potentials predicted essentially the same behavior of low-energy recoils, while in others there were strong differences.<sup>521</sup>

The threshold displacement energy in hexagonal Si NWs with a  $\langle 111 \rangle$ -oriented axis and with all side facets being  $\langle 112 \rangle$  was very recently studied.<sup>587</sup> It was reported that of the six nonequivalent surface positions (see Fig. 78), the highest two positions have clearly the lowest thresholds, whereas the bottommost surface atom position had essentially the same threshold as the bulk atoms.

In summary, extremely few studies have to date examined irradiation effects in NWs theoretically, especially compared to the case of carbon nanotubes where a wealth of studies exist. Considering that on the other hand a fair

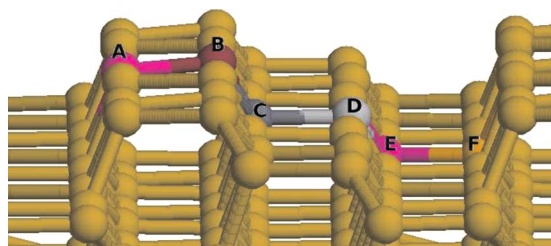


FIG. 78. (Color online) Surface reconstruction of a  $\langle 112 \rangle$  Si surface. A Si NW with a  $\langle 111 \rangle$ -oriented axis can have all six side surfaces be  $\langle 112 \rangle$  and hence be reconstructed as in the figure, with six nonequivalent atom positions. The A and B positions have the lowest threshold displacement energies, while the E and F have the highest ones. The F threshold displacement energy essentially agreed with the bulk threshold displacement. From Ref. 521.

amount of experimental information is available, often with little theoretical analysis, the field clearly needs additional theoretical and computational work.

## VIII. IRRADIATION EFFECTS IN FREESTANDING NANOCCLUSERS

With freestanding nanoclusters, we mean here particles in vacuum or on surfaces when they do not interact strongly with the substrate. The topic of irradiation of freestanding 0D nanostructures (nanoparticles, nanoclusters and NCs) has not been studied nearly as widely as that of nanotubes and NWs. This is most likely due to the fact that experimental study is difficult and that until recently there were no obvious practical applications of NC irradiation. However, recently a few potentially useful applications of irradiation of nanoclusters have been demonstrated, such as strong enhancement of secondary ion mass spectrometry (SIMS) signals for organic materials,<sup>589</sup> and the possibility to modify the crystal structure of metal nanoparticles.<sup>590</sup>

### A. Sputtering of nanoparticles

SIMS is a standard technique for analysis of depth profiles of hard condensed materials, but it is also useful for analyzing the composition of the top few monolayers of molecular solids. Previously molecular analysis was plagued by the problem of very low yields for sputtering of intact large molecules. However, in 2006, it was shown that the TOF SIMS analysis of molecular solids can be dramatically enhanced by first coating the sample with metal nanoparticles.<sup>589</sup> Citrate-capped Ag or Au nanoparticles were

first deposited on surfaces of poly(tetrafluoroethylene) and polystyrene-*g*-poly(ethylene glycol) (Tentagel) as polymer prototypes. A TOF-SIMS measurement was made using a pulsed 15 keV Ga ion beam and a TOF detection setup. The results showed that the mass range of molecules that can be analyzed was extended to 5000 Daltons (atomic mass units) and that the sputtering yield was enhanced up to a factor of 400 compared to a surface not treated with nanoparticles. The effect was attributed to metal ions which have been sputtered from the nanoparticle forming metastable complexes with the polymer molecules. The ionized polymers were then more stable during the SIMS experiments. Another possible mechanism is the loss of electrons from the polymer to the nanoparticle. The approach was developed further by attaching Au nanoparticles to well-controlled surfaces such as self-assembled monolayers.<sup>591</sup> This approach was applied for analysis of peptides (protein segments) with masses in the 1000 Dalton range.

The SIMS-enhancing effect of metal nanoparticles gives a clear motivation to study the sputtering of nanoparticles since regardless of the exact mechanism of the polymer sputtering, the metal nanoparticles are ejected by exposure to the incident ion beam.

Experiments on the sputtering of Ir nanoparticles created during sparking were carried out, and it was shown that even at the relatively high Ar ion energy of 34 keV, a surprisingly high fraction of the sputtered species were in the form of Ir-oxide, nitride, or carbide radicals.<sup>592</sup>

MD simulations of the sputtering of Au nanoclusters have been carried out by several groups.<sup>588,593–595</sup> Sputtering of Au nanoclusters by 38 keV Au ion bombardment with MD simulations was examined,<sup>588</sup> Fig. 79, and it was reported that the sputtering yield has no significant dependence on the impact point in the clusters (impact parameter). The average sputtering yield for a Au<sub>6051</sub> cluster was reported to be about 1200 atoms. Similar computer simulations of the sputtering of Au nanoclusters by impinging 180 eV/atom Au<sub>400</sub> nanoclusters<sup>593</sup> showed large sputtering yields of the order of several thousands of atoms. The bombardment of 8 nm diameter Au nanoclusters by even higher energy (100 keV) Au projectiles has also been examined.<sup>594</sup> This was shown to lead to most ions passing the nanoclusters with little or no effects on them, but a few collisions causing essentially the disintegration of the whole cluster. Simulations of 20 nm diameter Au nanoclusters by 16 and 64 keV Au projectiles were reported to lead to sputtering yields that could be more than a factor of 2 higher than the yield for a bulk target<sup>595</sup> (see Fig. 80).

MD simulations of sputtering as a function of size, to examine the enhancement of sputtering from nanoclusters,<sup>135</sup> were reported to show that the sputtering yield from Au clusters by 25 keV Ga ions can be as much as four times higher than the bulk sputtering yield. An analytical model for the sputtering yield as a function of cluster size that gave reasonable agreement with the MD simulation data was also developed (see Fig. 81).

A truly exotic case of nanoparticle sputtering is that of interstellar dust grains by cosmic ray ions.<sup>596,597</sup> Interstellar radiation contains a significant proportion of H and He ions

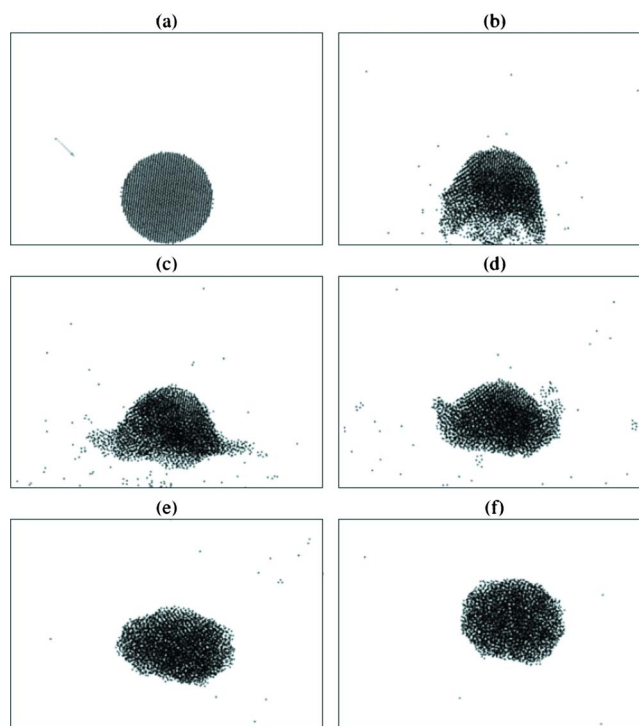


FIG. 79. (Color online) Time evolution of an Au<sub>6051</sub> nanocluster after 38 keV Au impact, shown as a time sequence a–f. Note the total disintegration of the shape of the cluster as well as the large amount of sputtering from it. From Ref. 588.

at keV and MeV energies. Experimentally it is known that these can sputter molecular grains consisting, for example, of water and carbon monoxide with very high yields.<sup>597</sup> This process was simulated by mimicking each grain as a Lennard-Jones solid with parameters giving cohesion energies similar to those of real molecular solids.<sup>596</sup> The results showed that at high excitation densities, the sputtering can be understood in terms of a swift heavy ion track process with two mechanisms contributing to the sputtering: prompt rapid ejection of matter during the initial heating, as well as late thermal evaporation due to the heating of the entire grain,<sup>597</sup> (see Fig. 82).

## B. Sputtering of nanoparticles by swift heavy ions

Also swift heavy ions can sputter materials due to electronic excitations.<sup>126,598</sup> With respect to nanostructures, the desorption of Au, Ag, Pt, In, Ge, UO<sub>2</sub>, and PbS nanocluster films by swift heavy ions has been studied.<sup>599,600</sup> For Au, nanodispersed films containing Au nanoclusters of different sizes were first manufactured on a surface by vapor deposition of gold on amorphous carbon at substrate temperatures of 20–400 °C (see Fig. 83), Ref. 600. The films were subsequently irradiated with 965 MeV Pb ions, and sputtered material was gathered on a collector consisting of several TEM grids. Postirradiation TEM analysis of the collectors showed clusters with a size distribution very similar to that of the initial irradiated films. This shows that a swift heavy ion could induce the sputtering of *intact* very large nanoclusters, with sizes up to the order of 100 nm in diameter. Moreover, the sputtered nanoclusters were more nearly spherical in shape than the initial ones, which suggests that they have

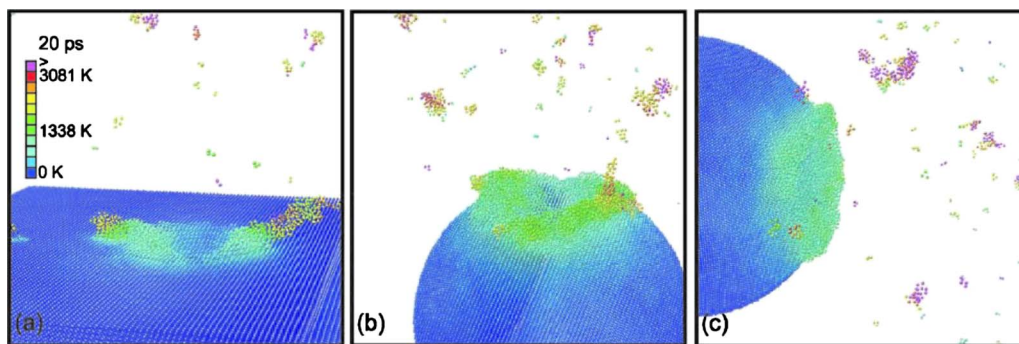


FIG. 80. (Color online) Sputtering of Au bulk (a) vs a nanocluster [(b) and (c)] by a 16 keV Au projectile. In cases (a) and (b), the bulk or nanocluster, respectively, was bombarded by a 16 keV ion from above. In case (c), the ion comes from the right toward the nanocluster. The colors represent the kinetic energy  $E$  of the atoms (given in units of K using the conversion  $E=3/2k_B T$ , where  $k_B$  is the Boltzmann's constant. The images have been selected from cases that give approximately the average yield for either bulk or cluster and can thus be considered representative. From Ref. 595.

been molten during the desorption process due to the energy deposition from the swift heavy ions.<sup>599,600</sup>

At somewhat lower ion energies, films containing Au nanoclusters were irradiated with 100 MeV Au ions, and the size distribution of the sputtered material was measured.<sup>601</sup> Sputtering of up to 300 000 atom particles was reported, and the size distribution of the sputtered material was shown to be described well by a power law with two exponents.

The sputtering yields from practically monodisperse 10.3 nm diameter Au nanoparticles prepared with a reverse micelle technique on top of Si and SiO<sub>2</sub> were measured.<sup>602</sup> 200 keV Ar irradiation was shown to lead to the burrowing of the nanoparticles into the substrate (an effect also known to occur without irradiation in certain other systems<sup>603</sup>). In this case, the effect was explained to be energetically due to minimization of the surface energy and kinetically due to an ion-enhanced viscosity. The nanoparticles were also shown to be sputtered with a strongly size-dependent sputtering yield.<sup>602</sup>

In summary, several experiments indicate that swift heavy ions can sputter nanocrystalline materials such that the initial nanoparticles or grains sputter at least roughly intact. The effect is not theoretically explained. However, studies of heavy ion irradiation at lower energies (in the heat spike

regime) have shown that heat spikes can lead to the emission of quite large atom clusters due to liquid flow, microexplosions, and corona formation.<sup>604–610</sup> The nanoparticle sputtering is likely explained by a similar effect arising from the swift heavy ion heat spikes.

In summary, several MD studies indicate that the sputtering yield from nanoparticles is enhanced compared to the bulk, and this effect can be reasonably well understood based on a heat spike model of sputtering. The sputtering from nanoparticles has a really promising practical application in being used to enhance SIMS signals.

### C. Phase changes in nanoparticles

It is well known that ion irradiation can induce phase changes such as amorphization or transitions to another crystalline state,<sup>87,611</sup> and thus it is natural to assume that phase

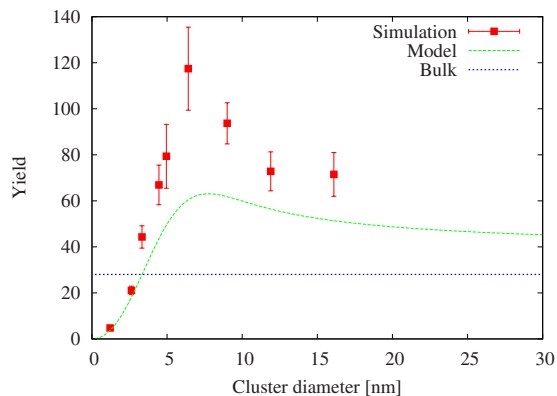


FIG. 81. (Color online) Sputtering yield of Au nanoclusters by 25 keV Ga bombardment as a function of the cluster diameter determined from MD simulations, compared to the bulk sample sputtering yield obtained using the same potential. Also shown are the results of an analytical model based on the Sigmund sputtering theory implemented for nanoclusters. Data are from Ref. 135. Figure courtesy of T. T. Järvi.

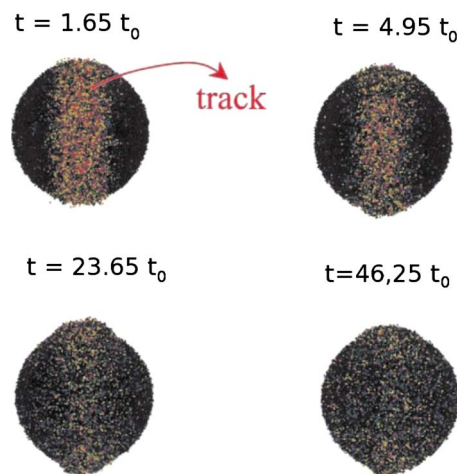


FIG. 82. (Color online) Heating and sputtering of an interstellar dust grain by a track produced by a cosmic ray ion. The ion came in the vertical direction and initially heated the cluster in a cylindrical track in the center. The heating subsequently spread in the grain by thermal diffusion. The colors show the kinetic energy of the molecules, red being hot and blue cold. The images show that while initially all heat is concentrated in the track and sputtering occurs where the track intersects the surface, eventually the energy is dissipated in the entire cluster, heating it up. The heated cluster can further lose atoms or molecules by thermal evaporation.  $t_0$  is the Lennard-Jones time unit,  $\approx 1.9$  ps for the modeled CO particles. Adapted from Ref. 596.

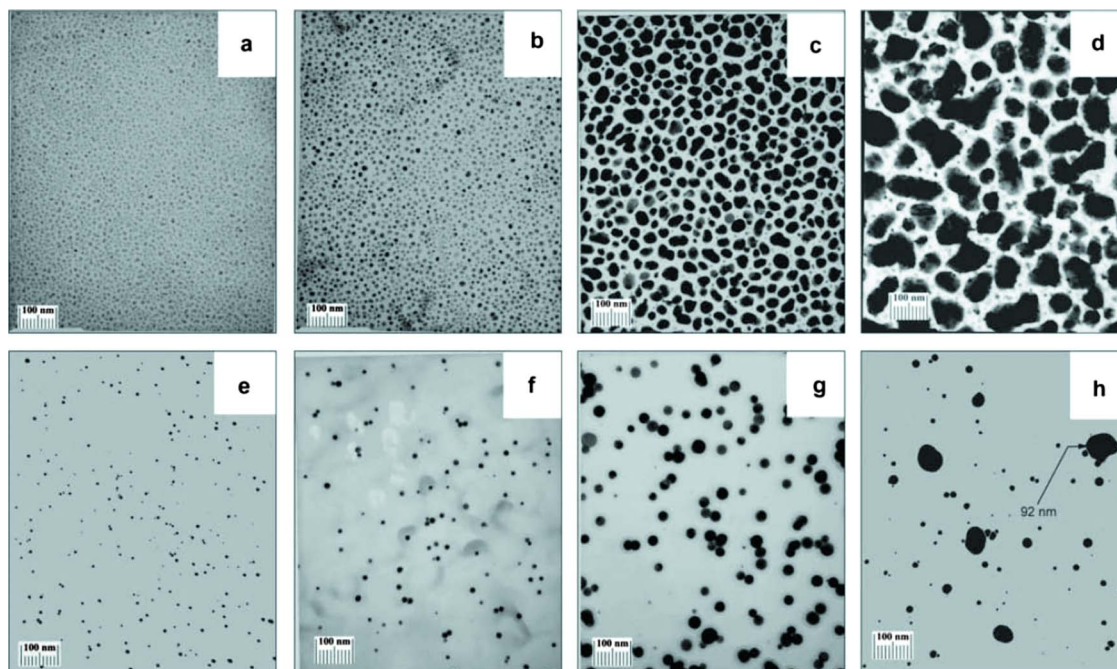


FIG. 83. (Color online) [(a)–(d)] TEM images of films of gold nanoclusters on amorphous carbon made by vapor deposition. [(e)–(h)] TEM images of collectors where some nanoclusters have landed after the initial film was irradiated with swift heavy ions. From Ref. 600.

changes can also result in nanoclusters. In fact, on the nano-scale this possibility is even more interesting since even nanoclusters of exactly the same material and size can exist in a multitude of different single- or polycrystalline as well as disordered states.<sup>612</sup> Different phases can exhibit different functionality, and thus it is natural to pose the question of whether irradiation can be used to modify the structure of nanoclusters in useful ways.

Ion beam effects on FePt nanoclusters have been examined<sup>135,613</sup> because such clusters are highly promising for magnetic applications if they have the ordered “L1<sub>0</sub>” single crystalline structure. However, as-prepared FePt nanoclusters tend to have the polycrystalline multiply twinned icosahedral structure. Using 5 keV He irradiation, it was shown that the icosahedral structure can be destabilized and transformed preferentially into the single crystalline fcc phase. However, this phase did not have the desired chemical ordering associated with the L1<sub>0</sub> crystal structure.<sup>613</sup> Other experiments indicated that the L1<sub>0</sub> ordering temperature of FePt nanoparticles can at least be lowered by He<sup>+</sup> ion irradiation.<sup>614</sup>

In summary, both experiments and simulations show that ion irradiation can be used to modify the structure of NCs, although the fluences needed to achieve major transformations are fairly high. This in turn may lead to a substantial reduction in the size of the clusters due to sputtering.

To understand the icosahedral to fcc transition,<sup>590,615</sup> experiments and MD simulations of the irradiation of FePt and CuAu nanoparticles have been carried out,<sup>590,615</sup> (see Fig. 84). The phase transition was explained to be due to irradiation-induced transient amorphization. A small fraction of the He ion impacts were shown to produce small disordered regions in the clusters, and if these were at one of the twin grain boundaries in the icosahedral structure, their re-

crystallization was shown to occur preferentially toward the single crystalline fcc phase.<sup>590,616</sup> However, this set of experiments did not show the appearance of chemically ordered nanoparticles. This was explained to be due to a high energy barrier separating the fcc and L1<sub>0</sub> structures.<sup>590</sup> Ion irradiation has also been shown to be able to induce structural modifications in diamond nanoparticles.<sup>617</sup>

The effects of irradiation on nanocluster thin films were studied by simulating the irradiation of porous nanocrystalline thin films with 5–30 keV Xe and Au ions.<sup>618</sup> It was reported that the films could be substantially densified by the irradiation while preserving nanocrystallinity. The densification was explained by local melting and associated viscous flow.<sup>618,619</sup> Experiments on the same system, albeit with larger crystallite size, showed a similar densification effect (see Fig. 85). Well in line with these results, 50 keV Ar irradiation of Ag NC films were reported to lead to growth of the average cluster size from 45 to 60 nm.<sup>621</sup>

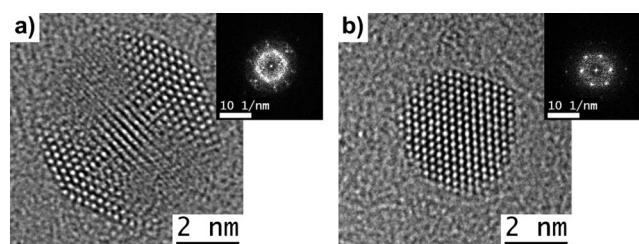


FIG. 84. CuAu nanocluster before (left) and after (right) He ion irradiation. The particle on the left has a multiply twinned icosahedral structure, whereas the one on the right has been transformed into a single crystalline state. Note, however, that at the same time the cluster has substantially decreased in size, apparently due to sputtering. From Ref. 590.

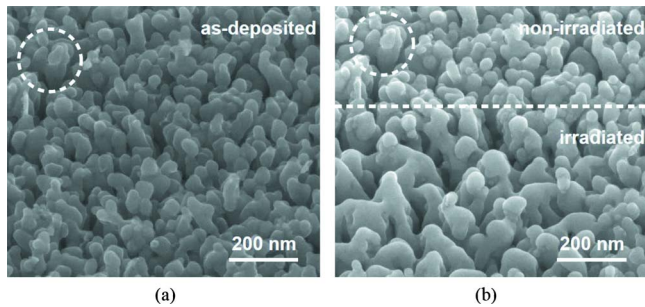


FIG. 85. (Color online) SEM images of (a) an as-deposited Cu cluster film, and (b) the same film after the lower part (below the dashed line) has been irradiated by a 30 keV focused Ga ion beam. The penetration depth of the Ga ions is not large enough to cause a densification of the entire thin film, but a clear difference can be seen, as surface layers of the film have been affected by the impinging ions. The same position has been encircled in both images, in order to ease the comparison between them. From Ref. 620.

## D. Irradiation of quantum dots

Quantum dot structures can be manufactured by growing or depositing nanoclusters on surfaces or in the bulk, with dimensions small enough that they exhibit quantum confinement effects. They have been modified with ion irradiation generally with the aim to modify their optical or electronic functionality. In this subsection, we discuss irradiation of quantum dots lying on surfaces, while effects of irradiation on embedded nanoclusters (with or without quantum dot functionality) are discussed in the next Sec. IX.

### 1. InAs quantum dots

InGaAs quantum dots grown on GaAs via the Stranski–Krastanov growth mode<sup>622</sup> are something of a model system for self-assembled quantum dots on surfaces.<sup>623</sup> Thus several groups have modified the properties of these systems with different kinds of ion irradiation.

Already in 1998, it was reported<sup>624</sup> that Mn ion implantation can be used to shift the QD luminescence of InAs quantum dots up to 150 meV toward higher energies. A fluence of  $10^{13}$  Mn/cm<sup>2</sup> was reported to reduce the PL intensity by only 20%, whereas fluence of  $10^{15}$  Mn/cm<sup>2</sup> led to a 75% decrease even after annealing.

The effects of 50 and 70 keV proton irradiation on a four-layer InAs quantum dot structure embedded in GaAs were reported in Ref. 625. An enhancement of the room-temperature PL by a factor of up to 80 due to the irradiations was reported. This effect was attributed to two effects: defect passivation causing a 20-fold increase and during continued irradiation a fourfold additional increase associated with an increased capture rate.<sup>625</sup> In apparent contradiction, InAs quantum dots were irradiated with 18 keV protons and shown to lead to a decrease of PL linewidth and the inter-sublevel spacing energy.<sup>626</sup> This was attributed to intermixing of InAs/GaAs by the irradiation and subsequent annealing. The differences are likely related to different kinds of sample preparation.

The effects of 25–40 keV proton and 450 keV phosphorus irradiation on InGaAs and InAs/InP quantum dots have been examined.<sup>627–629</sup> The results showed a PL energy shift by *p* irradiation in the quantum dots, which recovered

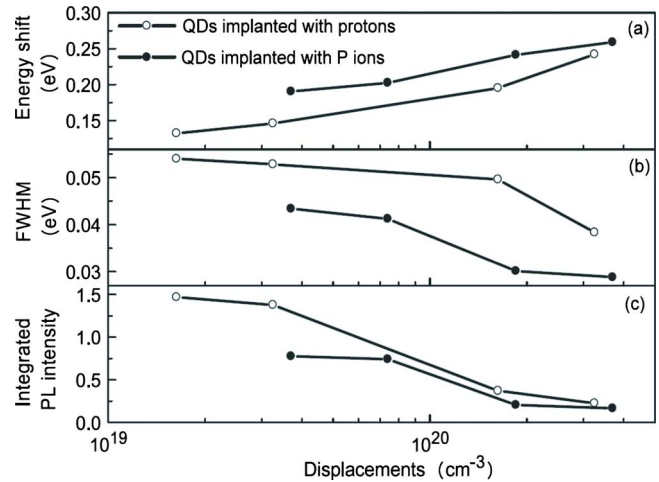


FIG. 86. (Color online) Effect of 40 keV proton and 450 keV P irradiations on the PL intensity in InAs/InP quantum dots. The irradiations were carried out at room temperature, but all samples were annealed at 850 °C after the irradiations. From Ref. 628.

during annealing much better than in InGaAs quantum wells.<sup>627</sup> The *p* irradiation was also found to result in less implantation-induced energy shift than the P implantations, which was attributed to more efficient dynamic annealing by the protons,<sup>628</sup> see Fig. 86. The irradiations also led to a substantially different temperature dependence than that found for unirradiated samples.<sup>629</sup>

A dramatic increase in the interdiffusion of InAs/InP quantum dots, and associated large PL shifts after annealing have been reported to result from irradiation of InAs/InP quantum dots with 30 keV P ions.<sup>630</sup> This was suggested as a means to achieve spatially selective band gap tuning.

The effects of FIBs on the optical properties of InGaAs quantum dots have also been considered.<sup>631</sup> The FIB treatment was used to remove a metallic mask deposited on top of the quantum dot, but it was found that the FIB caused damage on the dots, resulting in total inhibition of the luminescence properties of the InGaAs/GaAs quantum dots.

### 2. Other quantum dots

Also other quantum dots lying on surfaces other than InAs have been modified by ion beams. Chemically prepared ~5 nm CdS and CdSe quantum dot layers of about 4 μm thickness were irradiated with 1.2 MeV Au ions.<sup>632</sup> The irradiation was found to shift the absorption peak toward longer wavelength regions. The irradiation also led to a growth of the average quantum dot size from about 4 to about 10 nm.

PbS quantum dots of average size 10 nm were irradiated with 160 MeV Ni swift heavy ions.<sup>633</sup> The irradiation was reported to lead to a size increase of the nanoclusters to average sizes up to 120 nm, which was attributed to agglomeration. The PL intensity was found to increase significantly with increased ion fluence.

To summarize, several experiments show that irradiation can be used to strongly modify the optical properties of quantum dots, which may be potentially useful for tuning. However, some of the experiments appear contradictory, indicating that the effects are sensitive to effects such as the

processing conditions before and after irradiations, and further study is needed to understand and ensure controllability of the processes.

## IX. IRRADIATION EFFECTS IN EMBEDDED NANOCCLUSERS (NCS)

Ion implantation has an important role for the fabrication of nanoclusters embedded in solids. A standard way to achieve this is to implant atoms of a certain type into a matrix with which they are immiscible. After heating to temperatures high enough that the implanted atoms become mobile, they will segregate from the matrix and form nanoclusters if the implantation depth is suitable compared to the migration distance,<sup>634,635</sup> see Fig. 91. This topic has been studied extensively both by experiments and simulations (see, e.g., Refs. 634–640). Since this way of synthesizing embedded nanoclusters has been recently reviewed elsewhere,<sup>75</sup> we will not review the fabrication of nanoclusters with implantation in detail, but instead dwell on the ion modification of nanoclusters and nanoparticles *after* they have been synthesized. Also, it is important to know that embedded clusters can also be made with a variety of other techniques, such as thermal decomposition of thin grown layers<sup>641,642</sup> or cosputtering.<sup>643</sup>

Regardless of synthesis method, the end result is typically roughly spherical nanoclusters with sizes ranging from a couple of nm (even smaller nanoclusters may exist, but are very difficult to detect) to hundreds of nanometers. As in the case of the other nanostructures considered in this review, these nanoclusters can be further modified by ion irradiation.

### A. Effects of radiation on embedded NCs

#### 1. Si and Ge NCs in silica

One of the first studies of irradiation of NCs was carried out in 1999, when 30 and 130 keV He as well as 400 keV electron irradiation of Si NCs embedded in silica (“NC-Si/SiO<sub>2</sub>”) was examined.<sup>644,645</sup> The electron irradiation was reported not to lead to significant damage in the NCs. TEM analysis of the ion irradiated samples showed that the NCs were amorphized by a He dose of the order of 10<sup>16</sup> ions/cm<sup>2</sup>, i.e., about 1 dpa. The visible PL was reported to decrease and vanish after a He dose as low as one displacement per NC. This effect was ascribed to production of defect-induced nonradiative recombination centers, possibly situated at the Si nanocrystal/SiO<sub>2</sub> interface.<sup>644</sup> Annealing at 600 °C was reported to restore the PL to preirradiation levels.<sup>644</sup> On the other hand, a 1000 °C anneal was reported to be required to recrystallize the samples.<sup>645</sup> Remarkably, after this annealing the PL intensity was reported to be higher than before the irradiations.

Around the same time, Si NCs embedded in silica were irradiated with 400 keV or 3 MeV Si ions.<sup>646</sup> The irradiation was reported to reduce the NC-related luminescence at 806 nm down to 4% of the initial value for a dose of 5 × 10<sup>12</sup> ion/cm<sup>2</sup>. The reduction saturated at a dose of 5 × 10<sup>13</sup> ion/cm<sup>2</sup> (0.18 dpa), which was ascribed to amor-

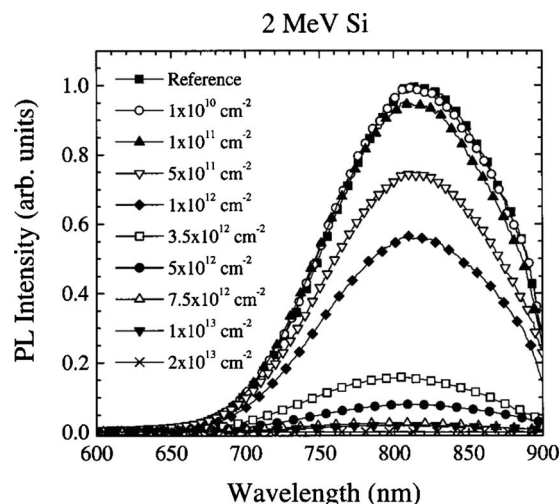


FIG. 87. PL spectra of a SiO<sub>x</sub> film with 39 at. % Si irradiated with a 2 MeV Si ion beam at different doses, from Ref. 647.

phization of the cluster at about this dose. On the other hand, the irradiation was also reported to lead to defect emission at 640 nm.

The same NC-Si/SiO<sub>2</sub> system was also subjected to 2 MeV He, Si, Ge, and Au ion irradiation.<sup>647,648</sup> Similarly to the other works, a strong decrease of the NC-related PL intensity was reported (see Fig. 87), but this drop was also found to be accompanied by a radiative lifetime quenching. This observation was ascribed to damage left by the beams (see Fig. 88).<sup>647</sup> Studies of the recovery of the NCs after the irradiations indicated that the recovery of the PL properties of completely amorphized Si NC could be characterized by a single activation energy of 3.4 eV (Ref. 648). This energy was associated with the transition between amorphous and crystalline phases of each Si grain.

Other studies of the same system include 150 keV P ion irradiation followed by annealing at 100 °C,<sup>649</sup> which was reported to enhance the PL intensity without a significant

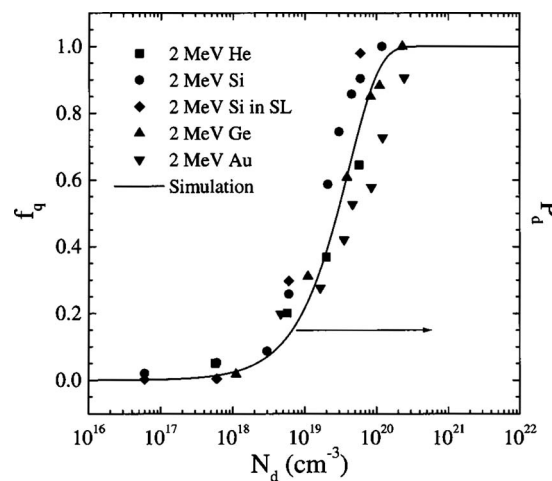


FIG. 88. Fraction of quenched Si NCs  $f_q$  vs defect concentration  $N_d$  left over by the ion beam for a Si/SiO<sub>2</sub> superlattice. The continuous line is a calculated probability  $P_d$  of a NC having at least one defect in its volume, obtained without any fitting parameters, thus providing strong evidence that the quenching can be explained by a NC having a single radiation-induced defect. From Ref. 647.

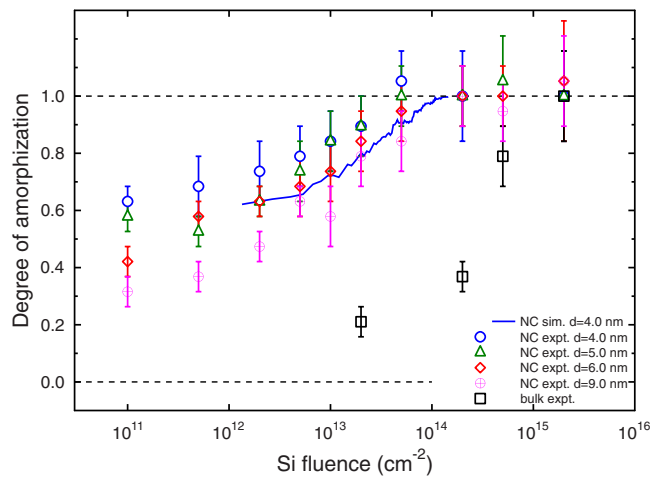


FIG. 89. (Color online) Amorphization of Ge NCs and bulk Ge by 5 MeV Si ions measured by the EXAFS Debye–Waller factor. Also shown are results from MD simulations (Ref. 653) for the same system. Figure courtesy of M. Backman.

shift in the emission peak position. A special variation of the theme was postimplanting of Si NCs with 100 keV Si ions (the same energy that was used in the synthesis of the crystals), thus leading to energy and ion deposition at exactly the same depth as the NC layer.<sup>650</sup> This irradiation was reported to lead to full or partial quenching of the PL signal, attributed to defect generation in the crystals.

Also 90 MeV Kr and 130 MeV Xe swift heavy ions have been used to irradiate the NC-Si/SiO<sub>2</sub> system, after which measurements were made of the current-voltage and capacitance-voltage characteristics at different frequencies.<sup>643</sup> This was reported to indicate the formation of arrays of NCs along the ion tracks.

Using Ge NCs instead of Si has the advantage that the crystals can be characterized by x-ray methods such as EXAFS and XANES.<sup>651,652</sup> Based on such studies, it was reported that already as-prepared NCs show a high degree of disorder as measured by the EXAFS Debye–Waller factor.<sup>651,652</sup> 5 MeV Si irradiation of the NC layer was found to lead to the amorphization of the NCs at about two orders of magnitude lower doses than for bulk Ge (see Fig. 89).

MD simulations have been used to examine the amorphization of NCs in silica.<sup>179,654</sup> Atomic models of Si and Ge NCs of the same sizes as those studied experimentally<sup>655</sup> were first created, and the response of these to irradiation was subsequently simulated by starting self-recoils in and near the NCs, Fig. 90. The results showed that already the as-prepared interfaces have a fairly high fraction (about 10%) of coordination defects and that irradiation does not substantially increase the fraction of defects at the interface.<sup>179</sup> While this result may seem contradictory to the experimental results cited above, it should be noted that not all defects are optically active, and in experimental situations many coordination defects are passivated by hydrogen. In good agreement with experiments, it was found that prolonged irradiation leads to the amorphization of the NCs at doses considerably lower than those needed to amorphize bulk Si or Ge,<sup>654</sup> (see Fig. 89).

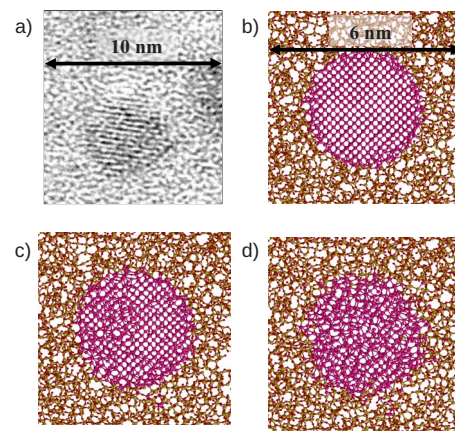


FIG. 90. (Color online) Amorphization of a Ge NC embedded in silica. (a) Experimental TEM image of Ge NC in silica. (b) Initial state in simulation. (c) Modification after irradiation dose of 1.7 eV/atom. (d) Modification after a dose of 4.0 eV/atom. Figures courtesy of L. Araujo, F. Djurabekova, and M. Backman.

It has also been shown that Ge NCs can be doped with Er to form erbium oxide phases, which promote EL.<sup>656</sup> For higher annealing temperatures, also the formation of Er<sub>2</sub>O<sub>3</sub> NCs and an Er<sub>2</sub>Ge<sub>2</sub>O<sub>7</sub> phase was reported. These phases were found to diminish the EL, and an Er content of 0.5% was reported to be optimal for maximizing the luminescence.

To summarize the current subsection, there is clear evidence that ion irradiation of NCs strongly reduces the PL intensity for Si NCs in silica, but that postirradiation annealing can be used to recover and in some cases even enhance the luminescence above the initial levels. The details seem to be very sensitive to the ways of processing the samples before and after irradiation. The embedded Si and Ge NCs amorphize at much lower doses than the corresponding bulk material.

## 2. Metal NCs

Radiation effects in Cu and Au NCs embedded in silica have been examined.<sup>166</sup> It is well known that elemental metals can never be rendered amorphous even by extremely large irradiation doses.<sup>182</sup> Thus it came as something of a surprise when it was shown that pure Cu NCs with diameters of the order of 3 nm could be rendered amorphous by 5 MeV Sn irradiation.<sup>166</sup> On the other hand, Cu NCs with a diameter of 8 nm were reported not to be amorphized, thus nicely showing where the limit for finite-size effects with respect to amorphization lies in this system.<sup>166</sup>

The disordering of Au nanoclusters in silica was also examined<sup>657,658</sup> and it was shown that Au nanoclusters can be dissolved into Au monomers and very small clusters (dimers, trimers) in the SiO<sub>2</sub> matrix. On the other hand, irradiation of 3D arrays of about 3 nm diameter Co nanoparticles in silica with 90 and 150 keV Ar and characterization of them with Rutherford backscattering spectroscopy and magnetic methods indicated that these nanoparticles had a very high resistance to radiation damage, surviving damage up to 33 dpa.<sup>659</sup> In contrast, higher energy and mass (9 MeV Au) irradiation, was reported to amorphize Co nanoclusters, evidenced by very good agreement with the radial distribution function of

MD-simulated bulk amorphous Co.<sup>660</sup> It was also shown that Co nanoclusters can be induced to undergo an fcc-to-hcp phase transition by swift heavy ion irradiation with 9–185 MeV Au ions.<sup>661</sup>

The effects of swift heavy ions on metallic nanoparticles in an Al matrix have also been studied.<sup>662</sup> It was reported that 30 MeV C<sub>60</sub> cluster ions induced amorphization of the core of about 6 nm diameter Bi NCs, but that Pb NCs of about the same size were not modified. This was attributed to overpressure being created at the particle-matrix interface. Comparison of the results cited in this subsection indicates that the issue of when elemental metal nanoparticles can be amorphized is complex, and further studies are needed before unequivocal conclusions can be drawn.

### 3. Inverse Ostwald ripening

A key aspect of NC growth is the Ostwald ripening process, where small particles are more likely than big ones to emit atoms, due to their higher surface curvature, leading to growth of large particles at the expense of small ones<sup>663</sup> (see Fig. 91). While this process is useful for increasing the size of NCs, it does not lead to a monodisperse size distribution. This process has been examined systematically with a combination of experiments, analytical theory, and KMC simulations.<sup>63,638,664</sup> It has been shown that by carrying out irradiation on existing nanoclusters, one can achieve an inverse Ostwald ripening process where high energy ion irradiation of existing NCs can, at least under suitable energy deposition conditions, be used to reduce the size of the largest nanoclusters. This is because a competition between the irradiation-induced detachment and the migration leads to a steady state condition where the system wants to achieve maximal interface area for a given amount of matter, which is reached at a monodisperse size distribution.<sup>63</sup> In practice, however, the large clusters tend to become surrounded by smaller satellite clusters, at least for the Au in SiO<sub>2</sub> system.<sup>664</sup> It was also shown that the mechanisms can be utilized to fabricate a thin layer of nanoclusters just above a flat interface in a semiconductor device,<sup>63</sup> Fig. 92.

Inverse Ostwald ripening was also observed in Ref. 657, where it was shown that an initial Au cluster size distribution with diameters between 2 and 8 nm can be reduced into one with clusters only between 2 and 3 nm, eventually leading to complete dissolution of the clusters. Another study of this process showed that as an intermediate stage, a clearly bimodal size distribution of small and large nanoclusters can be achieved.<sup>665</sup> In summary, inverse Ostwald ripening is a process by which the size distribution of nanoclusters can be controlled and is reasonably well understood by combinations of simulations and experiments.

### B. Elongation of nanoclusters by swift heavy ions

In 2003, it was shown that swift heavy ions can be used to elongate metal nanoparticles in the direction of the swift heavy ion track.<sup>513</sup> 10 nm diameter Co nanoparticles in silica were irradiated with 200 MeV I ions, and it was reported that at a fluence of 10<sup>13</sup> ions/cm<sup>2</sup>, the nanoparticles had grown along the incident beam direction into a prolate shape. At a

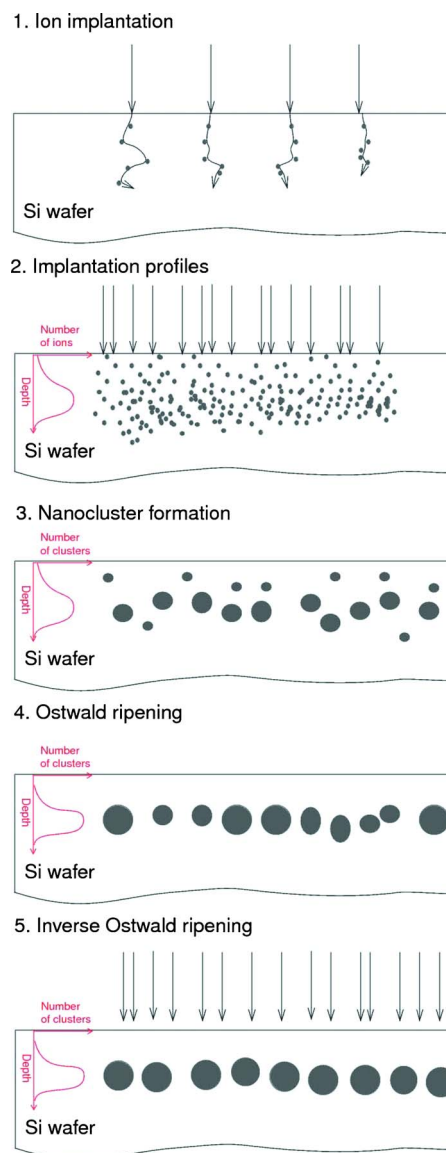


FIG. 91. (Color online) Schematic of the growth of nanoclusters by ion implantation, Ostwald ripening and inverse Ostwald ripening. [(1)–(2)] Conventional ion implantation is used to implant impurities into a crystal to high doses. (3) If the implanted material is immiscible in the matrix, it will start precipitating out of it to form clusters. This process can be sped up by annealing. (4) If the temperature is high enough, the precipitated clusters have some probability to also emit atoms. This probability is higher for smaller clusters due to higher surface curvature, leading to the growth of the larger clusters and vanishing of the smaller ones. (5) If high energy ion irradiation is carried out during or after the growth, the larger clusters are more likely to emit atoms than the smaller ones due to a large cross section for sputtering, leading ideally to a monodisperse cluster size distribution.

fluence of 10<sup>14</sup> ions/cm<sup>2</sup>, they had elongated to be on average about four times longer than wide (see Fig. 93).

This surprising finding has rapidly attracted a flurry of research activity.<sup>513,666–678</sup> The effect has been repeated in many systems, and as a general rule the results indicate that nanoparticles in a wide range of metals can be elongated with a suitable irradiation condition.

Irradiation of 5 nm Ag nanoparticles in silica with 8 MeV Si ions (which does not have an energy deposition high enough to be considered a swift heavy ion), was based on indirect optical measurements reported to produce particles

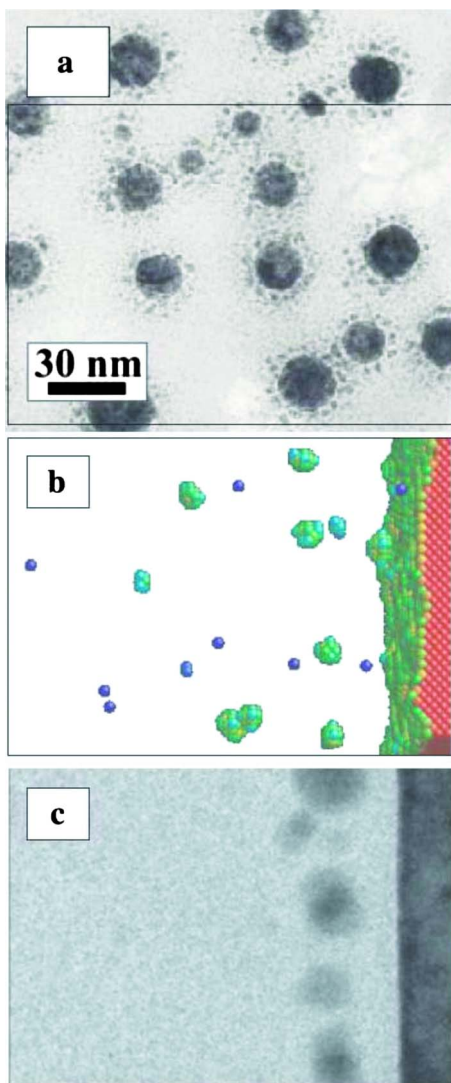


FIG. 92. (Color online) Formation of NCs at slightly curved or flat interfaces under ion irradiation. (a) TEM image of small Au NCs in SiO<sub>2</sub> formed around large Au inclusions by 4 MeV Au ion irradiation. (b) KMC simulation of ion irradiation of a flat interface. Small NCs appear in front of the interface. (c) XTEM image of a layer of Sn NCs in SiO<sub>2</sub> separated a few nanometers from the Si/SiO<sub>2</sub> interface. From Ref. 63.

with a prolate shape.<sup>668</sup> Irradiation of 1–6 nm sized Au nanoparticles near the surface with 100 MeV Au ions was reported to lead to a growth in size.<sup>670</sup> However, because of the vicinity of the surface, part of the Au was also sputtered.

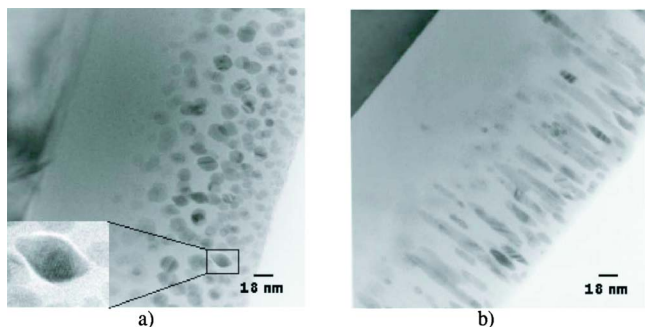


FIG. 93. (Color online) TEM images of initially spherical Co nanoclusters irradiated by (a) 10<sup>13</sup> 200 MeV ions/cm<sup>2</sup> and (b) 10<sup>14</sup> ions/cm<sup>2</sup>. From Ref. 513.

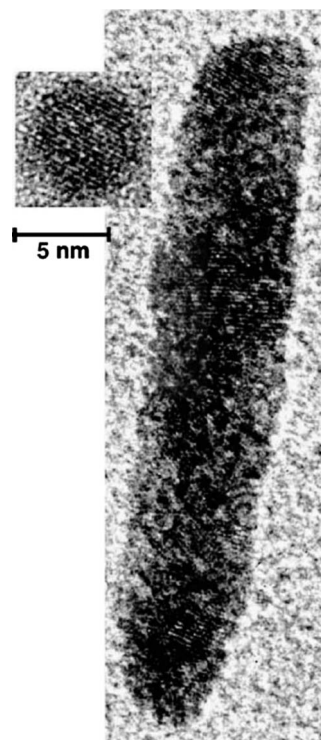


FIG. 94. TEM image of Pt nanoparticles before and after 185 MeV Au irradiation. From Ref. 679.

Several works indicate that there is a correlation between elongation and the swift heavy ion track diameter. Irradiation of Pt nanoparticles with an average diameter of about 145 nm with 27–185 MeV Au ions (see Fig. 94) was reported<sup>673</sup> to lead to elongations exceeding a factor of 10. But this work also showed that the elongated rods were subject to dissolution and breakup due to the Rayleigh instability.<sup>565</sup> Study of the relation of the elongation to electronic energy deposition indicated that the diameter of the molten track in silica confines the irradiation-induced phase transformation. Similarly, elongation of Au nanoparticles using 54–185 MeV Au irradiation was reported to lead to an energy-dependent saturation width for the elongation, which was directly correlated with the ion track diameter in silica.<sup>674</sup> In an independent study, irradiation of 20–80 nm Au nanoparticles with 90 MeV Cl, 100 MeV Cu, and 110 MeV Br ions showed that the Cl ions led to no elongation, whereas Cu and Br did.<sup>677</sup> This showed that the lower energy deposition density by Cl was not sufficient to induce elongation, and it was reported that the experiments could be well explained by the thermal spike track model of Toulemonde.<sup>114</sup>

Irradiation of 8–10 nm Ag nanoparticles in silica with 120 MeV Au ions was reported to lead to only a minor elongation, to an aspect ratio of about 1.5. However, smaller nanoparticles were reported to disappear under the same irradiations.<sup>675</sup> Thus one finds that major elongations are not observed in all metals, although it is not yet clear whether this is due to the choice of irradiating ion or is really a material's dependence. Contrary to the findings in metals, it has been reported that Ge nanoparticles were flattened into an oblate shape, when 38 MeV I irradiation was used to bombard 26 nm Ge nanoparticles.<sup>680</sup>

In more complex systems, the swift heavy 210 MeV Xe ion irradiation of about 2 nm diameter FePt nanoclusters embedded in alumina was reported to cause particles in the film interior to become elongated, with the particle centers being enriched with Pt.<sup>678</sup> It has also been shown that 80 MeV oxygen ions could modify CdS nanoparticles into elongated structures such as nanoneedles and nanorods.<sup>669</sup>

To summarize this subsection, there is already strong evidence that the elongation is linked to the width of the ion tracks. On the other hand, the mechanism is not fully established since for instance the observation of flattening of Ge nanoparticles is not consistent with the idea that the elongation is caused by the flow of liquid matter into the underdense core of an ion track.<sup>107</sup> Moreover, possible elongation of compound nanoparticles has been barely studied at all to date.

## X. CONCLUSIONS AND OUTLOOK

This review article has summarized the recent advances in our understanding of interactions of beams of energetic particles with nanostructured materials. Based on a wealth of experimental and theoretical data, it can be concluded that irradiation of nanostructures does not necessarily have only detrimental effects on the system. Similar to bulk materials, nanosystems can be doped with foreign atoms, and their properties can be changed in a controllable manner. In most cases considered in this review, the electronic, magnetic, and optoelectronic properties were found to be very sensitive to the presence of defects, but the origin of this sensitivity is a very nontrivial and interesting issue.

Moreover, under certain conditions the exposure to electron or ion beams can give rise to many fascinating and unexpected phenomena such as ordering and annealing of pre-existing defects, appearance of new phases, and in a wide sense, to self-organization in various systems. Many of these effects can be used for the engineering of various nanosystems and tailoring their properties. Both the “top-down” and “bottom-up” approaches can be realized.

With regard to the top-down approach, one of the most immediate applications of irradiation would be the use of electron or ion beams as “cutting tools” on the nanoscale. Various nano-objects can be shaped by the beams, and their dimensions can dramatically be reduced. For example, as discussed above, nanoribbons just a couple of nanometers across, and even chains of carbon atoms can be cut out from graphene sheets, and nanobridges in Si and ZnO wires can be manufactured. The same technique can be used to weld nanostructures to each other or to macroscopic systems, e.g., electrical contacts. Interconnections and strong covalent bonds between similar and chemically different nanostructures produced by irradiation may be one of the most promising tools to join these systems together. In particular, arrays of interconnected carbon nanotubes with different electronic properties can be manufactured by using spatially localized irradiation, which could be important for carbon-based electronics.<sup>681</sup> The main obstacle here is that defects may unintentionally be created in other parts of the system, but the amount of the undesired damage can be minimized after

making a device by high-temperature annealing. The defects produced in the desired position can also be beneficial, as the nanotube-based circuitry can gain from defected areas deliberately created to work as electron tunneling barriers and thus provide the desired functionality of the device. Somewhat similarly, ion beam introduction of defects into embedded semiconductor NCs can strongly affect their optical properties and sometimes enhance the luminescence.

Other enticing possibilities include the use of beams of energetic particles for functionalization of nanostructures. The chemical reactivity of graphitic nanostructures can be increased with irradiation-induced defects at the surface. This is important because a pristine basal plane of graphite is chemically almost inert. Thus, functional groups can be attached to graphene and nanotubes in preselected areas, which should be important for biological and other applications. Due to new irradiation-mediated covalent bonds between loosely connected parts of nanostructured carbon materials, irradiation can be used to improve on mechanical properties of macroscopic samples made from nanotubes and nanotube-polymer composite materials

Speaking of the irradiation-induced phenomena resulting in fabrication of nanostructures, which can be referred to as implementing the bottom-up approach, one can mention inverse Ostwald ripening, in which irradiation is used to induce atom emission from nanoclusters, which then by a balance of random atom migration and emission strive toward a steady state of equisized clusters.

Many other applications, such as nanocluster-enhanced sputter analysis of large organic molecules and electronics components with good radiation resistance, are envisaged, and the ongoing research will likely open up more new avenues for harnessing irradiation on the nanoscale. In a biological context, in addition to defect-mediated functionalization, creation of magnetic biocompatible systems by irradiating fullerenes, nanodiamonds, or nanotubes with nonmagnetic ions may be another interesting application.

Our progress, however, depends on the basic scientific understanding of irradiation-induced effects. This review has clearly shown that the understanding of radiation effects in carbon nanosystems is already good, thanks to extensive and systematic experimental and theoretical works. In many, but not all, cases the theories and simulation models developed for bulk systems can be applied, although cautiously. On the other hand, BN nanotubes are not so well understood; even though they would initially appear similar to carbon tubes, their response to irradiation is in many respects strikingly different. The understanding of the response of other kinds of NWs to irradiation is overall very poor, due to relatively little experimental and practically no theoretical work on these systems.

The research field of irradiation-induced modification of nanoparticles is even newer than that of NWs. Thanks to concerted experimental and theoretical works, however, a few key aspects such as the sputtering and amorphization of NCs start to be already well understood, but there remains a multitude of issues and systems that have not yet been studied at all. Composites between nanotubes, NWs and/or nanoparticles and other materials are only beginning to be ex-

plored, and an extremely wide range of systems and questions remain to be explored. Overall, this review has shown that there are numerous exciting scientific issues to study and possible applications coming out from the field of ion and electron beam interactions with nanostructures.

## ACKNOWLEDGMENTS

The authors would like to thank F. Banhart, R. Nieminen, A. S. Foster, J. Keinonen, and K. Albe and their research groups for many years of excellent collaboration on topics related to this review. The authors also gratefully acknowledge J. Baglin and F. Banhart for their critical comments on this review and valuable suggestions for the organization of the review and inclusion of the material. We further thank J. Kotakoski, T. T. Järvi, M. Backman, and F. Djurabekova for providing figures for this review. The authors are also indebted to the Academy of Finland for the support through several projects and the Centre of Excellence program.

## APPENDIX: WIKIPEDIA ARTICLES RELATED TO THE TOPIC

During the writing of this article, we also critically reviewed and contributed to several Wikipedia articles related to the topic (Ref. 682). Although we do *not* recommend using Wikipedia as a direct source for scholarly work, we do find that articles with proper original research citations can for nonexperts often serve as good introductions and provide lists of relevant references to a field or topic. Hence, we list here several related Wikipedia articles that we have reviewed. We found that the versions with the dates indicated below had proper references and did not contain outright errors. Several statements were certainly simplified, but this is justifiable in an encyclopedic work.

Note that in the Wikipedia system, all previous versions of an article remain permanently available, and hence the interested reader can access the exact versions of the articles listed below.

- “Particle radiation,” version of March 10, 2009.
- “Stopping power (particle radiation),” version of March 24, 2009.
- “Kinetic Monte Carlo,” version of April 8, 2009.
- “Molecular dynamics,” version of April 8, 2009.
- “Collision cascade,” version of January 24, 2009.
- “Threshold displacement energy,” version of December 8, 2008.
- “Carbon nanotube,” version of April 4, 2009.
- “Crystallographic defect,” version of February 22, 2009.
- “Vacancy defect,” version of February 1, 2009.
- “Interstitial defect,” version of March 22, 2009.
- “SRIM,” version of July 13, 2009.
- “Sputtering,” version of December 31, 2009.
- “Swift heavy ion,” version of November 26, 2009
- “Ion track,” version of December 30, 2009
- “Vapor-liquid-solid method,” version of December 23, 2009

- <sup>1</sup>J. A. Brinkman, *J. Appl. Phys.* **25**, 961 (1954).
- <sup>2</sup>F. Seitz and J. S. Koehler, in *Solid State Physics*, edited by F. Seitz and D. Turnbull (Academic, New York, 1956), Vol. 2, p. 307.
- <sup>3</sup>A. Seeger, *The Nature of Radiation Damage in Metals* (International Atomic Energy Agency, Vienna, 1962), Vol. 1, pp. 101–127.
- <sup>4</sup>J. W. Mayer and S. S. Lau, *Electronic Materials Science For Integrated Circuits in Si and GaAs* (MacMillan, New York, 1990).
- <sup>5</sup>E. Chason, S. T. Picraux, M. Poate, J. O. Borland, M. I. Current, T. Diaz de la Rubia, D. J. Eaglesham, O. W. Holland, M. E. Law, C. W. Magee, J. W. Mayer, J. Melngailis, and A. F. Tasch, *J. Appl. Phys.* **81**, 6513 (1997).
- <sup>6</sup>F. Banhart and P. M. Ajayan, *Nature (London)* **382**, 433 (1996).
- <sup>7</sup>A. Hashimoto, K. Suenaga, A. Gloter, K. Urita, and S. Iijima, *Nature (London)* **430**, 870 (2004).
- <sup>8</sup>B. Peng, M. Locascio, P. Zapol, S. Li, S. L. Mielke, G. C. Schatz, and H. D. Espinosa, *Nat. Nanotechnol.* **3**, 626 (2008).
- <sup>9</sup>B. W. Smith, M. Monthieux, and D. E. Luzzi, *Nature (London)* **396**, 323 (1998).
- <sup>10</sup>A. Kis, G. Csányi, J.-P. Salvetat, T.-N. Lee, E. Couteau, A. J. Kulik, W. Benoit, J. Brugger, and L. Förro, *Nature Mater.* **3**, 153 (2004).
- <sup>11</sup>C. Gómez-Navarro, P. J. De Pablo, J. Gómez-Herrero, B. Biel, F. J. García-Vidal, A. Rubio, and F. Flores, *Nature Mater.* **4**, 534 (2005).
- <sup>12</sup>M. Terrones, H. Terrones, F. Banhart, J.-C. Charlier, and P. M. Ajayan, *Science* **288**, 1226 (2000).
- <sup>13</sup>C. O. Girit, J. C. Meyer, R. Erni, M. D. Rossell, C. Kisielowski, L. Yang, C. Park, M. F. Crommie, M. L. Cohen, S. G. Louie, and A. Zettl, *Science* **323**, 1705 (2009).
- <sup>14</sup>D. Ugarte, *Nature (London)* **359**, 707 (1992).
- <sup>15</sup>A. V. Krasheninnikov and F. Banhart, *Nature Mater.* **6**, 723 (2007).
- <sup>16</sup>J. H. Warner, M. H. Rummeli, L. Ge, T. Gemming, B. Montanari, N. M. Harrison, B. Büchner, and G. Briggs, *Nat. Nanotechnol.* **4**, 500 (2009).
- <sup>17</sup>W. Mickelson, S. Aloni, W. Q. Han, J. Cumings, and A. Zettl, *Science* **300**, 467 (2003).
- <sup>18</sup>M. Terrones, F. Banhart, N. Grobert, J.-C. Charlier, H. Terrones, and P. M. Ajayan, *Phys. Rev. Lett.* **89**, 075505 (2002).
- <sup>19</sup>L. Sun, F. Banhart, A. V. Krasheninnikov, J. A. Rodríguez-Manzo, M. Terrones, and P. M. Ajayan, *Science* **312**, 1199 (2006).
- <sup>20</sup>L. Sun, A. V. Krasheninnikov, T. Ahlgren, K. Nordlund, and F. Banhart, *Phys. Rev. Lett.* **101**, 156101 (2008).
- <sup>21</sup>H. Stahl, J. Appenzeller, R. Martel, P. Avouris, and B. Lengeler, *Phys. Rev. Lett.* **85**, 5186 (2000).
- <sup>22</sup>B. Q. Wei, J. D’Arcy-Gall, P. M. Ajayan, and G. Ramanath, *Appl. Phys. Lett.* **83**, 3581 (2003).
- <sup>23</sup>M. S. Raghuvver, P. G. Ganesan, J. D’Arcy-Gall, G. Ramanath, M. Marshall, and I. Petrov, *Appl. Phys. Lett.* **84**, 4484 (2004).
- <sup>24</sup>M. S. Raghuvver, A. Kumar, M. J. Frederick, G. P. Louie, P. G. Ganesan, and G. Ramanath, *Adv. Mater.* **18**, 547 (2006).
- <sup>25</sup>M. Suzuki, K. Ishibashi, K. Toratani, D. Tsuya, and Y. Aoyagi, *Appl. Phys. Lett.* **81**, 2273 (2002).
- <sup>26</sup>K. Ishibashi, D. Tsuya, M. Suzuki, and Y. Aoyagi, *Appl. Phys. Lett.* **82**, 3307 (2003).
- <sup>27</sup>Y. J. Jung, Y. Homma, R. Vajtai, Y. Kobayashi, T. Ogino, and P. M. Ajayan, *Nano Lett.* **4**, 1109 (2004).
- <sup>28</sup>D.-H. Kim, H.-S. Jang, C.-D. Kim, D.-S. Cho, H.-D. Kang, and H.-R. Lee, *Chem. Phys. Lett.* **378**, 232 (2003).
- <sup>29</sup>D. Q. Yang, J. Rochette, and E. Sacher, *Langmuir* **21**, 8539 (2005).
- <sup>30</sup>B. Ni, R. Andrews, D. Jacques, D. Qian, M. B. J. Wijesundara, Y. Choi, L. Hanley, and S. B. Sinnott, *J. Phys. Chem. B* **105**, 12719 (2001).
- <sup>31</sup>C. Morant, J. Andrey, P. Prieto, D. Mendiola, J. M. Sanz, and E. Elizalde, *Phys. Status Solidi A* **203**, 1069 (2006).
- <sup>32</sup>Z. Osváth, G. Vértesy, L. Tapasztó, F. Wéber, Z. E. Horváth, J. Gyulai, and L. P. Biró, *Phys. Rev. B* **72**, 045429 (2005).
- <sup>33</sup>P. Vincent, A. Brioude, C. Journet, S. Rabaste, S. T. Purcell, J. L. Brusq, and J. C. Plenet, *J. Non-Cryst. Solids* **311**, 130 (2002).
- <sup>34</sup>H. M. Kim, H. S. Kim, S. K. Park, J. Joo, T. J. Lee, and C. J. Lee, *J. Appl. Phys.* **97**, 026103 (2005).
- <sup>35</sup>H. Schittenhelm, D. B. Geohegan, G. E. Jellison, A. A. Puretzky, M. J. Lance, and P. F. Britt, *Appl. Phys. Lett.* **81**, 2097 (2002).
- <sup>36</sup>V. A. Basiuk, K. Kobayashi, T. K. Y. Negishi, E. V. Basiuk, and J. M. Saniger-Blesa, *Nano Lett.* **2**, 789 (2002).
- <sup>37</sup>B. Khare, M. Meyyappan, M. H. Moore, P. Wilhite, H. Imanaka, and B. Chen, *Nano Lett.* **3**, 643 (2003).
- <sup>38</sup>P. P. Neupane, M. O. Manasreh, B. D. Weaver, B. J. Landi, and R. P. Raffaele, *Appl. Phys. Lett.* **86**, 221908 (2005).
- <sup>39</sup>K. Urita, K. Suenaga, T. Sugai, H. Shinohara, and S. Iijima, *Phys. Rev.*

- Lett.* **94**, 155502 (2005).
- <sup>40</sup>C.-H. Kiang, W. A. Goddard, R. Beyers, and D. S. Bethune, *J. Phys. Chem.* **100**, 3749 (1996).
- <sup>41</sup>P. M. Ajayan, V. Ravikumar, and J.-C. Charlier, *Phys. Rev. Lett.* **81**, 1437 (1998).
- <sup>42</sup>B. W. Smith and D. E. Luzzi, *J. Appl. Phys.* **90**, 3509 (2001).
- <sup>43</sup>V. H. Crespi, N. G. Chopra, M. L. Cohen, A. Zettl, and S. G. Louie, *Phys. Rev. B* **54**, 5927 (1996).
- <sup>44</sup>V. H. Crespi, N. G. Chopra, M. L. Cohen, A. Zettl, and V. Radmilović, *Appl. Phys. Lett.* **73**, 2435 (1998).
- <sup>45</sup>F. Banhart, J. X. Li, and M. Terrones, *Small* **1**, 953 (2005).
- <sup>46</sup>F. Banhart, J. X. Li, and A. V. Krasheninnikov, *Phys. Rev. B* **71**, 241408(R) (2005).
- <sup>47</sup>J. X. Li and F. Banhart, *Nano Lett.* **4**, 1143 (2004).
- <sup>48</sup>C. Mikó, M. Milas, J. W. Seo, E. Couteau, N. Barisić, R. Gaál, and L. Forró, *Appl. Phys. Lett.* **83**, 4622 (2003).
- <sup>49</sup>J. P. Salvetat, J. M. Bonard, N. H. Thomson, A. J. Kulik, L. Forró, W. Benoit, and L. Zuppiroli, *Appl. Phys. A: Mater. Sci. Process.* **69**, 255 (1999).
- <sup>50</sup>J. P. Salvetat, T. Fehér, C. L'Huillier, F. Beuneu, and L. Forró, *Phys. Rev. B* **72**, 075440 (2005).
- <sup>51</sup>S. Trasobares, O. Stéphan, C. Colliex, G. Hug, W. K. Hsu, H. W. Kroto, and D. R. M. Walton, *Eur. Phys. J. B* **22**, 117 (2001).
- <sup>52</sup>R. Caudillo, H. E. Troiani, M. A. L. M. Miki-Yoshida, A. Rubio, and M. J. Yacaman, *Radiat. Phys. Chem.* **73**, 334 (2005).
- <sup>53</sup>V. Skakalova, U. Dettlaff-Weglikowska, and S. Roth, *Diamond Related Materials* **13**, 296 (2004).
- <sup>54</sup>C. Mikó, M. Milas, J. W. Seo, R. Gaal, A. Kulik, and L. Forro, *Appl. Phys. Lett.* **88**, 151905 (2006).
- <sup>55</sup>A. Mangione, L. Torrisi, A. M. Visco, N. Campo, F. Bonaccorso, P. G. Gucciardi, and F. Belloni, *Radiat. Eff. Defects Solids* **163**, 453 (2008).
- <sup>56</sup>M. Hulman, V. Skákalová, S. Roth, and H. Kuzmany, *J. Appl. Phys.* **98**, 024311 (2005).
- <sup>57</sup>S. Talapatra, P. G. Ganesan, T. Kim, R. Vajtai, M. Huang, M. Shima, G. Ramanath, D. Srivastava, S. C. Deevi, and P. M. Ajayan, *Phys. Rev. Lett.* **95**, 097201 (2005).
- <sup>58</sup>P. Esquinazi, D. Spemann, R. Höhne, A. Setzer, and T. Butz, *Phys. Rev. Lett.* **91**, 227201 (2003).
- <sup>59</sup>C. Chappert, H. Bernas, J. Ferreacute, V. Kottler, J. Jamet, Y. Chen, E. Cambril, T. Devolder, F. Rousseaux, V. Mathet, and H. Launois, *Science* **280**, 1919 (1998).
- <sup>60</sup>H. Bernas, J.-P. Attané, K.-H. Heinig, D. Halley, D. Ravelosona, A. Marty, P. Auric, C. Chappert, and Y. Samson, *Phys. Rev. Lett.* **91**, 077203 (2003).
- <sup>61</sup>E. Akcöltekin, T. Peters, R. Meyer, A. Duvenbeck, M. Klusmann, I. Monnet, H. Lebius, and M. Schleberger, *Nat. Nanotechnol.* **2**, 290 (2007).
- <sup>62</sup>S. Dhar, R. P. Davis, and L. C. Feldman, *Nanotechnology* **17**, 4514 (2006).
- <sup>63</sup>K. H. Heinig, T. Muller, B. Schmidt, M. Strobel, and W. Möller, *Appl. Phys. A: Mater. Sci. Process.* **77**, 17 (2003).
- <sup>64</sup>S. Klumünzer, *Nucl. Instrum. Methods Phys. Res. B* **244**, 1 (2006).
- <sup>65</sup>A. Colli, A. Fasoli, C. Ronning, S. Pisana, S. Piscanec, and A. C. Ferrari, *Nano Lett.* **8**, 2188 (2008).
- <sup>66</sup>A. Kumar, D. K. Avasthi, J. C. Pivin, and P. M. Koinkar, *Appl. Phys. Lett.* **92**, 221904 (2008).
- <sup>67</sup>W. L. Brown, M. F. Jarrold, R. L. McEachern, M. Sosnowski, H. U. G. Takaoka, and I. Yamada, *Nucl. Instrum. Methods Phys. Res. B* **59-60**, 182 (1991).
- <sup>68</sup>S. Bouneau, A. Brunelle, S. Della-Negra, J. Depauw, D. Jacquet, Y. L. Beyec, M. Pautrat, M. Fallavier, J. C. Poizat, and H. H. Andersen, *Phys. Rev. B* **65**, 144106 (2002).
- <sup>69</sup>L. P. Allen, Z. Insepov, D. B. F. C. Santeufemio, W. Brooks, K. S. Jones, and I. Yamada, *J. Appl. Phys.* **92**, 3671 (2002).
- <sup>70</sup>H. H. Andersen, A. Johansen, M. Olsen, and V. Touboltsev, *Nucl. Instrum. Methods Phys. Res. B* **212**, 56 (2003).
- <sup>71</sup>J. Samela and K. Nordlund, *Phys. Rev. Lett.* **101**, 027601 (2008).
- <sup>72</sup>F. Banhart, *Rep. Prog. Phys.* **62**, 1181 (1999).
- <sup>73</sup>F. Banhart, *Philos. Trans. R. Soc. London, Ser. A* **362**, 2205 (2004).
- <sup>74</sup>A. V. Krasheninnikov and K. Nordlund, *Nucl. Instrum. Methods Phys. Res. B* **216**, 355 (2004).
- <sup>75</sup>S. Dhara, *Crit. Rev. Solid State Mater. Sci.* **32**, 1 (2007).
- <sup>76</sup>A. V. Krasheninnikov, *J. Comput. Theor. Nanosci.* **5**, 1828 (2008).
- <sup>77</sup>J. Kotakoski, A. V. Krasheninnikov, and K. Nordlund, *Radiat. Eff. Defects Solids* **162**, 157 (2007).
- <sup>78</sup>I. Utke, P. Hoffmann, and J. Melngailis, *J. Vac. Sci. Technol. B* **26**, 1197 (2008).
- <sup>79</sup>A. K. Geim and K. S. Novoselov, *Nature Mater.* **6**, 183 (2007).
- <sup>80</sup>A. H. Castro Neto, F. Guinea, N. M. R. Peres, K. S. Novoselov, and A. K. Geim, *Rev. Mod. Phys.* **81**, 109 (2009).
- <sup>81</sup>ISI Web of Science (formerly known as Science Citation Index), isiwebofknowledge.com. Web of Science is a registered trademark of Thomson Reuters Inc.
- <sup>82</sup>J. P. Briand, L. de Billy, P. Charles, S. Essabaa, P. Briand, R. Geller, J. P. Desclaux, S. Bliman, and C. Ristori, *Phys. Rev. Lett.* **65**, 159 (1990).
- <sup>83</sup>J. F. Ziegler, J. P. Biersack, and U. Littmark, *The Stopping and Range of Ions in Matter* (Pergamon, New York, 1985).
- <sup>84</sup>M. Nastasi, J. Mayer, and J. Hirvonen, *Ion-Solid Interactions—Fundamentals and Applications* (Cambridge University Press, Cambridge, 1996).
- <sup>85</sup>T. Diaz de la Rubia, R. S. Averback, R. Benedek, and W. E. King, *Phys. Rev. Lett.* **59**, 1930 (1987); **60**, 76(E) (1988).
- <sup>86</sup>S. E. Donnelly and R. C. Birtcher, *Phys. Rev. B* **56**, 13599 (1997).
- <sup>87</sup>A. Meldrum, S. J. Zinkle, L. A. Boatner, and R. C. Ewing, *Nature (London)* **395**, 56 (1998).
- <sup>88</sup>A. E. Stuchbery and E. Bezakova, *Phys. Rev. Lett.* **82**, 3637 (1999).
- <sup>89</sup>E. Fermi and E. Teller, *Phys. Rev.* **72**, 399 (1947).
- <sup>90</sup>L. M. Kishinevskii, *Bull. Acad. Sci. USSR, Phys. Ser. (Engl. Transl.)* **26**, 1433 (1962).
- <sup>91</sup>E. Bonderup and P. Hvelplund, *Phys. Rev. A* **4**, 562 (1971).
- <sup>92</sup>P. M. Echenique, R. M. Nieminen, and R. H. Ritchie, *Solid State Commun.* **37**, 779 (1981).
- <sup>93</sup>W. Brandt and M. Kitagawa, *Phys. Rev. B* **25**, 5631 (1982).
- <sup>94</sup>J. A. Golovchenko, D. E. Cox, and A. N. Goland, *Phys. Rev. B* **26**, 2335 (1982).
- <sup>95</sup>J. Oddershede and J. R. Sabin, *At. Data Nucl. Data Tables* **31**, 275 (1984).
- <sup>96</sup>E. J. McGuire, *Phys. Rev. A* **56**, 488 (1997).
- <sup>97</sup>A. F. Lifschitz and N. R. Arista, *Phys. Rev. A* **57**, 200 (1998).
- <sup>98</sup>J. F. Ziegler, *J. Appl. Phys.* **85**, 1249 (1999).
- <sup>99</sup>J. Wang, J. Mathar, S. B. Trickey, and J. R. Sabin, *J. Phys.: Condens. Matter* **11**, 3973 (1999).
- <sup>100</sup>J. I. Juaristi, C. Auth, H. Winter, A. Arnau, K. Eder, D. Semrad, F. Aumayr, P. Bauer, and P. Echenique, *Phys. Rev. Lett.* **84**, 2124 (2000).
- <sup>101</sup>V. U. Nazarov, J. M. Pitarke, C. S. Kim, and Y. Takada, *Phys. Rev. B* **71**, 121106(R) (2005).
- <sup>102</sup>N. Arista, *Mat. Fys. Medd. K. Dan. Vidensk. Selsk.* **52**, 595 (2006).
- <sup>103</sup>J. Krauser, J. Zollondz, A. Weidinger, and C. Trautmann, *J. Appl. Phys.* **94**, 1959 (2003).
- <sup>104</sup>D. Kanjijal, *Curr. Sci.* **80**, 1560 (2001).
- <sup>105</sup>C. Trautmann, S. Klumünzer, and H. Trinkaus, *Phys. Rev. Lett.* **85**, 3648 (2000).
- <sup>106</sup>A. Kumar, D. K. Avasthi, A. Tripathi, D. Kabiraj, F. Singh, and J. C. Pivin, *J. Appl. Phys.* **101**, 014308 (2007).
- <sup>107</sup>P. Kluth, C. S. Schnorr, O. H. Pakarinen, F. Djurabekova, D. J. Sprouster, R. Giulian, M. C. Ridgway, A. P. Byrne, C. Trautmann, D. J. Cookson, K. Nordlund, and M. Toulemonde, *Phys. Rev. Lett.* **101**, 175503 (2008).
- <sup>108</sup>F. Spaepen and D. Turnbull, *Crystallization Processes* (Academic, New York, 1982), Chap. 2, pp. 15–42.
- <sup>109</sup>I. Jencic, M. W. Bench, I. M. Robertson, and M. A. Kirk, *J. Appl. Phys.* **78**, 974 (1995).
- <sup>110</sup>M. W. Bench, I. M. Robertson, M. A. Kirk, and I. Jenčić, *J. Appl. Phys.* **87**, 49 (2000).
- <sup>111</sup>J. Frantz, J. Tarus, K. Nordlund, and J. Keinonen, *Phys. Rev. B* **64**, 125313 (2001).
- <sup>112</sup>E. Aprile, W. H.-M. Ku, and J. Park, *IEEE Trans. Nucl. Sci.* **35**, 37 (1988).
- <sup>113</sup>G. Szenes, *Nucl. Instrum. Methods Phys. Res. B* **122**, 530 (1997).
- <sup>114</sup>M. Toulemonde, W. Assmann, C. Dufour, A. Meftah, F. Studer, and C. Trautmann, *Mat. Fys. Medd. K. Dan. Vidensk. Selsk.* **52**, 263 (2006).
- <sup>115</sup>M. Guinan, *J. Nucl. Mater.* **53**, 171 (1974).
- <sup>116</sup>K. Nordlund, T. T. Järvi, K. Meinander, and J. Samela, *Appl. Phys. A: Mater. Sci. Process.* **91**, 561 (2008).
- <sup>117</sup>J. Samela, K. Nordlund, V. N. Popok, and E. E. B. Campbell, *Phys. Rev. B* **77**, 075309 (2008).
- <sup>118</sup>G. Abrasonis, W. Möller, and X. X. Ma, *Phys. Rev. Lett.* **96**, 065901 (2006).
- <sup>119</sup>C. Yang, N. P.-O. Homman, K. Malmqvist, L. Johansson, N. M. Halden, V. Barbin, S. H. Sie, and G. Remond, *Scanning Microsc.* **9**, 43 (1995).
- <sup>120</sup>J. Samela and K. Nordlund, *Phys. Rev. B* **76**, 125434 (2007).
- <sup>121</sup>J. Roth, in *Sputtering by Particle Bombardment*, edited by R. Behrisch

- (Springer, Berlin, 1981), Vol. I, pp. 91–146.
- <sup>122</sup> J. Küppers, *Surf. Sci. Rep.* **22**, 249 (1995).
- <sup>123</sup> E. Salonen, K. Nordlund, J. Keinonen, and C. H. Wu, *Phys. Rev. B* **63**, 195415 (2001).
- <sup>124</sup> A. V. Krasheninnikov, K. Nordlund, E. Salonen, J. Keinonen, and C. H. Wu, *Comput. Mater. Sci.* **25**, 427 (2002).
- <sup>125</sup> C. Björkas, K. Vörtler, K. Nordlund, D. Nishijima, and R. Doerner, *New J. Phys.* **11**, 123017 (2009).
- <sup>126</sup> M. Toulemonde, W. Assman, C. Trautmann, F. Gruner, H. D. Mieskes, H. Kucal, and Z. G. Wang, *Nucl. Instrum. Methods Phys. Res. B* **212**, 346 (2003).
- <sup>127</sup> K. Nakayama and J. H. Weaver, *Phys. Rev. Lett.* **82**, 980 (1999).
- <sup>128</sup> A. Meftah, F. Brisard, J. M. Costantini, E. Dooryhee, M. Hage-Ali, M. Hervieu, J. P. Stoquert, F. Studer, and M. Toulemonde, *Phys. Rev. B* **49**, 12457 (1994).
- <sup>129</sup> P. Ehrhart, *Atomic defects in metals*, Landolt-Bornstein, New Series III Vol. 25 (Springer, Berlin, 1991), Chap. 2, p. 88.
- <sup>130</sup> A. F. Voter, F. Montalenti, and T. C. Germann, *Annu. Rev. Mater. Res.* **32**, 321 (2002).
- <sup>131</sup> B. P. Uberuaga, S. J. Stuart, and A. F. Voter, *Phys. Rev. B* **75**, 014301 (2007).
- <sup>132</sup> J. Kotakoski, A. V. Krasheninnikov, and K. Nordlund, *J. Comput. Theor. Nanosci.* **4**, 1153 (2007).
- <sup>133</sup> A. J. Nozik, *Annu. Rev. Phys. Chem.* **52**, 193 (2001).
- <sup>134</sup> It is a matter of certain controversy whether temperature can be used to describe the atoms in a collision cascade since the system is of course not in thermodynamic equilibrium. However, it has been shown that after about three lattice vibrations, atoms do have a Maxwell–Boltzmann velocity distribution (Ref. 85). Hence we consider the use of Kelvin scale temperature as a practical way of describing the average kinetic energy of atoms. This also conforms to common usage of temperature units in other fields dealing with nonequilibrium systems, such as plasma physics.
- <sup>135</sup> T. T. Järvi, J. A. Pakarinen, A. Kuronen, and K. Nordlund, *EPL* **82**, 26002 (2008).
- <sup>136</sup> T. Kunert and R. Schmidt, *Phys. Rev. Lett.* **86**, 5258 (2001).
- <sup>137</sup> J. M. Pruneda, D. Sánchez-Portal, A. Arnau, J. I. Juaristi, and E. Artacho, *Phys. Rev. Lett.* **99**, 235501 (2007).
- <sup>138</sup> A. V. Krasheninnikov, Y. Miyamoto, and D. Tománek, *Phys. Rev. Lett.* **99**, 016104 (2007).
- <sup>139</sup> M. Quijada, R. Díez-Muñoz, and P. M. Echenique, *Nanotechnology* **16**, S176 (2005).
- <sup>140</sup> M. Ishigami, H. Choi, S. Aloni, S. G. Louie, M. L. Cohen, and A. Zettl, *Phys. Rev. Lett.* **93**, 196803 (2004).
- <sup>141</sup> L. Tapasztó, G. Dobrik, P. Nemes-Incze, G. Vertesy, P. Lambin, and L. P. Biró, *Phys. Rev. B* **78**, 233407 (2008).
- <sup>142</sup> G. Compagnini, F. Giannazzo, S. Sonde, V. Raineri, and E. Rimini, *Carbon* **47**, 3201 (2009).
- <sup>143</sup> K. Nordlund, J. Keinonen, and T. Mattila, *Phys. Rev. Lett.* **77**, 699 (1996).
- <sup>144</sup> D. B. Williams and C. B. Carter, *Transmission Electron Microscopy: A Textbook for Materials Science* (Plenum, New York, 1996).
- <sup>145</sup> R. C. Birtcher, S. E. Donnelly, M. Song, K. Furuya, K. Mitsuiishi, and C. W. Allen, *Phys. Rev. Lett.* **83**, 1617 (1999).
- <sup>146</sup> M. Haider, H. Rose, S. Uhlemann, E. Schwan, B. Kabius, and K. Urban, *Ultramicroscopy* **75**, 53 (1998).
- <sup>147</sup> M. I. Current, C.-Y. Wei, and D. N. Seidman, *Philos. Mag. A* **47**, 407 (1983).
- <sup>148</sup> M. I. Guseva, A. L. Suvorov, S. N. Korshunov, and N. E. Lazarev, *J. Nucl. Mater.* **266-269**, 222 (1999).
- <sup>149</sup> M. K. Miller, A. Cerezo, M. G. Hetherington, and G. D. W. Smith, *Atom Probe Field-Ion Microscopy* (Oxford University Press, Oxford, 1996), for a brief introduction, see also <http://www.materials.ox.ac.uk/fim/whatis3dap.html>.
- <sup>150</sup> J. Chen, W. G. Cullen, C. Jang, M. S. Fuhrer, and E. D. Williams, *Phys. Rev. Lett.* **102**, 236805 (2009).
- <sup>151</sup> G. D. Saraiva, A. G. S. Filho, G. Braunstein, E. B. Barros, J. M. Filho, E. C. Moreira, S. B. Fagan, D. L. Baptista, Y. A. Kim, H. Muramatsu, M. Endo, and M. S. Dresselhaus, *Phys. Rev. B* **80**, 155452 (2009).
- <sup>152</sup> R. Arenal, A. C. Ferrari, S. Reich, L. Wirtz, J. Mevellec, S. Lefrant, and A. L. A. Rubio, *Nano Lett.* **6**, 1812 (2006).
- <sup>153</sup> L. Khriachtchev, M. Räsänen, S. Novikov, and L. Pavesi, *Appl. Phys. Lett.* **85**, 1511 (2004).
- <sup>154</sup> L. Khriachtchev, *Top. Appl. Phys.* **100**, 403 (2006).
- <sup>155</sup> A. C. Ferrari and J. Robertson, *Phys. Rev. B* **61**, 14095 (2000).
- <sup>156</sup> Z. Ni, Q. Li, L. Yan, J. Gong, and D. Zhu, *Diamond Relat. Mater.* **17**, 365 (2008).
- <sup>157</sup> J. A. Nichols, H. Saito, C. Deck, and P. R. Bandaru, *J. Appl. Phys.* **102**, 064306 (2007).
- <sup>158</sup> S. Mathew, U. M. Bhatta, J. Ghatak, B. R. Sekhar, and B. N. Dev, *Carbon* **45**, 2659 (2007).
- <sup>159</sup> Y. Zhu, T. Yi, B. Zheng, and L. Cao, *Appl. Surf. Sci.* **137**, 83 (1999).
- <sup>160</sup> A. K. Chakraborty, R. A. J. Woolley, Y. V. Butenko, V. R. Dhanak, L. Siller, and M. R. C. Hunt, *Carbon* **45**, 2744 (2007).
- <sup>161</sup> F. Beuneu, C. l’Huillier, J.-P. Salvetat, J.-M. Bonard, and L. Forró, *Phys. Rev. B* **59**, 5945 (1999).
- <sup>162</sup> A. R. Adhikari, H. Bakhru, P. M. Ajayan, R. Benson, and M. Chipara, *Nucl. Instrum. Methods Phys. Res. B* **265**, 347 (2007).
- <sup>163</sup> E. Najafi, D. Hernández Cruz, M. Obst, A. P. Hitchcock, B. Douhard, J. Pireaux, and A. Felten, *Small* **4**, 2279 (2008).
- <sup>164</sup> B.-K. Teo, *EXAFS: Basic Principles and Data Analysis* (Springer, Berlin, 1986).
- <sup>165</sup> Q. Xu, I. Sharp, C. Yuan, D. Yi, C. Liao, A. Glaeser, A. Minor, J. Beeman, M. Ridgway, P. Kluth, J. W. Ager III, D. C. Chrzan, and E. E. Haller, *Phys. Rev. Lett.* **97**, 155701 (2006).
- <sup>166</sup> B. Johannessen, P. Kluth, D. J. Llewellyn, G. J. Foran, D. J. Cookson, and M. C. Ridgway, *Appl. Phys. Lett.* **90**, 073119 (2007).
- <sup>167</sup> V. Skakalova, S. Kaiser and A. B. Roth, *Phys. Status Solidi B* **2**, 62 (2008).
- <sup>168</sup> Y. Fan, B. R. Goldsmith, and P. G. Collins, *Nature Mater.* **4**, 906 (2005).
- <sup>169</sup> *Identification of Defects in Semiconductors (Semiconductors and Semimetals)*, edited by M. Stavola (Academic, San Diego, 1999), Vol. 51B.
- <sup>170</sup> K. Nordlund, T. Ahlgren, and E. Rauhala (unpublished).
- <sup>171</sup> L. A. Girifalco and V. G. Weizer, *Phys. Rev.* **114**, 687 (1959).
- <sup>172</sup> J. Tersoff, *Phys. Rev. B* **37**, 6991 (1988).
- <sup>173</sup> J. E. Jones, *Proc. R. Soc. London, Ser. A* **106**, 463 (1924).
- <sup>174</sup> A. V. Krasheninnikov, K. Nordlund, M. Sirviö, E. Salonen, and J. Keinonen, *Phys. Rev. B* **63**, 245405 (2001).
- <sup>175</sup> A. V. Krasheninnikov, K. Nordlund, and J. Keinonen, *Phys. Rev. B* **65**, 165423 (2002).
- <sup>176</sup> F. Z. Cui, Z. J. Chen, J. Ma, G. R. Xia, and Y. Zhai, *Phys. Lett. A* **295**, 55 (2002).
- <sup>177</sup> J. F. Ziegler and J. P. Biersack, Program TRIM, <http://www.srim.org>, 2003.
- <sup>178</sup> J. A. V. Pomoell, A. V. Krasheninnikov, K. Nordlund, and J. Keinonen, *J. Appl. Phys.* **96**, 2864 (2004).
- <sup>179</sup> F. Djurabekova, M. Backman, and K. Nordlund, *Nucl. Instrum. Methods Phys. Res. B* **266**, 2683 (2008).
- <sup>180</sup> *Atomic and Ion Collisions in Solids and at Surfaces: Theory, Simulation, and Applications*, edited by R. Smith (Cambridge University Press, Cambridge, 1997).
- <sup>181</sup> M. P. Allen and D. J. Tildesley, *Computer Simulation of Liquids* (Oxford University Press, Oxford, 1989).
- <sup>182</sup> R. S. Averback and T. Diaz de la Rubia, in *Solid State Physics*, edited by H. Ehrenfest and F. Spaepen (Academic, New York, 1998), Vol. 51, pp. 281–402.
- <sup>183</sup> K. Nordlund, *Comput. Mater. Sci.* **3**, 448 (1995).
- <sup>184</sup> W. A. McKinley and H. Feshbach, *Phys. Rev.* **74**, 1759 (1948).
- <sup>185</sup> L. R. Greenwood, *J. Nucl. Mater.* **216**, 29 (1994).
- <sup>186</sup> J. F. Ziegler, J. P. Biersack, and M. D. Ziegler, *SRIM—The Stopping and Range of Ions in Matter* (SRIM Co., Chester, 2008).
- <sup>187</sup> H. Zhu and R. S. Averback, *Nucl. Instrum. Methods Phys. Res. B* **83**, 334 (1993).
- <sup>188</sup> D. W. Brenner, *Phys. Rev. B* **42**, 9458 (1990).
- <sup>189</sup> D. W. Brenner, O. A. Shenderova, J. A. Harrison, S. J. Stuart, B. Ni, and S. B. Sinnott, *J. Phys.: Condens. Matter* **14**, 783 (2002).
- <sup>190</sup> S. J. Stuart, A. B. Tutein, and J. A. Harrison, *J. Chem. Phys.* **112**, 6472 (2000).
- <sup>191</sup> M. W. Finnis and J. E. Sinclair, *Philos. Mag. A* **50**, 45 (1984); **53**, 161(E) (1986).
- <sup>192</sup> M. S. Daw, S. M. Foiles, and M. I. Baskes, *Mater. Sci. Rep.* **9**, 251 (1993).
- <sup>193</sup> C. L. Kelchner, D. M. Halstead, L. S. Perkins, N. M. Wallace, and A. E. DePristo, *Surf. Sci.* **310**, 425 (1994) (and references therein).
- <sup>194</sup> F. Cleri and V. Rosato, *Phys. Rev. B* **48**, 22 (1993).
- <sup>195</sup> K. Albe, K. Nordlund, J. Nord, and A. Kuronen, *Phys. Rev. B* **66**, 035205 (2002).
- <sup>196</sup> K. Albe, K. Nordlund, and R. S. Averback, *Phys. Rev. B* **65**, 195124 (2002).
- <sup>197</sup> P. Erhart, N. Juslin, O. Goy, K. Nordlund, R. Muller, and K. Albe, *J.*

- Phys.: Condens. Matter* **18**, 6585 (2006).
- <sup>198</sup> J. Nord, K. Albe, P. Erhart, and K. Nordlund, *J. Phys.: Condens. Matter* **15**, 5649 (2003).
- <sup>199</sup> N. Juslin, P. Erhart, P. Träskelin, J. Nord, K. O. E. Henriksson, K. Nordlund, E. Salonen, and K. Albe, *J. Appl. Phys.* **98**, 123520 (2005).
- <sup>200</sup> K. O. E. Henriksson and K. Nordlund, *Phys. Rev. B* **79**, 144107 (2009).
- <sup>201</sup> W. G. Hoover, *Phys. Rev. A* **31**, 1695 (1985).
- <sup>202</sup> H. J. C. Berendsen, J. P. M. Postma, W. F. van Gunsteren, A. DiNola, and J. R. Haak, *J. Chem. Phys.* **81**, 3684 (1984).
- <sup>203</sup> E. M. Bringa and R. E. Johnson, *Nucl. Instrum. Methods Phys. Res. B* **143**, 513 (1998).
- <sup>204</sup> S. Mookerjee, M. Beuve, S. A. Khan, M. Toulemonde, and A. Roy, *Phys. Rev. B* **78**, 045435 (2008).
- <sup>205</sup> R. Martin, *Electronic Structure* (Cambridge University Press, Cambridge, 2004).
- <sup>206</sup> O. V. Yazyev, I. Tavernelli, U. Rothlisberger, and L. Helm, *Phys. Rev. B* **75**, 115418 (2007).
- <sup>207</sup> E. Holmström, A. Kuronen, and K. Nordlund, *Phys. Rev. B* **78**, 045202 (2008).
- <sup>208</sup> D. Porezag, T. Frauenheim, T. Köhler, G. Seifert, and R. Kaschner, *Phys. Rev. B* **51**, 12947 (1995).
- <sup>209</sup> M. Elstner, D. Porezag, G. Jungnickel, J. Elsner, M. Haugk, T. Frauenheim, S. Suhai, and G. Seifert, *Phys. Rev. B* **58**, 7260 (1998).
- <sup>210</sup> A. V. Krasheninnikov, F. Banhart, J. X. Li, A. S. Foster, and R. Nieminen, *Phys. Rev. B* **72**, 125428 (2005).
- <sup>211</sup> T. Lopenon, A. V. Krasheninnikov, M. Kaukonen, and R. M. Nieminen, *Phys. Rev. B* **74**, 073409 (2006).
- <sup>212</sup> A. Zobelli, A. Gloter, C. P. Ewels, G. Seifert, and C. Colliex, *Phys. Rev. B* **75**, 245402 (2007).
- <sup>213</sup> Z. Wang, F. Gao, J. Li, X. Zu, and W. J. Weber, *Nanotechnology* **20**, 075708 (2009).
- <sup>214</sup> T. Frauenheim, G. Seifert, M. Elstner, T. Niehaus, C. Köhler, M. Amkreutz, M. Sternberg, Z. Hajnal, A. Di Carlo, and S. Suhai, *J. Phys.: Condens. Matter* **14**, 3015 (2002).
- <sup>215</sup> A. V. Krasheninnikov, K. Nordlund, P. O. Lehtinen, A. S. Foster, A. Ayuela, and R. M. Nieminen, *Phys. Rev. B* **69**, 073402 (2004).
- <sup>216</sup> A. V. Krasheninnikov, P. O. Lehtinen, A. S. Foster, and R. M. Nieminen, *Chem. Phys. Lett.* **418**, 132 (2006).
- <sup>217</sup> C. Xu, C. Wang, C. Chan, and K. Ho, *J. Phys.: Condens. Matter* **4**, 6047 (1992).
- <sup>218</sup> M. Terrones, P. M. Ajayan, F. Banhart, X. Blasé, D. L. Carroll, J. C. Charlier, R. Czerw, B. Foley, N. Grobert, R. Kamalakaran, P. Kohler-Redlich, M. Ruhle, T. Seeger, and H. Terrones, *Appl. Phys. A: Mater. Sci. Process.* **65**, 355 (2002).
- <sup>219</sup> T. Schenkel, M. A. Briere, K. Schmidt-Böcking, K. Bethge, and D. H. Schneider, *Phys. Rev. Lett.* **78**, 2481 (1997).
- <sup>220</sup> Y. Miyamoto and H. Zhang, *Phys. Rev. B* **77**, 161402 (2008).
- <sup>221</sup> O. Sugino and Y. Miyamoto, *Phys. Rev. B* **59**, 2579 (1999); **66**, 089901(E) (2002).
- <sup>222</sup> Y. Miyamoto, S. Berber, M. Yoon, A. Rubio, and D. Tománek, *Chem. Phys. Lett.* **392**, 209 (2004).
- <sup>223</sup> Y. Miyamoto, A. Rubio, and D. Tománek, *Phys. Rev. Lett.* **97**, 126104 (2006).
- <sup>224</sup> J. F. Ziegler, SRIM-2003 software package, available online at <http://www.srim.org>.
- <sup>225</sup> M. T. Robinson and I. M. Torrens, *Phys. Rev. B* **9**, 5008 (1974).
- <sup>226</sup> M. T. Robinson, *Phys. Rev. B* **40**, 10717 (1989).
- <sup>227</sup> K. M. Beardmore and N. Grønbech-Jensen, *Phys. Rev. E* **57**, 7278 (1998).
- <sup>228</sup> J. Sillanpää, K. Nordlund, and J. Keinonen, *Phys. Rev. B* **62**, 3109 (2000).
- <sup>229</sup> J. Sillanpää, J. Peltola, K. Nordlund, J. Keinonen, and M. J. Puska, *Phys. Rev. B* **63**, 134113 (2001).
- <sup>230</sup> L. Zhigilei, P. B. S. Kodali, and B. J. Garrison, *J. Phys. Chem. B* **102**, 2845 (1998).
- <sup>231</sup> C. Schäfer, H. M. Urbassek, and L. V. Zhigilei, *Phys. Rev. B* **66**, 115404 (2002).
- <sup>232</sup> M. Toulemonde, C. Dufour, A. Meftah, and E. Paunier, *Nucl. Instrum. Methods Phys. Res. B* **166-167**, 903 (2000).
- <sup>233</sup> E. M. Bringa and R. E. Johnson, *Phys. Rev. Lett.* **88**, 165501 (2002).
- <sup>234</sup> H. M. Urbassek, H. Kafemann, and R. E. Johnson, *Phys. Rev. B* **49**, 786 (1994).
- <sup>235</sup> D. Schwen and E. M. Bringa, *Nucl. Instrum. Methods Phys. Res. B* **256**, 187 (2007).
- <sup>236</sup> R. Devanathan, P. Durham, J. Du, L. R. Corrales, and E. M. Bringa, *Nucl. Instrum. Methods Phys. Res. B* **255**, 172 (2007).
- <sup>237</sup> D. M. Duffy, N. Itoh, A. M. Rutherford, and A. M. Stoneham, *J. Phys.: Condens. Matter* **20**, 082201 (2008).
- <sup>238</sup> D. S. Ivanov and L. V. Zhigilei, *Phys. Rev. B* **68**, 064114 (2003).
- <sup>239</sup> L. Koči, E. M. Bringa, D. S. Ivanov, J. Hawreliak, J. McNaney, A. Higginbotham, L. V. Zhigilei, A. B. Belonoshko, B. A. Remington, and R. Ahuja, *Phys. Rev. B* **74**, 012101 (2006).
- <sup>240</sup> A. Caro and M. Victoria, *Phys. Rev. A Gen. Phys.* **40**, 2287 (1989).
- <sup>241</sup> M. W. Finnis, P. Agnew, and A. J. E. Foreman, *Phys. Rev. B* **44**, 567 (1991).
- <sup>242</sup> I. Koponen, *J. Appl. Phys.* **72**, 1194 (1992).
- <sup>243</sup> Q. Hou, M. Hou, L. Bardotti, B. Prevel, P. Melinon, and A. Perez, *Phys. Rev. B* **62**, 2825 (2000).
- <sup>244</sup> D. M. Duffy and A. M. Rutherford, *J. Phys.: Condens. Matter* **19**, 016207 (2007).
- <sup>245</sup> J. le Page, D. R. Mason, C. P. Race, and W. M. C. Foulkes, *New J. Phys.* **11**, 013004 (2009).
- <sup>246</sup> A. Duvenbeck, O. Weingart, V. Buss, and A. Wucher, *New J. Phys.* **9**, 38 (2007).
- <sup>247</sup> A. Duvenbeck, B. Weidtmann, O. Weingart, and A. Wucher, *Phys. Rev. B* **77**, 245444 (2008).
- <sup>248</sup> W. M. Young and E. W. Elcock, *Proc. Phys. Soc. London* **89**, 735 (1966).
- <sup>249</sup> A. B. Bortz, M. H. Kalos, and J. L. Lebowitz, *J. Comput. Phys.* **17**, 10 (1975).
- <sup>250</sup> K. A. Fichthorn and W. H. Weinberg, *J. Chem. Phys.* **95**, 1090 (1991).
- <sup>251</sup> F. G. Djurabekova, L. Malerba, C. Domain, and C. S. Becquart, *Nucl. Instrum. Methods Phys. Res. B* **255**, 47 (2007).
- <sup>252</sup> J. Dalla Torre, J. Bocquet, N. V. Doan, E. Adam, and A. Barbu, *Philos. Mag. A* **85**, 549 (2005).
- <sup>253</sup> T. Opplestrup, V. V. Bulatov, G. H. Gilmer, M. H. Kalos, and B. Sadigh, *Phys. Rev. Lett.* **97**, 230602 (2006).
- <sup>254</sup> P. E. Blöchl, *Phys. Rev. B* **50**, 17953 (1994).
- <sup>255</sup> H. W. Kroto, J. R. Heath, S. C. O'Brien, R. F. Curl, and R. E. Smalley, *Nature (London)* **318**, 162 (1985).
- <sup>256</sup> A. Jorio, G. Dresselhaus, and M. Dresselhaus, *Topics in Applied Physics* (Springer, Berlin, 2008), Vol. 111.
- <sup>257</sup> C. Jin, H. Lan, L. Peng, K. Suenaga, and S. Iijima, *Phys. Rev. Lett.* **102**, 205501 (2009).
- <sup>258</sup> A. Chuvilin, J. C. Meyer, G. Algara-Siller, and U. Kaiser, *New J. Phys.* **11**, 083019 (2009).
- <sup>259</sup> A. G. Nasibulin, P. V. Pikhitsa, H. Jiang, D. P. Brown, A. V. Krasheninnikov, A. S. Anisimov, P. Queipo, A. Moiala, D. Gonzalez, G. Lientschnig, A. Hassaniien, S. D. Shandakov, G. Lolli, D. E. Resasco, M. Choi, D. Tománek, and E. I. Kauppinen, *Nat. Nanotechnol.* **2**, 156 (2007).
- <sup>260</sup> D. Golberg, Y. Bando, O. Stéphan, and K. Kurashima, *Appl. Phys. Lett.* **73**, 2441 (1998).
- <sup>261</sup> D. Golberg, Y. Bando, K. Kurashima, and T. Sasaki, *Appl. Phys. Lett.* **72**, 2108 (1998).
- <sup>262</sup> J. A. Rodríguez-Manzo, M. Terrones, H. Terrones, H. W. Kroto, L. Sun, and F. Banhart, *Nat. Nanotechnol.* **2**, 307 (2007).
- <sup>263</sup> J. A. Rodríguez-Manzo, I. Janowska, C. Pham-Huu, A. Tolvanen, A. V. Krasheninnikov, K. Nordlund, and F. Banhart, *Small* **5**, 2710 (2009).
- <sup>264</sup> J. B. Gibson, A. N. Goland, M. Milgram, and G. H. Vineyard, *Phys. Rev.* **120**, 1229 (1960).
- <sup>265</sup> J. Pomoell, A. V. Krasheninnikov, K. Nordlund, and J. Keinonen, *Nucl. Instrum. Methods Phys. Res. B* **206**, 18 (2003).
- <sup>266</sup> J. A. Åström, A. V. Krasheninnikov, and K. Nordlund, *Phys. Rev. Lett.* **93**, 215503 (2004); **94**, 029902(E) (2005).
- <sup>267</sup> J. Kotakoski, J. Pomoell, A. V. Krasheninnikov, and K. Nordlund, *Nucl. Instrum. Methods Phys. Res. B* **228**, 31 (2005).
- <sup>268</sup> J. Kotakoski, A. V. Krasheninnikov, and K. Nordlund, *Nucl. Instrum. Methods Phys. Res. B* **240**, 810 (2005).
- <sup>269</sup> Y. Ma, A. S. Foster, A. V. Krasheninnikov, and R. M. Nieminen, *Phys. Rev. B* **72**, 205416 (2005).
- <sup>270</sup> J. Kotakoski and K. Nordlund, *New J. Phys.* **8**, 115 (2006).
- <sup>271</sup> S. K. Pregler and S. B. Sinnott, *Phys. Rev. B* **73**, 224106 (2006).
- <sup>272</sup> B. Ni and S. B. Sinnott, *Phys. Rev. B* **61**, R16343 (2000).
- <sup>273</sup> Y. Hu, D. L. Irving, and S. B. Sinnott, *Chem. Phys. Lett.* **422**, 137 (2006).
- <sup>274</sup> Z. Xu, W. Zhang, Z. Zhu, C. Ren, Y. Li, and P. Huai, *J. Appl. Phys.* **106**, 043501 (2009).
- <sup>275</sup> J. Nygård and D. Cobden, *Appl. Phys. Lett.* **79**, 4216 (2001).
- <sup>276</sup> A. Tolvanen, J. Kotakoski, A. V. Krasheninnikov, and K. Nordlund, *Appl. Phys. Lett.* **91**, 173109 (2007).

- <sup>277</sup> J. Kotakoski, A. V. Krasheninnikov, and K. Nordlund, *Phys. Rev. B* **74**, 245420 (2006).
- <sup>278</sup> J. M. Carlsson and M. Scheffler, *Phys. Rev. Lett.* **96**, 046806 (2006).
- <sup>279</sup> A. T. Lee, Y. Kang, K. J. Chang, and I. Lee, *Phys. Rev. B* **79**, 174105 (2009).
- <sup>280</sup> W. Orellana, *Phys. Rev. B* **80**, 075421 (2009).
- <sup>281</sup> A. V. Krasheninnikov, K. Nordlund, and J. Keinonen, *Appl. Phys. Lett.* **81**, 1101 (2002).
- <sup>282</sup> R. L. Federizzi, C. S. Moura, and L. Amaral, *J. Phys. Chem. B* **110**, 23215 (2006).
- <sup>283</sup> E. Salonen, A. V. Krasheninnikov, and K. Nordlund, *Nucl. Instrum. Methods Phys. Res. B* **193**, 603 (2002).
- <sup>284</sup> P. Wesolowski, Y. Lyutovich, F. Banhart, H. D. Carstanjen, and H. Kronmüller, *Appl. Phys. Lett.* **71**, 1948 (1997).
- <sup>285</sup> A. Kumar, D. K. Avasthi, J. C. Pivin, A. Tripathi, and F. Singh, *Phys. Rev. B* **74**, 153409 (2006).
- <sup>286</sup> I. Ponomareva and L. Chernozatonskii, *JETP Lett.* **79**, 375 (2004).
- <sup>287</sup> R. Astala, M. Kaukonen, R. M. Nieminen, G. Jungnickel, and T. Frauenheim, *Phys. Rev. B* **63**, 081402 (2001).
- <sup>288</sup> T. Yumura, M. Kertesz, and S. Iijima, *J. Phys. Chem. B* **111**, 1099 (2007).
- <sup>289</sup> I. Jang, S. B. Sinnott, D. Danailov, and P. Keblinski, *Nano Lett.* **4**, 109 (2004).
- <sup>290</sup> M. Yasuda, Y. Kimoto, K. Tada, H. Mori, S. Akita, Y. Nakayama, and Y. Hirai, *Phys. Rev. B* **75**, 205406 (2007).
- <sup>291</sup> T. Belytschko, S. P. Xiao, G. C. Schatz, and R. S. Ruoff, *Phys. Rev. B* **65**, 235430 (2002).
- <sup>292</sup> Y. Lifshitz, T. Köhler, T. Frauenheim, I. Guzman, A. Hoffman, R. Q. Zhang, X. T. Zhou, and S. T. Lee, *Science* **297**, 1531 (2002).
- <sup>293</sup> J. H. Warner, F. Schäffel, G. Zhong, M. H. Rummeli, B. Büchner, J. Robertson, and G. Briggs, *ACS Nano* **3**, 1557 (2009).
- <sup>294</sup> F. Ding, K. Jiao, M. Wu, and B. I. Yakobson, *Phys. Rev. Lett.* **98**, 075503 (2007).
- <sup>295</sup> M. H. Gass, U. Bangert, A. L. Bleloch, P. Wang, R. R. Nair, and A. K. Geim, *Nat. Nanotechnol.* **3**, 676 (2008).
- <sup>296</sup> P. Ehrhart, K. H. Robrock, and H. R. Shober, in *Physics of Radiation Effects in Crystals*, edited by R. A. Johnson and A. N. Orlov (Elsevier, Amsterdam, 1986), p. 3.
- <sup>297</sup> A. Misra, P. K. Tyagi, M. K. Singh, D. S. Misra, J. Ghatak, P. V. Satyam, and D. K. Avasthi, *Diamond Relat. Mater.* **15**, 300 (2006).
- <sup>298</sup> A. J. Lu and B. C. Pan, *Phys. Rev. Lett.* **92**, 105504 (2004).
- <sup>299</sup> J. Rossato, R. J. Baierle, A. Fazzio, and R. Mota, *Nano Lett.* **5**, 197 (2005).
- <sup>300</sup> S. Berber and A. Oshiyama, *Physica B* **376-377**, 272 (2006).
- <sup>301</sup> C. Wang and C. Y. Wang, *Eur. Phys. J. B* **54**, 243 (2006).
- <sup>302</sup> S. Berber and A. Oshiyama, *Phys. Rev. B* **77**, 165405 (2008).
- <sup>303</sup> P. O. Lehtinen, A. S. Foster, Y. Ma, A. V. Krasheninnikov, and R. M. Nieminen, *Phys. Rev. Lett.* **93**, 187202 (2004).
- <sup>304</sup> R. Telling, C. Ewels, A. El-Barbary, and M. Heggie, *Nature Mater.* **2**, 333 (2003).
- <sup>305</sup> A. A. El-Barbary, R. H. Telling, C. P. Ewels, M. I. Heggie, and P. R. Briddon, *Phys. Rev. B* **68**, 144107 (2003).
- <sup>306</sup> L. Li, S. Reich, and J. Robertson, *Phys. Rev. B* **72**, 184109 (2005).
- <sup>307</sup> A. M. Stoneham, *Theory of Defects in Solids* (Clarendon, Oxford, 1975).
- <sup>308</sup> A. Kis, K. Jensen, S. Aloni, W. Mickelson, and A. Zettl, *Phys. Rev. Lett.* **97**, 025501 (2006).
- <sup>309</sup> R. G. Amorim, A. Fazzio, A. Antonelli, F. D. Novaes, and A. da Silva, *Nano Lett.* **7**, 2459 (2007).
- <sup>310</sup> G. Lee, C. Z. Wang, E. Yoon, N. Hwang, D. Kim, and K. M. Ho, *Phys. Rev. Lett.* **95**, 205501 (2005).
- <sup>311</sup> R. Y. Oeiras, F. M. Araújo-Moreira, and E. Z. da Silva, *Phys. Rev. B* **80**, 073405 (2009).
- <sup>312</sup> J. C. Meyer, C. Kisielowski, R. Erni, M. D. Rossell, M. F. Crommie, and A. Zettl, *Nano Lett.* **8**, 3582 (2008).
- <sup>313</sup> O. Gülseren, T. Yildirim, and S. Ciraci, *Phys. Rev. Lett.* **87**, 116802 (2001).
- <sup>314</sup> M. Zhao, Y. Xia, Y. Ma, M. Ying, X. Liu, and L. Mei, *Phys. Rev. B* **66**, 155403 (2002).
- <sup>315</sup> A. V. Krasheninnikov, K. Nordlund, P. O. Lehtinen, A. S. Foster, A. Ayuela, and R. M. Nieminen, *Carbon* **42**, 1021 (2004).
- <sup>316</sup> P. O. Lehtinen, A. S. Foster, A. Ayuela, A. Krasheninnikov, K. Nordlund, and R. M. Nieminen, *Phys. Rev. Lett.* **91**, 017202 (2003).
- <sup>317</sup> R. Singh and P. Kroll, *J. Phys.: Condens. Matter* **21**, 196002 (2009).
- <sup>318</sup> M. T. Lusk and L. D. Carr, *Phys. Rev. Lett.* **100**, 175503 (2008).
- <sup>319</sup> T. Hashi, Y. Uramoto, and M. Saito, *Jpn. J. Appl. Phys.* **47**, 6623 (2008).
- <sup>320</sup> L. Tsetseris and S. T. Pantelides, *Carbon* **47**, 901 (2009).
- <sup>321</sup> Y. Ma, *Phys. Rev. B* **76**, 075419 (2007).
- <sup>322</sup> A. J. Stone and D. J. Wales, *Chem. Phys. Lett.* **128**, 501 (1986).
- <sup>323</sup> Z. Wang, F. Gao, J. Li, X. Zu, and W. J. Weber, *J. Appl. Phys.* **106**, 084305 (2009).
- <sup>324</sup> K. Suenaga, H. Wakabayashi, M. Koshino, Y. Sato, K. Urita, and S. Iijima, *Nat. Nanotechnol.* **2**, 358 (2007).
- <sup>325</sup> B. I. Yakobson, *Appl. Phys. Lett.* **72**, 918 (1998).
- <sup>326</sup> M. B. Nardelli, B. I. Yakobson, and J. Bernholc, *Phys. Rev. B* **57**, R4277 (1998).
- <sup>327</sup> G. G. Samsonidze, G. G. Samsonidze, and B. I. Yakobson, *Phys. Rev. Lett.* **88**, 065501 (2002).
- <sup>328</sup> E. Ertekin, D. C. Chrzan, and M. S. Daw, *Phys. Rev. B* **79**, 155421 (2009).
- <sup>329</sup> B. C. Pan, W. S. Yang, and J. Yang, *Phys. Rev. B* **62**, 12652 (2000).
- <sup>330</sup> L. G. Zhou and S. Shi, *Appl. Phys. Lett.* **83**, 1222 (2003).
- <sup>331</sup> J. Ma, D. Alfè, A. Michaelides, and E. Wang, *Phys. Rev. B* **80**, 033407 (2009).
- <sup>332</sup> A. da Silva, A. Fazzio, and A. Antonelli, *Nano Lett.* **5**, 1045 (2005).
- <sup>333</sup> J. A. Rodríguez-Manzo and F. Banhart, *Nano Lett.* **9**, 2285 (2009).
- <sup>334</sup> O. Lehtinen, L. Sun, T. Nikitin, A. V. Krasheninnikov, L. Khriachtchev, J. A. Rodríguez-Manzo, M. Terrones, F. Banhart, and J. Keinonen, *Physica E (Amsterdam)* **40**, 2618 (2008).
- <sup>335</sup> Y. H. Lee, S. G. Kim, and D. Tománek, *Phys. Rev. Lett.* **78**, 2393 (1997).
- <sup>336</sup> M. Heggie, B. R. Eggen, C. P. Ewels, P. Leary, S. Ali, G. Jungnickel, R. Jones, and P. R. Briddon, *Proc.-Electrochem. Soc.* **98**, 60 (1998).
- <sup>337</sup> F. Banhart, T. Füller, P. Redlich, and P. M. Ajayan, *Chem. Phys. Lett.* **269**, 349 (1997).
- <sup>338</sup> Y. Gan, J. Kotakoski, A. V. Krasheninnikov, K. Nordlund, and F. Banhart, *New J. Phys.* **10**, 023022 (2008).
- <sup>339</sup> P. A. Thrower and R. M. Mayer, *Phys. Status Solidi A* **47**, 11 (1978).
- <sup>340</sup> C. Xu, C. L. Fu, and D. Pedraza, *Phys. Rev. B* **48**, 13273 (1993).
- <sup>341</sup> Y. Gan and F. Banhart, *Adv. Mater.* **20**, 4751 (2008).
- <sup>342</sup> C. P. Ewels, M. I. Heggie, and P. R. Briddon, *Chem. Phys. Lett.* **351**, 178 (2002).
- <sup>343</sup> C. Jin, K. Suenaga, and S. Iijima, *Nano Lett.* **8**, 1127 (2008).
- <sup>344</sup> T. Tanabe, *Phys. Scr., T* **64**, 7 (1996).
- <sup>345</sup> K. Niwase, *Phys. Rev. B* **52**, 15785 (1995).
- <sup>346</sup> S. K. Pregler, T. Hayakawa, H. Yasumatsu, T. Kondow, and S. B. Sinnott, *Nucl. Instrum. Methods Phys. Res. B* **262**, 240 (2007).
- <sup>347</sup> E. Kaxiras and K. C. Pandey, *Phys. Rev. Lett.* **61**, 2693 (1988).
- <sup>348</sup> C. P. Ewels, R. H. Telling, A. A. El-Barbary, M. I. Heggie, and P. R. Briddon, *Phys. Rev. Lett.* **91**, 025505 (2003).
- <sup>349</sup> F. Tournus, J. Charlier, and P. Mélinon, *J. Chem. Phys.* **122**, 094315 (2005).
- <sup>350</sup> K. Kim, J. Choi, H. Lee, H.-K. Lee, T.-H. Kang, Y.-H. Han, B.-C. Lee, S. Kim, and B. Kim, *J. Phys. Chem. C* **112**, 13062 (2008).
- <sup>351</sup> J. C. Meyer, A. K. Geim, M. I. Katsnelson, K. S. Novoselov, T. J. Booth, and S. Roth, *Nature (London)* **446**, 60 (2007).
- <sup>352</sup> D. Teweldebrhan and A. A. Balandin, *Appl. Phys. Lett.* **94**, 013101 (2009).
- <sup>353</sup> M. Sammalkorpi, A. V. Krasheninnikov, A. Kuronen, K. Nordlund, and K. Kaski, *Nucl. Instrum. Methods Phys. Res. B* **228**, 142 (2005).
- <sup>354</sup> M. Sammalkorpi, A. Krasheninnikov, A. Kuronen, K. Nordlund, and K. Kaski, *Phys. Rev. B* **70**, 245416 (2004); **71**, 169906(E) (2005).
- <sup>355</sup> D. E. Luzzi and B. W. Smith, *Carbon* **38**, 1751 (2000).
- <sup>356</sup> E. Hernández, V. Meunier, B. W. Smith, R. Rurali, H. Terrones, M. Nardelli, M. Terrones, D. E. Luzzi, and J. Charlier, *Nano Lett.* **3**, 1037 (2003).
- <sup>357</sup> H. Terrones, M. Terrones, E. Hernández, N. Grobert, J. Charlier, and P. M. Ajayan, *Phys. Rev. Lett.* **84**, 1716 (2000).
- <sup>358</sup> J. A. Rodríguez-Manzo, F. Banhart, M. Terrones, H. Terrones, N. Grobert, P. M. Ajayan, B. G. Sumpter, V. Meunier, M. Wang, Y. Bando, and D. Golberg, *Proc. Natl. Acad. Sci. U.S.A.* **106**, 4591 (2009).
- <sup>359</sup> F. Banhart, *Nanoscale* **1**, 201 (2009).
- <sup>360</sup> T. Aref, M. Remeika, and A. Bezryadin, *J. Appl. Phys.* **104**, 024312 (2008).
- <sup>361</sup> M. D. Fischbein and M. Drndić, *Appl. Phys. Lett.* **93**, 113107 (2008).
- <sup>362</sup> T. G. Pedersen, C. Flindt, J. Pedersen, N. A. Mortensen, A. Jauho, and K. Pedersen, *Phys. Rev. Lett.* **100**, 136804 (2008).
- <sup>363</sup> Y. Son, M. L. Cohen, and S. G. Louie, *Nature (London)* **444**, 347 (2006).
- <sup>364</sup> Y. Son, M. L. Cohen, and S. G. Louie, *Phys. Rev. Lett.* **97**, 216803 (2006).
- <sup>365</sup> T. D. Yuzvinsky, A. M. Fennimore, W. Mickelson, C. Esquivias, and A.

- Zettl, *Appl. Phys. Lett.* **86**, 053109 (2005).
- <sup>366</sup>P. W. Sutter and E. A. Sutter, *Nature Mater.* **6**, 363 (2007).
- <sup>367</sup>Z. Liu, M. Koshino, K. Suenaga, A. Mrzel, H. Kataura, and S. Iijima, *Phys. Rev. Lett.* **96**, 088304 (2006).
- <sup>368</sup>D. Golberg and Y. Bando, *Recent Res. Dev. Appl. Phys.* **2**, 1 (1999).
- <sup>369</sup>D. Golberg, P. S. Dorozhkin, Y. Bando, M. Mitome, and C. C. Tang, *Diamond Relat. Mater.* **14**, 1857 (2005).
- <sup>370</sup>K. Pi, K. M. McCreary, W. Bao, W. Han, Y. F. Chiang, Y. Li, S. Tsai, C. N. Lau, and R. K. Kawakami, *Phys. Rev. B* **80**, 075406 (2009).
- <sup>371</sup>A. V. Krasheninnikov, P. O. Lehtinen, A. S. Foster, P. Pyykkö, and R. M. Nieminen, *Phys. Rev. Lett.* **102**, 126807 (2009).
- <sup>372</sup>E. J. G. Santos, A. Ayuela, S. B. Fagan, J. Mendes Filho, D. L. Azevedo, A. G. Souza Filho, and D. Sánchez-Portal, *Phys. Rev. B* **78**, 195420 (2008).
- <sup>373</sup>A. V. Krasheninnikov and V. F. Elesin, *Surf. Sci.* **454-456**, 519 (2000).
- <sup>374</sup>E. Stolyarova, D. Stolyarov, K. Bolotin, S. Ryu, L. Liu, K. T. Rim, M. Klima, M. Hybertsen, I. Pogorelsky, I. Pavlishin, J. Hone, P. Kim, H. L. Stormer, V. Yakimenko, and G. Flynn, *Nano Lett.* **9**, 332 (2009).
- <sup>375</sup>M. Hulman, V. Skákalová, A. V. Krasheninnikov, and S. Roth, *Appl. Phys. Lett.* **94**, 071907 (2009).
- <sup>376</sup>G. H. Jeong, R. Hatakeyama, T. Hirata, K. Tohji, K. Motomiya, N. Sato, and Y. Kawazoe, *Appl. Phys. Lett.* **79**, 4213 (2001).
- <sup>377</sup>G. H. Jeong, R. Hatakeyama, T. Hirata, K. Tohji, K. Motomiya, T. Yaguchi, and Y. Kawazoe, *Chem. Commun. (Cambridge)* **2003**, 152.
- <sup>378</sup>Z. Ni, A. Ishaq, L. Yan, J. Gong, and D. Zhu, *J. Phys. D* **42**, 075408 (2009).
- <sup>379</sup>K. Maehashi, H. Ozaki, Y. Ohno, K. Inoue, K. Matsumoto, S. Seki, and S. Tagawa, *Appl. Phys. Lett.* **90**, 023103 (2007).
- <sup>380</sup>D. W. Boukhvalov and M. I. Katsnelson, *Nano Lett.* **8**, 4373 (2008).
- <sup>381</sup>A. V. Krasheninnikov, *Solid State Commun.* **118**, 361 (2001).
- <sup>382</sup>A. V. Krasheninnikov and K. Nordlund, *J. Vac. Sci. Technol. B* **20**, 728 (2002).
- <sup>383</sup>V. Skákalová, A. B. Kaiser, Z. Osváth, G. Vértesy, L. P. Biró, and S. Roth, *Appl. Phys. A: Mater. Sci. Process.* **90**, 597 (2008).
- <sup>384</sup>B. D. Weaver, B. J. Landi, and R. P. Raffaele, *Proceedings of the 2nd International Energy Conversion Engineering Conference, Providence, Rhode Island, 16–19 August 2004 (unpublished)*.
- <sup>385</sup>R. H. Baughman, C. Cui, A. A. Zakhidov, Z. Iqbal, J. N. Barisci, G. M. Spinks, G. G. Wallace, A. Mazzoldi, D. De Rossi, A. G. Rinzler, O. Jaschinski, S. Roth, and M. Kertesz, *Science* **284**, 1340 (1999).
- <sup>386</sup>A. Rinzler, J. Liu, H. Dai, P. Nikolaev, C. B. Huffman, F. J. Rodriguez-Macias, P. J. Boul, A. H. Lu, D. Heymann, D. T. Colbert, R. S. Lee, J. E. Fische, A. M. Rao, P. C. Eklund, and R. E. Smalley, *Appl. Phys. A: Mater. Sci. Process.* **67**, 29 (1998).
- <sup>387</sup>T. V. Sreekumar, T. Liu, S. Kumar, L. Ericson, R. H. Hauge, and R. E. Smalley, *Chem. Mater.* **15**, 175 (2003).
- <sup>388</sup>K. Nordlund, *Mat. Fys. Medd. K. Dan. Vidensk. Selsk.* **52**, 357 (2006).
- <sup>389</sup>A. V. Krasheninnikov, K. Nordlund, J. Keinonen, and F. Banhart, *Phys. Rev. B* **66**, 245403 (2002).
- <sup>390</sup>Z. Wang, L. Yu, W. Zhang, Y. Ding, Y. Li, J. Han, Z. Zhu, H. Xu, G. He, Y. Chen, and G. Hu, *Phys. Lett. A* **324**, 321 (2004).
- <sup>391</sup>Z. Ni, Q. Li, L. Yan, J. Gong, and D. Zhu, *Carbon* **46**, 376 (2008).
- <sup>392</sup>A. Bachtold, M. Henny, C. Terrier, C. Strunk, C. Schonenberger, J.-P. Salvetat, J.-M. Bonard, and L. Forró, *Appl. Phys. Lett.* **73**, 274 (1998).
- <sup>393</sup>M. Fujii, X. Zhang, H. Xie, H. Ago, K. Takahashi, T. Ikuta, H. Abe, and T. Shimizu, *Phys. Rev. Lett.* **95**, 065502 (2005).
- <sup>394</sup>R. S. Lee, H. J. Kim, J. E. Fisher, A. Thess, and R. E. Smalley, *Nature (London)* **388**, 854 (1997).
- <sup>395</sup>A. M. Rao, P. C. Eklund, S. Bandow, A. Thess, and R. E. Smalley, *Nature (London)* **388**, 257 (1997).
- <sup>396</sup>L. Grigorian, G. U. Sumanasekera, A. L. Loper, S. Fang, J. L. Allen, and P. C. Eklund, *Phys. Rev. B* **58**, R4195 (1998).
- <sup>397</sup>C. P. Ewels and M. Glerup, *J. Nanosci. Nanotechnol.* **5**, 1345 (2005).
- <sup>398</sup>A. H. Nevidomskyy, G. Csányi, and M. C. Payne, *Phys. Rev. Lett.* **91**, 105502 (2003).
- <sup>399</sup>R. Droppa, Jr., C. T. M. Ribeiro, A. R. Zanatta, M. C. dos Santos, and F. Alvarez, *Phys. Rev. B* **69**, 045405 (2004).
- <sup>400</sup>J. W. Jang, C. E. Lee, S. C. Lyu, T. J. Lee, and C. J. Lee, *Appl. Phys. Lett.* **84**, 2877 (2004).
- <sup>401</sup>D. Srivastava, M. Menon, C. Daraio, S. Jin, B. Sadanadan, and A. M. Rao, *Phys. Rev. B* **69**, 153414 (2004).
- <sup>402</sup>L. H. Chan, K. H. Hong, D. Q. Xiao, T. C. Lin, S. H. Lai, W. J. Hsieh, and H. C. Shih, *Phys. Rev. B* **70**, 125408 (2004).
- <sup>403</sup>R. C. Che, L.-M. Peng, and M. S. Wang, *Appl. Phys. Lett.* **85**, 4753 (2004).
- <sup>404</sup>H. C. Choi, S. Y. Bae, J. Park, K. Seo, C. Kim, B. Kim, H. J. Song, and H.-J. Shin, *Appl. Phys. Lett.* **85**, 5742 (2004).
- <sup>405</sup>H. S. Kang and S. Jeong, *Phys. Rev. B* **70**, 233411 (2004).
- <sup>406</sup>M. Glerup, J. Steinmetz, D. Samaille, O. Stéphan, S. Enouz, A. Loiseau, S. Roth, and P. Bernier, *Chem. Phys. Lett.* **387**, 193 (2004).
- <sup>407</sup>Q. Zhao, M. B. Nardelli, and J. Bernholc, *Phys. Rev. B* **65**, 144105 (2002).
- <sup>408</sup>J. Kotakoski, A. V. Krasheninnikov, Y. Ma, A. S. Foster, K. Nordlund, and R. M. Nieminen, *Phys. Rev. B* **71**, 205408 (2005).
- <sup>409</sup>I. Shimoyama, G. Wu, T. Sekiguchi, and Y. Baba, *Phys. Rev. B* **62**, R6053 (2000).
- <sup>410</sup>M. Mehring, W. Scherer, and A. Weidinger, *Phys. Rev. Lett.* **93**, 206603 (2004).
- <sup>411</sup>C. Morant, R. Torres, I. Jimenez, J. M. Sanz, and E. Elizalde, *J. Nanosci. Nanotechnol.* **9**, 3633 (2009).
- <sup>412</sup>F. Xu, M. Minniti, P. Barone, A. Sindona, A. Bonanno, and A. Oliva, *Carbon* **46**, 1489 (2008).
- <sup>413</sup>F. Xu, M. Minniti, C. Giallombardo, A. Cupolillo, P. Barone, A. Oliva, and L. Papagno, *Surf. Sci.* **601**, 2819 (2007).
- <sup>414</sup>W. S. Yun, J. Kim, K. H. Park, J. S. Ha, Y. J. Ko, K. Park, S. K. Kim, Y. J. Doh, H. J. Lee, J. P. Salvetat, and L. Forro, *J. Vac. Sci. Technol. A* **18**, 1329 (2000).
- <sup>415</sup>C. Thelander and L. Samuelson, *Nanotechnology* **13**, 108 (2002).
- <sup>416</sup>G. Hobler, *Radiat. Eff. Defects Solids* **139**, 21 (1996).
- <sup>417</sup>A. V. Krasheninnikov and K. Nordlund, *Phys. Rev. B* **71**, 245408 (2005).
- <sup>418</sup>A. V. Krasheninnikov and K. Nordlund, *Nucl. Instrum. Methods Phys. Res. B* **228**, 21 (2005).
- <sup>419</sup>C. S. Moura and L. Amaral, *J. Phys. Chem. B* **109**, 13515 (2005).
- <sup>420</sup>G. V. Dedkov, *Surf. Coat. Technol.* **158-159**, 75 (2002).
- <sup>421</sup>P. Král and D. Tománek, *Phys. Rev. Lett.* **82**, 5373 (1999).
- <sup>422</sup>Z. Mao and S. B. Sinnott, *Phys. Rev. Lett.* **89**, 278301 (2002).
- <sup>423</sup>B. C. Regan, S. Aloni, R. O. Ritchie, U. Dahmen, and A. Zettl, *Nature (London)* **428**, 924 (2004).
- <sup>424</sup>C. S. Moura and L. Amaral, *Carbon* **45**, 1802 (2007).
- <sup>425</sup>L. Zheng, Z. Zhu, Y. Li, D. Zhu, and H. Xia, *Nucl. Instrum. Methods Phys. Res. B* **266**, 849 (2008).
- <sup>426</sup>S. Bellucci, V. M. Biryukov, Y. A. Chesnokov, V. Guidic, and W. Scandale, *Nucl. Instrum. Methods Phys. Res. B* **202**, 236 (2003).
- <sup>427</sup>Y.-N. Wang and Z. L. Mišković, *Phys. Rev. A* **69**, 022901 (2004).
- <sup>428</sup>Y.-N. Wang and Z. L. Mišković, *Phys. Rev. A* **66**, 042904 (2002).
- <sup>429</sup>N. K. Zhevago and V. I. Glebov, *Phys. Lett. A* **310**, 301 (2003).
- <sup>430</sup>D. Borka, D. J. Mowbray, Z. L. Miskovic, S. Petrovic, and N. Neskovic, *J. Phys.: Condens. Matter* **20**, 474212 (2008).
- <sup>431</sup>Zh. Zhu, private communication.
- <sup>432</sup>J. X. Li and F. Banhart, *Adv. Mater.* **17**, 1539 (2005).
- <sup>433</sup>D. Ugarte, *Chem. Phys. Lett.* **209**, 99 (1993).
- <sup>434</sup>*Carbon Nanotubes: Synthesis, Structure, Properties and Applications*, edited by M. S. Dresselhaus, G. Dresselhaus, and P. Avouris (Springer, Berlin, 2001).
- <sup>435</sup>S. Zhang, S. L. Mielke, R. Khare, D. Troya, R. S. Ruoff, G. C. Schatz, and T. Belytschko, *Phys. Rev. B* **71**, 115403 (2005).
- <sup>436</sup>S. L. Mielke, D. Troya, S. Zhang, J. L. Li, S. Xiao, R. Car, R. S. Ruoff, G. C. Schatz, and T. Belytschko, *Chem. Phys. Lett.* **390**, 413 (2004).
- <sup>437</sup>T. Dumitrica, M. Hua, and B. I. Yakobson, *Proc. Natl. Acad. Sci. U.S.A.* **103**, 6105 (2006).
- <sup>438</sup>J. Yuan and K. M. Liew, *Carbon* **47**, 1526 (2009).
- <sup>439</sup>M.-F. Yu, O. Lourie, M. J. Dyer, K. Moloni, T. F. Kelly, and R. S. Ruoff, *Science* **287**, 637 (2000).
- <sup>440</sup>M. Huhtala, A. V. Krasheninnikov, J. Aittoniemi, K. Nordlund, and K. Kaski, *Phys. Rev. B* **70**, 045404 (2004).
- <sup>441</sup>E. M. Byrne, M. A. McCarthy, Z. Xia, and W. A. Curtin, *Phys. Rev. Lett.* **103**, 045502 (2009).
- <sup>442</sup>B. Vigolo, A. Penicaud, C. Coulon, C. Sauder, R. Paillet, C. Journet, P. Bernier, and P. Poulin, *Science* **290**, 1331 (2000).
- <sup>443</sup>B. Vigolo, P. Poulin, M. Lucas, P. Launois, and P. Bernier, *Appl. Phys. Lett.* **81**, 1210 (2002).
- <sup>444</sup>P. Poulin, B. Vigolo, and P. Launois, *Carbon* **40**, 1741 (2002).
- <sup>445</sup>N. Neophytou, D. Kienle, E. Polizzi, and M. P. Anantram, *Appl. Phys. Lett.* **88**, 242106 (2006).
- <sup>446</sup>M. P. Anantram and T. R. Govindan, *Phys. Rev. B* **58**, 4882 (1998).
- <sup>447</sup>H.-F. Song, J.-L. Zhu, and J.-J. Xiong, *Phys. Rev. B* **65**, 085408 (2002).
- <sup>448</sup>C. G. Rocha, T. G. Dargam, and A. Latge, *Phys. Rev. B* **65**, 165431 (2002).

- <sup>449</sup>T. Kostyrko, M. Bartkowiak, and G. D. Mahan, *Phys. Rev. B* **60**, 10735 (1999).
- <sup>450</sup>H. J. Choi, J. Ihm, S. G. Louie, and M. L. Cohen, *Phys. Rev. Lett.* **84**, 2917 (2000).
- <sup>451</sup>L. Chico, L. X. Benedict, S. G. Louie, and M. L. Cohen, *Phys. Rev. B* **54**, 2600 (1996).
- <sup>452</sup>A. Tolvanen, G. Buchs, P. Ruffieux, P. Groening, O. Groening, and A. V. Krasheninnikov, *Phys. Rev. B* **79**, 125430 (2009).
- <sup>453</sup>G. Buchs, A. V. Krasheninnikov, P. Ruffieux, P. Gröning, A. S. Foster, R. M. Nieminen, and O. Gröning, *New J. Phys.* **9**, 275 (2007).
- <sup>454</sup>A. Högele, C. Galland, M. Winger, and A. Imamoglu, *Phys. Rev. Lett.* **100**, 217401 (2008).
- <sup>455</sup>V. Skákalová, A. B. Kaiser, U. Dettlaff, K. Arstila, A. V. Krasheninnikov, J. Keinonen, and S. Roth, *Phys. Status Solidi C* **245**, 2280 (2008).
- <sup>456</sup>A. Ishaq, L. Yan, and D. Zhu, *Nucl. Instrum. Methods Phys. Res. B* **267**, 1779 (2009).
- <sup>457</sup>Y. Kopelevich, P. Esquinazi, J. Torres, and S. Moehlecke, *J. Low Temp. Phys.* **119**, 691 (2000).
- <sup>458</sup>A. V. Rode, E. G. Gamaly, A. G. Christy, J. G. Fitz Gerald, S. T. Hyde, R. G. Elliman, B. Luther-Davies, A. I. Veinger, J. Androulakis, and J. Giapintzakis, *Phys. Rev. B* **70**, 054407 (2004).
- <sup>459</sup>A. W. Mombrú, H. Pardo, R. Faccio, O. F. de Lima, E. R. Leite, G. Z. To, A. J. C. Lanfredi, C. A. Cardoso, and F. M. Araújo-Moreira, *Phys. Rev. B* **71**, 100404 (2005).
- <sup>460</sup>J. Barzola-Quiquia, P. Esquinazi, M. Rothermel, D. Spemann, T. Butz, and N. Garcia, *Phys. Rev. B* **76**, 161403 (2007).
- <sup>461</sup>*Carbon Based Magnetism*, edited by T. Makarova and F. Palacio (Elsevier, Amsterdam, 2006).
- <sup>462</sup>R. Sielemann, Y. Kobayashi, Y. Yoshida, H. P. Gunnlaugsson, and G. Weyer, *Phys. Rev. Lett.* **101**, 137206 (2008).
- <sup>463</sup>M. P. López-Sancho, F. de Juan, and M. A. H. Vozmediano, *Phys. Rev. B* **79**, 075413 (2009).
- <sup>464</sup>A. N. Andriotis, M. Menon, R. M. Sheetz, and L. Chernozatonskii, *Phys. Rev. Lett.* **90**, 026801 (2003).
- <sup>465</sup>J. A. Chan, B. Montanari, J. D. Gale, S. M. B. J. W. Taylor, and N. M. Harrison, *Phys. Rev. B* **70**, 041403(R) (2004).
- <sup>466</sup>D. W. Boukhalov and M. I. Katsnelson, *Eur. Phys. J. B* **68**, 529 (2009).
- <sup>467</sup>O. V. Yazzyev, *Phys. Rev. Lett.* **101**, 037203 (2008).
- <sup>468</sup>L. Pisani, B. Montanari, and N. M. Harrison, *New J. Phys.* **10**, 033002 (2008).
- <sup>469</sup>H. Lee, Y. Miyamoto, and J. Yu, *Phys. Rev. B* **79**, 121404 (2009).
- <sup>470</sup>K. Kusakabe and M. Maruyama, *Phys. Rev. B* **67**, 092406 (2003).
- <sup>471</sup>Y.-H. Kim, J. Choi, K. J. Chang, and D. Tománek, *Phys. Rev. B* **68**, 125420 (2003).
- <sup>472</sup>S. Okada and A. Oshiyama, *J. Phys. Soc. Jpn.* **72**, 1510 (2003).
- <sup>473</sup>K. Nakada, M. Fujita, G. Dresselhaus, and M. S. Dresselhaus, *Phys. Rev. B* **54**, 17954 (1996).
- <sup>474</sup>J. Barzola-Quiquia, R. Hoehne, M. Rothermel, A. Setzer, P. Esquinazi, and V. Heera, *Eur. Phys. J. B* **61**, 127 (2008).
- <sup>475</sup>Y. Zhang, S. Talapatra, S. Kar, R. Vajtai, S. K. Nayak, and P. M. Ajayan, *Phys. Rev. Lett.* **99**, 107201 (2007).
- <sup>476</sup>H. Xia, W. Li, Y. Song, X. Yang, X. Liu, M. Zhao, Y. Xia, C. Song, T.-W. Wang, D. Zhu, J. Gong, and Z. Zhu, *Adv. Mater.* **20**, 4679 (2008).
- <sup>477</sup>N. G. Chopra, R. J. Luyken, K. Cherrey, V. H. Crespi, M. L. Cohen, S. G. Louie, and A. Zettl, *Science* **269**, 966 (1995).
- <sup>478</sup>D. Golberg, Y. Bando, M. Eremets, K. Takemura, K. Kurashima, and H. Yusa, *Appl. Phys. Lett.* **69**, 2045 (1996).
- <sup>479</sup>D. Pacilé, J. C. Meyer, Ç. Ö. Girit, and A. Zettl, *Appl. Phys. Lett.* **92**, 133107 (2008).
- <sup>480</sup>N. Alem, R. Erni, C. Kisielowski, M. D. Rossell, W. Gannett, and A. Zettl, *Phys. Rev. B* **80**, 155425 (2009).
- <sup>481</sup>D. Golberg, Y. Bando, C. Tang, and C. Zhi, *Adv. Mater.* **19**, 2413 (2007).
- <sup>482</sup>J. Ullmann, J. E. E. Baglin, and A. J. Kellock, *J. Appl. Phys.* **83**, 2980 (1998).
- <sup>483</sup>I. Jiménez, A. F. Jankowski, L. J. Terminello, D. G. J. Sutherland, J. A. Carlisle, G. L. Doll, W. M. Tong, D. K. Shuh, and F. J. Himpsel, *Phys. Rev. B* **55**, 12025 (1997).
- <sup>484</sup>S. Eyhusein, I. Gerhards, H. Hofsäss, C. Ronning, M. Blomenhofer, J. Zweck, and M. Seibt, *Diamond Relat. Mater.* **12**, 1877 (2003).
- <sup>485</sup>E. Bengu, L. D. Marks, R. V. Ovali, and O. Gulseren, *Ultramicroscopy* **108**, 1484 (2008).
- <sup>486</sup>D. Golberg, private communication.
- <sup>487</sup>D. Golberg, Y. Bando, M. Eremets, K. Takemura, K. Kurashima, T. Tamiya, and H. Yusa, *Chem. Phys. Lett.* **279**, 191 (1997).
- <sup>488</sup>D. Golberg, Y. Bando, W. Han, L. Bourgeois, K. Kurashima, and T. Sato, *Mater. Res. Soc. Symp. Proc.* **593**, 27 (2000).
- <sup>489</sup>A. Celik-Aktas, J. F. Stubbins, and J. Zuo, *J. Appl. Phys.* **102**, 024310 (2007).
- <sup>490</sup>C. Jin, F. Lin, K. Suenaga, and S. Iijima, *Phys. Rev. Lett.* **102**, 195505 (2009).
- <sup>491</sup>J. C. Meyer, A. Chuvilin, G. Algara-Siller, J. Biskupek, and U. Kaiser, *Nano Lett.* **9**, 2683 (2009).
- <sup>492</sup>O. Lehtinen, T. Nikitin, A. V. Krasheninnikov, L. Sun, L. Khriachtchev, F. Banhart, T. Terao, D. Golberg, and J. Keinonen, *Phys. Status Solidi C* **7** (2010).
- <sup>493</sup>H. F. Bettinger, T. Dumitric, G. E. Scuseria, and B. I. Yakobson, *Phys. Rev. B* **65**, 041406 (2002).
- <sup>494</sup>G. Y. Gou, B. C. Pan, and L. Shi, *Phys. Rev. B* **76**, 155414 (2007).
- <sup>495</sup>S. Azevedo, J. R. Kaschny, C. M. C. de Castilho, and F. de Brito Mota, *Nanotechnology* **18**, 495707 (2007).
- <sup>496</sup>S. Azevedo, J. R. Kaschny, C. M. C. de Castilho, and F. de Brito Mota, *Eur. Phys. J. B* **67**, 507 (2009).
- <sup>497</sup>A. Zobelli, C. Ewels, A. Gloter, G. Seifert, O. Stephan, S. Csillag, and C. Colliex, *Nano Lett.* **6**, 1955 (2006).
- <sup>498</sup>W. Orellana and H. Chacham, *Phys. Rev. B* **63**, 125205 (2001).
- <sup>499</sup>A. Zobelli, A. Gloter, C. P. Ewels, and C. Colliex, *Phys. Rev. B* **77**, 045410 (2008).
- <sup>500</sup>A. Zobelli, C. P. Ewels, A. Gloter, and G. Seifert, *Phys. Rev. B* **75**, 094104 (2007).
- <sup>501</sup>T. M. Schmidt, R. J. Baierle, P. Piquini, and A. Fazzio, *Phys. Rev. B* **67**, 113407 (2003).
- <sup>502</sup>R.-F. Liu and C. Cheng, *Phys. Rev. B* **76**, 014405 (2007).
- <sup>503</sup>M. S. Si and D. S. Xue, *Phys. Rev. B* **75**, 193409 (2007).
- <sup>504</sup>Y. F. Zhukovskii, S. Bellucci, S. Piskunov, L. Trinkler, and B. Berzina, *Eur. Phys. J. B* **67**, 519 (2009).
- <sup>505</sup>M. Topsakal, E. Aktürk, and S. Ciraci, *Phys. Rev. B* **79**, 115442 (2009).
- <sup>506</sup>Y. Miyamoto, A. Rubio, S. Berber, M. Yoon, and D. Tománek, *Phys. Rev. B* **69**, 121413(R) (2004).
- <sup>507</sup>S. Okada, *Phys. Rev. B* **80**, 161404 (2009).
- <sup>508</sup>O. Stéphan, Y. Bando, A. Loiseau, F. Willaime, N. Shramchenko, T. Tamiya, and T. Sato, *Appl. Phys. A: Mater. Sci. Process.* **67**, 107 (1998).
- <sup>509</sup>Y. Xia, P. Yang, Y. Sun, Y. Wu, B. Mayers, B. Gates, Y. Yin, F. Kim, and H. Yan, *Adv. Mater.* **15**, 353 (2003).
- <sup>510</sup>D. Sood, P. Sekhar, and S. Bhansali, *Appl. Phys. Lett.* **88**, 143110 (2006).
- <sup>511</sup>R. S. Wagner and W. C. Ellis, *Appl. Phys. Lett.* **4**, 89 (1964).
- <sup>512</sup>J. Ahopelto, M. Sopanen, H. Lipsanen, S. Lourduos, E. R. Messmer, E. Höfling, J. P. Reithmaier, A. Forchel, A. Petersson, and L. Samuelsson, *Appl. Phys. Lett.* **70**, 2828 (1997).
- <sup>513</sup>C. D'Orléans, J. P. Stoquert, C. Estournes, C. Cerruti, J. J. Grob, J. L. Guille, F. Haas, D. Muller, and M. Richard-Plouet, *Phys. Rev. B* **67**, 220101 (2003).
- <sup>514</sup>T. Muller, K. H. Heinig, and B. Schmidt, *Mater. Sci. Eng., C* **19**, 209 (2002).
- <sup>515</sup>V. A. Nebol'sin and A. A. Shchetinin, *Inorg. Mater.* **39**, 899 (2003).
- <sup>516</sup>D. Bell, Y. Wu, C. Barrelet, S. Gradecak, J. Xiang, B. Timko, and C. Lieber, *Microsc. Res. Tech.* **64**, 373 (2004).
- <sup>517</sup>Y. Su, X. Liang, S. Li, Y. Chen, Q. Zhou, S. Yin, X. Meng, and M. Kong, *Mater. Lett.* **62**, 1010 (2008).
- <sup>518</sup>C. B. Duke, *Chem. Rev. (Washington, D.C.)* **96**, 1237 (1996).
- <sup>519</sup>C. H. Grein, *J. Cryst. Growth* **180**, 54 (1997).
- <sup>520</sup>C. Fulk, S. Sivanathan, D. Zavitz, R. Singh, M. Trenary, Y. P. Chen, G. Brill, and N. Dhar, *J. Electron. Mater.* **35**, 1449 (2006).
- <sup>521</sup>E. Holmström, A. V. Krasheninnikov, and K. Nordlund, in *Ion Beams and Nano-Engineering*, edited by D. Ila, J. K. N. Lindner, P. K. Chu, J. Baglin, and N. Kishimoto (MRS, Warrendale, 2009).
- <sup>522</sup>S. Hofmann, C. Ducati, R. J. Neill, S. Piscanec, A. C. Ferrari, J. Geng, and R. E. Dunin-Borkowski, *J. Appl. Phys.* **94**, 6005 (2003).
- <sup>523</sup>E. de Vasconcelos, F. dos Santos, E. da Silva, and H. Boudinov, *Appl. Surf. Sci.* **252**, 5572 (2006).
- <sup>524</sup>S.-Y. Lee, C.-O. Jang, J.-H. Hyung, D.-J. Kim, T.-H. Kim, S.-K. Lee, S.-M. Koo, and M.-D. Kim, *J. Korean Phys. Soc.* **55**, 28 (2009).
- <sup>525</sup>J. Li, K. J. V. Vilet, T. Zhu, S. Yip, and S. Suresh, *Nature (London)* **418**, 307 (2002).
- <sup>526</sup>S. Hoffmann, J. Bauer, C. Ronning, T. Stelzner, J. Michler, C. Ballif, V. Sivakov, and S. H. Christiansen, *Nano Lett.* **9**, 1341 (2009).
- <sup>527</sup>R. G. Elliman, A. R. Wilkinson, T. Kim, P. Sekhar, and S. Bhansali, *Nucl. Instrum. Methods Phys. Res. B* **266**, 1362 (2008).
- <sup>528</sup>P. K. Sekhar, A. R. Wilkinson, R. G. Elliman, T.-H. Kim, and S. Bhansali,

- J. Phys. Chem. C* **112**, 20109 (2008).
- <sup>529</sup> S. Dhara, A. Datta, C. Wu, Z. Lan, K. Chen, Y. Wang, Y. Chen, C. Hsu, L. Chen, H. Lin, and C. C. Chen, *Appl. Phys. Lett.* **84**, 3486 (2004).
- <sup>530</sup> V. M. Ayres, B. W. Jacobs, M. E. Englund, E. H. Carey, M. A. Crimp, R. M. Ronningen, A. F. Zeller, J. B. Halpern, M. Q. He, G. L. Harris, D. Liu, H. C. Shaw, and M. P. Petkov, *Diamond Relat. Mater.* **15**, 1117 (2006).
- <sup>531</sup> D. C. Look, J. W. Hemsky, and J. R. Sizelove, *Phys. Rev. Lett.* **82**, 2552 (1999).
- <sup>532</sup> Y. V. Gorelinskii and G. D. Watkins, *Phys. Rev. B* **69**, 115212 (2004).
- <sup>533</sup> C. Coskun, D. C. Look, G. C. Farlow, and J. R. Sizelove, *Semicond. Sci. Technol.* **19**, 752 (2004).
- <sup>534</sup> K. Lorenz, E. Alves, E. Wendler, O. Bilani, W. Wesch, and M. Hayes, *Appl. Phys. Lett.* **87**, 191904 (2005).
- <sup>535</sup> D. C. Look, G. C. Farlow, P. Reunchan, S. Limpijumnong, S. Zhang, and K. Nordlund, *Phys. Rev. Lett.* **95**, 225502 (2005).
- <sup>536</sup> W.-K. Hong, S.-S. Kwon, G. Jo, S. Song, B. S. Choi, and T. Lee, *J. Korean Phys. Soc.* **52**, 848 (2008).
- <sup>537</sup> L. Liao, Z. Zhang, Y. Yang, B. Yan, H. T. Cao, L. L. Chen, G. P. Li, T. Wu, Z. X. Shen, B. K. Tay, T. Yu, and X. W. Sun, *J. Appl. Phys.* **104**, 076104 (2008).
- <sup>538</sup> R. H. Baughman, A. A. Zakhidov, and W. A. de Heer, *Science* **297**, 787 (2002).
- <sup>539</sup> X. W. Sun, B. Ling, J. L. Zhao, S. T. Tan, Y. Yang, Y. Q. Shen, Z. L. Dong, and X. C. Li, *Appl. Phys. Lett.* **95**, 133124 (2009).
- <sup>540</sup> S. Ju, K. Lee, D. B. Janes, R. C. Dwivedi, H. Baffour-Awuah, R. Wilkins, M.-H. Yoon, A. Facchetti, and T. J. Mark, *Appl. Phys. Lett.* **89**, 073510 (2006).
- <sup>541</sup> J. Wang, M. J. Zhou, S. K. Hark, Q. Li, D. Tang, M. W. Chu, and C. H. Chen, *Appl. Phys. Lett.* **89**, 221917 (2006).
- <sup>542</sup> H. Liu, G.-A. Cheng, C. Liang, and R. Zheng, *Nanotechnology* **19**, 245606 (2008).
- <sup>543</sup> S. Tsukuda, M. Sugimoto, S. Tagawa, and S.-I. Tanaka, *J. Ceram. Proc. Res.* **9**, 466 (2008).
- <sup>544</sup> Y. Kondo and K. Takayanagi, *Phys. Rev. Lett.* **79**, 3455 (1997).
- <sup>545</sup> S. Xu, M. Tian, J. Wang, H. Xu, J. Redwing, and M. Chan, *Small* **1**, 1221 (2005).
- <sup>546</sup> J. Hu, Q. Li, J. Zhan, Y. Jiao, Z. Liu, S. P. Ringer, Y. Bando, and D. Golberg, *ACS Nano* **2**, 107 (2008).
- <sup>547</sup> J. Zhan, Y. Bando, J. Hu, and D. Golberg, *Appl. Phys. Lett.* **89**, 243111 (2006).
- <sup>548</sup> D. Weissenberger, D. Gerthsen, A. Reiser, G. M. Prinz, M. Feneberg, K. Thonke, H. Zhou, J. Sartor, J. Fallert, C. Klingshirn, and H. Kalt, *Appl. Phys. Lett.* **94**, 042107 (2009).
- <sup>549</sup> M. Takeguchi, M. Shimojo, M. Tanaka, R. Che, W. Zhang, and K. Furuya, *Surf. Interface Anal.* **38**, 1628 (2006).
- <sup>550</sup> C. Lai, J. Dai, X. Zhang, H. Chan, Y. Xu, Q. Li, and H. Ong, *J. Cryst. Growth* **282**, 383 (2005).
- <sup>551</sup> Y. C. Choi, J. Kim, and S. D. Bu, *J. Korean Phys. Soc.* **51**, 2045 (2007).
- <sup>552</sup> J. Hu, Y. Bando, J. Zhan, and D. Golberg, *Adv. Mater.* **17**, 1964 (2005).
- <sup>553</sup> Y. K. Hong, D. H. Park, S. K. Park, and J. Joo, *J. Korean Phys. Soc.* **53**, 2627 (2008).
- <sup>554</sup> C. Akhmadaliev, B. Schmidt, and L. Bischoff, *Appl. Phys. Lett.* **89**, 223129 (2006).
- <sup>555</sup> V. Pott and A. M. Ionescu, *Microelectron. Eng.* **83**, 1718 (2006).
- <sup>556</sup> L. Bischoff, B. Schmidt, C. Akhmadaliev, and A. Mucklich, *Microelectron. Eng.* **83**, 800 (2006).
- <sup>557</sup> S. K. Tripathi, N. Shukla, and V. N. Kulkarni, *Nucl. Instrum. Methods Phys. Res. B* **266**, 1468 (2008).
- <sup>558</sup> Z.-M. Liao, J.-B. Xu, X.-M. Sun, Y.-D. Li, J. Xu, and D.-P. Yu, *Phys. Lett. A* **373**, 1181 (2009).
- <sup>559</sup> L. Bischoff, C. Akhmadaliev, and B. Schmidt, *Microelectron. Eng.* **84**, 1459 (2007).
- <sup>560</sup> N. Chekurov, K. Grigoros, A. Peltonen, S. Franssila, and I. Tittonen, *Nanotechnology* **20**, 065307 (2009).
- <sup>561</sup> M. Savolainen, V. Touboltsev, P. Koppinen, K.-P. Riikonen, and K. Arutyunov, *Appl. Phys. A: Mater. Sci. Process.* **79**, 1769 (2004).
- <sup>562</sup> M. Zgirska, K.-P. Riikonen, V. Touboltsev, P. Jalkanen, T. T. Hongisto, and K. Y. Arutyunov, *Nanotechnology* **19**, 055301 (2008).
- <sup>563</sup> V. Touboltsev and J. Raisanen, *Nanotechnology* **20**, 335302 (2009).
- <sup>564</sup> M. Zgirska, K.-P. Riikonen, V. Touboltsev, and K. Y. Arutyunov, *Phys. Rev. B* **77**, 054508 (2008).
- <sup>565</sup> L. Rayleigh, *Proc. R. Soc. London* **29**, 71 (1879).
- <sup>566</sup> C. Akhmadaliev, L. Bischoff, and B. Schmidt, *Mater. Sci. Eng., C* **26**, 818 (2006).
- <sup>567</sup> T. Stelzner, G. Andra, F. Falk, E. Wendler, W. Wesch, R. Scholz, and S. Christiansen, *Nucl. Instrum. Methods Phys. Res. B* **257**, 172 (2007).
- <sup>568</sup> A. Lugstein, C. Schoendorfer, M. Weil, C. Tomastik, A. Jauss, and E. Bertagnolli, *Nucl. Instrum. Methods Phys. Res. B* **255**, 309 (2007).
- <sup>569</sup> Y. Ok, T. Seong, C. Choi, and K. Tu, *Appl. Phys. Lett.* **88**, 043106 (2006).
- <sup>570</sup> J. B. Condon and T. Schober, *J. Nucl. Mater.* **207**, 1 (1993).
- <sup>571</sup> W. Jiang, W. Weber, C. Wang, J. Young, L. Boatner, J. Lian, L. Wang, and R. Ewing, *Adv. Mater.* **17**, 1602 (2005).
- <sup>572</sup> J. Chen and R. Konekamp, *Appl. Phys. Lett.* **82**, 4782 (2003).
- <sup>573</sup> S. Tsukuda, S. Seki, S. Tagawa, M. Sugimoto, A. Idesaki, S. Tanaka, and A. Oshima, *J. Phys. Chem. B* **108**, 3407 (2004).
- <sup>574</sup> M. Lindeberg and K. Hjort, *Sens. Actuators, A* **105**, 150 (2003).
- <sup>575</sup> D. Fink, P. Alegaonkar, A. Petrov, M. Wilhelm, P. Szymkowiak, A. Behar, D. Sinha, W. Fahrner, K. Hoppe, and L. Chadderton, *Nucl. Instrum. Methods Phys. Res. B* **236**, 11 (2005).
- <sup>576</sup> M. Skupinski, M. Toulemonde, M. Lindeberg, and K. Hjort, *Nucl. Instrum. Methods Phys. Res. B* **240**, 681 (2005).
- <sup>577</sup> F. Maurer, A. Dangwal, D. Lysenkov, G. Muller, M. Toimil-Molares, C. Trautmann, J. Brotz, and H. Fuess, *Nucl. Instrum. Methods Phys. Res. B* **245**, 337 (2006).
- <sup>578</sup> R. Sanz, M. Vazquez, K. R. Pirola, and M. Hernandez-Velez, *J. Appl. Phys.* **101**, 114325 (2007).
- <sup>579</sup> A. Navitski, G. Müller, V. Sakharuk, T. W. Cornelius, C. Trautmann, and S. Karim, *Eur. Phys. J.: Appl. Phys.* **48**, 30502 (2009).
- <sup>580</sup> C. Chien, L. Sun, M. Tanase, L. Bauer, A. Hultgren, D. Silevitch, G. Meyer, P. Seanson, and D. Reich, *J. Magn. Magn. Mater.* **249**, 146 (2002).
- <sup>581</sup> S. Seki, S. Tsukuda, K. Maeda, S. Tagawa, H. Shibata, M. Sugimoto, K. Jimbo, I. Hashitomi, and A. Kohyama, *Macromolecules* **38**, 10164 (2005).
- <sup>582</sup> S. Tsukuda, S. Seki, M. Sugimoto, and S. Tagawa, *Surf. Coat. Technol.* **201**, 8526 (2007).
- <sup>583</sup> J. Kang, J. Seo, K. Byun, and H. Hwang, *Phys. Rev. B* **66**, 125405 (2002).
- <sup>584</sup> J. Tersoff, *Phys. Rev. B* **38**, 9902 (1988).
- <sup>585</sup> F. H. Stillinger and T. A. Weber, *Phys. Rev. B* **31**, 5262 (1985).
- <sup>586</sup> C. Moura and L. Amaral, *Nucl. Instrum. Methods Phys. Res. B* **228**, 37 (2005).
- <sup>587</sup> E. Holmström, A. V. Krasheninnikov, and K. Nordlund, Quantum and Classical Molecular Dynamics Studies of the Threshold Displacement Energy in Si Bulk and Nanowires, Proceedings of MRS Spring Meeting 2009, Paper No. 1181.
- <sup>588</sup> E. E. Zhurkin, *Surf. Invest. X-Ray Synchrotron Neutron Tech.* **2**, 193 (2008).
- <sup>589</sup> A. Marcus and N. Winograd, *Anal. Chem.* **78**, 141 (2006).
- <sup>590</sup> T. T. Järvi, D. Pohl, K. Albe, B. Rellinghaus, L. Schultz, J. Fassbender, A. Kuronen, and K. Nordlund, *EPL* **85**, 26001 (2009).
- <sup>591</sup> Y.-P. Kim, E. Oh, H. K. Shon, D. W. Moon, T. G. Lee, and H.-S. Kim, *Appl. Surf. Sci.* **255**, 1064 (2008).
- <sup>592</sup> W. Szymczak, N. Menzel, W. G. Kreyling, and K. Wittmaack, *Int. J. Mass Spectrom.* **254**, 70 (2006).
- <sup>593</sup> E. E. Zhurkin, *Surf. Invest. X-Ray Synchrotron Neutron Tech.* **3**, 192 (2009).
- <sup>594</sup> R. Kissel and H. M. Urbassek, *Nucl. Instr. Methods Phys. Res. B* **180**, 293 (2001).
- <sup>595</sup> S. Zimmermann and H. M. Urbassek, *Int. J. Mass Spectrom.* **272**, 91 (2008).
- <sup>596</sup> E. M. Bringa and R. E. Johnson, *Nucl. Instrum. Methods Phys. Res. B* **193**, 365 (2002).
- <sup>597</sup> E. M. Bringa and R. E. Johnson, *Astrophys. J.* **603**, 159 (2004).
- <sup>598</sup> R. E. Johnson and J. Schou, *Mat. Fys. Medd. K. Dan. Vidensk. Selsk.* **43**, 403 (1993).
- <sup>599</sup> I. Baranov, P. Håkansson, S. Kirillov, J. Kopniczyk, A. Novikov, V. Obnorskii, A. Pchelintsev, A. P. Quist, G. Torzo, S. Yarmiychuk, and L. Zennaro, *Nucl. Instrum. Methods Phys. Res. B* **193**, 798 (2002).
- <sup>600</sup> I. Baranov, S. Kirillov, A. Novikov, V. Obnorskii, M. Toulemonde, K. Wien, S. Yarmiychuk, V. A. Borodin, and A. Volkov, *Nucl. Instrum. Methods Phys. Res. B* **230**, 495 (2005).
- <sup>601</sup> P. K. Kuri, B. Joseph, H. P. Lenka, G. Sahu, J. Ghatak, D. Kanjilal, and D. P. Mahapatra, *Phys. Rev. Lett.* **100**, 245501 (2008).
- <sup>602</sup> A. Klimmer, P. Ziemann, J. Biskupek, U. Kaiser, and M. Fleisch, *Phys. Rev. B* **79**, 155427 (2009).
- <sup>603</sup> C. Zimmermann, M. Yeadon, K. Nordlund, J. M. Gibson, R. S. Averback, U. Herr, and K. Samwer, *Phys. Rev. B* **64**, 085419 (2001).

- <sup>604</sup>M. Ghaly and R. S. Averback, *Phys. Rev. Lett.* **72**, 364 (1994).
- <sup>605</sup>A. Wucher and B. J. Garrison, *J. Chem. Phys.* **105**, 5999 (1996).
- <sup>606</sup>R. E. Birtcher, S. E. Donnelly, and S. Schlutig, *Phys. Rev. Lett.* **85**, 4968 (2000).
- <sup>607</sup>L. E. Rehn, R. C. Birtcher, S. E. Donnelly, P. M. Baldo, and L. Funk, *Phys. Rev. Lett.* **87**, 207601 (2001).
- <sup>608</sup>K. O. E. Henriksson, K. Nordlund, and J. Keinonen, *Phys. Rev. B* **71**, 014117 (2005).
- <sup>609</sup>J. Samela and K. Nordlund, *Nucl. Instrum. Methods Phys. Res. B* **263**, 375 (2007).
- <sup>610</sup>K. Nordlund and J. Samela, *Nucl. Instrum. Methods Phys. Res. B* **267**, 1420 (2009).
- <sup>611</sup>M. O. Ruault, J. Chaumont, J. M. Penisson, and A. Bourret, *Philos. Mag. A* **50**, 667 (1984).
- <sup>612</sup>F. Baletto and R. Ferrando, *Rev. Mod. Phys.* **77**, 371 (2005).
- <sup>613</sup>O. Dmitrieva, B. Rellinghaus, J. Kästner, M. O. Liedke, and J. Fassbender, *J. Appl. Phys.* **97**, 10N112 (2005).
- <sup>614</sup>U. Wiedwald, A. Klimmer, B. Kern, L. Han, H.-G. Boyen, P. Ziemann, and K. Fauth, *Appl. Phys. Lett.* **90**, 062508 (2007).
- <sup>615</sup>T. T. Järvi, A. Kuronen, K. Nordlund, and K. Albe, *J. Appl. Phys.* **102**, 124304 (2007).
- <sup>616</sup>T. T. Järvi, A. Kuronen, K. Nordlund, and K. Albe, *Phys. Rev. B* **80**, 132101 (2009).
- <sup>617</sup>S. Talapatra, J.-Y. Cheng, N. Chakrapani, S. Trasobares, A. Cao, R. Vajtai, M. B. Huang, and P. M. Ajayan, *Nanotechnology* **17**, 305 (2006).
- <sup>618</sup>K. Meinander and K. Nordlund, *Phys. Rev. B* **79**, 045411 (2009).
- <sup>619</sup>T. T. Järvi, A. Kuronen, K. Nordlund, and K. Albe, *J. Appl. Phys.* **106**, 063516 (2009).
- <sup>620</sup>K. Meinander, Ph.D. thesis, University of Helsinki, Helsinki, Finland, 2009.
- <sup>621</sup>D. Datta, S. Bhattacharyya, I. Shyjumon, D. Ghose, and R. Hippler, *Surf. Coat. Technol.* **203**, 2452 (2009).
- <sup>622</sup>C. P. Poole and F. J. Owens, *Introduction to Nanotechnology* (Wiley, New Jersey, 2003).
- <sup>623</sup>S. Guha, A. Madhukar, and K. C. Rajkumar, *Appl. Phys. Lett.* **57**, 2110 (1990).
- <sup>624</sup>P. J. Wellmann, W. V. Schoenfeld, J. M. Garcia, and P. M. Petroff, *J. Electron. Mater.* **27**, 1030 (1998).
- <sup>625</sup>W. Lu, Y. L. Ji, G. B. Chen, N. Y. Tang, X. S. Chen, S. C. Shen, Q. X. Zhao, and M. Willander, *Appl. Phys. Lett.* **83**, 4300 (2003).
- <sup>626</sup>Z. Zaâboub, B. Ilahi, L. Sfaki, H. Maaref, B. Salem, V. Aimez, and D. Morris, *Nanotechnology* **19**, 285715 (2008).
- <sup>627</sup>P. Lever, H. H. Tan, C. Jagadish, P. Reece, and M. Gal, *Appl. Phys. Lett.* **82**, 2053 (2003).
- <sup>628</sup>S. Barik, H. H. Tan, and C. Jagadish, *Nanotechnology* **18**, 175305 (2007).
- <sup>629</sup>Q. Li, S. Barik, H. H. Tan, and C. Jagadish, *J. Phys. D: Appl. Phys.* **41**, 205107 (2008).
- <sup>630</sup>C. Dion, P. Desjardins, M. Chicoine, F. Schiettekatte, P. J. Poole, and S. Raymond, *Nanotechnology* **18**, 015404 (2007).
- <sup>631</sup>E. Bellini, A. Taurino, M. Catalano, M. Lomascolo, A. Passaseo, and L. Vasanelli, *Nanotechnology* **20**, 255306 (2009).
- <sup>632</sup>N. Venkatram, T. Reddeppa, R. Sathyavathi, U. M. Bhatta, P. V. Satyam, and D. N. Rao, *Nucl. Instrum. Methods Phys. Res. B* **266**, 1816 (2008).
- <sup>633</sup>S. Choudhury, D. Mohanta, G. Ahmed, S. Dolui, D. Avasthi, and A. Choudhury, *J. Lumin.* **114**, 95 (2005).
- <sup>634</sup>K. H. Heinig, B. Schmidt, A. Markwitz, R. Grötzchel, M. Strobel, and S. Oswald, *Nucl. Instrum. Methods Phys. Res. B* **148**, 969 (1999).
- <sup>635</sup>C. Bonafos, M. Carrada, N. Cherkashin, H. Coffin, D. Chassaing, G. B. Assayag, A. Claverie, T. Müller, K. H. Heinig, M. Perego, and M. Fanciulli, *J. Appl. Phys.* **95**, 5696 (2004).
- <sup>636</sup>C. W. White, J. D. Budai, S. P. Withrow, J. G. Zhu, E. Sonder, R. A. Zuhr, A. Meldrum, D. M. Hembree, D. O. Henderson, and S. Prawer, *Nucl. Instrum. Methods Phys. Res. B* **141**, 228 (1998).
- <sup>637</sup>P. G. Kik and A. Polman, *J. Appl. Phys.* **88**, 1992 (2000).
- <sup>638</sup>K.-H. Heinig, B. Schmidt, M. Strobel, and H. Bernas, in *Ion Beam Synthesis and Processing of Advanced Materials*, edited by D. B. Poker, S. C. Moss, and K.-H. Heinig (MRS, Warrendale, 2000), Vol. 647.
- <sup>639</sup>F. Ren, X. H. Xiao, G. X. Cai, J. B. Wang, and C. Z. Jiang, *Appl. Phys. A: Mater. Sci. Process.* **96**, 317 (2009).
- <sup>640</sup>K. Baba, T. Kaneko, and R. Hatakeyama, *Appl. Phys. Express* **2**, 035006 (2009).
- <sup>641</sup>L. Khriachtchev, S. Novikov, and O. Kilpelä, *J. Appl. Phys.* **87**, 7805 (2000).
- <sup>642</sup>L. Khriachtchev, M. Räsänen, and S. Novikov, *Appl. Phys. Lett.* **88**, 013102 (2006).
- <sup>643</sup>I. V. Antonova, A. G. Cherkov, V. A. Skuratov, M. S. Kagan, J. Jedrzejewski, and I. Balberg, *Nanotechnology* **20**, 185401 (2009).
- <sup>644</sup>G. A. Kachurin, M. O. Ruault, A. K. Gutakovskiy, O. Kaitasov, S. G. Yanovskaya, K. S. Zhuravlev, and H. Bernas, *Nucl. Instrum. Methods Phys. Res. B* **147**, 356 (1999).
- <sup>645</sup>G. A. Kachurin, S. G. Yanovskaya, M. O. Ruault, A. K. Gutakovskii, K. S. Zhuravlev, O. Kaitasov, and H. Bernas, *Semiconductors* **34**, 965 (2000).
- <sup>646</sup>S. Cheylan, N. Langford, and R. G. Elliman, *Nucl. Instrum. Methods Phys. Res. B* **166-167**, 851 (2000).
- <sup>647</sup>D. Pacifici, E. C. Moreira, G. Franzo, V. Martorino, F. Priolo, and F. Iacona, *Phys. Rev. B* **65**, 144109 (2002).
- <sup>648</sup>D. Pacifici, G. Franzo, F. Iacona, and F. Priolo, *Physica E (Amsterdam)* **16**, 404 (2003).
- <sup>649</sup>D. I. Tetelbaum, S. A. Trushin, V. A. Burdov, A. I. Golovanov, D. G. Revin, and D. M. Gaponova, *Nucl. Instrum. Methods Phys. Res. B* **174**, 123 (2001).
- <sup>650</sup>U. Serincan, M. Kulacsi, R. Turan, S. Foss, and T. G. Finstad, *Nucl. Instrum. Methods Phys. Res. B* **254**, 87 (2007).
- <sup>651</sup>M. C. Ridgway, G. M. Azevedo, R. G. Elliman, C. J. Glover, D. J. Llewellyn, R. Miller, W. Wesch, G. J. Foran, J. Hansen, and A. Nylandsted-Larsen, *Phys. Rev. B* **71**, 094107 (2005).
- <sup>652</sup>L. L. Araujo, R. Giuliani, B. Johannessen, D. J. Llewellyn, P. Kluth, G. D. M. Azevedo, D. J. Cookson, G. J. Foran, and M. C. Ridgway, *Nucl. Instrum. Methods Phys. Res. B* **266**, 3153 (2008).
- <sup>653</sup>M. Backman, F. Djurabekova, O. H. Pakarinen, K. Nordlund, L. L. Araujo, and M. C. Ridgway, *Phys. Rev. B* **80**, 144109 (2009).
- <sup>654</sup>F. Djurabekova, M. Backman, O. H. Pakarinen, K. Nordlund, L. Araujo, and M. Ridgway, *Nucl. Instrum. Methods Phys. Res. B* **267**, 1235 (2009).
- <sup>655</sup>F. Djurabekova and K. Nordlund, *Phys. Rev. B* **77**, 115325 (2008).
- <sup>656</sup>A. Kanjilal, L. Rebohle, N. K. Baddela, S. Zhou, M. Voelskow, W. Skorupa, and M. Helm, *Phys. Rev. B* **79**, 161302 (2009).
- <sup>657</sup>P. Kluth, B. Johannessen, G. J. Foran, D. J. Cookson, S. M. Kluth, and M. C. Ridgway, *Phys. Rev. B* **74**, 014202 (2006).
- <sup>658</sup>P. Kluth, B. Johannessen, R. Giuliani, C. S. Schnohr, G. J. Foran, D. J. Cookson, A. P. Byrne, and M. C. Ridgway, *Radiat. Eff. Defects Solids* **162**, 501 (2007).
- <sup>659</sup>L. G. Jacobsohn, J. D. Thompson, Y. Wang, A. Misra, R. K. Schulze, and M. Nastasi, *Nucl. Instrum. Methods Phys. Res. B* **250**, 201 (2006).
- <sup>660</sup>D. J. Sprouster, R. Giuliani, L. L. Araujo, P. Kluth, B. Johannessen, K. Nordlund, and M. C. Ridgway, "Ion irradiation induced amorphization on cobalt nanoparticles," *Phys. Rev. B* (submitted).
- <sup>661</sup>D. J. Sprouster, R. Giuliani, C. S. Schnohr, L. L. Araujo, P. Kluth, A. P. Byrne, G. J. Foran, B. Johannessen, and M. C. Ridgway, *Phys. Rev. B* **80**, 115438 (2009).
- <sup>662</sup>G. Rizza, A. Dunlop, and A. Dezellus, *Nucl. Instrum. Methods Phys. Res. B* **256**, 219 (2007).
- <sup>663</sup>W. Ostwald, *Z. Elektrochem. Angew. Phys. Chem.* **22**, 289 (1897).
- <sup>664</sup>G. C. Rizza, M. Strobel, K. H. Heinig, and H. Bernas, *Nucl. Instrum. Methods Phys. Res. B* **178**, 78 (2001).
- <sup>665</sup>G. Rizza, H. Cheverry, T. Gacoin, A. Lamas, and S. Henry, *J. Appl. Phys.* **101**, 014321 (2007).
- <sup>666</sup>C. Dorleans, J. P. Stoquert, C. Estournes, J. J. Grob, D. Muller, J. L. Guille, M. Richard-Plouet, C. Cerruti, and F. Haas, *Nucl. Instrum. Methods Phys. Res. B* **216**, 372 (2004).
- <sup>667</sup>C. Cerruti, J. P. Stoquert, C. D'Orleans, C. Estournes, J. J. Grob, J. L. Guille, F. Haas, D. Muller, and M. Richard-Plouet, *Nucl. Instrum. Methods Phys. Res. B* **216**, 329 (2004).
- <sup>668</sup>A. Oliver, J. A. Reyes-Esqueda, J. C. Cheang-Wong, C. E. Roman-Velazquez, A. Crespo-Sosa, L. Rodriguez-Fernandez, J. A. Seman, and C. Noguez, *Phys. Rev. B* **74**, 245425 (2006).
- <sup>669</sup>D. Mohanta, G. A. Ahmed, A. Choudhury, F. Singh, D. K. Avasthi, G. Boyer, and G. A. Stanciu, *Eur. Phys. J.: Appl. Phys.* **35**, 29 (2006).
- <sup>670</sup>B. Joseph, J. Ghatak, H. P. Lenka, P. K. Kuri, G. Sahu, N. C. Mishra, and D. P. Mahapatra, *Nucl. Instrum. Methods Phys. Res. B* **256**, 659 (2007).
- <sup>671</sup>B. Schmidt, A. Muecklich, L. Roentzsch, and K.-H. Heinig, *Nucl. Instrum. Methods Phys. Res. B* **257**, 30 (2007).
- <sup>672</sup>M. Gilliot, A. E. Naciri, L. Johann, J. P. Stoquert, J. J. Grob, and D. Muller, *Phys. Rev. B* **76**, 045424 (2007).
- <sup>673</sup>R. Giuliani, P. Kluth, L. L. Araujo, D. J. Sprouster, A. P. Byrne, D. J. Cookson, and M. C. Ridgway, *Phys. Rev. B* **78**, 125413 (2008).
- <sup>674</sup>P. Kluth, R. Giuliani, D. J. Sprouster, C. S. Schnohr, A. P. Byrne, D. J.

- Cookson, and M. C. Ridgway, *Appl. Phys. Lett.* **94**, 113107 (2009).
- <sup>675</sup>F. Singh, S. Mohapatra, J. P. Stolquert, D. K. Avasthi, and J. C. Pivin, *Nucl. Instrum. Methods Phys. Res. B* **267**, 936 (2009).
- <sup>676</sup>J. C. Pivin, F. Singh, Y. Mishra, D. K. Avasthi, and J. P. Stoquert, *Surf. Coat. Technol.* **203**, 2432 (2009).
- <sup>677</sup>K. Awazu, X. Wang, M. Fujimaki, J. Tominaga, H. Aiba, Y. Ohki, and T. Komatsubara, *Phys. Rev. B* **78**, 054102 (2008).
- <sup>678</sup>M. Shirai, K. Tsumori, M. Kutsuwada, K. Yasuda, and S. Matsumura, *Nucl. Instrum. Methods Phys. Res. B* **267**, 1787 (2009).
- <sup>679</sup>M. C. Ridgway, P. Kluth, R. Giulian, D. J. Sprouster, L. L. Araujo, C. S. Schnohr, D. J. Llewellyn, A. P. Byrne, G. J. Foran, and D. J. Cookson, *Nucl. Instrum. Methods Phys. Res. B* **267**, 931 (2009).
- <sup>680</sup>B. Schmidt, K.-H. Heinig, A. Mucklich, and C. Akhmadaliev, *Nucl. Instrum. Methods Phys. Res. B* **267**, 1345 (2009).
- <sup>681</sup>P. L. McEuen, *Nature (London)* **393**, 15 (1998).
- <sup>682</sup>Wikipedia, the free encyclopedia, <http://en.wikipedia.org/>.